Global Sulfur and Nitrogen Depositions – Distribution, Source Contribution, Critical Loads and Phosphorus Deposition

A Dissertation Presented for the

Doctor of Philosophy

Degree

The University of Tennessee, Knoxville

Jiani Tan

December 2019

ACKNOWLEDGEMENTS

I would like to express great gratitude to my supervisor, Dr. Joshua S. Fu, for his invaluable guidance on my research during my pursuit of the Ph.D. degree. During the last five years and a half, I have received countless helps and advices from him regarding both fundamental skills to conduct researches, and more important, the attitude towards scientific research. By working with him, I have learnt about many valuable lessons as a scientific researcher about being motivated, responsible to my researches, critical thinking and fearless of obstacles, which I think are the priceless experiences for my future career.

I am highly thankful to all my committee members: Dr. Forrest M. Hoffman, Dr. John S. Schwartz and Dr. Frank Yin for providing precious comments and suggestions to my presentation and dissertation. I would like to acknowledge Dr. Frank Dentener, Dr. John Seinfeld and Dr. Jason Lynch, for providing their insightful comments on my researches and publications. My research is also supported by the datasets from all modelling groups of HTAP-II and monitoring datasets from NADP, EMEP and EANET. Thank for the scholarships, awards and funding provided by the AWMA southern section and UTK graduate school. It's a great pleasure to receive your recognition.

Finally, I want to express my sincerely thank to my parents for their endless love, company and support. Many thanks to my friends Kan Huang, Juan Li and Bob Conrad, who provided me help when I first came to the United States. My special thanks to my friends, Liu Cao and Zhenghao Zhu, for their encouragement and company when I was down. I would like to express my special thanks to my colleagues, Melissa R. Allen, Kan Huang, Xinyi Dong, Jian Sun, Cheng-En Yang and Qingzhao Zhu for the enjoyable moments we have spent together.

ABSTRACT

The increasing nitrogen (N) emissions caused by human activities lead to elevations of N deposition in the ecosystems. And excessive N deposition is associated with a host of environmental issues. This study investigates several issues about N deposition. First, we map the global distribution of N deposition with ensemble results of several global climate models. The model predictions of N wet deposition generally agree well with site observations over North America, Europe and East Asia, but model underestimation of NH_4^+ wet deposition exists over all three regions. And more studies are required for measurement-poor regions, some of which happen to be the most heavily polluted regions (i.e. China and India). Then, we investigate the two predominant drivers of future N deposition: anthropogenic emissions and climate changes. We examine the effectiveness of emission control on reducing N deposition over United States via modelling approach. NH_3 emission abatement is not likely to cause significant reduction of reduced forms of nitrogen (NH_x) deposition, owing to the current atmospheric level of gas-phase NH_3. Long-range transport of air pollutants, as a potential impact of climate changes, increases the N burden on low emission intensity regions (i.e. Russia), coastal regions and Open Ocean, especially on those in the downwind regions of intensive emission sources. The impacts of excessive N deposition on terrestrial ecosystems are assessed by critical loads (CL), which is a threshold to show the natural capability on bearing N deposition. We collect several CLs from literature, and most of them were developed on regional scale (i.e. United States, Europe and China). In the practice of applying these datasets to access the exceedance of CLs, we find large uncertainties related to the land type classification, which may challenge the interpolation of results. We conduct a preliminary study on the deposition of phosphorus (P). The switches of nutrient limitation patterns from N-limited to P-limited by many ecosystems, due to inputs of N by human activities, draw the public attention on P deposition. But the lack of long-term measurement data and uncertainty on major parameters in the numerical simulations limit our understanding on the P budget.

TABLE OF CONTENTS

LIST OF FIGURES

LIST OF TABLES

CHAPTER 1
INTRODUCTION

1.1 The nitrogen (N) cycles in earth systems

Figure 1.1 demonstrates a simplified nitrogen (N) cycle in the atmosphere, biosphere and hydrosphere. Reactive N (N_r), defined as biologically, photochemically and radically reactive N, mainly includes oxidized N (denoted as NO_y) and reduced form N (denoted as NH_x). It comes from both anthropogenic and natural sources. The main anthropogenic sources of N_r are fossil fuel combustion, mobile emission, fertilizers production, fertilizer application and livestock cultivation (Galloway et al., 2008; Vitousek et al., 1997). The natural sources include biomass burning (lightening-induced burning) and N_2O released from soil. The processes that covert the unreactive N_2 gas into different forms of N_r are called natural and anthropogenic "N fixation". N_r takes parts in series of reactions in the atmosphere. The most important ones are (1) N_r servers as a reactant in the photochemical production of O_3; (2) both NO_x and NH_3 are the main reactants in the formation of particulate matters. Wet and dry depositions are the main pathways to remove N_r from the atmosphere. They are the main ways for the exchange of N_r between the atmosphere and biosphere/hydrosphere. Through atmospheric deposition, the N_r is also re-distributed so that many regions may receive more N_r than they have emitted, likewise the coastal and open ocean.

Figure 1.2 illustrates the N cycle in soils. The N generally exists in three forms in soils: organic N, NO_y (mainly in form of NO_3^-) and NH_x (mainly in form of ammonium (NH_4^+)). The inputs of N into soil can be categorized as (1) animal manures, biosolids and crop residues; (2) industrial fixation, such as application of fertilizer; (3) atmospheric fixation through natural processes (such as lightening) and atmospheric depositions; (4) biological N fixation, which converts N_2 to inorganic N via bacteria in soils. All sources beside source (1) are inorganic N. The balance between organic and inorganic N in soils are controlled by several processes: (1) Mineralization process decomposes chemical components in the organic matter. The outcomes are conversion of organic N to inorganic N; (2) Immobilization is the reverse process of

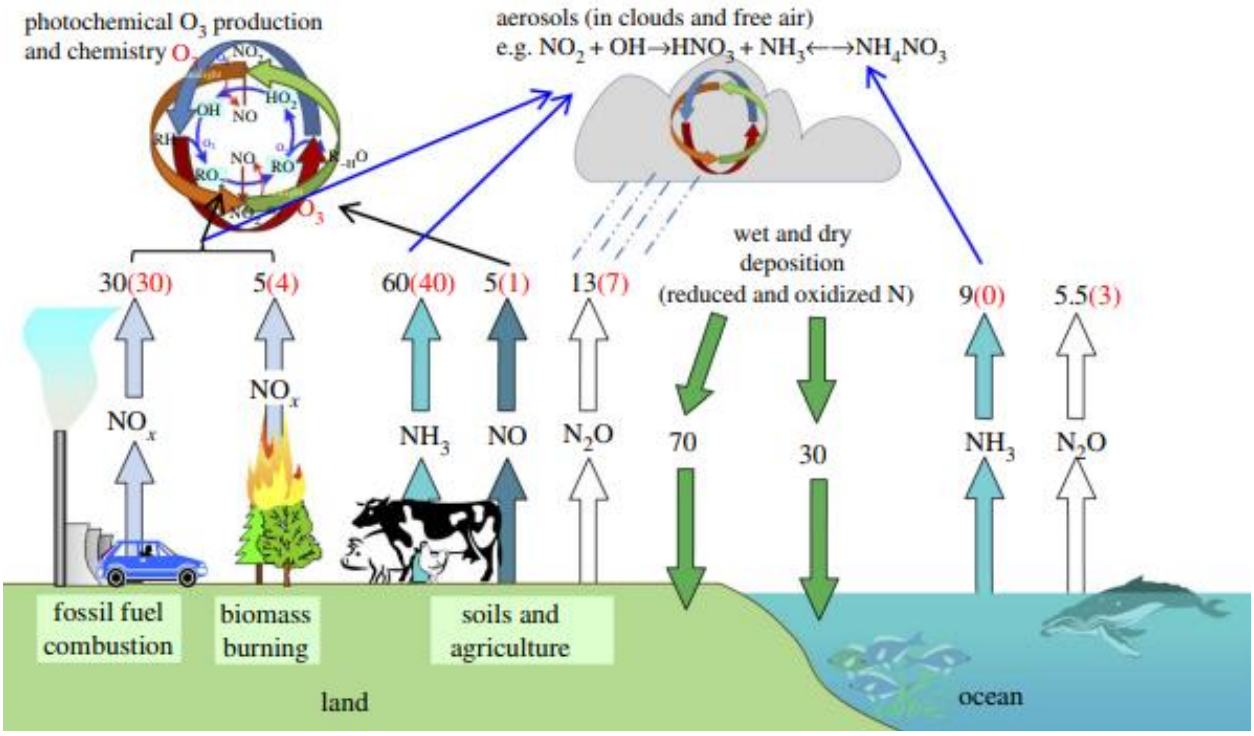

Figure 1. 1 The global atmospheric processing of reactive N, illustrating the main sources, the main chemical pathways and products and the magnitudes of the fluxes (units Tg yr^{-1}) (adopt from (Fowler, Pyle, Raven, & Sutton, 2013)).

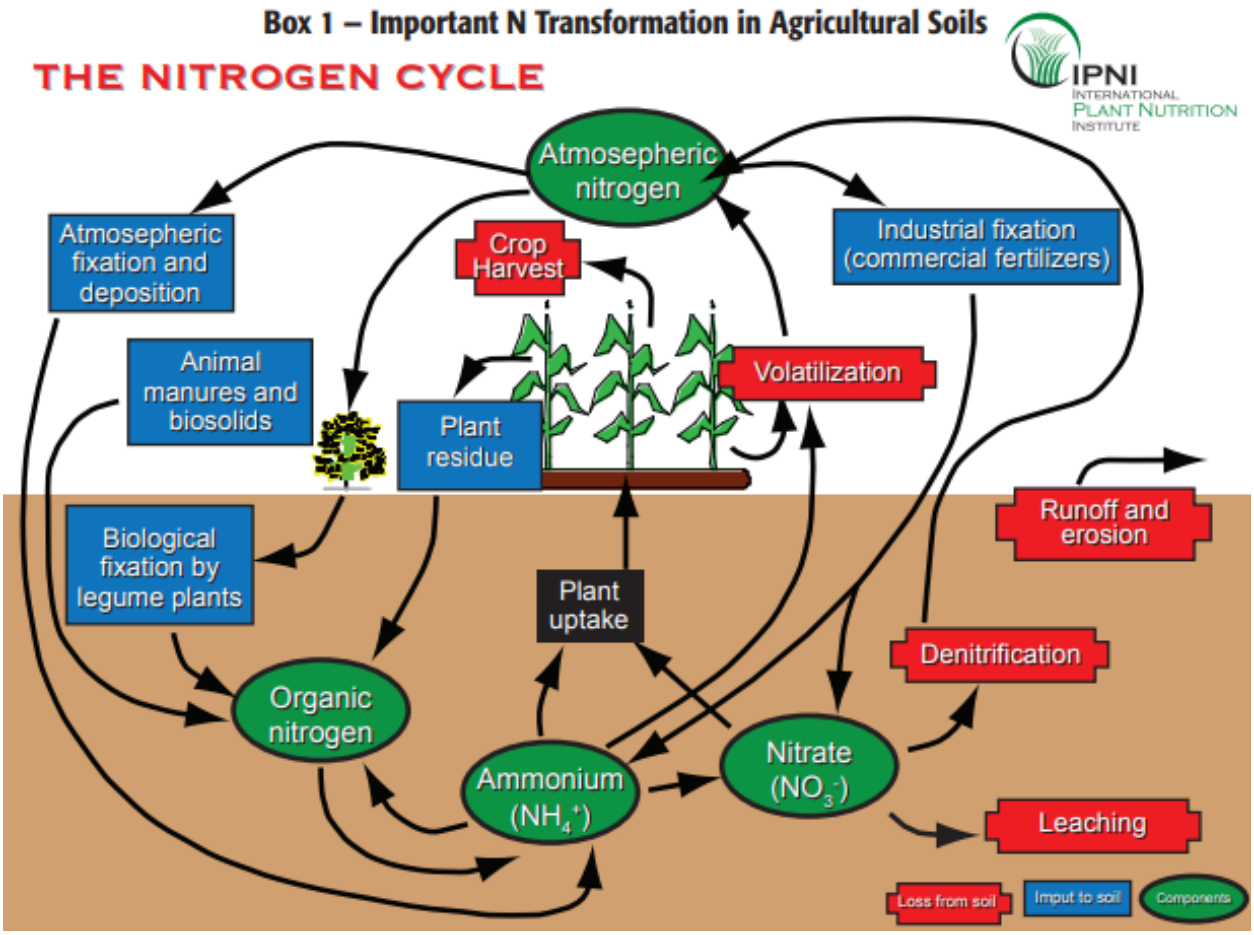

Figure 1. 2 N cycle in soils (adopt from (International Plant Nitrition Institute, 2018))

mineralization. The micro-organisms consume inorganic N in order to decompose carbon when materials (i.e. compost) with high C:N ratios are incorporated into soil. (3) Nitrification coverts NH_4^+ to NO_3^-. The loss of N in soil includes plant harvesting, volatilization of NH_3 gas, denitrification, leaching, runoff and erosion. Following are the main processes: (1) Harvesting plants removes N from the ecosystem; (2) Volatilization process releases NH_3 gas into the atmosphere. It is affected by the earth temperature, precipitation and soil pH values. Urea- or NH_4^+-based fertilizers are easily lost by this process in condition of low precipitation and high temperature; (3) Denitrification is the process that converts NO_3^- to N_2 gas, especially when O_2 concentration is low in soil; (4) Leaching moves NO_3^- from the root zones (leaching of NH_4^+ is generally negligible); (5) Run off and erosion processes bring N into the aquatic ecosystem.

1.2 Environmental issues related to atmospheric deposition

The increasing consumptions of energy by human activities have enhanced the atmospheric deposition largely over the terrestrial and marine ecosystems (Duce et al., 2008; Galloway et al., 2008; T. W. Kim, Lee, Najjar, Jeong, & Jeong, 2011). And the increasing trend is estimated to continue in the near future in many regions (Bleeker, Hicks, Dentener, Galloway, & Erisman, 2011; Kanakidou et al., 2016; Lamarque et al., 2013; Lamarque et al., 2005; Paulot, Jacob, & Henze, 2013). According to measurement data and modelling studies, the global total N deposition is about 101-122 Tg(N) yr^{-1} in 2000 (Kanakidou et al., 2016; Lamarque et al., 2013; Lamarque et al., 2005; Vet et al., 2014). And the amount is estimated to be increased by a factor of ~2.5 in 2100 under the IPCC SRES A2 scenario (Lamarque et al., 2005).

Elevated N deposition leads to exceedance of deposition required by the ecosystems (Sanderson, Collins, Johnson, & Derwent, 2006; Sun, Fu, Lynch, Huang, & Gao, 2017). About 7-17% of the world's natural vegetation has already received excessive N deposition in late 1990s and early 2000s (A. F. Bouwman, Van Vuuren, Derwent, & Posch, 2002; Dentener et al., 2006). This percentage will be increased to 40% for the world's protected areas in 2030 (Bleeker et al., 2011). The most affected regions are Eastern EU, South Asia (SA) and East Asia (EA). Excessive

S and N depositions are associated with a host of environmental issues related to over-richness in nutrient and acidification.

Impacts on the soil and terrestrial ecosystems. Following are the short-term and long-term impacts of excessive atmospheric depositions on the terrestrial ecosystems:

- Direct toxicity to vegetation. Short-time and long-term exposures of SO_2, NO_x and NH_3 air pollutants to vegetation can cause acute and chronic effects (*Critical Loads and Dynamic Risk Assessments*, 2015).
- Impacts on chemical and biogenic reactions in soils. High acidity environment will reduce the enzymatic activity (*Critical Loads and Dynamic Risk Assessments*, 2015) and affect the chemical and biogenic processes in soils, including the mineralization, immobilization, nitrification and leaching processes. For instance, the increase in leaching of NO_3^-will increase the leaching of base cations and affect the uptake of base cations by vegetation (Fang, Gundersen, Mo, & Zhu, 2009). Soil acidity also affects the heterotrophic respiration of soil and further influence the soil decomposition process (Janssens et al., 2010).
- Impacts on heavy metals in soils. Soil pH is also closely related to the solubility of heavy metals in soils (*Critical Loads and Dynamic Risk Assessments*, 2015). The heavy metals are more soluble under acid environment. And the excessive uptake of some heavy metals (Hg, Cd and Pb) is toxic to crops. Furthermore, the heavy metal can be transferred by food chains to accumulate in animals and humans.
- Benefits on vegetation. Increase in N nutrient benefit the productivity of crops and reduce the demand of fertilizer. It also favors the forest growth, which benefit the carbon uptake by land processes (de Vries & Posch, 2011; Holland et al., 1997; Reay, Dentener, Smith, Grace, & Feely, 2008). But at the same time this will increase the demand for cation uptake. This may result in an increase of biomass production to certain extent, after which the growth of vegetation will be limited to other sources than N. See Fig. S1.1 in Appendix for more details about the interactions between N and carbon (C) cycle.
- Impacts on biodiversity of ecosystems. High N intensity in soils favors the growth of species that are more adaptable to high-nutrient soil environment. This can drive the switch of species (Bobbink et al., 2010; Stevens et al., 2011) and result in extinction of certain species and loss of ecosystem biodiversity (Clark & Tilman, 2008).

Impacts on the aquatic ecosystems. The extra N that could not be uptake by the root systems could be brought to the waterbody (river, lake or ocean) by runoff and erosion. This will cause both acidification and eutrophication of the aquatic ecosystems (Fang et al., 2009).

- Ocean acidification. Acidification of the ocean and leads to release of inorganic carbon from sea to air (Doney et al., 2007). The impact on the ocean is small due to corresponding reduction in alkalinity, but the influence might be amplified over the coastal regions.
- Waterbody eutrophication. Eutrophication in waterbody increases production of phytoplankton, (Bergstrom & Jansson, 2006) and is reflected by algal blooms, which reduce the water quality, harm the health of marine livings and reduce the harvest of fishes (Smith & Schindler, 2009). For oceans, the atmospheric N deposition is relatively small compared to inner fluxes of oceanic N, but the impact might be significant over the coastal regions (T. Jickells, 2006).
- Promote the productivity of ocean and increase the oceanic carbon sequestration (T. D. Jickells et al., 2017).

Other impacts. Increase in Nr also promotes the formation of O_3 at surface layer, which harms the productivity of plants and human health. While the O_3 loss in the stratosphere increases human exposure to solar radiation and increases the probability of skin cancer. Exposure to O_3 harms the vegetation by the plant stomata. An accumulated hourly exposure of 40 ppb O_3 (AOT40) can result in about 5% yield reduction in crops, 2-4% reduction in the growth reduction of forests and 10% reduction in biomass production (*Critical Loads and Dynamic Risk Assessments*, 2015).

1.3 Motivations and overview of this study

The huge amount of nitrogen (N) emitted by human activities is disturbing the natural N cycle. The elevated N deposition causes exceedance of deposition over ecosystems. The natural feedbacks to overload of N deposition are mostly negative on human lives. Therefore, the prevention of excessive atmospheric deposition is of vital importance in the protection of a sustainable ecosystem and avoiding the in-reversible damages in the future.

Study on understanding the global and regional N budgets. During the last decade, several global-scale studies have been conducted to understand the distribution and intensity of Sulfur (S) and N deposition with measurements and model simulations, such as the ACCENT IPCC-AR4 experiment (PhotoComp) (Dentener et al., 2006), the Task Force Hemispheric Transport of Air Pollution (HTAP) (Vet et al., 2014), the Atmospheric Chemistry and Climate Model Intercomparison Project (ACCMIP) (Kanakidou et al., 2016; Lamarque et al., 2013). However, most studies are conducted for the early 2000s, while large changes in the emissions have been taken place since then (van der A et al., 2008), with increases in China (Kurokawa et al., 2013; M. Li, Zhang, et al., 2017; Richter, Burrows, Nuss, Granier, & Niemeier, 2005; van der A et al., 2006; Q. Zhang et al., 2009; Q. Zhang et al., 2007) and general decreases in both Europe (EU) (Tørseth et al., 2012) and Eastern U.S. (S. W. Kim et al., 2006). Follow-up study is required to understand the change of S and N depositions with the emission change and depict the S and N depositions in 2010s. **Chapter 2** estimates the distributions of S and N depositions in early 2010s at global scale, as an update to the previous studies in the early 2000s. The mapping of deposition is developed base on multi-model ensemble results of an international corporative project. The model accuracies on simulation amount of deposition are evaluated with site measurement data. The results are compared with previous multi-model studies to investigate the improvement of model abilities on predicting the spatial distributions of deposition in recent years. The developed deposition field in 2010 is compared with the deposition in 2001 to check the changes in the amount and distribution in the last decade and link the changes with the changes in emission.

Study on the main drivers of future N deposition. Anthropogenic emission and climate change are suggested as the major factors that affect the N deposition (Dentener et al., 2006; Lamarque et al., 2013). Recent studies (Tagaris et al., 2008; J. X. Zhang et al., 2019) declared a dominant importance of the former one on the change of deposition. Human activities and population growth have increased the natural burden of N in the environment, which is in the form of oxidized N deposition (NO_y sum of all oxidized nitrogen species, except nitrous oxide (NO_2)) and reduced forms of N deposition (NH_x, ammonia (NH_3) plus ammonium (NH_4^+)), produced as byproducts of fossil fuel combustion and emissions from croplands and livestock feeding operations. Implementation of emission control strategies and associated policies is an effective avenue to

reduce acid deposition (Tagaris et al., 2008; J. X. Zhang et al., 2019). Control of nitrogen oxides (NO_x) emissions from combustion sources, has led to reduced deposition of NO_y. NH_x deposition, on the other hand, has increased due to lacking control strategies and offset the benefits from NO_y deposition reduction (Y. Li et al., 2016). As deposition of NH_x (the sum of NH_3 and NH_4^+) gains in importance, stringent control of NH_3 emissions is being considered. But few studies have examined the benefit of reducing NH_3 emission on NH_x deposition. Whereas studies have investigated the effectiveness of NH_3 emission abatement on reducing fine particle levels (Robert W. Pinder, Adams, & Pandis, 2007). However, the actual efficiency of this strategy has been lower than expectation (H. Y. Guo et al., 2018; Holt, Selin, & Solomon, 2015; R. W. Pinder, Gilliland, & Dennis, 2008), due to that conversion between NH_3 gas and NH_4^+ particulate matter is highly dependent on acid components in aerosols such as SO_4^{2-} and NO_3^-, since NH_4^+ is the main alkali neutralizer to balance aerosol pH value. The same situation is likely to arise associated with the control of NH_x deposition. **Chapter 3** estimates the effectiveness of controlling NH_3 emissions as a means to reduce NH_x deposition, with a comparison with the benefit of NO_x emission abatement on reducing NO_y deposition. We first review the consistency between the trends (2000-2014) of NH_3 emissions and NH_x deposition over the conterminous US (CONUS) based on measurement data. Then we quantify the effectiveness of controlling NH_3 emissions on NH_x deposition via modelling analysis of emission control scenarios.

The impacts of climate change are reflected on multiple aspects. This study focuses on the influences related to meteorological factors such as precipitation and long-range transport. Hemispheric transport of air pollutants plays an important role in the re-distribution of air pollutants. A series of studies have been conducted on the hemispheric transport of air pollutants (Fiore et al., 2009; Fu, Dong, Gao, Wong, & Lam, 2012; Sudo & Akimoto, 2007; Wild & Akimoto, 2001). Recent studies have reported increased concentrations of air pollutants in the hemispheric transport from Asia to NA from the mid-1980s to late-2000s (Jaffe, Price, Parrish, Goldstein, & Harris, 2003; Parrish et al., 2004; Parrish, Millet, & Goldstein, 2009; L. Zhang et al., 2008), due to the rapid growth of Asian emissions (Lu et al., 2010; Richter et al., 2005; van der A et al., 2008; van der A et al., 2006; Q. Zhang et al., 2007). However, the impact of hemispheric transport on deposition has been given little attention in the past, with limited number of global-scale studies for the 1990s and early 2000s (Arndt & Carmichael, 1995; Sanderson et al., 2008; L. Zhang et al., 2012). Furthermore, most studies focused on the emission intensive regions such as U.S. and

China. However, studies on the low emission intensity regions have not been evaluated in the same detail. A systematical study is required to evaluate the contribution of hemispheric transport on local deposition, especially for the coastal regions and low emission intensity regions. **Chapter 4** investigates the hemispheric transport of air pollutants and its impact on regional depositions for six world regions: North America, Europe, Middle East, Russia, East Asia and South Asia. A source-receptor relationship is developed among the six regions to quantify the exchange of air pollutants between continents and the impacts on local deposition. We also compare the contributions of hemispheric transport and own region emissions on local deposition

Study on the impacts of excessive deposition on ecosystems. Adverse influences occur on the ecosystems when they have received excessive amounts of deposition. The term Critical Loads (CLs) is used to represent this up-bound limit, which is defined as the highest load that will not cause chemical changes leading to long-term harmful effects on most sensitive ecological systems (Nilsson, 1988). The CLs has been widely used to quantify the exceedance of deposition in both global-wide and regional studies (A. F. Bouwman et al., 2002; Duan, Xie, Zhou, Ye, & Hao, 2001; Ellis et al., 2013; Posch, Duan, Reinds, & Zhao, 2015; Rodriguez-Lado & Macias, 2006). However, most of CLs were developed on country-scale or regional-scale and there is no global scale CLs, probably due to the requirement for site-specific variables and expertise knowledge. **Chapter 5** collects the available CLs over U.S., EU and China from publications and reports and compares the data inputs and processes used to calculate the CLs by different studies. Then we use these datasets to assess the exceedance of CLs with the S and N depositions created in Chapter 2. The exceedance of CLs in 2001 and 2010 over U.S. and EU are compared to investigate the changes in the last decade.

Study on Phosphorus (P) deposition. The bioavailability of N and P nutrients determines the productivity of the ecosystems. Human activities have been altering the N and P cycles and even changing the nutrient limitation patterns of many ecosystems. And the atmospheric deposition was found with significate contributions on these changes (Camarero & Catalan, 2012; Elser et al., 2009). Compared to the long-term measurement and modelling studies on N species and N

depositions, much less attention has been given to the P budgets, owing to the fact that P neither the regular detected specie in current observation networks nor a variable in the CTMs and most earth system models (ESMs) projects (Y. Sun et al., 2017), which makes the mapping of P deposition more difficult than N deposition. **Chapter 6** reviews the previous studies on P budget via both measurement and modelling approaches. We collect the measurement dataset on P deposition and compile them into a database for further studies on the characteristics of P and for the model evaluation. We compare the different methodologies to form the emission inventory of P and collect the issues found in the numerical modelling studies of P. Based on the information, we summarize our understanding on the global P budget and discuss the problems to be solved in future studies.

CHAPTER 2
MULTI-MODEL STUDY OF HTAP II ON SULPHUR AND NITROGEN DEPOSITION

A version of this chapter was originally published by (J. N. Tan, Fu, Dentener, Sun, Emmons, Tilmes, Sudo, et al., 2018):

Tan, J. N., Fu, J. S., Dentener, F., Sun, J., Emmons, L., Tilmes, S., . . . Keating, T. (2018). Multi-model study of HTAP II on sulfur and nitrogen deposition. *Atmospheric Chemistry and Physics*, *18*(9), 6847-6866.

Statement: J.T. and J.-S.F. designed the study. J.T. prepared the multi-model ensemble results and analyzed the data with help from J.-S.F., F.D. and J.S. F.D. suggested data analysis. F.D. and T.K. coordinated HTAP II. L.E. and S.T. provided CAM-Chem model results. J.F. provided C-IFS_v2 model results. T.T. provided SPRINTARS model results. H.B. provided GEOS5 model results. J.T. wrote the manuscript and J.-S.F. and F.D. edited it with contributions from all co-authors. Section 2.4.4 was added after publication of the paper. This section discussed the unsolved questions we found and the comments we received when presenting the results of this chapter in conferences and workshops.

2.1 Abstract

This study uses multi-model ensemble results of eleven models from the 2nd phase of Task Force Hemispheric Transport of Air Pollution (HTAP II) to calculate the global sulfur (S) and nitrogen (N) deposition in 2010. Modelled wet deposition is evaluated with observation networks in North America, Europe and Asia. The modelled results agree well with observations, with 76-83% of stations having predicted within ±50% of observations. The results underestimate SO_4^{2-}, NO_3^- and NH_4^+ wet depositions in some European and East Asian stations, but overestimate NO_3^- wet deposition in Eastern US. Inter-comparison with previous projects (PhotoComp, ACCMIP and HTAP I) shows HTPA II has considerably improved the estimation of deposition at European and East Asian stations. Modelled dry deposition is generally higher than the "inferential" data calculated by observed concentration and modelled velocity in North America, but the inferential data has high uncertainty, too. The global S deposition is 84 Tg(S) in 2010, with 49% of the deposits on continental regions and 51% on ocean (19% on coastal). The global N deposition consists of 59 Tg(N) oxidized nitrogen (NO_y) deposition and 54 Tg(N) reduced nitrogen (NH_x)

deposition in 2010. About 65% of N is deposited on the continental regions and 35% is on ocean (15% on coastal). The estimated outflow of pollution from land to ocean is about 4 Tg(S) for S deposition and 18 Tg(N) for N deposition. Compared our results to the results in 2001 from HTAP I, we find that the global distributions of S and N depositions have changed considerably during the last 10 years. The global S deposition decreases 2 Tg(S) (3%) from 2001 to 2010, with significant decreases in Europe (5 Tg(S) and 55%), North America (3 Tg(S) and 29%) and Russia (2 Tg(S) and 26%), and increases in South Asia (2 Tg(S) and 42%) and the Middle East (1 Tg(S) and 44%). The global N deposition increases by 7 Tg(N) (6%), mainly contributed by South Asia (5 Tg(N) and 39%), East Asia (4 Tg(N) and 21%) and Southeast Asia (2 Tg(N) and 21%). The NH_x deposition is increased with no control policy on NH_3 emission in North America. On the other hand, NO_y deposition starts to dominate in East Asia (especially China) due to boosted NO_x emission.

2.2 Introduction

Global-scale studies have been conducted to understand atmospheric depositions via modelling approach. Following are the main findings of previous efforts on mapping the global depositions. The multi-model ensemble results of PhotoComp project were used to investigate the distributions of S and N depositions in 2000 and 2030 (Dentener et al., 2006). Model evaluation with site measurements showed that 60-70% of modelled wet depositions were within ±50% of measurements at sites over EU and North America (NA). NH_x depositions were overestimated in South Asian sites and NO_y depositions were underestimated in East Asian sites.

The model ensemble results of the first phase of HTAP (HTAP I) (http://www.htap.org/) were used to estimate the S and N depositions in 2000. A comprehensive evaluation was conducted on the model performance with site observations (Vet et al., 2014). The ensemble results underestimated the wet deposition at observation sites where the observed depositions are high over NA, Southern and Northern EU and EA. Dry deposition in the Unites States was found to deviate with “observation” data (inferential data as a combination of observation and modelling data, see sect. 2.3.4 for details). Another study used the HTAP I multi-model results to study the

long-range transport of oxidized N among several regions including EU, NA, SA and EA (Sanderson et al., 2008). Results showed that 8-15% of NO_x from source regions could be transported and deposited beyond the distance of 1000 km, which indicated the inter-continental transport of air pollutants and possible impacts on local deposition.

The multi-model ensemble of the ACCMIP was used to estimate the atmospheric deposition in 2000 (Lamarque et al., 2013). The model performance of ACCMIP models is compared with that of PhotoComp and HTAP. Model performance on NO_3^- wet deposition was comparable with that of PhotoComp and HTAP I, but the accuracy on NH_4^+ wet deposition was worse than the previous two, due to mapping errors in NH_3 emission over China. Simulations with projected emissions in 2100 under four Representative Concentration Pathways (RCP) indicated that N deposition is likely to substantially increase in Latin America, Africa and parts of Asia (especially SA) in the future. Another study analyzed the ACCMIP simulation results under historical, RCP 6.0 and RCP 8.5 emission scenarios to estimate the changes in N deposition driven by human activity in the past (1850), present (2005) and future (2050) (Kanakidou et al., 2016). The results found significant importance of organic N (ON) from primary emission and secondary organic aerosol (SOA), which accounted for 20-30% of total N deposition. The impact of human activity on N deposition has increased from 15% in the past to 60% in present years (2000). And this impact was likely to persist in the future.

This study uses the multi-model ensemble results from the second phase of HTAP (HTAP II) to develop the deposition map in 2010. Two companion studies are conducted to update our understanding of atmospheric deposition in this decade. The third phase of Air Quality Model Evaluation International Initiative (AQMEII) is multi-model cooperative study over Europe. A study developed the S and N depositions over Europe with ensemble results of fourteen models and assessed the exceedance of CL in six habitats with model ensemble (Vivanco et al., 2018). Another project is the third phase of Aerosol Comparisons between Observations and Models (AeroCom III) (*https://wiki.met.no/aerocom/phase3-experiments*). A study used the results of nine models to study the possible factors causing the inter-model diversity in simulating NO_3^- and NH_4^+ depositions (Bian et al., 2017). Large differences were found in the calculation of the pH adjustment for the effective Henry's law constant by different models, which could largely influence the simulation of wet NH_x deposition.

The previous studies on the distribution and amount of deposition give a clear view to S and N depositions in the early 2000s. However, updates in more recent years are required due to large changes in the global N emissions in the last decade (van der A et al., 2008), including a large increase in China (Kurokawa et al., 2013; M. Li, Zhang, et al., 2017; Richter et al., 2005; van der A et al., 2006; Q. Zhang et al., 2009; Q. Zhang et al., 2007), and general decreases in both EU (Tørseth et al., 2012) and Eastern U.S. (S. W. Kim et al., 2006). The NO_x emissions have increased by about 10 Tg(N) from 2001 to 2010, due to the large increase in the Asia regions (J. N. Tan, Fu, Dentener, Sun, Emmons, Tilmes, Sudo, et al., 2018), while recent studies have reported year 2011 as the turning point for NO_x emissions from China (M. Li, Liu, et al., 2017; F. Liu et al., 2016). On the other hand, the global S emissions have declined by about 5 Tg(S) from 2000 to 2010 (J. N. Tan, Fu, Dentener, Sun, Emmons, Tilmes, Sudo, et al., 2018). The global amounts of SO_2 emissions from fossil fuel have been decreased since 1980, owing to the significant decline of emissions from EU and U.S. (Chin et al., 2014). The SO_2 emission in China has experienced increases before 2005 due to energy consumption and decreases after 2006 thanks to the implementation of the eleventh Five-Year-Plan (FYP). In addition, ground observations and satellite measurements show large increases in the dry deposition in the western US, Eastern EU and East China, together with decreases in Eastern US, Western EU and Japan (Jia et al., 2016).

This chapter estimates the S and N depositions at global scale in 2010, as a fundamental study for further researches and as a follow-up study for the previous studies. The multi-model ensemble depositions of eleven models of HTAP II were used to map the distribution of S and N depositions in 2010. The main targets of this study include the following aspects:

a. Understand the model accuracy on simulating wet and dry depositions of S and N. This study evaluates both modelled wet and dry depositions of S and N with available site measurements. The model performance is also compared with previous studies PhotoComp (Dentener et al., 2006), HTAP I (Vet et al., 2014), and ACCMIP (Lamarque et al., 2013) to find the improvements on modelling deposition.
b. Map the distributions of S and N depositions over continental, coastal and ocean regions. The characteristics of deposition are also investigated, including the balance between wet and dry depositions and between NO_y and NH_x depositions.

c. Compare the depositions in 2010 (this study) with that in 2001 to investigate the changes of deposition in the past ten years. The 2001 results are derived from multi-model ensemble results of first phase of HTAP (HTAP I). The comparison aims at performing a review to the changes of S and N depositions in the last decade.

2.3 Methods

2.3.1 Model description and experiment setup

The HTAP was developed in 2005 under the direction of Unite Nation Economic Commission for Europe. It is an international cooperation aiming at understanding the long-range transport of air pollutants and their potential impacts on regional air quality and deposition issues. HTAP I involved more than twenty global models with base simulation year of 2001. A comprehensive assessment has been published to summarize the findings in HTAP I with respect to the long-range transport of (1) ozone and particulate matter (2) mercury and (3) persistent organic pollutants. The report is available to the public at *http://www.htap.org/*.

The HTAP II was initialed in 2012 with the participation of twenty global models (Galmarini et al., 2017). The simulations were conducted on the base year of 2010 with different emission control scenarios (Galmarini et al., 2017). The accuracies of models on simulating the concentrations of O_3 (Huang et al., 2017; C. K. Liang et al., 2018), particles (Dong et al., 2018; C. K. Liang et al., 2018) and depositions (J. N. Tan, Fu, Dentener, Sun, Emmons, Tilmes, Sudo, et al., 2018) have been evaluated with observations. This dataset has been widely used to studies environmental issues related to air quality and deposition. The multi-model ensemble model results were used to estimate the impact of domestic and foreign emission changes of black carbon, organic carbon and sulfate on regional radiative forcing (Stjern et al., 2016) and the contribution of world-wide emission on O_3 burden over EU (Jonson et al., 2018). The ensemble results were also used as boundary conditions for regional scale studies, including the contribution of East Asian outflow to O_3 pollution over NA (Huang et al., 2017) and the impacts of boundary condition on simulating O_3 burden (Hogrefe et al., 2018).

Eleven of the twenty models from HTAP II (i.e. CAM-Chem, CHASER_re1, CHASER_t106, EMEP_rv48, GEMMACH, GEOS5, GEOSCHEMAJOINT, OsloCTM3v.2, GOCARTv5, SPRINTARS and C-IFS_v2) submitted the model outputs of S and N depositions. The configurations of models are listed in Table 2.1 (adopt from (Stjern et al., 2016)). The ensemble results, which have been reported to perform better than single model results, are used so that we can get more accurate estimation of depositions. The model evaluation of this study also proved that ensemble results are closer to the observations than single model results. This study uses multi-model mean (MMM) to present the ensemble results. To develop the MMM, all models are interpolated to a uniform $0.1^{o} \times 0.1°$ horizontal resolution (the same resolution as the emission inventory) by linear interpolation. Then the MMM quantities of S and N depositions are calculated by averaging (arithmetic mean) all available model outputs. More details are demonstrated in sect. 2.3.3 of this document. The simulations are conducted on whole year of 2010, with additional six-month run as model spin-up.

2.3.2 Data quality check and method for calculating MMM

Before constructing the MMM, the qualities of model outputs are checked with two criteria. The first criterion is to check mass balance of each model by comparing its global deposition with its emission. Models are excluded if their deposition values fall outside the range of ±20% of their emission values. The second criterion is to check if the result of a model is away from the mean value of all models. The upper and lower limits are adopted as median of models $\pm 1.5 \times$ interquartile by (Vet et al., 2014). The values are checked separately for all species of deposition and emission. The models used to develop the MMM and their values are summarized in Tables 2.2-2.4.

2.3.3 Method for calculating MMM

To make the discussion clear, we define the terms as follows: The continental regions refer to all land regions including the Antarctic. The coastal regions are defined in Fig. 2.1. The S deposition contains gas phase SO_2 deposition and aerosol SO_4^{2-} deposition. The N deposition includes NO_y

Table 2. 1 Model used for this study with relevant information (adopt from (Stjern et al., 2016))

Model	Version	Horizontal resolution	Vertical layers	Meteorology input source
SPRINTARS	Atmosphere, MIROC5.2	1.1° × 1.1°	56	ECMWF Interim
OsoloCTM3_v2	v02, all aerosol modules from OsloCTM2	2.8° × 2.8°	60	ECMWF's Integrated Forecast System (IFS) model
GOCART	v5 2010	1.3° × 1.0°	72	MERRA
C-IFS	IFS CY40r2	0.7° × 0.7°	54	Relaxed to ERA-Interim
CHASER_re1	v4.0, MIROCESM version	2.8° × 2.8°	32	ERA-Interim (u, v, T) and HadLSST
CHASER_t106	V4.0, MIROCESM version	1.1° × 1.1°	32	ERA-Interim (u, v, T) and HadLSST
CAM-Chem	CESM1-CAM4-chemSD	1.9° × 2.5°	56	GEOS5 v5.2 meteorology
GEOS5	v5	1.3° × 1.0°	72	MERRA
GEOSCHEMADJOINT	v35f	2.0° × 2.5°	47	GEOS-5 (MERRA)
EMEPrv48	Rv4.8	0.5° × 0.5°	20	ECMWF's Integrated Forecast System (IFS) model
GEMMACH	v2	0.9° × 0.9°	79	-

Table 2. 2 Summary of global total deposition and emission of S in 2010 from individual models (Tg(S) yr^{-1})

Models/Species	Deposition			Emission			
	Dry	Wet	Total	Surface SO_2	Surface SO_4^{2-}	DMS	Total
CAM-Chem	18	-	-	55	-	28	83
CHASER_re1	25	54	79	55	-	25	80
CHASER_t106	23	53	77	55	-	23	78
EMEP_rv48	16	42	58	-	-	-	-
GEMMACH	-	-	-	66	-	-	-
GEOS5	34	43	77	53	2	31	85
GEOSCHEMADJOINT	32	52	85	62	1	-	-
OsloCTM3.v2	40	63	103	77	2	-	-
GOCARTv5	29	47	76	66	2	-	-
SPRINTARS	26	-	-	60	1	22	84
C-IFS_v2	-	-	-	77	-		77
Multimodel mean	28	56	84	62	1	27	91

Note: S deposition is the sum of SO_2, SO_4^{2-}, Methanesulfonic acid (MSA) and Dimethyl sulfide (DMS) deposition. S emission is the sum of SO_2, SO_4^{2-} (sulfate dry aerosol particles due to emission) and Dimethyl sulfide (DMS) emission.

Table 2. 3 Same as table 2.2, but for NO_x emission (Tg(N) yr^{-1})

Model/Species	Deposition			Emission		
	Dry	Wet	Total	NO_x	Lightening NO_x	Total
CAM-Chem	16	-	-	-	4	-
CHASER_re1	23	28	51	57	4	60
CHASER_t106	25	27	52	58	5	63
EMEP_rv48	15	45	59	-	-	-
GEMMACH	-	-	-	44	-	44
GEOSCHEMADJOINT	26	28	54	54	-	54
OsloCTM3.v2	25	-	-	51	-	51
Multimodel mean	22	38	59	57	4	60

Note: NO_y deposition is the sum of all simulated oxidized N species (expressed as N) including NO, NO_2, HNO_3, HNO_4, NO_3aerosol, NO_3(radical), N_2O_5, Peroxyacyl nitrates (PAN), other organic nitrates other than PAN, but not N_2O (Orgn) deposition. NO_x emission is sum of anthropogenic NO_X emission, aircraft NO emission, soil NO emission and lightening NOx emission.

Table 2. 4 Same as table 2.2, but for NH_x emission (Tg(N) yr^{-1})

Model/Species	Dry deposition		Wet deposition		Total Deposition	NH_3 Emission
	NH_3	NH_4^+	NH_3	NH_4^+		
CAM-Chem	12	8	-	-	-	54
EMEP_rv48	11	3	13	-	-	-
GEOSCHEMADJOINT	14	4	13	24	55	55
OsloCTM3.v2	19	4	-	21	-	54
Multimodel mean	14	5	13	22	54	54

Note: NH_X deposition is the sum of NH_3 and NH_4^+ deposition.

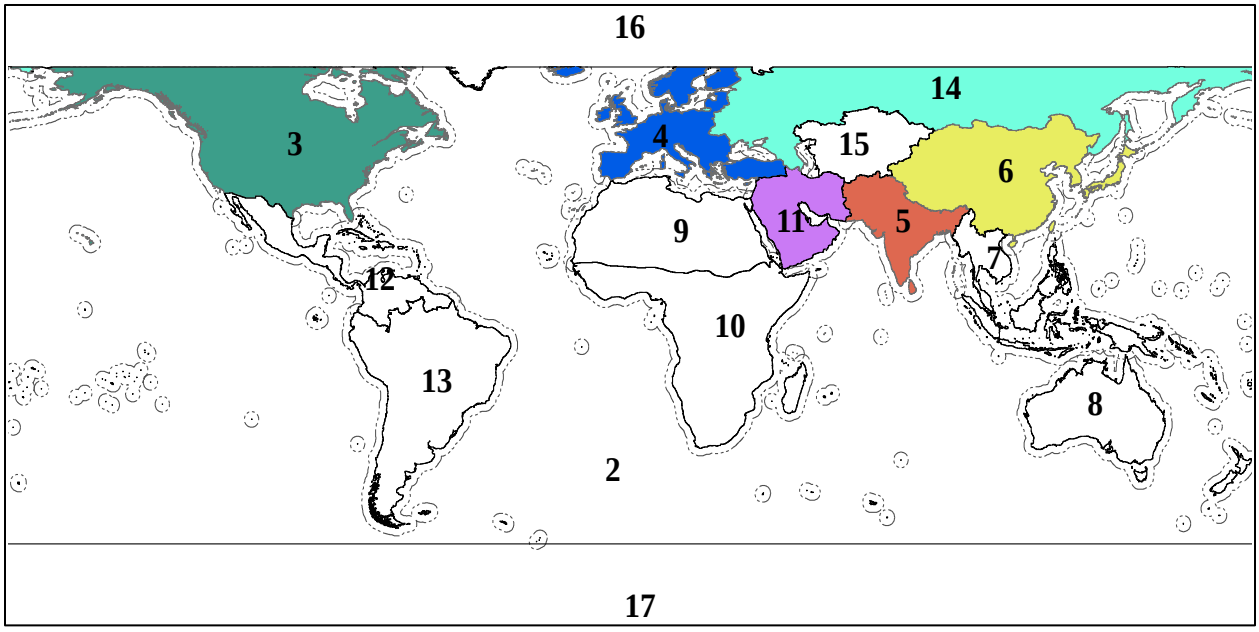

Figure 2. 1 Boundaries of regions and coastal areas (dashed). Six regions with perturbation experiments: 3-North America (NA), 4-Europe (EU), 5-South Asia (SA), 6-East Asia (EA), 11-Middle East (ME) and 14-Russia, Belarussia, Ukraine (RU). Others: 1-Global, 2-Ocean (including Arctic), 7-Southeast Asia, 8-Australia, 9-North Africa, 10- Sub Saharan Africa, 12- Mexico, Central America, Caribbean, Guyanas, Venezuela, Columbia (Central America), 13-South America, 15-Central Asia, 16-Arctic and 17-Antarctic. The continental regions refer to all land regions including the Antarctic.

deposition and NH_x deposition. NO_y deposition is composed of all oxidized nitrogen species except N_2O. Based on the model outputs, NO_y deposition mainly includes NO_2, HNO_3, aerosol NO_3^-, peroxyacyl nitrate (PAN) and other organic nitrates than PAN (Orgn). NH_x deposition consists of gas phase NH_3 deposition and aerosol NH_4^+ deposition.

Following are the methods to form the MMM results. We calculate the mean value of each species using Eq. *(2-1)* with all available model outputs. Then, we combine all related species into total deposition or emission by Eq. *(2-2)*.

$$S_{MMM}(j) = \frac{1}{n}\sum_{i=1}^{n} S_i(j) \qquad (2\text{-}1)$$

$$S_{MMM}(NO_y, NH_x \text{ or } S) = \sum_{j=1}^{s} S_{MMM}(j) \qquad (2\text{-}2)$$

where, *i* is the individual model and *j* is the species of deposition/emission from model outputs. $S_i(j)$ is the species *j* from model *i* and $S_{MMM}(j)$ is the MMM of species *j*.

2.3.4 Observation datasets and evaluation metrics

The model results of SO_4^{2-}, NO_3^- and NH_4^+ wet depositions are evaluated with site observations in US, EU and EA. The MMM result is annual deposition in 2010 and the observation data is three-year annual average deposition during 2009-2011. The observation data in U.S. comes from the National Atmospheric Deposition Program (NADP) (*http://nadp.sws.uiuc.edu/*). The quality and completeness of the observations are checked according to the four criteria established by the NADP technical committee (*http://nadp.sws.uiuc.edu/documentation/notes-depo.html*). Data from 136 stations of the 267 available stations are used for evaluation. The observations in EU are derived from the European Monitoring and Evaluation Programme (EMEP) CCC reports (*http://www.nilu.no/projects/ccc/reports.html*). After checking the data quality and completeness, data from 82 stations of the 102 available stations are used. The observations in Asia are from the Acid Deposition Monitoring Network in East Asia (EANET) (*http://www.eanet.asia/*). Data from 43 stations of the 52 available stations are used for evaluation.

In terms of dry deposition, the number of dry deposition measurements is limited due to difficulty in measuring the dry deposition directly by instruments. This study evaluates the dry deposition in CONUS with the Clean Air Status and Trends Network (CASTNET). Instead of

direct measurements, these data are processed by an "inferential" method, using calculations of the measured concentration of species and modelled dry deposition velocities. Same as the wet deposition measurements, the three-year average data of 2009-2011 from CASTNET are used for evaluation with the same selection criteria adopted for the wet deposition. Data from 81 stations out of 85 available stations is used for comparison.

The model performance of this study is compared with previous projects. In order to make the comparison consistent, we adopt the following metrics used in literature (Lamarque et al., 2013): Linear fit slope (Slope), mean bias (MB), mean of observation, mean of model, correlation coefficient between model and observation (R) and fraction of model results within ± 50% of observations (F50%). In addition, we use four statistical metrics following Eqs. *(2-3)* - *(2-6)*.

$$\text{NMB (normalized mean bias)} = \frac{\sum_{i=1}^{n}(M_i - O_i)}{\sum_{i=1}^{n} O_i} \times 100 \qquad (2\text{-}3)$$

$$\text{NME (normalized mean error)} = \frac{\sum_{i=1}^{n}|M_i - O_i|}{\sum_{i=1}^{n} O_i} \times 100 \qquad (2\text{-}4)$$

$$\text{MFB (mean fractional bias)} = \frac{1}{n}\sum_{i=1}^{n}\frac{M_i - O_i}{(M_i + O_i)/2} \times 100 \qquad (2\text{-}5)$$

$$\text{MFE (mean fractional gross error)} = \frac{1}{n}\sum_{i=1}^{n}\frac{|M_i - O_i|}{(M_i + O_i)/2} \times 100 \qquad (2\text{-}6)$$

where M_i is the model result, O_i is the observation and n is the sample size. NMB, NME, MFB and MFE normalize the model mean bias to avoid data inflation in case of large data range. NMB and NME normalize the mean bias by the observation data and thus may tend toward model overestimation. MFB and MFE normalize the mean bias by the average of observations and model results, considering both model overestimation and underestimation, and thus are less biased. Therefore, MFB and MFE are used as the main metrics to evaluate the model performance.

2.4 Results and discussion

2.4.1 Evaluation of model performance

Wet deposition. In this section, the wet deposition of SO_4^{2-}, NO_3^- and NH_4^+ from MMM are compared with observations at the NADP, EMEP and EANET stations. The SO_4^{2-} wet deposition

comprises gas phase SO_2 and aerosol SO_4^{2-} wet deposition. The NO_3^- wet deposition includes gas phase HNO_3 and aerosol NO_3^- wet deposition. The NH_4^+ wet deposition contains gas phase NH_3 and aerosol NH_4^+ wet deposition.

Figure 2.2 shows the scatter plots of the MMM results with observation. Performances of individual models can be found in Fig. S2.1-S2.3 in the Appendix. Figure 2.3 displays the spatial distributions of MMM SO_4^{2-}, NO_3^- and NH_4^+ wet deposition (contours) with observations (filled circles). In terms of SO_4^{2-} wet deposition, the MMM results are consistent with observations at the NADP stations with a close to 1 slope (0.9) and a high R value (0.8) (Fig. 2.2(a)). The MFB and MFE are 9% and 32%, indicating slight overestimation. According to Fig. 2.3(a), the observed SO_4^{2-} wet deposition is highest in north-eastern US, and this spatial distribution is well captured by MMM. The EMEP stations are well simulated with low MFB (-7%) and MFE (25%) (Fig. 2.2(b)). The MMM predictions are within ±50% of observations at 87% of the stations. According to Fig. 2.3(b), one station in Poland and one station in Norway, with observed SO_4^{2-} wet deposition of 1000 and 500 mg (S) m^{-2} yr^{-1} respectively, are both underestimated by 50%.

The model performances on simulating precipitation are shown in Fig. 2.4 and Fig. 2.5. The individual model performances can be found in Fig. S2.4 in the Appendix. For the Norway site, the observed precipitation is 1566 mm yr^{-1} and the mmm underestimated the precipitation by 49%, which fits well for the 50% underestimation of SO_4^{2-} wet deposition at this site. For the Polish site, the observed precipitation is 1137 mm yr^{-1} and the mmm underestimated the precipitation by 21%. The underestimation in precipitation could partly explain the negative model bias in simulating SO_4^{2-} wet deposition. Another possible reason is the high topography of the sites. The Polish site is 1603 meters above sea, which is one of the highest sites among the European sites. Similar to the Polish site, one site in Spain, which is 1360 meters height, is underestimated by 142 mg (S) m^{-2} yr^{-1} (59%) for SO_4^{2-} wet deposition, while its precipitation is well simulated with a slight positive model bias of 5%.

At the EANET stations, very high SO_4^{2-} concentrations were measured at some stations, probably correlated with dust emission (Dentener et al., 2006). Therefore, we ignore the measurements coincident with measured calcium (Ca^{2+}) deposition larger than 20 mole m^{-2} yr^{-1}. The evaluation (Fig. 2.2(c)) shows that the SO_4^{2-} wet deposition is generally underestimated at the

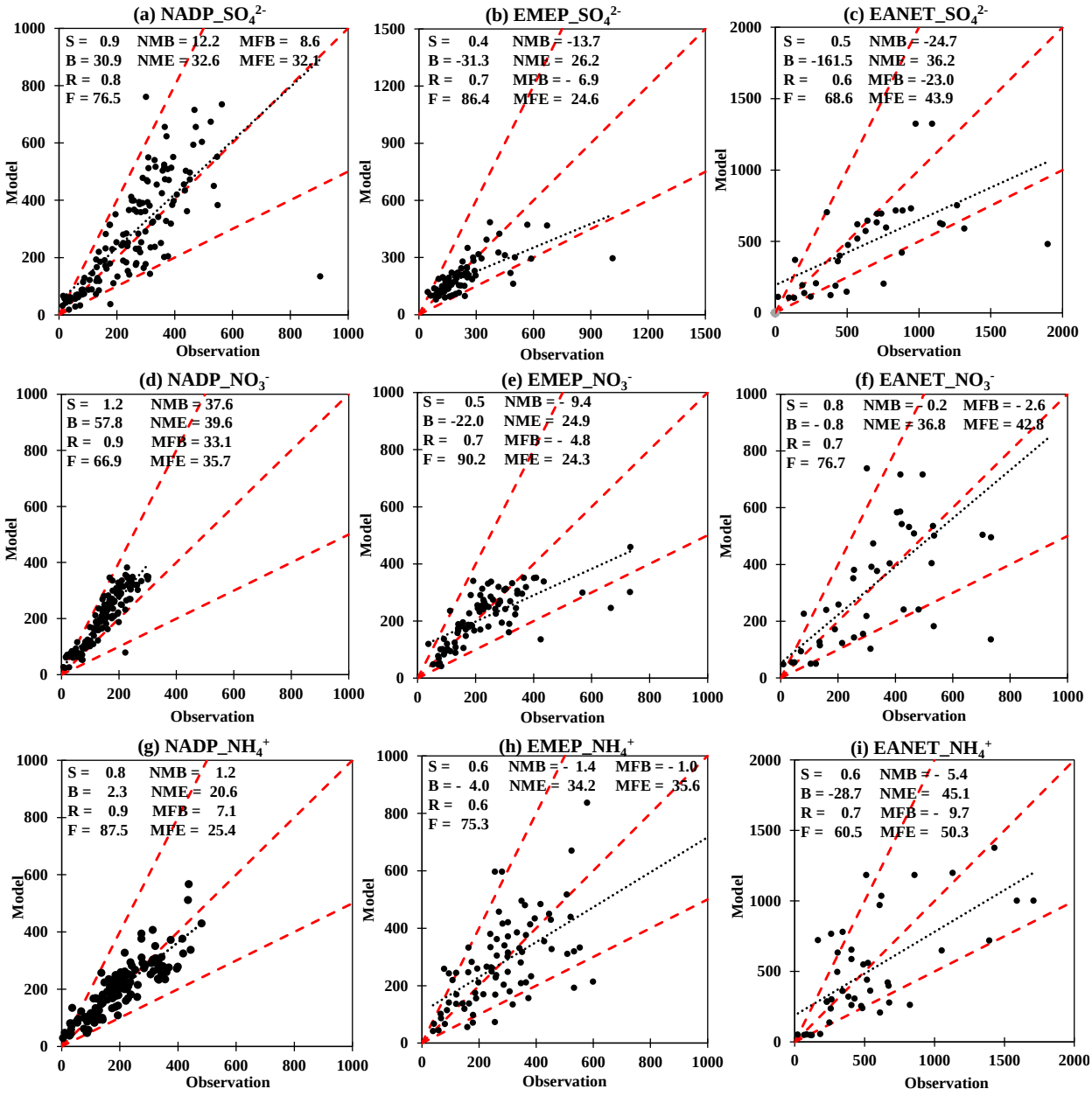

Figure 2. 2 Evaluation of MMM performance of SO_4^{2-}, NO_3^- and NH_4^+ wet deposition (mg (N or S) m^{-2} yr^{-1}) at NADP (left), EMEP (middle) and EANET (right) stations. The MMM is the annual wet deposition in 2010 and the observations are three-year average annual data of 2009-2011.

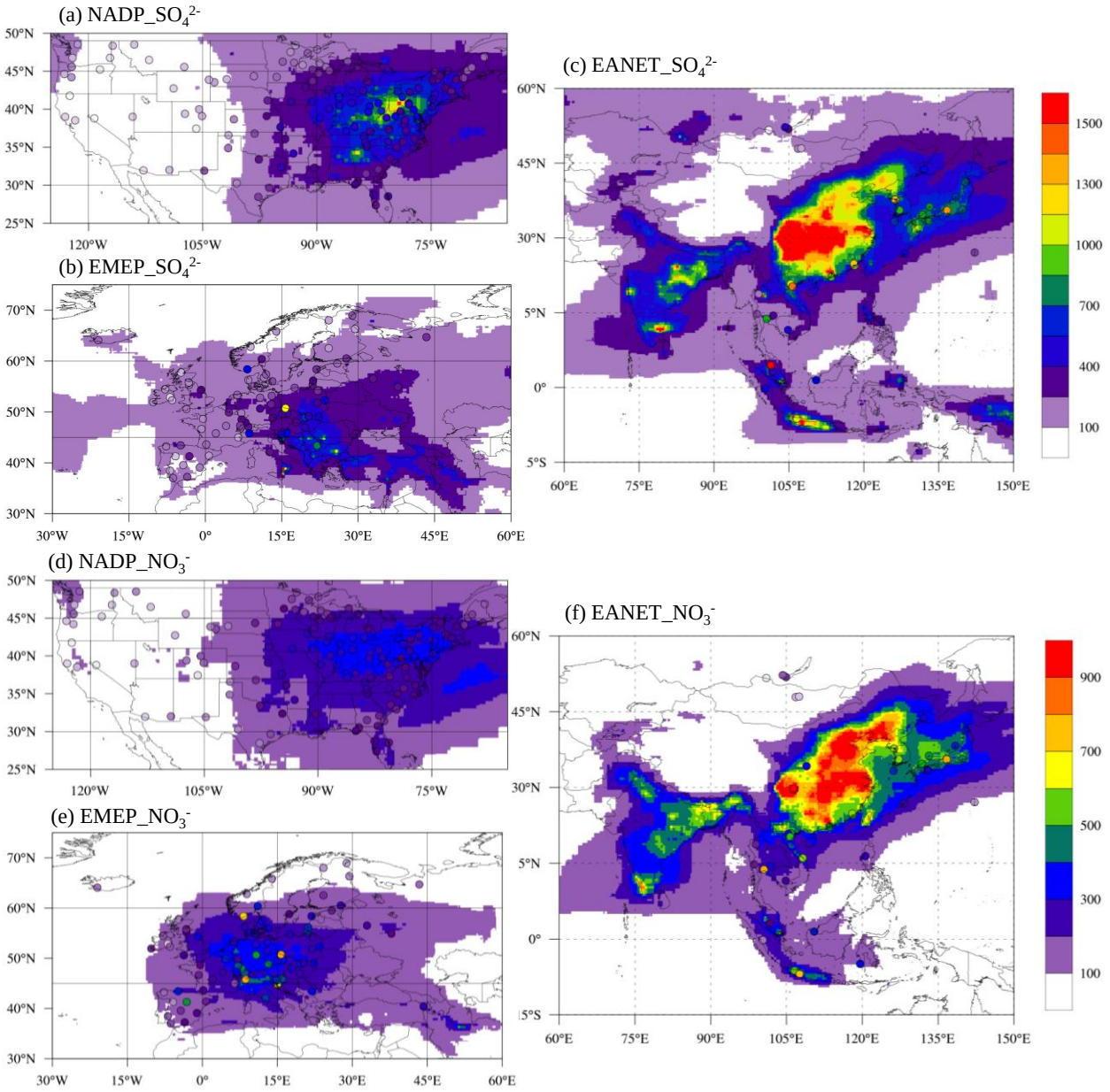

Figure 2. 3 Distribution of SO_4^{2-}, NO_3^- and NH_4^+ wet deposition (mg (N or S) m^{-2} yr^{-1}) of MMM and observation. The MMM is the annual wet deposition in 2010 and the observations are three-year average annual data of 2009-2011.Contours are MMM results and filled circles are observations.

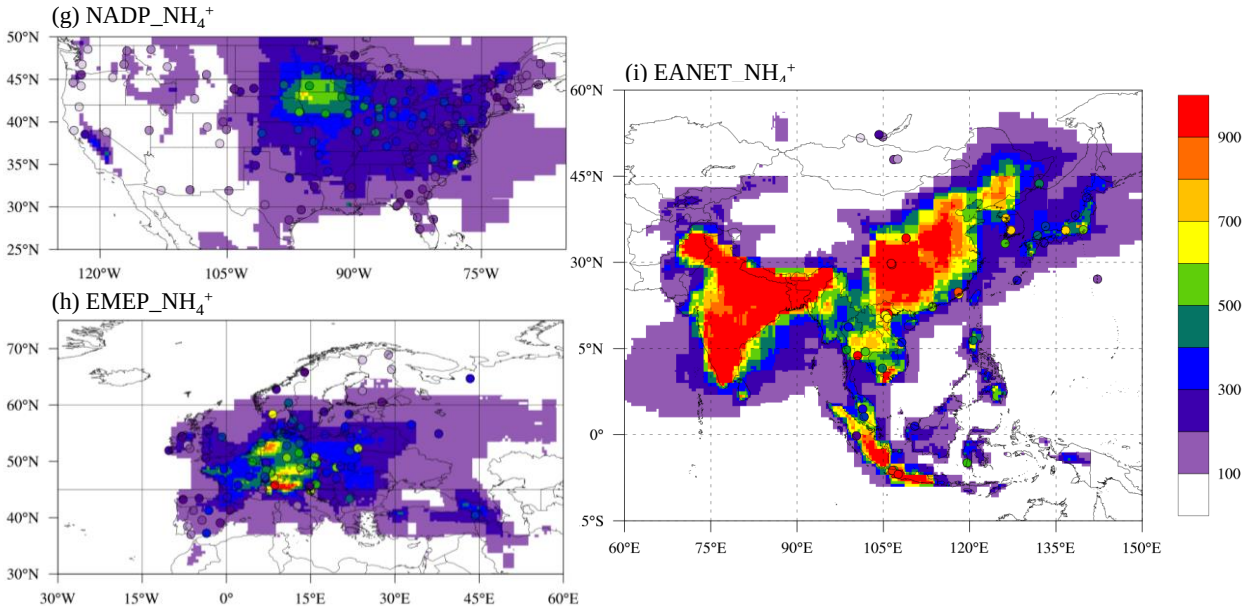

Figure 2. 3 Continued.

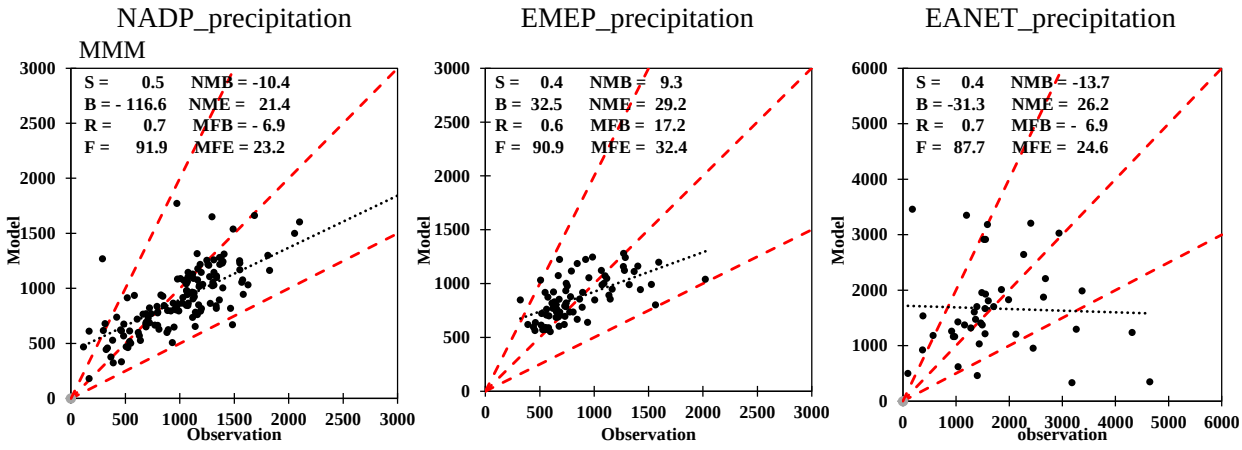

Figure 2. 4 Model performances on precipitation (mm yr^{-1}). The model result is the annual precipitation in 2010 and the observations are three-year average annual data of 2009-2011.

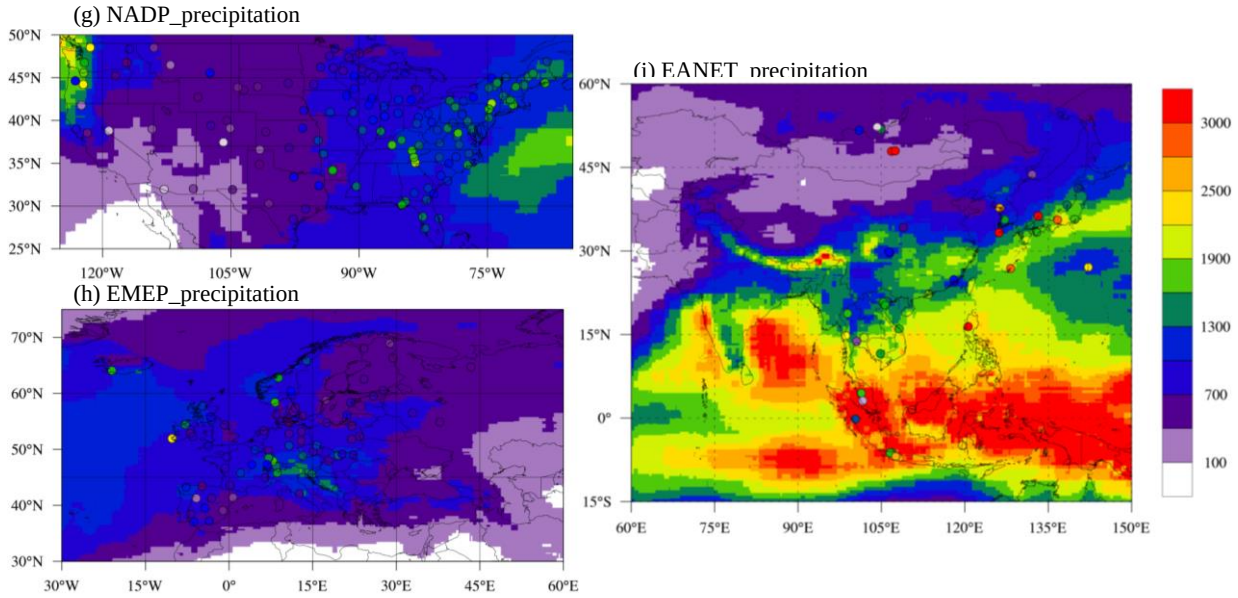

Figure 2. 5 Distribution of precipitation (mm yr^{-1}) of MMM and observation. The MMM is the annual total precipitation in 2010 and the observations are three-year average annual data of 2009-2011.Contours are MMM results and filled circles are observations.

EANET stations by 23% (MFB) and 44% (MFE). The stations in Korea and Vietnam are generally underestimated by more than 200 mg (S) m^{-2} yr^{-1} (Fig. 2.3(c)). On the other hand, the SO_4^{2-} wet deposition is generally well simulated in Indonesia, Philippines, Thailand and Japan. Overall, 76% of the stations of all networks predicted quantities within ±50% of observations. The EANET stations have the highest model bias among the three networks. It should be noted that for the three excluded stations (located in China) with high Ca^{2+} deposition, the SO_4^{2-} wet deposition is largely underestimated by more than 1000 mg (S) m^{-2} yr^{-1} (not shown in figures). If these stations are included in the model evaluation, the mean bias for EA will change from -160 mg (S) m^{-2} yr^{-1} to -300 mg (S) m^{-2} yr^{-1}. The observation stations in China are mainly located along the eastern and southern coast, while the highest modelled deposition is found in the inland areas. Therefore, it is hard to conduct a comprehensive evaluation over this region due to unavailable measured data in the inland areas.

For NO_3^- wet deposition, the MMM results agree well with observations at the NADP stations, as shown by the linear regression line in Fig. 2.2(d) with slope of 1.2 and R value of 0.9. However, the amount of deposition is overestimated by 33% (MFB) and 36% (MFE). According to Fig. 2.3(d), there is a general tendency of overestimation throughout the stations in US, especially the stations located in Midwest and Southeast. At the EMEP stations, the NO_3^- wet deposition is well simulated with low MFB of -5% and MFE of 24% (Fig. 2.2(e)). The modelled deposition is within ±50% of observed deposition at more than 90% of the stations. The MMM results are close to the observations at stations with deposition lower than 400 mg (N) m^{-2} yr^{-1}, but generally underestimate the deposition at stations with higher observations. According to Fig. 2.3(e), wet deposition at three stations in Poland, Norway and Spain were underestimated by 430 (59%), 420 (63%) and 290 (67%) mg N m^{-2} yr^{-1}, respectively. Besides, the stations in Germany generally under-predict these values by 100-200 mg (N) m^{-2} yr^{-1}. The NO_3^- wet deposition at the EANET stations is well simulated with MFB (-3%) and MFE (43%) (Fig. 2.2(f)). The model estimations are within ±50% of observations for 77% of the stations. According to Fig. 2.3(f), one station in Central China is overestimated by 400 (130%) mg (N) m^{-2} yr^{-1}. On the contrary, three stations in Thailand, Vietnam and Malaysia are underestimated by 570 (78%), 350 (66%) and 200 (64%) mg (N) m^{-2} yr^{-1}. Overall, 83% of the MMM results are within ±50% of observations at stations of all networks. The NADP stations have the highest MFB due to a generally positive bias

in the eastern US. The EANET stations have the highest MFE value, mainly due to the underestimation in Southeast Asia.

The modelled NH_4^+ wet deposition agrees well with observations at the NADP stations with MFB of 7% and MFE of 25% (Fig. 2.2(g)). About 88% of modelled deposition is within ±50% of observations as shown by the R value of 0.9. The MMM has well captured the high deposition in the U.S. Midwest, but slightly underestimates the deposition in the Southeast (Fig. 2.3(g)). At the EMEP stations, the NH_4^+ wet deposition is well simulated with MFB of -1% and MFE of 36% (Fig. 2.2(h)). The MMM results are close to the observations at most stations and well reproduce the high deposition in Germany and Italy (Fig. 2.3(h)). Some stations in Norway and Poland are slightly underestimated by 100-200 mg (N) m^{-2} yr^{-1}. These stations all report observations of higher deposition than 500 mg (N) m^{-2} yr^{-1}. The NH_4^+ wet deposition is underestimated at the EANET stations by 10% (MFB) and 50% (MFE) (Fig. 2.2(i)). The MMM has well captured the high deposition in Eastern China and Indonesia, but generally underestimates the NH_4^+ wet deposition at the Russian stations (Fig. 2.3(i)). In addition, the observed deposition at the three Korean stations is relatively high (~500-600 mg (N) m^{-2} yr^{-1}), but the MMM fails to reproduce any of them. There could be a missing emission source in that region. Overall, 81% of the MMM predictions are within ±50% of observations at stations of all networks. The NH_4^+ wet deposition is somewhat underestimated in all three regions, especially in EA.

Table 2.5 compares the model performance of this study with previous studies for PhotoComp (Dentener et al., 2006), HTAP I (Vet et al., 2014) and ACCMIP (Lamarque et al., 2013). It should be noted that the emission inputs, simulation periods and participating groups of this study (year 2010) are different from those of the previous projects (year 2001). Although the observations are from the same networks, the previous projects used three-year averaged observations of 2000-2002 and this study used those of 2009-2011. Due to these differences, the model performances may not be totally comparable. In terms of SO_4^{2-} wet deposition, the model performance is similar to that for previous projects in NA, with 4-6% higher percentage of stations within ±50% of observations. Large improvement is found in EU. The absolute mean bias decreases from 50-130 mg (S) m^{-2} yr^{-1} to 30 mg (S) m^{-2} yr^{-1}. There is 10% increase in the f50% of observations. At the East Asian stations, the absolute mean bias decreases slightly from 180~290 mg (S) m^{-2} yr^{-1} to 160 mg (S) m^{-2} yr^{-1}. But the R value and f50% have somewhat declined.

Table 2. 5 Comparison of HTAP II with previous studies on wet deposition. The unit is mg (N or S) m^{-2} yr^{-1}.

Wet SO_4^{2-} Deposition	NA				EU				EA			
	PhotoComp	HTAP I	ACCMIP	HTAP II	PhotoComp	HTAP I	ACCMIP	HTAP II	PhotoComp	HTAP I	ACCMIP	HTAP II
Slope	0.9	1	0.6	0.9	0.4	0.6	0.3	0.4	0.4	0.5	0.3	0.5
MB	46.3	50	-18.8	30.9	-67.1	51.5	-125.3	-31.3	-218.6	-182.1	-292.4	-161.5
Mean Obs	309.8	309.8	309.8	253.7	404.5	404.5	404.5	228.7	686.1	686.1	686.1	653.7
Mean Model	356.1	359.8	291	284.6	337.3	456.1	279.3	197.4	467.5	504.1	393.7	492.2
R	0.9	0.9	0.9	0.8	0.6	0.6	0.6	0.7	0.9	0.9	0.8	0.6
F50%	70.4	70	72.2	76.5	78.7	52.8	78.7	86.4	80	88	72	68.6
No. of stations	346	346	346	136	126	126	126	82	49	49	49	43
Wet NO_3^- Deposition	NA				EU				EA			
	PhotoComp	HTAP I	ACCMIP	HTAP II	PhotoComp	HTAP I	ACCMIP	HTAP II	PhotoComp	HTAP I	ACCMIP	HTAP II
Slope	1	1	0.9	1.2	0.3	0.3	0.3	0.5	0.5	0.5	0.4	0.8
MB	34.8	21.9	44.3	57.8	-41.4	-60	-75.2	-22.0	-47.8	-49.3	-46.4	-0.8
Mean Obs	191.3	191.3	191.3	153.7	300.5	300.5	300.5	237.3	263	263	263	356.4
Mean Model	226.1	213.3	235.6	211.5	259.1	240.5	225.3	215.4	215.2	213.7	216.7	355.7
R	0.8	0.9	0.9	0.9	0.6	0.6	0.6	0.7	0.8	0.8	0.8	0.7
F50%	77	84.3	68.7	66.9	75	85.2	85.2	90.2	84	84	88	76.7
No. of stations	346	346	346	136	126	126	126	82	49	49	49	43
Wet NH_4^+ Deposition	NA				EU				EA			
	PhotoComp	HTAP I	ACCMIP	HTAP II	PhotoComp	HTAP I	ACCMIP	HTAP II	PhotoComp	HTAP I	ACCMIP	HTAP II
Slope	0.8	0.9	0.5	0.8	0.4	0.4	0.3	0.6	0.8	0.7	0.1	0.6
MB	5.5	10.9	-12.1	2.3	-23.9	-49.7	-94.7	-4.0	-69.7	-63.4	-136.2	-28.7
Mean Obs	161.3	161.3	161.3	195.5	336	336	336	286.1	400.5	400.5	400.5	534.5
Mean Model	166.8	172.2	149.2	197.9	312.1	286.4	241.3	282.2	330.8	337.1	264.4	505.8
R	0.9	0.9	0.8	0.9	0.8	0.6	0.6	0.6	0.8	0.8	0.2	0.7
F50%	82.2	84.8	75.7	87.5	73.9	79.5	78.4	75.3	76	68	56	60.5
No. of stations	346	346	346	136	126	126	126	82	49	49	49	43

For NO_3^- wet deposition, HTAP II performs similar to the ensembles used in previous projects in NA, but slightly better in EU with lower mean bias and 5% increase in the f50% of observations. The model mean bias at the Asian stations has decreased significantly from ~50 mg (N) m^{-2} yr^{-1} to ~1 mg (N) m^{-2} yr^{-1}. However, the biases for individual models are large (Fig. S2.2). Large negative model bias is found in Southeast Asia and improvements are needed in the future.

In terms of NH_4^+ wet deposition, HTAP II shows similar R values to those of ensembles used for the previous projects at the NADP stations, with slightly lower model bias. However, HTAP II shows considerable improvement in EU. The slope of the regression line increases from 0.3-0.4 to 0.6 and the mean bias decreases from as large as -95 mg (N) m^{-2} yr^{-1} to -4 mg (N) m^{-2} yr^{-1}. For Asia, the slope, mean bias and R values for HTAP II are all within the ranges of the previous projects, while the absolute mean bias decreases form 70~140 mg (N) m^{-2} yr^{-1} to 30 mg (N) m^{-2} yr^{-1}.

Dry deposition. This study evaluates the dry deposition in CONUS with inferential data for CASTNET due to limited number of measurements. Figure 2.6 shows the scatter plots of the MMM SO_2, SO_4^{2-}, NO_3^-, HNO_3 and NH_4^+ dry deposition with inferential data at the CASTNET stations. Performances of individual models can be found in Fig. S2.5-S2.9 in the Appendix. The modelled SO_2 dry deposition is 240 (170%) mg (S) m^{-2} yr^{-1} higher than the inferential data and only 5% of the stations is within ±50% of the inferential values. There are smaller discrepancies for values of SO_4^{2-} dry deposition (14 mg (S) m^{-2} yr^{-1} and 60%) between model and inferential results. Modelled NO_3^-, HNO_3 and NH_4^+ dry deposition is generally 50-100% higher than the inferential data and the f50% is about 15%.

Figure 2.7 shows the spatial distributions of MMM dry deposition (contours) with the inferential data (filled circles). The MMM results are consistent with the inferential data in the western US, where the dry deposition is generally low. And both datasets predict high NO_3^- dry deposition in western California. Large disagreements are found in the eastern US. In the U.S. Midwest (mainly Indiana and Ohio states), although both results estimate higher N (NO_3^-, HNO_3 and NH_4^+) dry deposition in this region than the others, the prediction of MMM is 20-30 mg (N) m^{-2} yr^{-1} higher than the inferential data at every station. In addition, the MMM estimates much

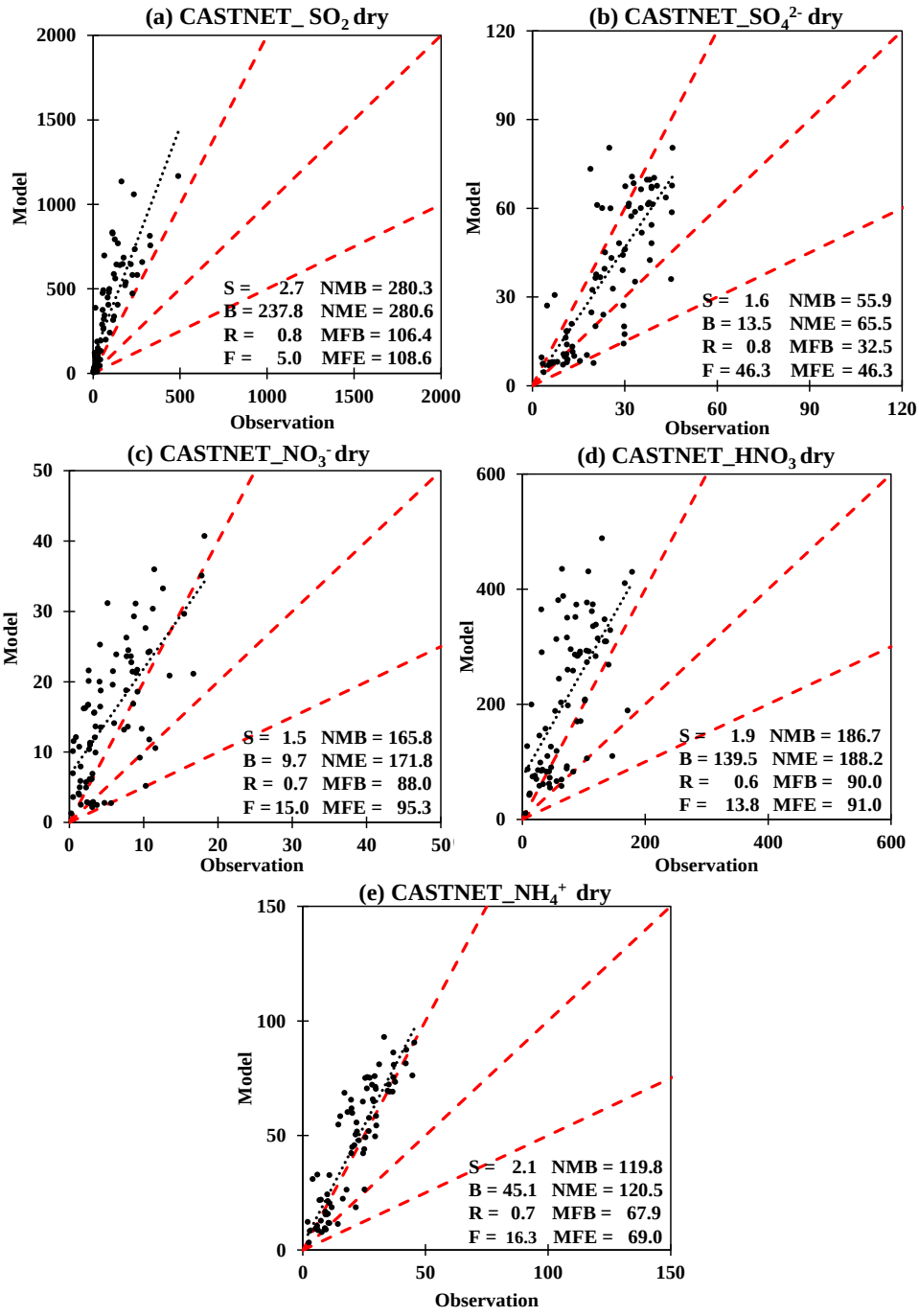

Figure 2. 6 Evaluation of MMM performance of SO_2, SO_4^{2-}, NO_3^-, HNO_3 and NH_4^+ dry depositions (mg (N or S) m^{-2} yr^{-1}) at CASTNET stations. The MMM is the annual dry deposition in 2010 and the observations are three-year average annual data during 2009-2011 from CASTNET network.

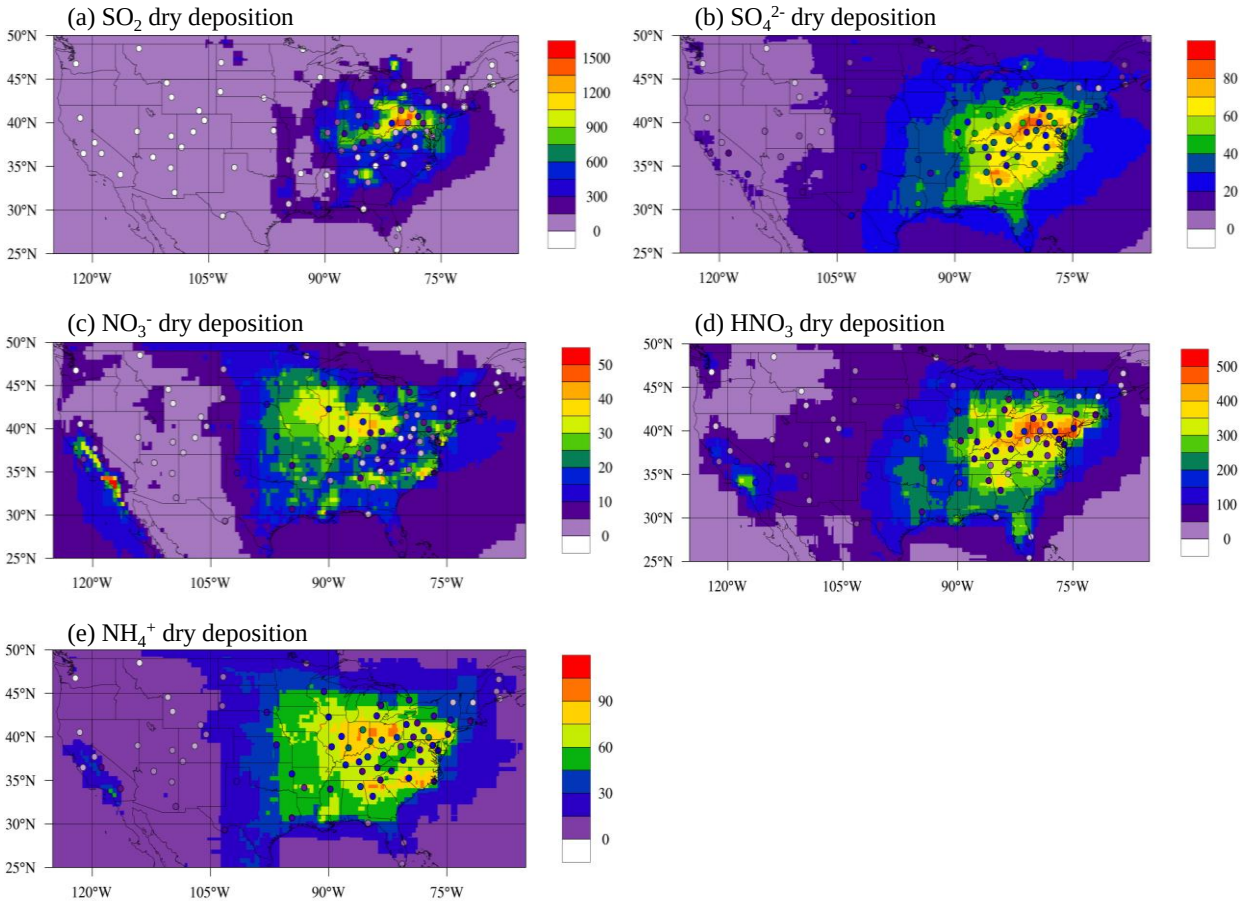

Figure 2. 7 Distribution of SO_2, SO_4^{2-}, NO_3^-, HNO_3 and NH_4^+ dry depositions (mg (N or S) m^{-2} yr^{-1}) of MMM and observations. The MMM is the annual dry deposition in 2010 and the observations are three-year average annual data of 2009-2011. Contours are MMM results and filled circles are inferential data from CASTNET.

higher deposition in southern and north-eastern U.S. than in the western US, but this gradient is much weaker in the inferential data.

Table 2.6 compares the model performance of this study (HTAP II) with that of the models used in the previous projects of HTAP I (Vet et al., 2014) and ACCMIP (J. Sun et al., 2017). HTAP I used the 2001 simulation results and compared them with three-year average (2000-2002) CASTNET data. ACCMIP used ten-year averages of both MMM and CASTNET data from 2000 to 2009. The N dry deposition values for all projects contain NO_3^-, NH_4^+ and HNO_3 and the S dry deposition includes SO_2 and SO_4^{2-}. Both HTAP I and HTAP II overestimated the S and N dry deposition, but HTAP II has ~100 mg(S) m^{-2} yr^{-1} and ~80 mg(N) m^{-2} yr^{-1} lower mean bias than HTAP I. The comparison with ACCMIP results may not be solid since there are large differences in simulation periods. Generally, the HTAP II performance is close to ACCMIP for NH_4^+, SO_2 and SO_4^{2-} dry deposition simulation, but has larger mean bias for HNO_3 dry deposition prediction.

Since the CASTNET dry deposition is not actually measured but instead a calculation of measured concentration of species and modelled dry deposition velocities, it is necessary to investigate which factor of these two contributes to the model bias. We compare the modelled air pollutant concentrations with CASENET measurements as shown in Table 2.7 (individual model performances can be found in Table S2.1-S2.5 in the Appendix). The MMM overestimates the SO_2, SO_4^{2-}, HNO_3, NO_3^- and NH_4^+ concentrations by 394%, 40%, 217%, 135% and 173%, respectively. It should be noted that the CASTNET sites are generally located in rural regions that are away from emission sources (Sickles & Shadwick, 2008), thus the measured concentrations of air pollutants are relatively low compared with those of urban sites. While the resolutions of the HTAP II models range from 0.5° to 3° and are not fine enough to reproduce the characteristic of some rural sites. The models with finer resolutions except CHASER_t106 model (i.e. EMEP_rv48 (0.5° × 0.5°) and SPRINTARS (1.1° × 1.1°)) generally perform better than the others, while models with coarse resolutions (i.e. CHASER_re1 (2.8° × 2.8°) and OsloCTM3.v2 (2.8° × 2.8°)) are generally not performing well for all species. This could explain the overestimation of air pollutant concentrations at the CASTNET sites.

Table 2. 6 Comparison of HTAP II MMM with previous projects on dry deposition. The unit is mg (N or S) m^{-2} yr^{-1}. S dry deposition is the sum of SO_2 and SO_4^{2-} dry depositions. N dry deposition is the sum of HNO_3, NO_3^- and NH_4^+ dry depositions (not include NO_2 and NH_3 depositions).

	S dry deposition			SO_2 dry deposition			SO_4^{2-} dry deposition		
	ACCMIP	HTAP I	HTAP II	ACCMIP	HTAP I	HTAP II	ACCMIP	HTAP I	HTAP II
Slope	1	-	2.7	1	-	2.7	1	-	1.6
MB	280.9	367	251.2	264	-	237.8	17	-	13.5
Mean Obs	225.6	-	108.9	191	-	84.8	35	-	24.1
Mean Model	506.5	-	360.2	455	-	322.6	52	-	37.5
R	0.8	0.8	0.8	0.8	-	0.8	0.9	-	0.8
F50%	6	-	12.5	6	-	5	48	-	46.3
	N dry deposition			**HNO_3 dry deposition**			**NH_4^+ dry deposition**		
	ACCMIP	HTAP I	HTAP II	ACCMIP	HTAP I	HTAP II	ACCMIP	HTAP I	HTAP II
Slope	-	-	2.1	1	-	1.9	2	-	2.1
MB	-	411 (eastern NA) 114 (western NA)	185.1	75	-	139.5	33	-	24.6
Mean Obs	-	-	101.1	119	-	74.7	28	-	20.5
Mean Model	-	-	286.1	195	-	214.2	60	-	45.1
R	-	0.8	0.7	0.8	-	0.6	0.8	-	0.7
F50%	-	-	13.8	38	-	13.8	18	-	16.3

Table 2. 7 Comparison of modelled concentrations of air pollutants with CASTNET. The unit is μg (S) m^{-3}.

Species	SO_2	SO_4^{2-}	HNO_3	NO_3^-	NH_4^+
Mean obs	0.82	0.64	0.17	0.17	0.56
Mean model	4.06	0.89	0.55	0.4	1.54
Slope	5.03	1.57	3.01	1.63	2.74
MB	0	0	0	0	0
Bias[1]	394.73	40.36	216.83	135.05	172.79
R	0.9	0.91	0.84	0.77	0.95
F50%	11.25	63.75	3.75	17.5	5
NMB	394.73	40.36	216.83	135.05	172.79
NME	396.47	46.73	216.83	144.21	172.79
MFB	99.26	23.84	98.66	76.92	88.42
MFE	106.31	33.98	98.66	87.53	88.42
No. of stations	80	80	80	80	80

Note: [1] Bias is calculated as dividing MB with mean observation. The unit is %.

In order to check the differences of modelled dry deposition velocity between CASNET and HTAP II models, we adopt the general approach for calculating dry deposition velocity by Eq. *(2-7)*.

$$V_d = \frac{-F_c}{C_a} \qquad (2\text{-}7)$$

where V_d is the deposition velocity. F_c is the dry deposition flux. C_a is the concentration of species. The negative mark indicates the direction of the dry deposition velocity. This scheme has been widely adopted in global models studies with some modifications in the parameters (Wesely & Hicks, 2000). The calculated dry deposition velocity of models and CASTNET are compared in Table 2.8 (Individual model comparison can be found in Table S2.6-S2.10 in the Appendix). The mean bias of dry deposition velocities for MMM are -8%, 0.3%, 7%, 19% and 2% for SO_2, SO_4^{2-}, HNO_3, NO_3^- and NH_4^+, respectively, which are much lower than those of air pollutants. The model bias for dry deposition at the CASTNET sites mainly comes from the model over-prediction of air pollutant concentration.

In addition, the estimation of CASENET dry deposition has been reported with high uncertainties. The uncertainties are estimated to be 10-20% in the measurement of mixing ratio of species, 20% in the calculated velocity and about 20% when lacking of hourly concentration for species with strong diurnal variation (L. Zhang, R. Vet, et al., 2009). And the CASTNET dry deposition is found to be lower than the value reported by the Canadian Air and Precipitation Monitoring Network (CAPMoN) by 54% for SO_2 dry deposition and 47% for HNO_3 dry deposition. The main differences are caused by using different models to calculate the dry velocity (Schwede, Zhang, Vet, & Lear, 2011).

2.4.2 Distributions of S and N depositions

S deposition. Table 2.9 lists the calculated amount of S emission and deposition on continents, coastal regions and oceans. Fig. 2.8 presents the distribution of S emission and deposition from MMM results. The distributions of components of S deposition are shown in Fig. S2.10 in the Appendix. The global S deposition is 84 Tg(S) in 2010, with 49% deposits on non-coastal continents, 32% deposits on non-coastal ocean and 19% deposits on coastal area. For continental

Table 2. 8 Comparison of modelled dry deposition velocities of air pollutants with CASTNET (cm s^{-1}).

	SO_2	SO_4^{2-}	HNO_3	NO_3^-	NH_4^+
Mean Obs	0.27	0.13	1.34	0.12	0.12
Mean Model	0.24	0.13	1.25	0.14	0.12
Slope	0.04	0.1	-0.1	0.06	0.13
MB	-0.02	0	-0.1	0.02	0
Bias%	-8.39	0.3	-7.27	18.69	-1.72
R	0.06	0.34	-0.12	0.05	0.27
F50%	77.5	88.75	85	73.75	87.5
NMB	-9.03	0.3	-7.27	18.69	-1.72
NME	34.88	21.12	27.47	37.35	22.13
MFB	-3.83	4.56	-7.01	17.29	2.01
MFE	35	21.73	29.52	32.05	22.67
No. of stations	80	80	80	80	80

Table 2. 9 MMM estimates of S deposition and emission in 2010 (Tg(S) yr-1) and comparison with HTAP I results. Δ is the difference between 2010 and 2001 calculated as (HTAP II – HTAP I). The numbers in parentheses are the percentage of changes, calculated as $\frac{(\text{HTAP II} - \text{HTAP I})}{\text{HTAP I}} \times 100\%$.

Regions	S emission					
	Non-coastal			Coastal		
	HTAP II (2010)	HTAP I (2001)	Δ	HTAP II (2010)	HTAP I (2001)	Δ
3. North America	6.2	9.5	-3.3 (-34.3)	1	1.3	-0.2 (-19.2)
4. Europe	3.9	10	-6.1 (-60.8)	1.6	3.6	-1.9 (-54.2)
5. South Asia	5.2	3.3	1.9 (56.4)	0.8	0.8	0.0 (-3.6)
6. East Asia	15	15.6	-0.6 (-4.0)	1.8	3.2	-1.4 (-42.8)
7. Southeast Asia	2.5	1.7	0.7 (42.4)	2.6	2.4	0.1 (6.0)
8. Australia	1.5	1	0.5 (56.0)	2	1.4	0.6 (42.0)
9. North Africa	0.7	1.1	-0.4 (-37.0)	0.9	0.9	0.0 (-2.9)
10. Sub Saharan Africa	2.5	2.8	-0.4 (-12.6)	0.9	0.7	0.2 (24.2)
11. Middle East	3.2	1.9	1.3 (68.9)	1.1	0.5	0.6 (108.1)
12. Central America	2.2	2.1	0.2 (7.7)	1.4	1.7	-0.3 (-15.2)
13. South America	3.1	2.7	0.4 (16.9)	0.8	1	-0.2 (-23.3)
14. RBU	2.9	5.1	-2.2 (-43.9)	0.5	0.5	0.0 (-5.8)
15. Central Asia	1.6	1.4	0.2 (18.3)	0	0	0.0 (-5.9)
17. Antarctic	1.1	1.1	-0.1 (-7.2)	0	0	0.0 (0)
Continental	51.5	59.3	-7.7 (-13.1)	15.3	18	-2.7 (-14.8)
2. Ocean	23.9	18.1	5.8 (31.9)			
1. World Total	75.4	77.4	-2.0 (-2.6)	15.3	18	-2.7 (-14.8)

Table 2.9 continued

Regions	S deposition					
	Non-coastal			Coastal		
	HTAP II (2010)	HTAP I (2001)	Δ	HTAP II (2010)	HTAP I (2001)	Δ
3. North America	4.7	7.2	-2.5 (-34.8)	1.3	1.3	0.0 (-1.2)
4. Europe	2.7	6.4	-3.7 (-58.2)	1.5	2.9	-1.4 (-49.6)
5. South Asia	3.7	2.4	1.4 (57.8)	1	0.9	0.1 (17.0)
6. East Asia	11.2	11.9	-0.7 (-5.6)	2.9	3.3	-0.4 (-13.3)
7. Southeast Asia	2.4	1.9	0.5 (27.6)	2.8	2.4	0.4 (16.1)
8. Australia	1	0.7	0.3 (43.9)	1.5	1.1	0.3 (28.0)
9. North Africa	1	1.1	-0.1 (-12.3)	0.5	0.6	-0.1 (-11.3)
10. Sub Saharan Africa	2.7	2.6	0.1 (4.8)	0.7	0.7	0.0 (-4.9)
11. Middle East	1.7	1.2	0.5 (47.0)	0.6	0.4	0.2 (50.4)
12. Central America	1.4	1.4	0.0 (1.6)	1.4	1.4	0.0 (2.0)
13. South America	2.4	2.1	0.3 (14.3)	0.6	0.6	0.0 (1.6)
14. RBU	3.6	5.3	-1.7 (-32.1)	0.9	0.8	0.1 (9.7)
15. Central Asia	1.2	1.2	0.0 (2.7)	0.1	0.1	0.0 (-13.5)
17. Antarctic	1.4	0.8	0.6 (73.7)	0	0	0.0 (0)
Continental	41	46	-4.9 (-10.7)	15.6	16.5	-0.8 (-5.1)
2. Ocean	26.9	23.3	3.6 (15.5)			
1. World Total	67.9	69.2	-1.3 (-1.9)	15.6	16.5	-0.8 (-5.1)

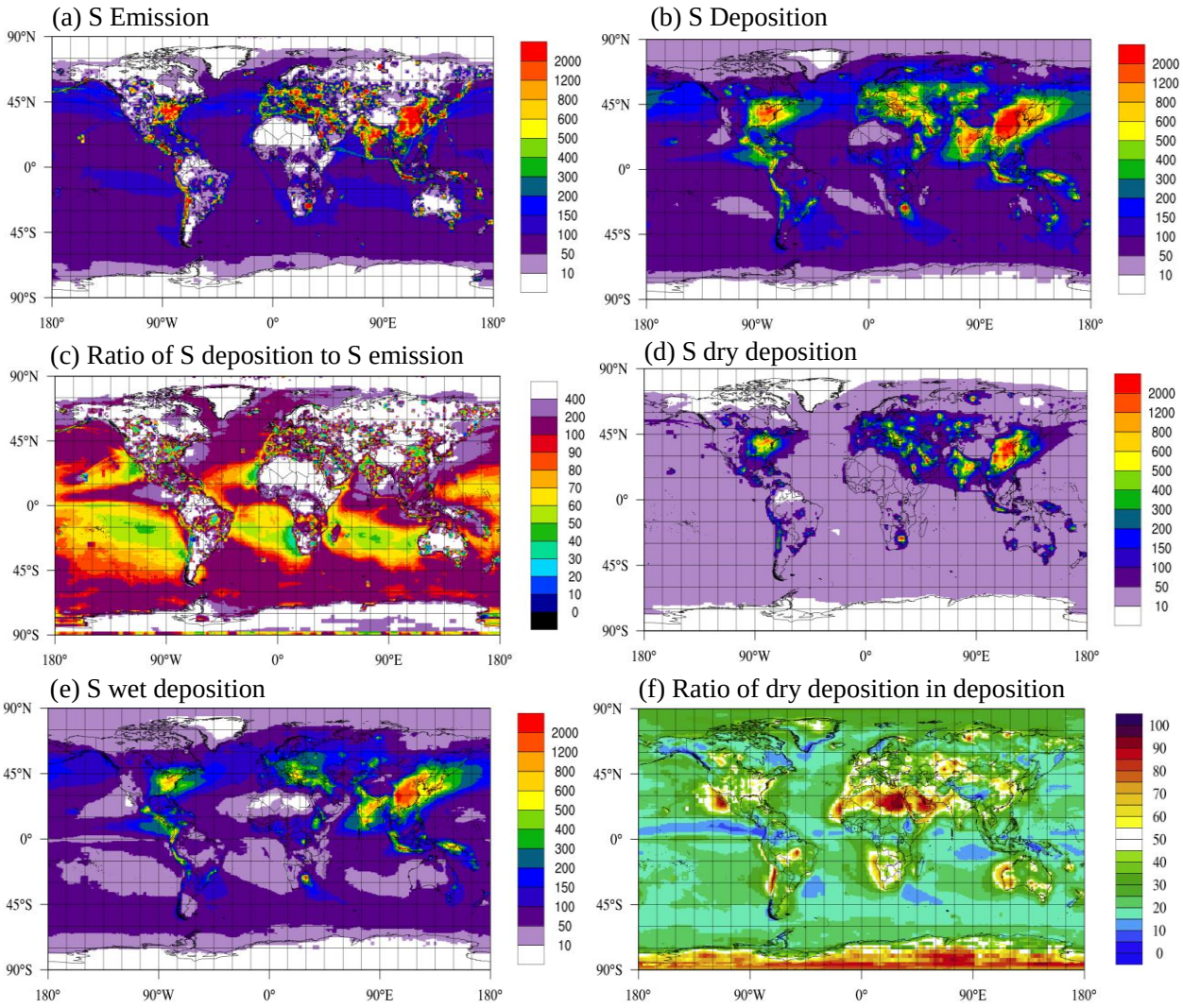

Figure 2. 8 MMM results of S emission and deposition in 2010 (mg(S) m^{-2} yr^{-1}) and ratio of S deposition in S emission (%). (bottom panel) MMM results of S dry and wet depositions in 2010 (mg(S) m^{-2} yr^{-1}) and ratio of dry deposition to total (wet + dry) deposition (%).

non-coastal regions, EA receives the largest amount of S deposition (17%). The highest S deposition is found in Eastern China (2000 mg(S) m^{-2} yr^{-1}) (Fig. 2.8(b)). Other regions with largely extended areas of high S deposition are the Indian peninsula (800-1200 mg(S) m^{-2} yr^{-1}), Malaysia and Indonesia (~1200 mg(S) m^{-2} yr^{-1}), U.S. Midwest (800-2000 mg(S) m^{-2} yr^{-1}), Mexico and Central America (400-800 mg(S) m^{-2} yr^{-1}), Peru and Chile (400-600 mg(S) m^{-2} yr^{-1}), Eastern EU (~800 mg(S) m^{-2} yr^{-1}) and the northeastern ME (500-1200 mg(S) m^{-2} yr^{-1}). The distribution of high deposition regions agrees very well with high S emission regions (Fig. 2.8(a)). For coastal regions, EA and Southeast Asia receive the most S deposition (3% and 3% respectively). The east coast of EA and NA and all coasts of India have relatively high deposition (400-800 mg(S) m^{-2} yr^{-1}), followed by the west coast of Mexico (~400 mg(S) m^{-2} yr^{-1}). This study estimates 43 Tg(S) of S deposition on the ocean and coastal regions in 2010, and accounts for 51% of global S deposition. The ratio is similar to the 46%-51% estimated by previous studies for 2001 (Dentener et al., 2006; Vet et al., 2014).

The ratio of S deposition to S emission is shown in Fig. 2.8(c). Because it is not clear what fraction of dimethyl sulphide (DMS) emission is transferred to S deposition, this ratio could not represent the transformation of S emission to deposition. For continental non-coastal regions, the average ratio is 85% (86% if taking consideration of coastal regions). In high emission regions, this ratio can be viewed as the "scavenging" effect of S pollution by deposition. In major source regions of S emission (i.e. North China Plain, Midwest of U.S. and India), the ratios are only slightly higher than 50%, while in low S emission regions (<10 mg(S) m^{-2} yr^{-1}), the ratios could exceed 400 % (areas with white color in Fig. 2.8(c)). This result indicates that the deposition in these regions is largely affected by long-range transport of pollution from other regions. The impact of intercontinental transport of air pollutants on deposition can be quantified by the emission perturbation experiments in HATP II.

NO_y deposition. Table 2.10 summarizes the NO_y emission and deposition in each region. Figure 2.9 presents the spatial distribution from MMM results. Distributions of components of NO_y deposition are shown in Fig. S2.11 in the Appendix. The global NO_y deposition is 59 Tg(N) in 2010, with 62% of deposits on non-coastal continents, 22% of deposits on non-coastal ocean and

Table 2.10 The numbers in the parenthesis are the percentages in world total emission/deposition.

Regions	NO_X emission		NO_y deposition		NH_3 emission	
	Non-coastal	Coastal	Non-coastal	Coastal	Non-coastal	Coastal
3. North America	6.6 (10.9)	0.6 (1.1)	4.4 (7.5)	0.8 (1.4)	3.7 (6.9)	0.2 (0.3)
4. Europe	3.7 (6.2)	1.2 (1.9)	2.6 (4.4)	1.2 (2.1)	3.2 (5.9)	0.6 (1.1)
5. South Asia	4.4 (7.3)	0.4 (0.7)	3.6 (6.0)	0.7 (1.2)	10.4 (19.2)	0.7 (1.3)
6. East Asia	10.1 (16.8)	1.3 (2.1)	8.3 (14.0)	2.2 (3.7)	7.8 (14.4)	0.7 (1.3)
7. Southeast Asia	2.6 (4.4)	1.3 (2.1)	1.9 (3.1)	1.4 (2.3)	3.1 (5.8)	1.5 (2.7)
8. Australia	1.4 (2.3)	0.3 (0.6)	0.6 (1.0)	0.4 (0.7)	0.7 (1.2)	0.4 (0.8)
9. North Africa	1.5 (2.5)	0.4 (0.7)	1.4 (2.3)	0.4 (0.6)	0.9 (1.7)	0.2 (0.3)
10. Sub Saharan Africa	7.4 (12.2)	0.4 (0.7)	4.7 (7.9)	0.6 (1.1)	4.0 (7.5)	0.3 (0.6)
11. Middle East	1.9 (3.1)	0.5 (0.7)	1.4 (2.4)	0.3 (0.6)	0.7 (1.2)	0.1 (0.2)
12. Central America	2.1 (3.5)	0.8 (1.3)	1.2 (2.1)	0.8 (1.4)	1.4 (2.6)	0.5 (0.9)
13. South America	5.4 (8.9)	0.3 (0.5)	3.4 (5.8)	0.3 (0.5)	4.4 (8.1)	0.3 (0.5)
14. RBU	2.4 (4.1)	0.2 (0.3)	2.4 (4.1)	0.5 (0.9)	1.7 (3.1)	0.1 (0.2)
15. Central Asia	0.7 (1.1)	0.0 (0)	0.6 (1.1)	0.0 (0.1)	0.5 (0.9)	0.0 (0)
17. Antarctic	0.0 (0.1)	0.0 (0)	0.1 (0.2)	0.0 (0)	0.0 (0.1)	0.0 (0)
Continental	50.2 (83.2)	7.7 (12.8)	36.7 (61.9)	9.7 (16.4)	42.6 (78.5)	5.6 (10.3)
2. Ocean	2.4 (4)		12.9 (21.7)		6.0 (11.1)	
1. World Total	52.7 (87.2)	7.7 (12.8)	49.6 (83.6)	9.7 (16.4)	48.7 (89.7)	5.6 (10.3)

Table 2.10 continued

Regions	NH_X deposition		N emission		N deposition	
	Non-coastal	Coastal	Non-coastal	Coastal	Non-coastal	Coastal
3. North America	3.4 (6.3)	0.4 (0.7)	10.3 (9.0)	0.8 (0.7)	7.8 (6.9)	1.2 (1.0)
4. Europe	2.5 (4.6)	0.8 (1.4)	6.9 (6.0)	1.8 (1.6)	5.1 (4.5)	2.0 (1.8)
5. South Asia	8.6 (15.9)	1.0 (1.9)	14.8 (12.9)	1.1 (1.0)	12.1 (10.7)	1.7 (1.5)
6. East Asia	6.7 (12.5)	1.0 (1.9)	18.0 (15.7)	2.0 (1.7)	15.1 (13.3)	3.2 (2.8)
7. Southeast Asia	3.2 (5.9)	1.6 (2.9)	5.8 (5.0)	2.7 (2.4)	5. 1 (4.5)	2.9 (2.6)
8. Australia	0.4 (0.8)	0.4 (0.8)	2.0 (1.8)	0.8 (0.7)	1.0 (0.9)	0.9 (0.8)
9. North Africa	0.7 (1.3)	0.2 (0.3)	2.5 (2.1)	0.6 (0.5)	2.1 (1.9)	0.5 (0.5)
10. Sub Saharan Africa	3.4 (6.4)	0.4 (0.7)	11.4 (10.0)	0.7 (0.6)	8.1 (7.2)	1.0 (0.9)
11. Middle East	0.5 (0.9)	0.1 (0.2)	2.5 (2.2)	0.6 (0.5)	1.9 (1.7)	0.5 (0.4)
12. Central America	1.4 (2.5)	0.6 (1.1)	3.5 (3.1)	1.2 (1.1)	2.6 (2.3)	1.4 (1.3)
13. South America	3.8 (7.1)	0.3 (0.6)	9.8 (8.5)	0.6 (0.5)	7.3 (6.4)	0.6 (0.5)
14. RBU	1.8 (3.4)	0.3 (0.6)	4.1 (3.6)	0.3 (0.2)	4.3 (3.8)	0.8 (0.7)
15. Central Asia	0.5 (0.8)	0.0 (0)	1.1 (1.0)	0.0 (0)	1.1 (1.0)	0.1 (0.1)
17. Antarctic	0.1 (0.2)	0.0 (0)	0.1 (0.1)	0.0 (0)	0.2 (0.2)	0.0 (0)
Continental	37.0 (68.6)	7.1 (13.1)	92.9 (81.0)	13.3 (11.6)	73.7 (65.1)	16.8 (14.8)
2. Ocean	9.9 (18.3)		8.5 (7.4)		22.8 (20.1)	
1. World Total	46.9 (86.9)	7.1 (13.1)	101.3 (88.4)	13.3 (11.6)	96.5 (85.2)	16.8 (14.8)

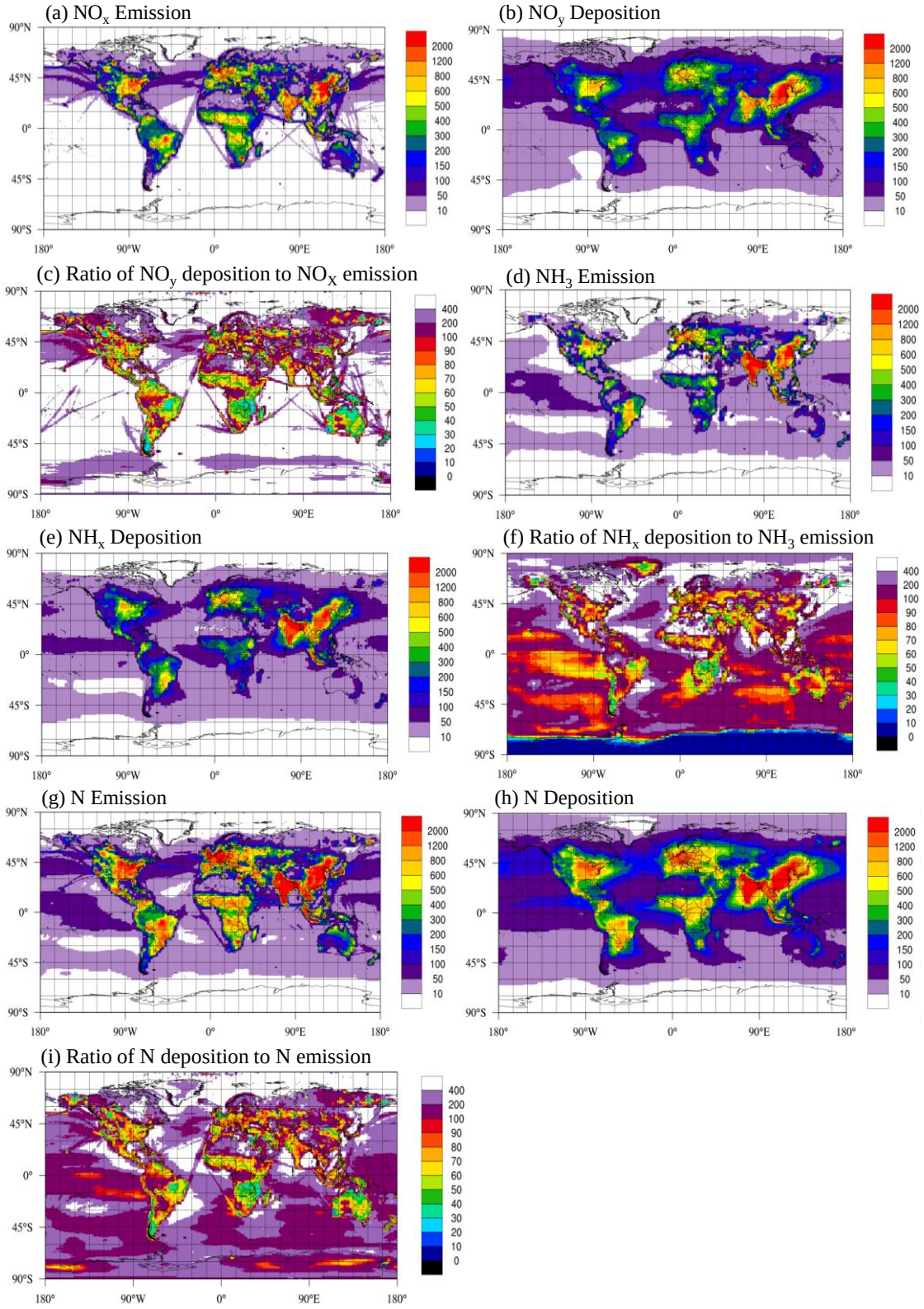

Figure 2. 9 MMM results of NO_X, NH_3 and N(NO_X + NH_3) emissions and depositions (mg(N) m^{-2} yr^{-1}), ratio of NO_y deposition to NO_X emission, ratio of NH_X deposition to NH_3 emission and N deposition to total N(NO_X + NH_3) emission (%). Purple colors represent regions where depositions are larger than emissions.

16% of deposits on coastal areas. For continental non-coastal regions, EA receives the largest NO_y deposition (14%). The highest NO_y deposition is found in north-eastern China (2000 mg(N) m^{-2} yr^{-1}), followed by the Indian peninsula (800-1200 mg(N) m^{-2} yr^{-1}), Malaysia and Indonesia (500-800 mg(N) m^{-2} yr^{-1}), Germany, Switzerland and Poland (500-600 mg(N) m^{-2} yr^{-1}), northern Sub-Saharan Africa (300-500 mg(N) m^{-2} yr^{-1}), north-eastern ME (400-500 mg(N) m^{-2} yr^{-1}), U.S. Midwest (500-600 mg(N) m^{-2} yr^{-1}) and Brazil (300-600 mg(N) m^{-2} yr^{-1}). For coastal regions, the east coast of EA also receives the largest amount of NO_y deposition (600 mg(N) m^{-2} yr^{-1} and 4%). Relatively high deposition is found on the east coast of NA (150-400 mg(N) m^{-2} yr^{-1}), all coasts of India (300-500 mg(N) m^{-2} yr^{-1}), the west coast of EU and all coasts of Southeast Asia (150-200 mg(N) m^{-2} yr^{-1}). This study estimates 23 Tg(N) of NO_y deposition on the ocean in 2010 (include ocean non-coastal and coastal), similar to the values of 23 Tg(N) (Dentener et al., 2006), 14-32 Tg(N) (Duce et al., 2008) and 20 Tg(N) (Vet et al., 2014) in literature. About 38% of global NO_y deposits on the ocean, similar to the estimations of 43% (Dentener et al., 2006), 42% (Vet et al., 2014) and 30% (Lamarque et al., 2005) in literatures. It should be noted that the calculation partly depend on the land-ocean mask, which may cause differences among studies.

For non-coastal ocean regions, the NO_y deposition is 13 Tg(N), accounts for 22% of the global deposition. While the emission from oceans is only 2 Tg(N), about 4% of global emission. The difference of 11 Tg(N) indicates NO_y transport from continents to the open ocean. Antarctic has near zero NO_x emission but receives 0.1 Tg(N) NO_y deposition. Deposition has been a non-negligible pathway that human pollution is contaminating the nearly untouched areas. We calculate the ratio of NO_y deposition to NO_x emission (Fig. 2.9(c)). In continental non-coastal regions, the average ratio is 74% (81% if taking consideration of coastal regions). In high NO_x emission regions (i.e. NA, EA and SA), an average 60-80% of the NO_y is removed by deposition, with large regional variation. For low emission regions (i.e. North Africa and Central Asia), the ratio can reach higher than 90%. The ratios in coastal regions and Open Ocean are generally over 200%. Instead of the local emission, the transport of air pollutants from elsewhere is the major source of deposition.

NH_x Deposition. The global NH_x deposition is 54 Tg(N) in 2010, with 69% of deposits on continental non-coastal regions, 19% of deposits on ocean non-coastal regions and 13% of deposits

on coastal regions (Table 2.10). For continental non-coastal regions, SA receives 16% of global NH_x depositions, followed by EA (13%). The whole Indian peninsula receives higher NH_x depositions than 2,000 mg(N) m^{-2} yr^{-1} (Fig. 2.9(e)). The Asian regions have several high deposition areas: North China Plain and Indonesia (1,200-2,000 mg(N) m^{-2} yr^{-1}), Japan, Thailand, Vietnam and Myanmar (500-600 mg(N) m^{-2} yr^{-1}). Other regions with high NH_x deposition are: the U.S. Midwest, Germany, France, Northern Italy, Southern Brazil and Ethiopia (400-800 mg(N) m^{-2} yr^{-1}). Distributions of components of NH_x deposition are shown in Fig. S2.12 in the Appendix.

Coastal regions of Southeast Asia (3%), EA (2%) and SA (2%) receive the largest NH_x deposition (~200-400 mg(N) m^{-2} yr^{-1}). The east coast of NA and Mexico also have high NH_x deposition (150-200 mg(N) m^{-2} yr^{-1}). Compared to NO_y deposition, the amounts of NH_x deposition on coastal regions are relatively lower. The ocean receives 17 Tg(N) of NH_x deposition in 2010, within the range of 13-29 Tg(N) (Duce et al., 2008), but slightly lower than the estimations of 23.5 Tg(N) (Dentener et al., 2006) and 21.4 Tg(N) (Vet et al., 2014) in literatures. About 31% of NH_3 emission is deposited on ocean areas, similar to estimation of 31% (Dentener et al., 2006) and 30% (Lamarque et al., 2005), but slightly lower than 37% (Dentener et al., 2006) and 37% (Vet et al., 2014) in literatures. The ocean emits 12 Tg(N) of NH_3 in 2010, which means that at least 5 Tg(N) of NH_x deposition on oceans in 2010 comes from continental regions. This value is considerably lower than the 13 Tg(N) of deposition-emission difference for NO_y (including the 2 Tg(N) difference on coastal regions). A possible explanation is that NH_3 has a short lifetime in the atmosphere, which makes it more likely to deposit close to where it is emitted (Shen et al., 2016), while NO_x can be oxidized to organic nitrate (Moxim, Levy, & Kasibhatla, 1996), which facilitates the long-range transport from land to open ocean.

The ratio of NH_x deposition to NH_3 emission is shown in Fig. 2.9(f). The average ratio is 87% for continental non-coastal regions (92% if also considers the coastal regions). The ratios are generally higher than those of NO_y deposition (74% and 81%), since large a proportion of NH_x deposits near the sources. The ratios are generally over 400% for coastal areas, but less than 100% on Open Ocean (70-90%). This is because there is less continental NH_x transported to the open ocean than to coastal regions.

Total N deposition as sum of NO_y and NH_x depositions. The global N deposition in 2010 is 113 Tg(N), with 65% of deposits on the continental non-coastal regions, 20% on non-coastal oceans and 15% on coastal regions (Table 2.10). EA (13%) and SA (11%) receive the largest amount of N deposition, consistent with the fact that they are also the largest N emission sources (16% and 13% respectively). The deposition reaches 3000 mg(N) m^{-2} yr^{-1} over Eastern China (especially North China Plain) and 2000 mg(N) m^{-2} yr^{-1} over India and Southeast Asia (Thailand, Vietnam and Malaysia). Other regions of high N deposition are the US, northeast Western EU (800-1200 mg(N) m^{-2} yr^{-1}), Mexico, Central America, Brazil, northern Sub-Saharan Africa and the north-eastern ME (500-600 mg(N) m^{-2} yr^{-1}). For coastal regions, the east coast of the US, all coasts of India and the east coast of EA are identified with relatively high deposition (>600 mg(N) m^{-2} yr^{-1}).

The global N dry and wet deposition is 40 Tg(N) yr^{-1} and 73 Tg(N) yr^{-1} in 2010, respectively. We calculate the ratio of dry deposition to total deposition as $\frac{dry\ deposition}{dry\ deposition+wet\ deposition} \times 100\%$. The spatial distributions are shown in Fig. 2.10. For continental non-coastal regions, about 44% (range from 35-61%) of the N deposition comes from dry deposition (42% if take coastal regions into consideration). If the overestimation of N dry deposition in Sect. 2.4.1 is considered, this ratio could be even lower. Desert areas (e.g., the Sonoran, Mojave and Chihuahuan deserts near the west coast of NA, the Sahara Desert in North Africa, the Arabian Desert in ME and the Great Victoria Desert in Australia) are seen with high ratios of dry deposition (80%) (Red color regions in Fig. 2.10(c)). This outcome is reasonable since these areas generally lack precipitation. Low fractions of dry deposition (30%) are found in RU, Western China, Southeast Asia, Australia and Central America.

Almost all coastal regions are dominated by wet deposition. Studies reported a dry deposition ratio of 21-45% for the east coast of the U.S. (T. Jickells, 2006) and a ratio of 15-22% for the Atlantic Ocean (Baker, Lesworth, Adams, Jickells, & Ganzeveld, 2010). Our study finds similar ratios for these coastal regions. An outflow of NO_y is exported from Asia over the Western Pacific Ocean through deposition (Bey, Jacob, Logan, & Yantosca, 2001). According to this study, about 70% of this land-to-ocean export of NO_y deposition is through wet deposition (Fig. 2.10(a)).

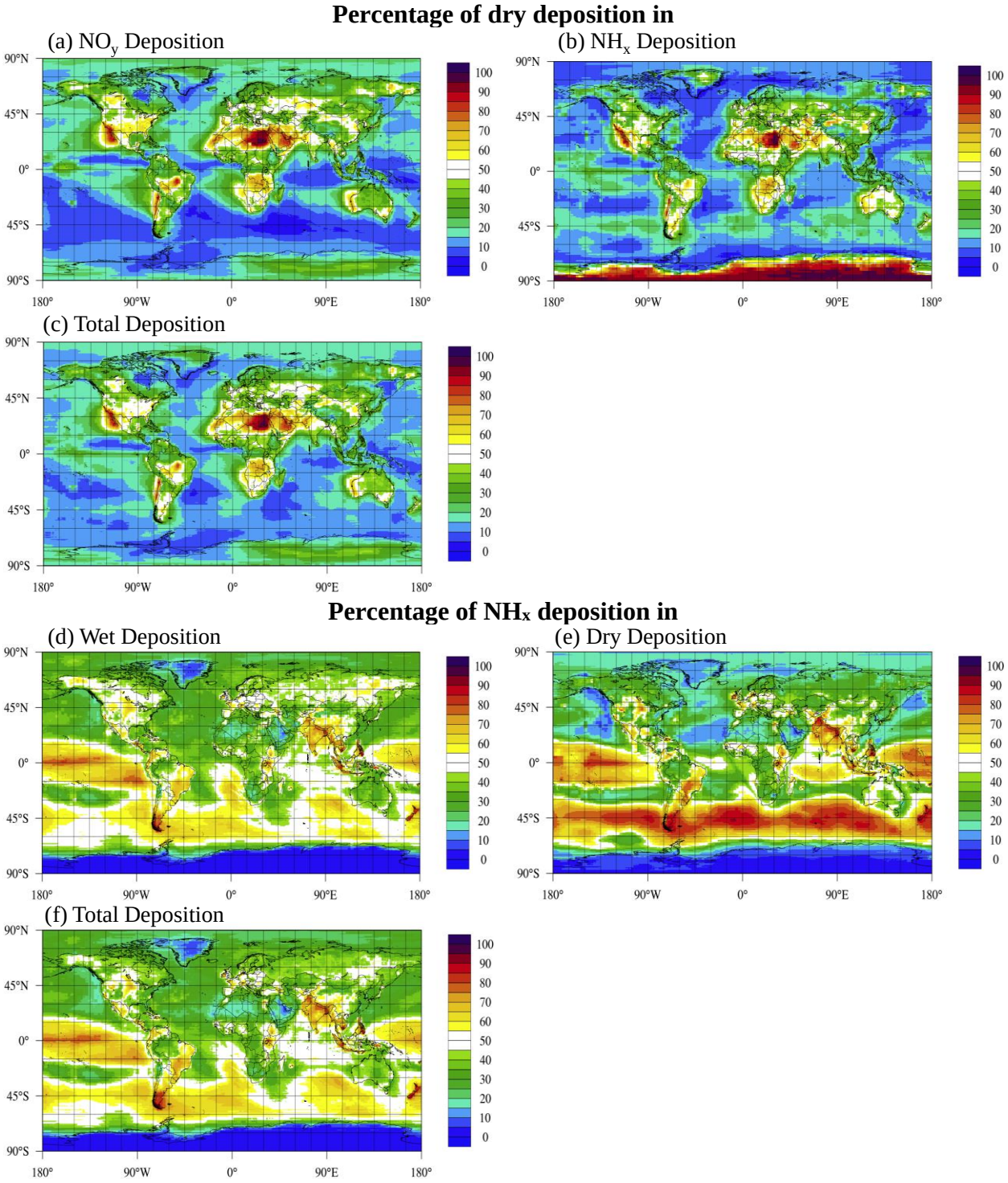

Figure 2. 10 (a-c) The percentage of dry deposition in wet + dry deposition for NO_y, NH_x and N (NO_y + NH_x) deposition. The ratio is calculated as (dry deposition)/ (dry + wet deposition) ×100%. (d-f) The percentage of NH_x deposition in N (NO_y + NH_x) deposition for wet, dry and (wet + dry) deposition. The ratio is calculated as (NH_x deposition)/ (NO_y + NH_x deposition).

The NH_x and NO_y deposition is 54 Tg(N) yr^{-1} and 59 Tg(N) yr^{-1} in 2010, respectively. The average ratio of NH_x deposition (calculated as $\frac{NH_x\ deposition}{NH_x\ deposition + NO_y\ deposition} \times 100\%$) for continental non-coastal regions is 47% (45% if coastal regions are taken into consideration). SA (71%) and Southeast Asia (63%) are dominated by NH_x deposition, owing to high local NH_3 emission, while the ME (25%) and North Africa (34%) are dominated by NO_y deposition. Fig. 2.10(f) shows the global distribution of the ratio of NH_x deposition. Except the high ratios found in the Indian peninsula, Southeast Asia, Southeast Brazil, South Argentina and New Zealand (70-80%) and Eastern Asia (~60%), other continental non-coastal regions are mainly dominated by NO_y deposition. This is consistent with finding by the ACCMIP study (Sun, Fu, & Huang, 2016).

2.4.3 Changes in deposition from 2001 to 2010

Changes in S and N depositions. The S emission and deposition in 2010 from HTAP II are compared with those in 2001 from HTAP I (Vet et al., 2014) (Table 2.9). The HTAP I deposition in regions are re-calculated according to the definition of regions of HTAP II, so the HTAP I results may look different from the reference (Vet et al., 2014). Because different models are used for each of the two ensembles compared, associated uncertainty is expected. In addition, emissions in HTAP I were not prescribed, so each modelling group used its own best estimation of emissions (Sanderson et al., 2008). Conversely, all models in HTAP II use the same anthropogenic emission values (although there were still differences in natural emissions).

Globally, the S emission decreases by 5 Tg(S) from 2001 to 2010, with 8 Tg(S) (13%) decrease in continental non-coastal regions, 6 Tg(S) (32%) increase in non-coastal ocean regions and 3 Tg(S) (15%) decrease in coastal regions. For continental non-coastal regions, there are large drops in S emissions from EU (6 Tg(S) and 61%), NA (3 Tg(S) and 34%) and RU (2 Tg(S) and 44%). On the other hand, SA and ME have 2 Tg(S) (56%) and 1 Tg(S) (69%) increase in S emissions. EA, one of the main contributors to S emission seems to show little change between 2001 and 2010. However, it has experienced large changes during these ten years, with stable annual increases from 2000 to 2005 due to increased energy consumption and decreases after 2006 owing to the successful implementation of the SO_2 control policies in China's eleventh FYP (Lu et al., 2010). For coastal regions, EU has experienced a 2 Tg(S) (54%) decrease and EA has

experienced a 1 Tg(S) (43%) decrease in S emission. Other regions have relatively small (0-0.6 Tg(S)) changes. The global S deposition decreases by 2 Tg(S), with 5 Tg(S) (11%) decrease in continental non-coastal regions, 4 Tg(S) (16%) increase in non-coastal ocean regions and 1 Tg(S) (5%) decrease in coastal regions. The regions with the largest change in deposition coincide with those having big changes in emission.

Figure 2.11 shows the comparison of S emission and deposition in HTAP II with those in HTAP I. Declined S deposition is found in large areas of the eastern U.S. and EU (400-1,500 mg(S) m^{-2} yr^{-1}). Regions with increased S deposition are India and Indonesia (100-800 mg(S) m^{-2} yr^{-1}). In China, there is a mixture of both increases and decreases in S deposition over different areas. The changes in S depositions agree well with changes in S emissions (Fig. 2.11(a)). During China's 11th FYP, the Flue Gas Desulfurization (FGD) systems were installed on power plants as the main technologies to control the SO_2 emission (Cao, Garbaccio, & Ho, 2009). The effectiveness of this technology in removing SO_2 emission varies considerably regionally. On the other hand, new sources of SO_2 emission, such as newly built power plants, are found responsible for the increased S emissions and deposition over some areas in China (J. Tan et al., 2017).

Table 2.11 compares the N emission and deposition in HTAP II with HTAP I. The global N emission increases from 105 Tg(N) to 115 Tg(N), with a 12 Tg(N) (15%) increase in continental non-coastal regions and a 2 Tg(N) (14%) decrease in coastal regions. The change on the ocean is small due to increased NO_y deposition but decreased NH_x deposition. For continental non-coastal regions, increases in N emission are found in SA (5 Tg(N), 56%), EA (4 Tg(N), 26%) and Southeast Asia (2 Tg(N), 58%), while the emission in EU decreases by 1 Tg(N) (12%). The emission changes in coastal regions are relatively small. The global N deposition increases by 7 Tg(N), with a 9 Tg(N) (14%) increase in continental non-coastal regions and a 2 Tg(N) decrease in ocean regions. Asian regions also have experienced the largest increases in deposition, and the amounts are identical with corresponding emission changes. Figure 2.12 shows the comparison of N emission and deposition in HTAP II with those in HTAP I. Elevated N deposition is found in India, Indonesia and North Chain Plain (1,500 mg(N) m^{-2} yr^{-1}). Regions with small increases are Japan, the northern ME, north-western Brazil and Mexico (~200 mg(N) m^{-2} yr^{-1}). On the other hand, the N deposition in the eastern U.S. and EU have decreased by 200-400 mg(N) m^{-2} yr^{-1}.

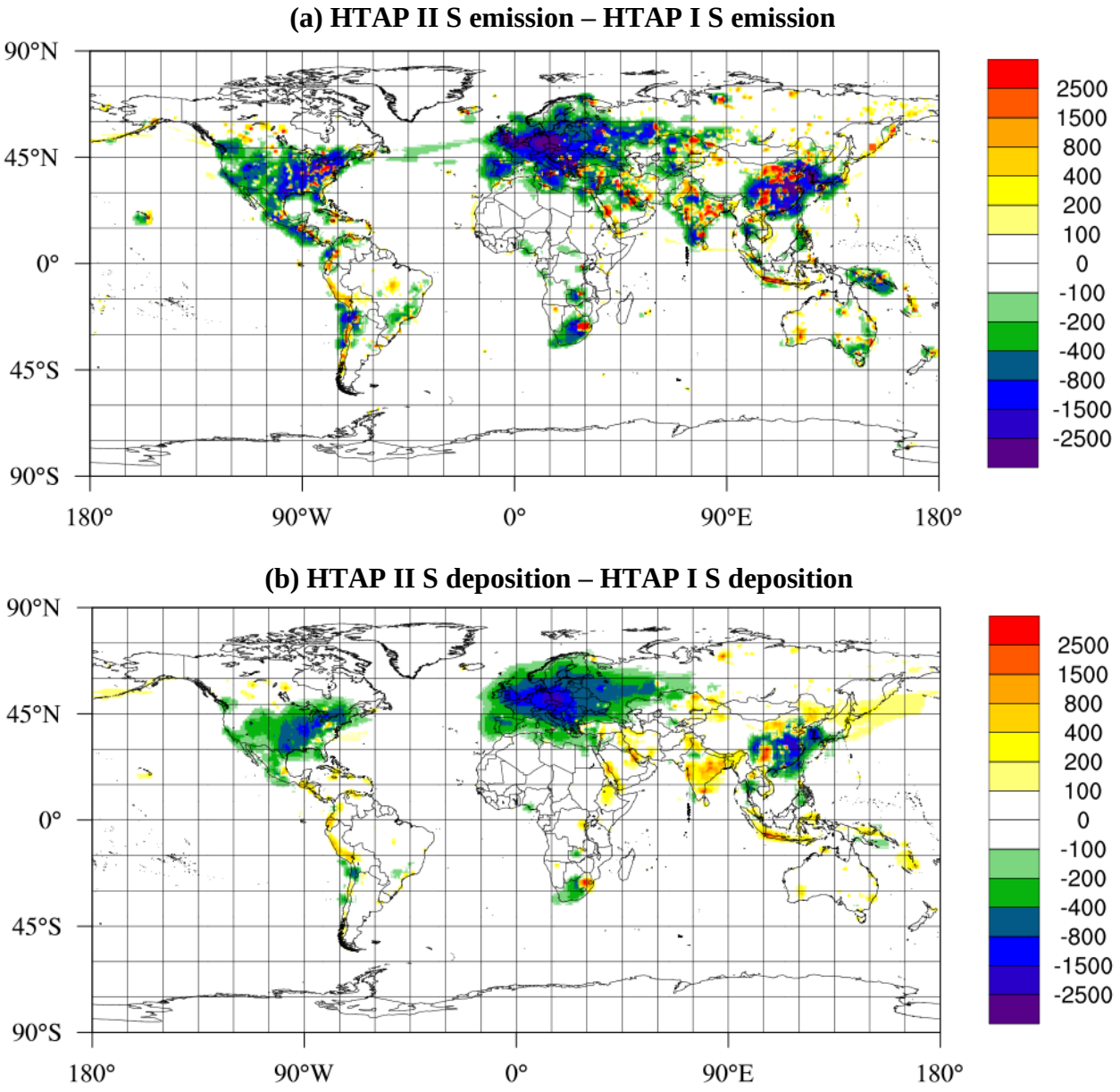

Figure 2. 11 Differences between MMM of HTAP II and HTAP I for (a) S emission (b) S Deposition. Unit: mg(S) m^{-2} yr^{-1}.

Table 2. 10 Comparison of N deposition and emission between 2010 (HTAP II) and 2001 (HTAP I) (Tg (N) yr^{-1}). Δ is the difference between 2010 and 2001 calculated as (HTAP II – HTAP I). The numbers in parentheses are the percentage of changes, calculated as $\frac{(\text{HTAP II} - \text{HTAP I})}{\text{HTAP I}} \times 100\%$.

Regions	N emission					
	Non-coastal			Coastal		
	HTAP II (2010)	HTAP I (2001)	Δ	HTAP II (2010)	HTAP I (2001)	Δ
3. North America	10.3	10.2	0.1 (0.5)	0.8	1.0	-0.2 (-16.8)
4. Europe	6.9	7.8	-0.9 (-11.8)	1.8	2.7	-0.9 (-33.6)
5. South Asia	14.8	9.5	5.3 (56.0)	1.1	1.3	-0.2 (-15.5)
6. East Asia	18.0	14.3	3.7 (25.9)	2.0	2.2	-0.2 (-8.1)
7. Southeast Asia	5.8	3.7	2.1 (57.4)	2.7	2.7	0.0 (0.5)
8. Australia	2.0	2.1	-0.1 (-5.3)	0.8	0.9	-0.2 (-16.6)
9. North Africa	2.5	2.1	0.3 (15.6)	0.6	0.6	0.1 (9.6)
10. Sub Saharan Africa	11.4	11.8	-0.4 (-3.1)	0.7	1.1	-0.3 (-30.6)
11. Middle East	2.5	1.8	0.8 (44.7)	0.6	0.4	0.2 (36.8)
12. Central America	3.5	3.2	0.3 (9.6)	1.2	1.5	-0.2 (-16.5)
13. South America	9.8	8.6	1.1 (12.8)	0.6	0.8	-0.2 (-23.4)
14. RBU	4.1	4.7	-0.6 (-12.4)	0.3	0.3	-0.1 (-17.4)
15. Central Asia	1.1	1.1	0.0 (4.1)	0.0	0.0	0.0 (24.5)
17. Antarctic	0.1	0.1	0.0 (-17.5)	0.0	0.0	0.0 (0)
Continental	92.9	81.1	11.8 (14.5)	13.3	15.5	-2.2 (-14.1)
2. Ocean	8.5	8.4	0.0 (0.2)			
1. World Total	101.3	89.6	11.8 (13.1)	13.3	15.5	-2.2 (-14.1)

Table 2. 11 continued

Regions	N deposition					
	Non-coastal			Coastal		
	HTAP II (2010)	HTAP I (2001)	Δ	HTAP II (2010)	HTAP I (2001)	Δ
3. North America	7.8	8.1	-0.2 (-3.1)	1.2	1.2	-0.1 (-4.8)
4. Europe	5.1	5.7	-0.7 (-11.4)	2	2.6	-0.6 (-23.6)
5. South Asia	12.1	6.7	5.4 (79.7)	1.7	1.7	0.1 (3.8)
6. East Asia	15.1	11.9	3.2 (26.8)	3.2	2.6	0.6 (21.9)
7. Southeast Asia	5.1	3.3	1.8 (54.4)	2.9	3	0.0 (-0.7)
8. Australia	1	1.3	-0.3 (-23.0)	0.9	1.1	-0.2 (-21.0)
9. North Africa	2.1	2	0.1 (7.5)	0.5	0.6	-0.1 (-12.2)
10. Sub Saharan Africa	8.1	9.1	-1.0 (-10.9)	1	1.5	-0.4 (-30.2)
11. Middle East	1.9	1.4	0.5 (37.3)	0.5	0.5	0.0 (0.2)
12. Central America	2.6	2.4	0.2 (8.3)	1.4	1.6	-0.2 (-12.7)
13. South America	7.3	6.8	0.5 (7.0)	0.6	0.8	-0.2 (-27.9)
14. RBU	4.3	4.9	-0.6 (-12.6)	0.8	0.7	0.1 (20.9)
15. Central Asia	1.1	1.2	-0.1 (-5.1)	0.1	0.1	0.0 (0)
17. Antarctic	0.2	0.2	0.0 (-10.3)	0	0	0.0 (0)
Continental	73.7	64.9	8.8 (13.5)	16.8	17.9	-1.1 (-6.1)
2. Ocean	22.8	23.5	-0.7 (-2.9)			
1. World Total	96.5	88.4	8.1 (9.2)	16.8	17.9	-1.1 (-6.1)

Table 2. 11 continued

	NO_X emission		NO_y deposition		NH_3 emission		NH_X deposition	
	Non-coastal	Coastal	Non-coastal	Coastal	Non-coastal	Coastal	Non-coastal	Coastal
	Δ	Δ	Δ	Δ	Δ	Δ	Δ	Δ
3. North America	-0.1	-0.1	-0.4	-0.1	0.1	0.0	0.1	0.0
4. Europe	-0.4	-0.5	-0.3	-0.3	-0.6	-0.4	-0.4	-0.3
5. South Asia	2.4	0.0	2.1	0.2	3.0	-0.2	3.3	-0.1
6. East Asia	5.3	0.0	4.5	0.8	-1.6	-0.2	-1.3	-0.2
7. Southeast Asia	1.1	0.1	0.7	0.1	1.0	-0.1	1.1	-0.2
8. Australia	0.2	0.0	-0.1	0.0	-0.3	-0.1	-0.2	-0.2
9 North Africa	0.6	0.1	0.3	0.0	-0.2	0.0	-0.1	-0.1
10. Sub Saharan Africa	1.1	-0.1	0.3	-0.1	-1.5	-0.2	-1.3	-0.4
11 Middle East	0.9	0.2	0.6	0.1	-0.1	0.0	-0.1	-0.1
12. Central America	0.6	0.0	0.2	0.0	-0.3	-0.2	0.0	-0.2
13. South America	1.5	0.0	0.7	0.0	-0.3	-0.2	-0.3	-0.2
14. RBU	0.1	0.0	0.1	0.2	-0.7	-0.1	-0.7	0.0
15. Central Asia	0.2	0.0	0.1	0.0	-0.1	0.0	-0.1	0.0
17. Antarctic	0.0	0.0	0.0	0.0	0.0	0.0	-0.1	0.0
Continental	13.5	-0.4	8.9	0.9	-1.7	-1.8	-0.1	-2.0
2. Ocean	0.7		1.7		-0.7		-2.4	
1. World Total	14.2	-0.4	10.7	0.9	-2.4	-1.8	-2.6	-2.0

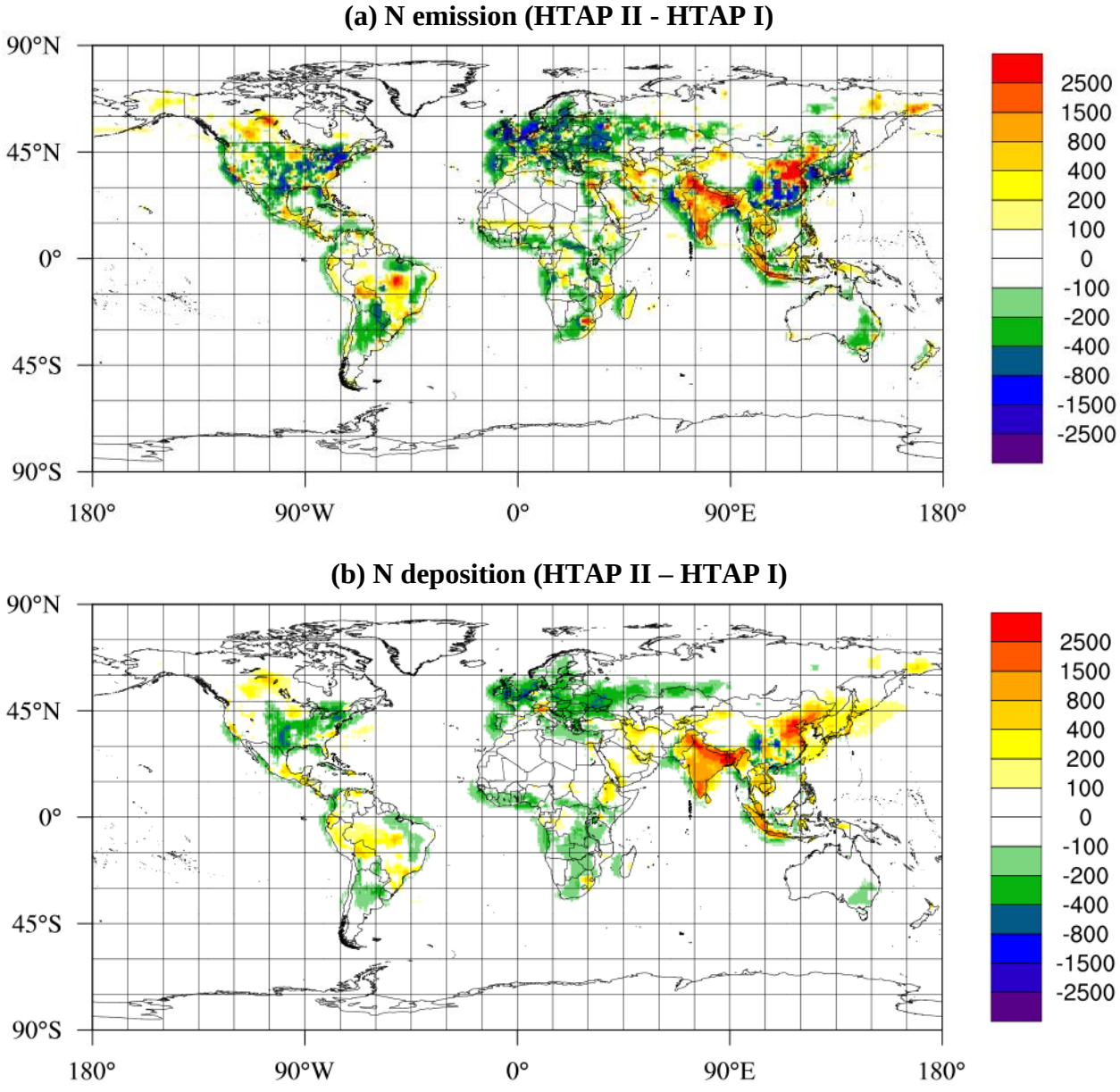

Figure 2. 12 Differences between MMM of HTAP II and HTAP I for (a) N emission (b) N Deposition. Unit: mg(N) m^{-2} yr^{-1}.

Changes in ratio of NH_x deposition to total (NH_x plus NO_y) depositions. The ratios of NH_x deposition in 2010 (HTAP II) are compared with those in 2001 (HTAP I) in Fig. 2.13. Generally, a 10% worldwide decrease of the ratio of NH_x deposition in found from 2001 to 2010. In particular, a 30% decrease is found in southeastern China, mainly due to the large increase in NO_x emission during the last decade. On the other hand, the ratio of NH_x deposition in California was 15-20% in 2001 and increases to 40-60% in 2010. The ratio in Alaska also increases from 30-40% to 50%. There is a generally 5-10% increase over the eastern US. This is consistent with an observed large increase of the NH_x depositions and decrease of NO_y depositions in northeastern U.S. from 1990s to 2010s (Du, de Vries, Galloway, Hu, & Fang, 2014; Y. Li et al., 2016). A possible explanation is that the implementation of emission control stretegies such as the Clean Air Act has resulted in a large reduction in NO_x emssions, which lowered the NO_y deposition in the U.S. (Lloret & Valiela, 2016). This benefit is compensated by increasing NH_x deposition because no limitation is implemented on NH_3 emission (Kanakidou et al., 2016; Y. Li et al., 2016). Some regions have small increases in the ratio of NH_x deposition, such as North EU (Norway) (5%), Southeast Asia (10%) and Western Australia (10%).

2.4.4 Problems and uncertainties

Multi-model ensemble approach. This approach has been widely used in recent studies to eliminate the 'random' errors from single model results. We find some problems when processing data from multiple models. We find that the total amounts of deposition of some models are much lower than the amounts of their emissions, which indicates that these models may not meet the mass balance for some species. Thus, a pre-check of model results is required before forming the multi-model ensemble to avoid "unreasonable" results of individual models. In this study, we allow a ±20% differences in the amounts between model inputs and outputs. But it is an arbitrary value and other studies may use more stringent/loose values. We also find that the depositions of some model might be inconsistent with those of majority of models (here we use mean of all models). We compare model results with each other and excluded the models with values away from MMM. However, this assumes that the results of majority models are more reasonable than single model.

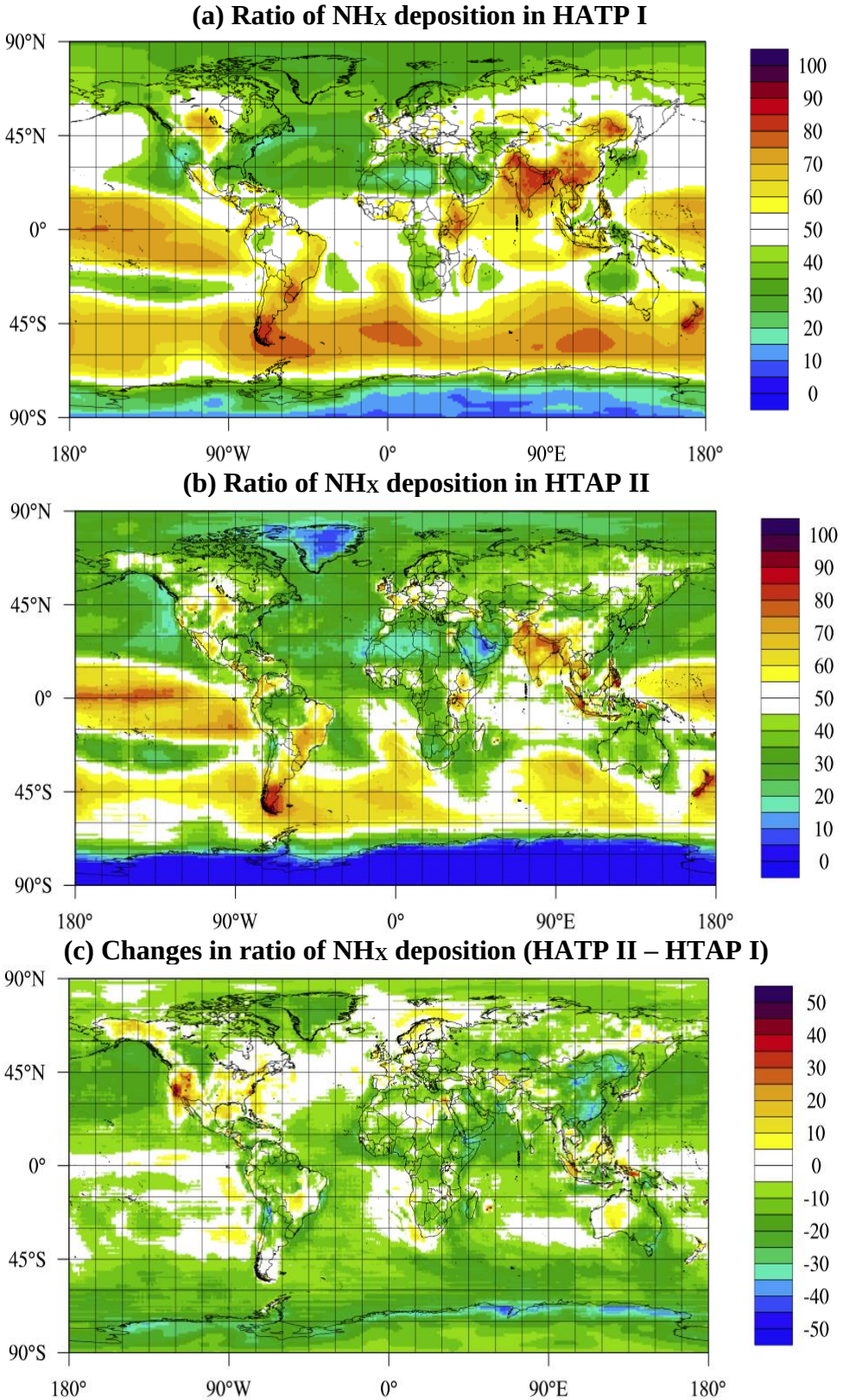

Figure 2. 13 Ratio of NHx deposition to N (NO_y + NH_x) deposition from MMM results of (a) HTAP 1 (b) HTAP II. (c) Changes from HTAP I to HTAP II (calculated as HTAP II – HTAP I). Unit: %.

Missing/underestimated species in model simulations. Most studies, include the present study, only evaluate the model performances on those species with regularly measurement data, such as wet deposition of inorganic species. Therefore, model performance on other components, such as the organic forms of nitrogen (ON), are still unknown and can be subjected to large uncertainty. Take deposition of organic nitrogen (ON) for instance. We plot the individual model results on ON in Fig 2.14. According to the definition of species in HTAP II, the deposition of ON was calculated as the sum of the depositions of PAN and Orgn. The blue bars indicate the global total amounts of ON deposition (wet + dry). The red markers indicate the percentages of ON deposition in total N deposition.

Predictions of the amounts of ON vary largely from 1 Tg yr^{-1} to 3.5 Tg yr^{-1} among different models. And the percentages of ON deposition in total N deposition range from 2% to 3.5%. The differences between models indicate model uncertainties in simulating the ON deposition. The MMM result of ON deposition is about 3 Tg(N) yr^{-1}, which accounts for 3% of total N deposition (5% of total NO_y deposition). But many measurement studies suggested much higher proportions (20-30%) of ON deposition (Laj et al., 2009; Neff, Holland, Dentener, McDowell, & Russell, 2002). The underestimation of the proportion of ON in total N deposition by models indicate possibility of underestimation of total N budgets in present work. Further study on the formation mechanism of ON in models is suggested.

Comprehensive model evaluation at global scale. We are unclear about the model performances in poorly observed regions. In this study, although we conduct an assessment over Asia with EANET observation network, most of the observation sites are located in Japan and Korea, whereas China and India are supposed to be the most heavily polluted regions in Asia. In addition, there is much more attention on the North Hemisphere than the South Hemisphere according to our review of previous studies. And the model performance in South America, Africa and Australia have not been fully studied. This issue can be solved by extending the current measurement network to these regions or using new datasets with better coverage and data availability for model evaluation such as satellite data.

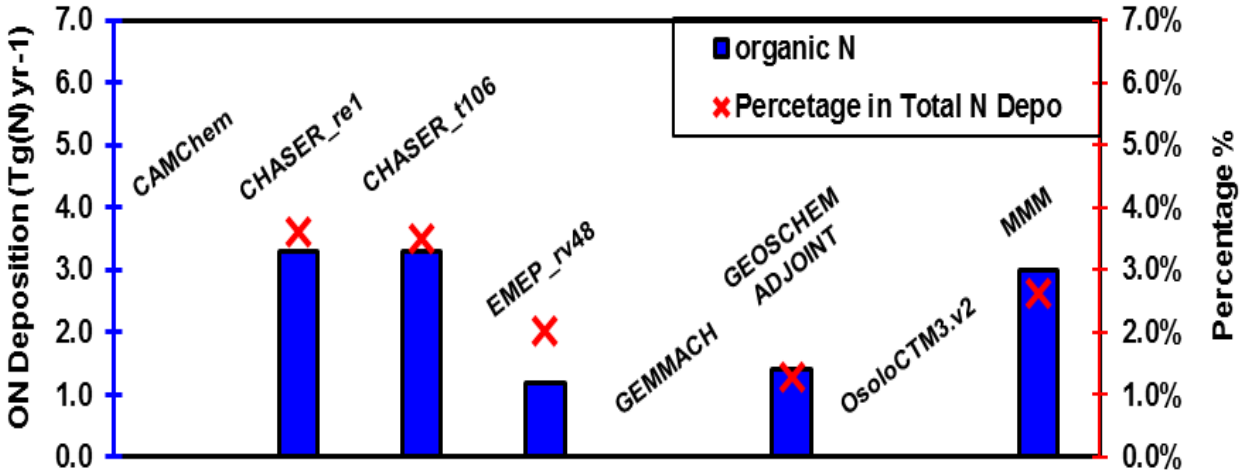

Figure 2. 14 Multi-model results of organic nitrogen deposition. The blue bar indicates the annual accumulated global total amounts of organic nitrogen deposition. The red mark indicates the proportional of organic nitrogen deposition in total nitrogen deposition.

2.5 Conclusion

The S and N depositions in 2010 are calculated with the ensemble results of eleven models from HTAP II. The model performance on wet deposition is evaluated with measurement networks of NADP over NA, EMEP over EU and EANET over EA. The modelled wet deposition compares favorably with the observations. About 76-83% of stations are predicted within ±50% of observations. For SO_4^{2-} wet deposition, stations in EA are underestimated by 20%, especially the 3 Chinese stations with high Ca^{2+} concentration. Because the limited number of Chinese stations and the locations couldn't cover the areas with highest deposition in China, it is hard to provide a comprehensive evaluation over this region. For NO_3^- wet deposition, about 20% positive model bias is generally found at stations in eastern US, while some European (Poland, Norway and Spain) and East Asian (in Southeast Asia) stations with high observed deposition are underestimated by about 60-70%. NH_4^+ wet deposition is generally underestimated in EU (especially Norway and Poland) and EA (especially RU and Korea). An inter-comparison with previous projects of PhotoComp, ACCMIP and HTAP I show that the model accuracy in predicting wet deposition of S and N has been significantly improved in HTAP II, especially at the European and East Asian stations. In terms of dry deposition, model results are compared with the inferential data from CASTNET in NA. The MMM results are generally higher than the inferential data by 50-170%, which has been reported in ACCMIP and HTAP I studies.

The amounts and intensities of S and N depositions are calculated over lands, costal zones and open oceans. The global S deposition is 84 Tg(S) in 2010, with 49% deposits on continental non-coastal regions, 32% deposits on non-coastal oceans and 19% deposits on coastal regions. The global N deposition is 113 Tg(N) in 2010, of which 59 Tg(N) is NO_y deposition and 64 Tg(N) is NH_x deposition. About 65% of N is deposited on the continental non-coastal regions and 35% is on oceans (including 15% on coastal regions). For continental regions, high S deposition is found in Asia regions (EA, SA and Southeast Asia), U.S. Midwest, Central America and Eastern EU. For N deposition, high deposition is also identified in the above-mentioned regions plus the Sub Sahara Africa and Brazil. For coastal regions, the east coast of Asia, all coasts of India and Malaysia and east coast of U.S. are seen with relatively high S and N depositions. According to our estimation, about 4 Tg(S) of S deposition and 18 Tg(N) of N deposition are exported from land to ocean, including 0.3 Tg(S) and 4 Tg(N) on coastal regions.

The deposition in HTAP II for 2010 are compared with that in HTAP I for 2001. The S deposition decreases 2 Tg(S) from 2001 to 2010, with significant decreases in EU (5 Tg(S)), NA (3 Tg(S)) and RU (2 Tg(S)) and increases in SA (2 Tg(S)) and the ME (1 Tg(S)). EA doesn't have large net changes in its S deposition due to increased S emission from 2001-2005 and a continuous reduction of S emission starting from 2006 owing to the SO_2 control policies in China's 11^{th} FYP. The N deposition increases by 7 Tg(N). The increased N emissions from SA (5 Tg(N)), EA (4 Tg(N)) and Southeast Asia (2 Tg(N)) lead to identical amounts of elevation in deposition in the corresponding regions. We also compare the ratio of NH_x deposition to total N deposition between HTAP I and HTAP II. The ratio has increased in some regions of NA, especially in California (~20%), Alaska (~10%) and the eastern U.S. (5-10%), which agrees well with recent observational and modelling studies. A small increase in the ratio of NH_x deposition is found in North EU (Norway) (5%), Southeast Asia (10%) and Western Austrilia (10%). On the other hand, NO_y deposition starts to dominate in EA (especially China) due to increased NO_x emission in recent years.

This study updates the knowledge about the global S and N depositions in 2010, as an update to the previous studies focusing on the early 2000s. The global distributions of S and N depositions have changed considerably during the last ten years, with decreases in NA and EU and increases in Asian regions. Further studies are proposed to understand how these changes could affect the source-receptor relationship on deposition between continents and the impacts on the ecosystems.

CHAPTER 3
EFFECTS OF EMISSION CONTROL ON REDUCING NITROGEN DEPOSITION

A version of this chapter has been submitted as a scientific paper titled “Is Ammonia Emission Abatement an Efficient Way to Control Reduced Form of Nitrogen Deposition?” coauthored by Jiani Tan, Joshua S Fu and John H. Seinfeld.

Statement: J.T. and J.-S.F. design the study. J.T. collected and analyzed the data. J.-S.F. provided the financial support for the project. J.T. created the initial draft. J.-S.F. and J.-H.S. reviewed and edited the manuscript.

3.1 Abstract

Human activities and population growth have increased the natural burden of Nitrogen (N) in the environment. The excessive N deposition on earth’s surface leads to adverse feedbacks on ecosystems and humans. Prevention of excessive N deposition is a crucial component of a sustainable future. Similar to that of air pollution, emission control is recognized as an efficient means to control acid deposition. Control of nitrogen oxides (NO_x = NO + NO_2) emissions has led to reduced deposition of oxidized nitrogen (NO_y, the sum of all oxidized nitrogen species, except nitrous oxide (N_2O)). Reduced forms of nitrogen (NH_x = ammonia (NH_3) + ammonium (NH_4^+)) deposition have, otherwise, increased, offsetting the benefit of reduction in NO_y deposition. Stringent control of NH_3 emissions is being considered. In this study, we assess the effectiveness of NH_3 emission control on reducing NH_x deposition. We show that significant reduction of NH_x deposition is unlikely to be achieved at the early stages of implementing control strategies on NH_3 emissions, owing to the current atmospheric level of NH_3. Effectiveness of NH_3 emission abatement on control of NH_x deposition is shown to range from 60% to 80%, which is significantly lower than the demonstrated 80-120% benefit of controlling NO_x emissions on NO_y deposition.

3.2 Introduction

Atmospheric deposition is a principal pathway for the exchange of nitrogen (N) between earth cycles. Elevated N deposition on earth’s surface has occurred, due to increasing human

consumption of energy. Global total N deposition is estimated to have increased from 51 Tg(N) yr^{-1} in 1850 (Kanakidou et al., 2016) to 101-123 Tg(N) yr^{-1} in the 2000s (Kanakidou et al., 2016; Lamarque et al., 2013; Lamarque et al., 2005; J. N. Tan, Fu, Dentener, Sun, Emmons, Tilmes, Sudo, et al., 2018; Vet et al., 2014), with estimates of continuing growth in the near future (Bleeker et al., 2011; Kanakidou et al., 2016; Lamarque et al., 2013; Lamarque et al., 2005; Paulot et al., 2013). Nature responds when the loading of N deposition exceeds certain thresholds (so called critical load (CL), defined as the highest load that the ecosystem can bear before the occurrence of long-term harmful impacts on the most sensitive ecological elements (Nilsson, 1988)). It is estimated that about 11% of the world's natural vegetation has exceeded CL for N deposition (Dentener et al., 2006). In the US, N deposition over 10-15% of forest soils (McNulty, Cohen, Myers, Sullivan, & Li, 2007; J. Sun et al., 2017) and 24 out of 45 national parks (Ellis et al., 2013) has exceeded critical loads. Response to excessive N deposition is mainly exhibited by eutrophication and acidification of terrestrial and aquatic ecosystems (A. F. Bouwman et al., 2002; Duce et al., 2008; Galloway et al., 2008; T. W. Kim et al., 2011). The well-studied influences are damage and toxicity to vegetation and soil systems (Janssens et al., 2010), impact on natural dominant species (Bobbink et al., 2010; Stevens et al., 2011), and even loss of ecosystem biodiversity (Clark & Tilman, 2008). Therefore, prevention of excessive atmospheric N deposition is of vital importance in the protection of a sustainable ecosystem and in avoiding irreversible future damages.

Atmospheric emissions and climate change are the major drivers of future N deposition (Dentener et al., 2006; Lamarque et al., 2013). Implementation of emission control strategies and associated policies is an effective avenue to reduce acid deposition (Tagaris et al., 2008; J. X. Zhang et al., 2019). Moreover, the main components of N deposition have been changing over time. In the US, for example, oxidized nitrogen (NO_y, sum of all oxidized nitrogen species except N_2O) deposition, a result of nitrogen oxides (NO_x, NO plus NO_2) emissions from combustion, has been less and less a public issue since implementation of the Clean Air Act (CAA) in the 1970s. Recent studies have raised attention to the rapid growth of deposition of reduced forms of nitrogen (NH_x, NH_3 plus NH_4^+) (Y. Li et al., 2016), owing to lack of constraints on ammonia (NH_3) emissions.

NH_x deposition results from wet deposition (precipitation) and dry deposition (driven by gravity) of gaseous NH_3. Few studies have examined the benefit of reducing NH_3 emissions on NH_x deposition, whereas studies have investigated the effectiveness of NH_3 emission abatement on reducing fine particle levels (Robert W. Pinder et al., 2007). However, the actual efficiency of reducing fine particle levels has been lower than expectation (H. Y. Guo et al., 2018; Holt et al., 2015; R. W. Pinder et al., 2008), as a result of the fact that conversion between NH_3 gas and NH_4^+ particulate matter is highly dependent on the presence of acid components in aerosols such as SO_4^{2-} and NO_3^-, since NH_4^+ is the main alkali neutralizer to balance aerosol pH. The same situation is likely to arise associated with the control of NH_x deposition.

Here, we estimate the effectiveness of controlling NH_3 emissions as a means to reduce NH_x deposition. This study was motivated by a comparison with the benefit of NO_x emission abatement on reducing NO_y deposition. We first review the consistency between the temporal trends (2000-2017) of NH_3 emissions, NH_x deposition and NO_2 ambient concentrations over the conterminous U.S. (CONUS) based on both national and site measurement data. Then we quantify the effectiveness of controlling NH_3 emissions on NH_x deposition via modelling analysis of emission control scenarios.

3.3 Methods

3.3.1 Site measurement of deposition and air concentration

Site observations of wet NO_3^- deposition and wet NH_4^+ deposition were provided by the National Trends Network (NTN) of the National Atmospheric Deposition Program (NADP) (http://nadp.slh.wisc.edu/NTN/). NTN measured the precipitation chemistry, including precipitation amount and concentrations of free acidity H^+, conductance, calcium, magnesium, sodium, potassium, sulfate, nitrate, ammonium and chloride, at 373 sites located throughout the entire U.S. (Fig. 3.1) from 1980s until present day. This study used the annual accumulated wet deposition data from 244 sites with available data in the study period over nine climate regions (Table 3.1) defined by the National Centers for Environmental Information (https://www.ncdc.noaa.gov/monitoring-references/maps/us-climate-regions.php). The sites were

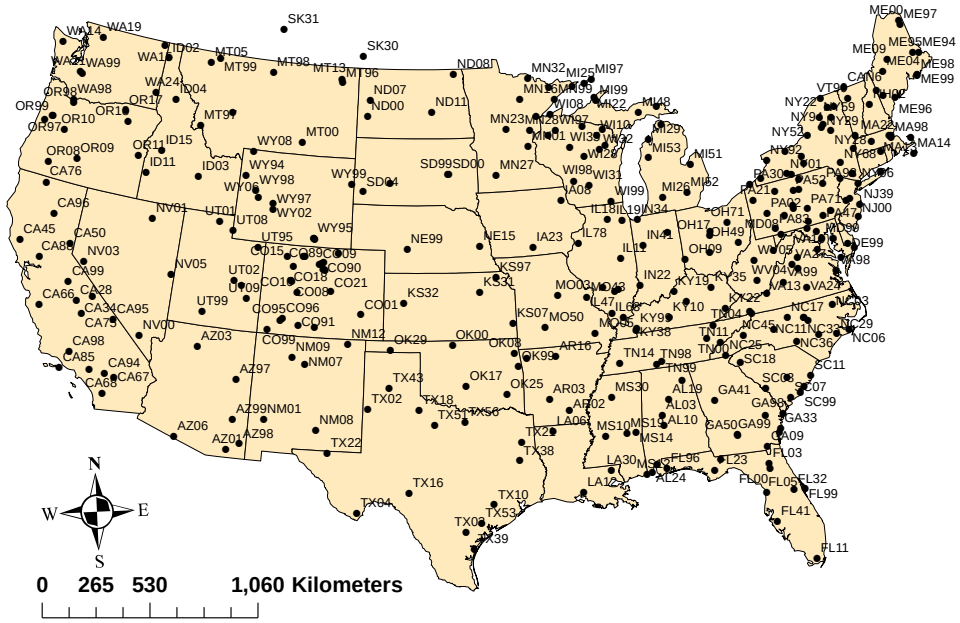

Figure 3. 1 Location of NADP sites for wet deposition over CONUS.

Table 3. 1 Numbers of sites in each region. Insufficient NO_2 observation exist in the Northwest.

Number of sites	AQS sites for NO_2 air concentration	NADP sites for N wet deposition
Central	12	31
Northeast	25	36
Northwest	-	15
Rockies	6	22
South	36	25
Southeast	14	37
Southwest	10	31
Upper Midwest	2	32
West	48	15
Total	153	244

located away from urban and point pollution sources. Samples were collected weekly in wet deposition collectors and shipped in bottles to the Illinois State Water Survey at the University of Illinois at Urbana-Champaign (before March 1, 2018) and the Central Analytical Laboratory at the Wisconsin State Laboratory of Hygiene (after March 1, 2018). The data quality has been checked with the NTN procedures and documentation (http://nadp.slh.wisc.edu/lib/qaReports.aspx).

Site observations of airborne NO_2 concentrations were provided by Air Quality System (AQS). Monitoring Network of U.S. EPA (https://www.epa.gov/air-trends/nitrogen-dioxide-trends). AQS observed the airborne concentrations of CO_2, PM, NO_2, O_3 and SO_2 at 153 sites over U.S. (Fig. 3.2 and Table 3.1). The Ammonia Monitoring Network (AMoN) of NADP (http://nadp.slh.wisc.edu/AMoN/) can provide airborne NH_3 concentrations for 50 sites beginning in 2007, but the numbers of sites in regions are much less than those of N deposition and NO_2 air observation. Thus, this dataset was not used in this study, but will be considered in future studies.

3.3.2 Annual gradient maps of deposition

The spatial distributions of NO_y and NH_x deposition were developed by the Total Deposition Science Committee (TDEP) of NADP by spatial interpolation of quality-controlled observation sites with model simulation (http://nadp.slh.wisc.edu/NTN/maps.aspx). Maps were available from 1985 to 2017. The quality and uncertainty associated with these maps have not been fully evaluated, an uncertainty that may affect the interpretation of the results.

3.3.3 Emissions

NO_x and NH_3 emissions were provided by U.S. EPA's National Emissions Inventory (NEI) (https://www.epa.gov/air-emissions-inventories/national-emissions-inventory-nei). Annual emissions at the country scale were available during 2000-2014. Annual emissions of individual states were only available for years 2002, 2005, 2008, 2011 and 2014. Contiguous emissions for other years were calculated by linear interpolation of country-scale data. We compared this emission dataset with site observations of wet deposition and air concentration. Comparability was

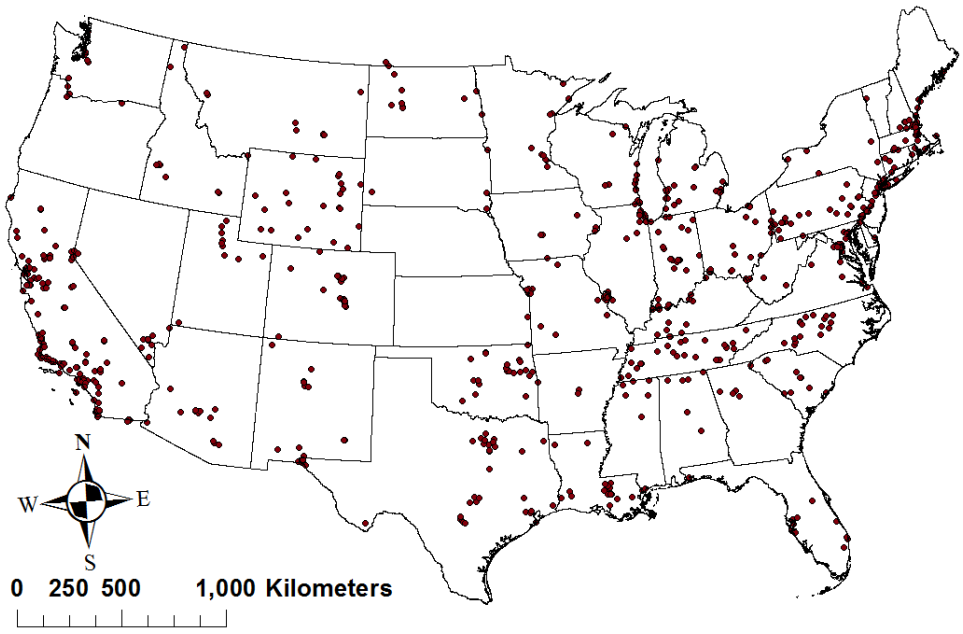

Figure 3. 2 Location of AQS sites for NO_2 air concentration over CONUS.

subject to the extent to which the NADP sites were more or less evenly located. In this regard, stations in western and central U.S. tended to be more scattered than those in the eastern U.S. (Figs. 3.1-3.2 and Table 3.1). Further analysis with more observation data is suggested for these regions. Spatial distributions of emissions were obtained from the Emissions Database for Global Atmospheric Research (EDGARv4.3.2) (http://edgar.jrc.ec.europa.eu/overview.php?v=432). Spatial resolutions of both NO_x and NH_3 emissions were 0.1 × 0.1 degree (~11.1 km × 11.1 km). The EDGAR emissions over CONUS were developed based on information from U.S. EPA NEI (Crippa et al., 2018).

3.3.5 Emission control scenario and calculation of effectiveness

Following Eqs. *(3-1)* - (*3-3)* showed the calculation of the effectiveness of emission control on deposition.

$$\Delta Emis_{NO_x\ or\ NH_3} = \frac{Emission_{NO_x\ or\ NH_3}(Control\ Case) - Emission_{NO_x\ or\ NH_3}(Base\ Case)}{Emission_{NO_x\ or\ NH_3}(Base\ Case)} \quad (3\text{-}1)$$

$$\Delta Depo_{NO_y\ or\ NH_x} = \frac{Deposition_{NO_y\ or\ NH_x}(Control\ Case) - Deposition_{NO_y\ or\ NH_x}(Base\ Case)}{Deposition_{NO_y\ or\ NH_x}(Base\ Case)} \quad (3\text{-}2)$$

$$Effectiveness_{NO_y\ or\ NH_x} = \frac{\Delta Deposition_{NO_y\ or\ NH_x}}{\Delta Emission_{NO_x\ or\ NH_3}} \quad (3\text{-}3)$$

where $\Delta Emis_{NOx\ or\ NH3}$ is the percentage change of emission under emission control. $\Delta Depo_{NOx\ or\ NH3}$ is the percentage change of deposition (wet plus dry) under emission control. $Effectiveness_{NOy\ or\ NHx}$ is the effectiveness of NO_x (NH_3) emission control on NO_y (NH_x) deposition.

In the base case, the models used the HTAPv2.2 emission inventory (Chapter 2). In the emission control scenario, the models used a modified emission inventory with 20% reduction in the anthropogenic emissions of North America, including SO_2, NO_x and NH_3, and emissions in other world regions maintained the same as the base case. The 20% reduction in anthropogenic emissions was considered as a reasonable and practical target for an emission control strategy. Note that since only anthropogenic emissions were reduced by 20% and natural emissions kept the same, the $\Delta Emis_{NOx\ or\ NH3}$, which included changes in both anthropogenic and natural emissions, was lower than 20% (Fig 3.3). Since the same meteorology fields and model parameters were used

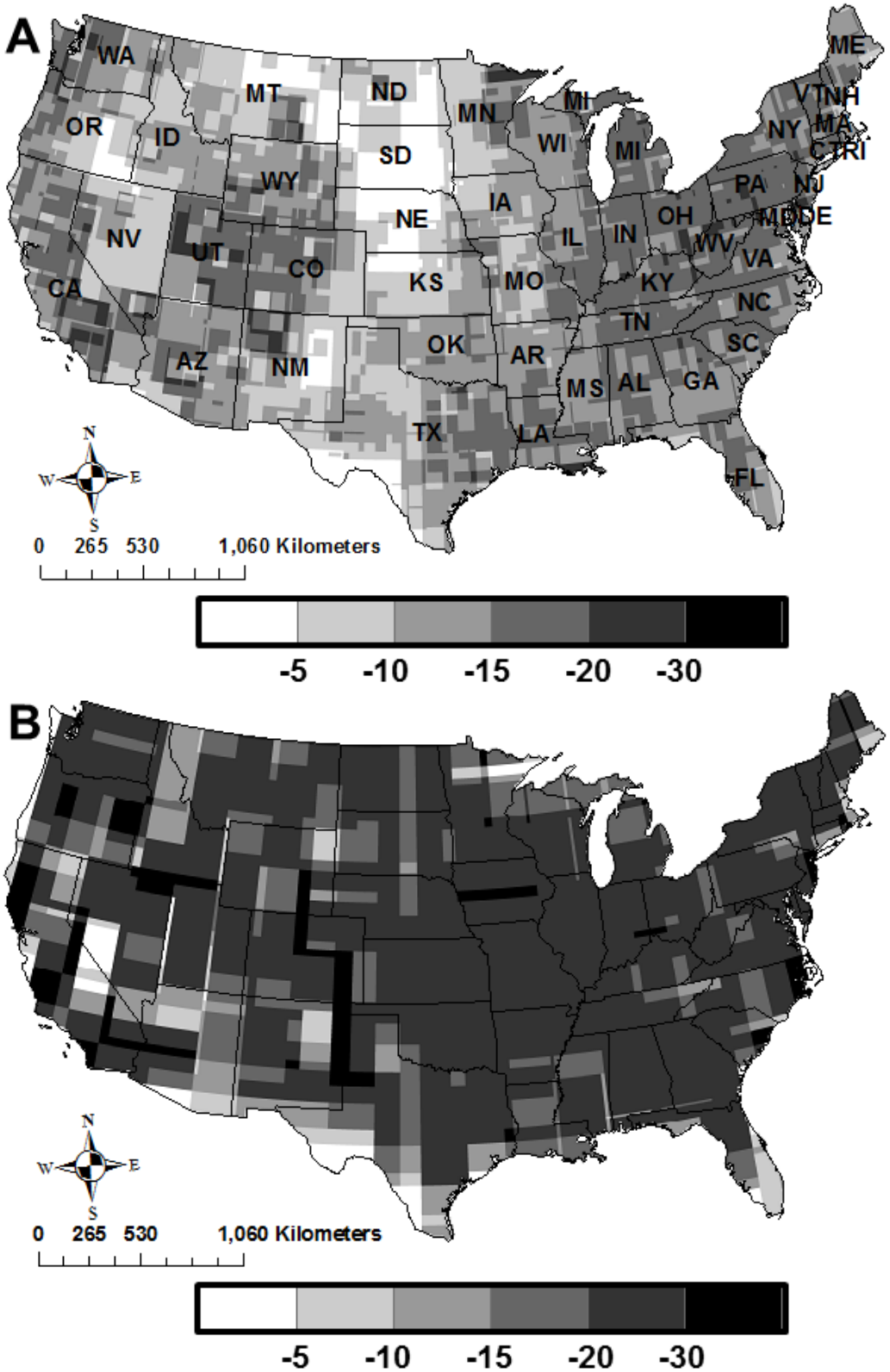

Figure 3. 3 Percentage changes of (A) NO_x emissions and (B) NH_3 emissions in the emission control scenarios (%).

in the base case and control scenarios, emission change was the main factor that contributed to the variation of deposition.

3.4 Results

3.4.1 Temporal trends of N emissions and N wet deposition

We analyzed the temporal trends of N wet deposition, N emissions and NO_2 air concentrations for measurement data in eight CONUS regions from 2000 to 2017 (Fig. 3.4). NO_3^- and NH_4^+ wet deposition and NO_2 air concentrations are annual values averaged from all sites in the regions. NO_x and NH_3 emissions are state-level values derived from NEI. NO_x emissions (Fig. 3.4B, red lines) peaked in 2002 in all CONUS regions, with amounts dropping by 10% each year following for all regions, except the Northern Rockies and Plains (Rockies) and Southwest. This reduction of NO_x emissions, associated with the implementation of the CAA since the 1970s, was reflected in the reduction of NO_2 levels (Fig. 3.4B, red ×'s). NO_3^- wet deposition (Fig. 3.4B, red bars) also started to decrease after 2002 in all regions, although levels in all regions did not decrease at the same rate. For instance, it took seven years for the Rockies to show a significant decrease of NO_3^- wet deposition, while clear and rapid (1-2 years after 2002) responses occurred in the Upper Midwest, Northeast, South and Central U.S. The response times between decreases of NO_x emissions and decrease of NO_y wet deposition were associated with the effectiveness of emission reductions. Overall, clear consistency existed between temporal trends of NO_x emissions and NO_y wet deposition in all CONUS regions.

The relationship between NH_3 emissions and NH_x wet deposition, on the other hand, was considerably more complex than that between NO_x emissions and NO_y wet deposition. For example, a decrease in NH_4^+ wet deposition occurred during an increase of NH_3 emissions during 2004-2012 in the Upper Midwest (Fig. 3.4(c)). Also, with continuously decreasing NH_3 emissions after 2006 (Fig. 3.4B(d)), the Northeast was still experiencing increases in NH_4^+ wet deposition after 2011. Generally, it was difficult to establish a clear relationship between the trends of NH_3 emissions and NH_x wet deposition.

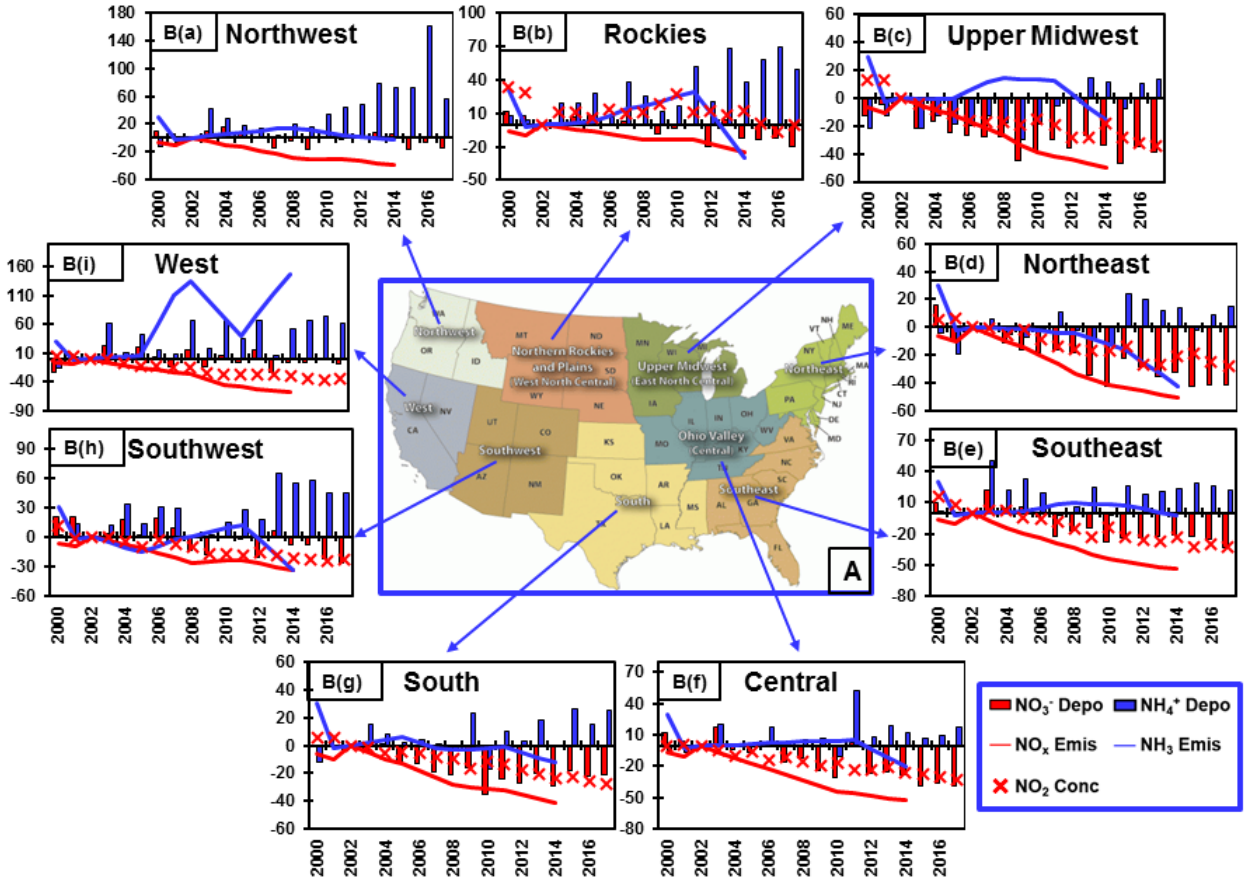

Figure 3. 4 Trends of annual N emissions and N deposition over nine CONUS regions from 2000 to 2017. (A) Definition of the nine CONUS regions in this study. (B(a)-(i)) Percentage changes of N emission, NO_2 concentration and N deposition in regions (unit: %). The percentage changes were calculated based on 2002 level, calculated as 100 × [Emissions of target year – Emissions of 2002] / [Emissions of 2002].

Considering the relationship between N emissions and N wet deposition (Fig. 3.5), the temporal changes of NO_3^- wet deposition exhibited strong and positive linear correlations with those of NO_x emissions for several regions, such as the U.S. Northeast, Central and South (Fig. 3.5A) and the correlations (R values) between these trends (Fig. 3.5C, green bar) were about 0.8 in these regions. For NH_3 emissions and NH_4^+ wet deposition (Fig. 3.5B), the correlations were either unclear (most CONUS regions) or weakly negative (Upper Midwest), and R values between the trends were low (Fig. 3.5C, blue bars). We then explored possible explanations for this uncertain relationship.

3.4.2 Spatial changes of N emissions and N deposition

We plotted the spatial distributions of percentage changes of N emissions and N deposition (wet + dry) from 2001 to 2010 (Fig. 3.6). The annual maps of N deposition were developed by combining the site observation data with deposition fields simulated by a chemical transport model. NO_x emissions (Fig. 3.6A) were reduced by about 15-30% over CONUS, with slight increases in some regions such as MT and NV states. Responses of NO_y deposition (Fig. 3.6B) were generally consistent with the changes of NO_x emissions in both amount and distribution.

Concerning NH_3 emissions and NH_x deposition, NH_3 emissions (Fig. 3.6C) increased by 10-30% over CONUS from 2001 to 2010, whereas NH_x deposition (Fig. 3.6D) exhibited mixed responses in different states. Increased NH_x deposition occurred only in regions with increased NO_y deposition (Fig. 3.6B, contours with yellow and orange) and increased S deposition (Fig. 3.7), despite a nation-wide increase in NH_3 emissions (Fig. 3.6C).

Changes in NH_4^+ wet deposition were strongly influenced by the acidic components of wet deposition (mainly SO_4^{2-} and NO_3^-), since NH_4^+ is the main alkali neutralizer. Thus, in regions with decreased NO_y deposition, only a portion of the increased NH_3 emissions partitioned to the aerosol phase (NH_4^+). Once NH_3 emissions are controlled, the remaining NH_3 in the atmosphere will be converted to the NH_4^+particle phase as the aerosol becomes more acidic (Weber, Guo, Russell, & Nenes, 2016).

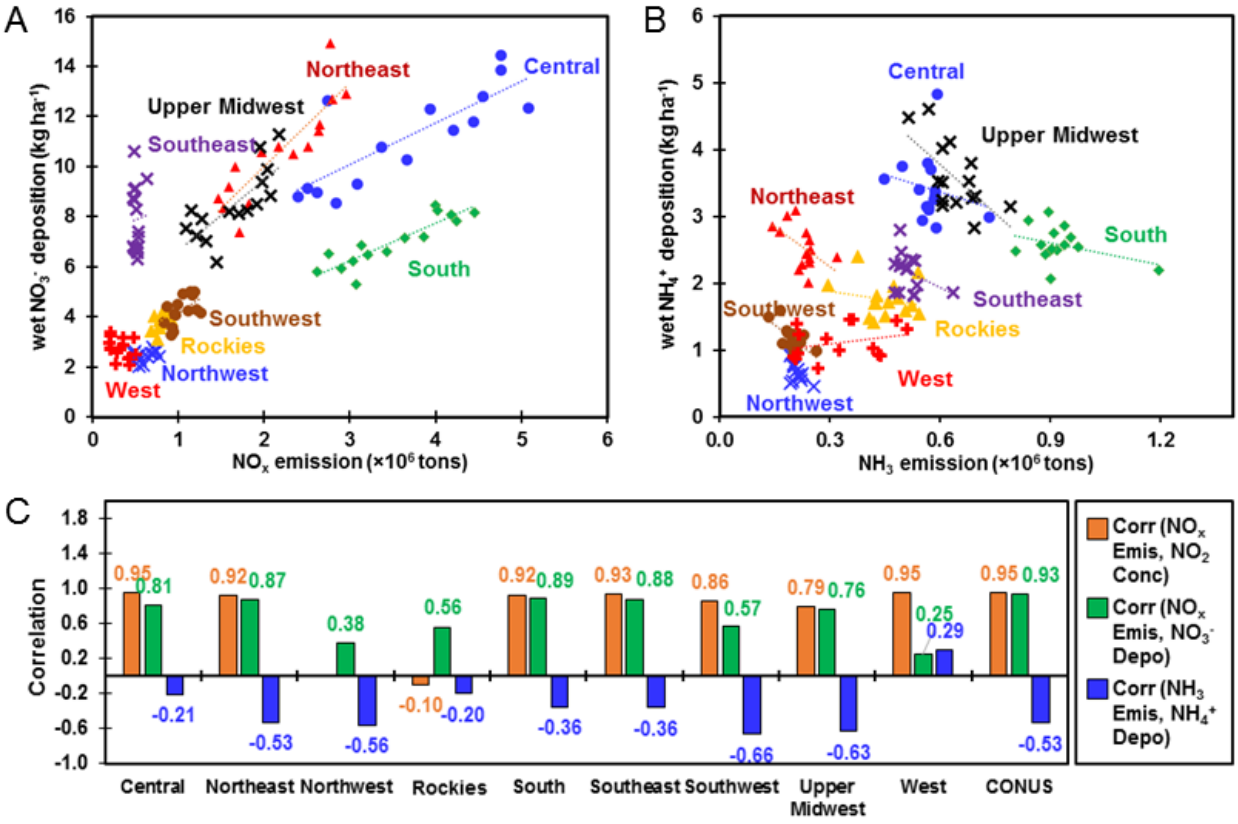

Figure 3. 5 Relationships between N emissions and N deposition. Scatter plots of regional emissions with deposition for (A) NO_x emission and NO_3^- wet deposition (B) and NH_3 emission and NH_4^+ wet deposition from 2000 to 2014 for nine CONUS regions. (C) Correlations between NO_x emissions and NO_2 concentration (orange bars), between NO_x emissions and NO_3^- wet deposition (green bars), and between NH_3 emissions and NH_4^+ wet deposition (blue bars). Northwest lacked sufficient NO_2 observations.

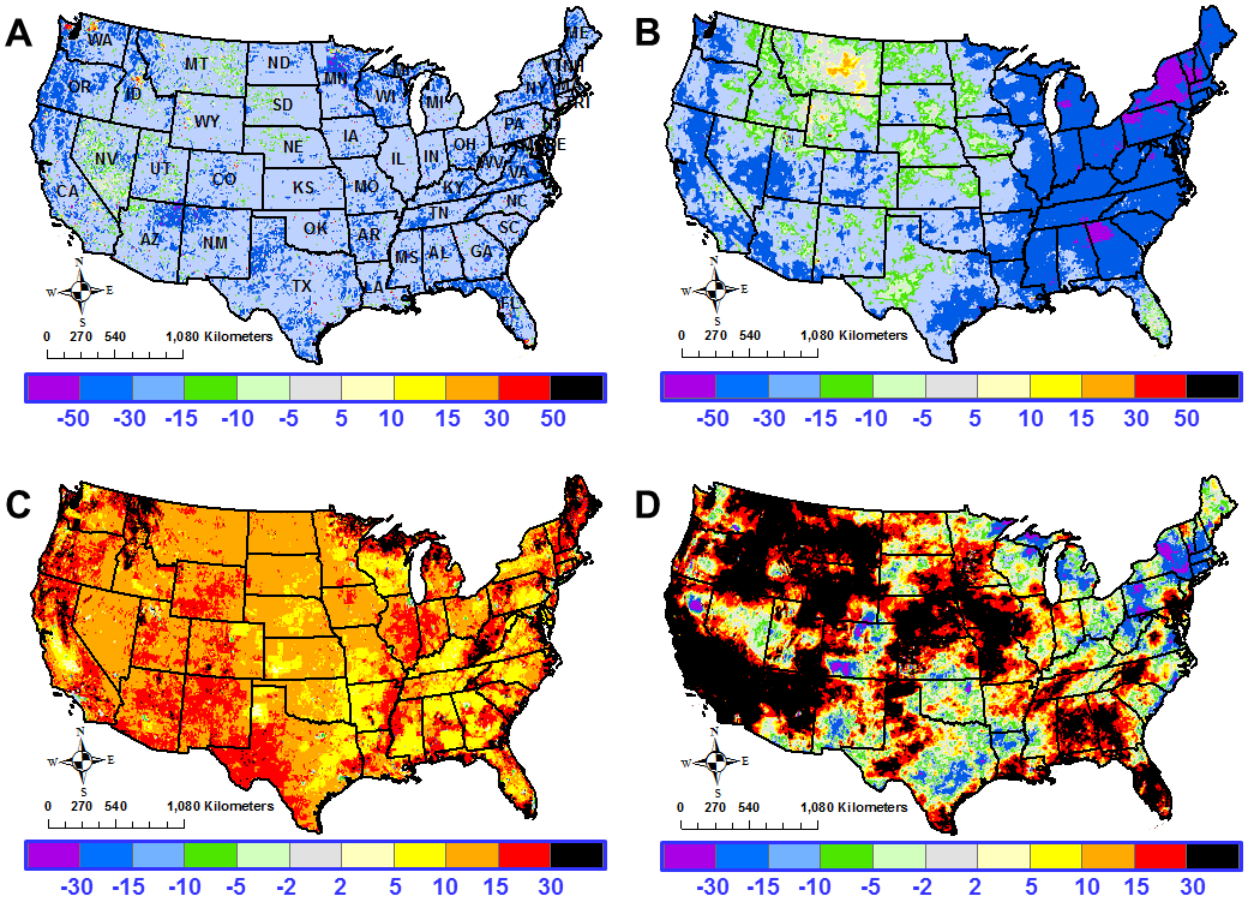

Figure 3. 6 Spatial distributions of the percentage changes of N emissions and deposition from 2001 to 2010. Percentage changes of (A) NO_x emissions (B) NO_y deposition (C) NH_3 emissions (D) NH_x deposition (unit: %). The percentage changes were calculated as 100 × [Emission of 2010 – Emission of 2001] / Emission of 2001.

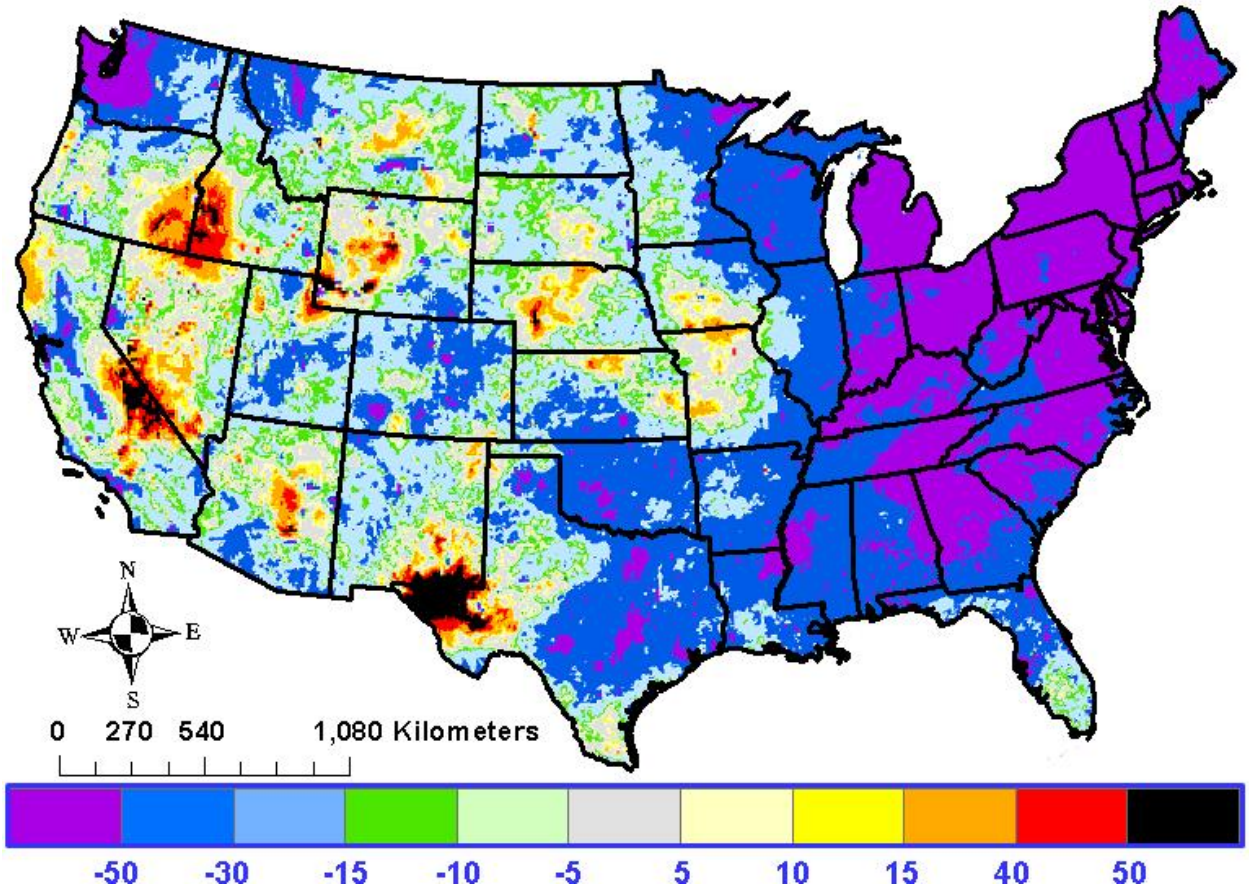

Figure 3. 7 Percentage change of S (wet + dry) deposition from 2001 to 2010 (calculated as [2010] - [2001]) / [2001] × 100%) (Unit: %). Spatial distributions of deposition were interpolation maps from NADP site observation (see Methods).

3.4.3 Effectiveness of N emission abatement on controlling N deposition.

We calculated the effectiveness of emission control on reducing deposition by Eq. *(3-3)*. Note that high effectiveness values (around 100%) were considered as cost-effective. The effectiveness of controlling NO_x emissions on reducing NO_y deposition ($Effectiveness_{NOy}$) (Fig. 3.8A) ranged from 80% to 120% over most CONUS regions (the ±20% variation around 100% could be a result of meteorological factors such as precipitation and long-range transport, which agreed with findings from HTAP-II simulations (J. N. Tan, Fu, Dentener, Sun, Emmons, Tilmes, Flemming, et al., 2018), and can be viewed as potential impacts of long-term climate change). Some areas in MT, SD and NE exhibited extraordinary values (~200%) (Fig. 3.8A, rust color), owing to very low (<5%) reduction rates of NO_x emissions (thus the denominator of Eq. (1) was close to zero) (Fig. 3.3A). Overall, the average $Effectiveness_{NOy}$ was very close to the ideal value of 100%, which indicates that a "full" control benefit can be expected on the application of NO_x emission control policies.

The effectiveness of controlling NH_3 emissions on NH_x deposition ($Effectiveness_{NHx}$) (Fig 3.8B) on most CONUS regions ranged from 60% to 80%. Gaseous NH_3 is removed mainly by atmospheric moisture, surface water, and dry deposition from the atmosphere, with minor consumption in slow oxidation of NH_3 by OH radicals in the atmosphere (Renard, Calidonna, & Henley, 2004). Spatial distributions of the effectiveness were more consistent among nearby regions for NH_x deposition (Fig. 3.8B) than NO_y deposition (Fig. 3.8A), since NO_x can be transported over long distance via reservoir species such as peroxyacetylnitrate (PAN) (J. N. Tan, Fu, Dentener, Sun, Emmons, Tilmes, Flemming, et al., 2018). The 20-40% shortfall to the "full" effectiveness indicates that additional reduction of NH_3 emissions should be considered to reach the control target for NH_x deposition.

3.5 Discussion and Implications

The present work shows a strong connection between NO_y wet deposition and NO_x emissions, whereas no clear relationship exists between NH_3 emissions and NH_x wet deposition. NH_x wet deposition, as the main alkali neutralizer in precipitation, is tied to pH values and the availability

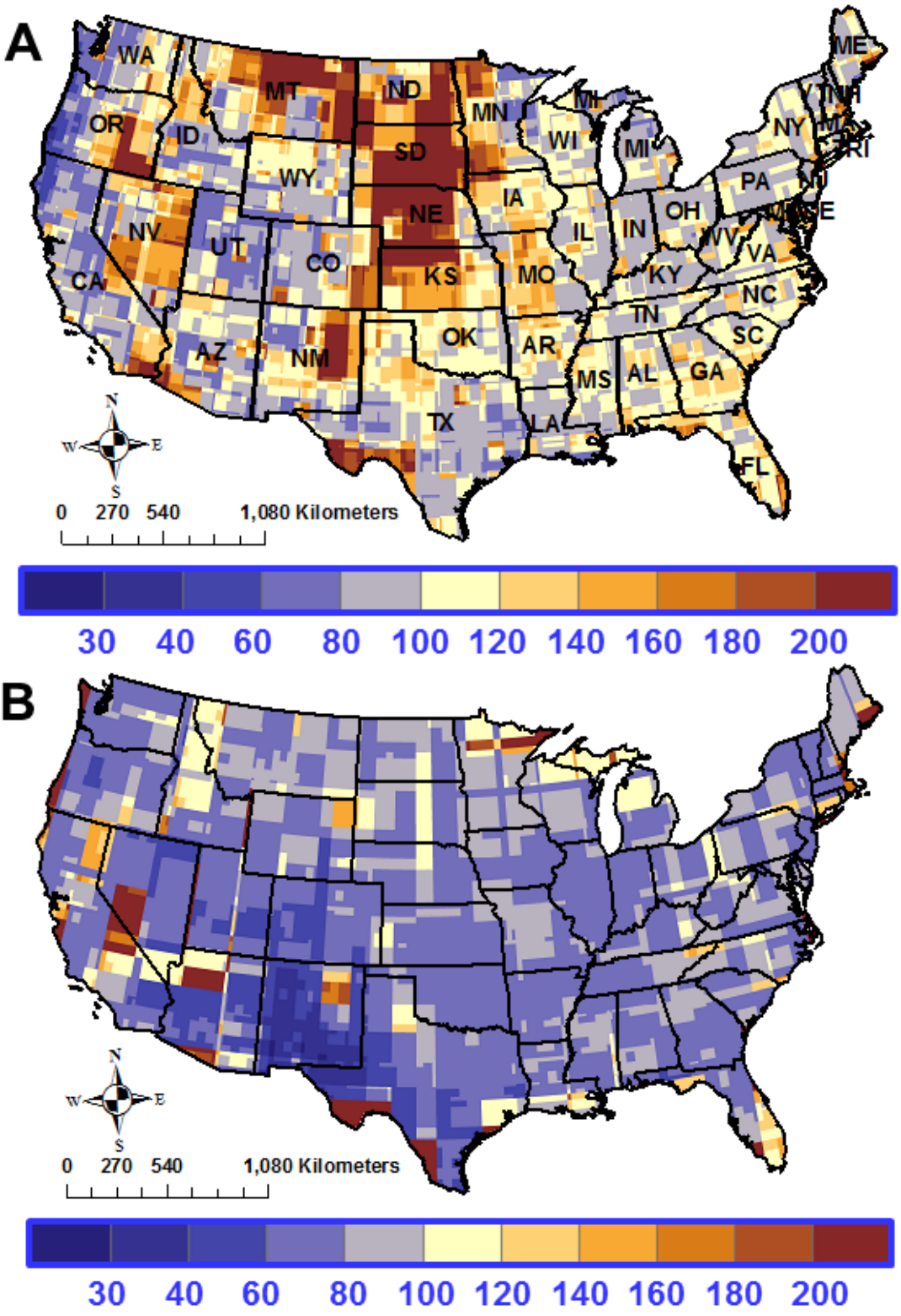

Figure 3. 8 Predicted effectiveness of controlling N emissions on N deposition (wet plus dry) in 2010. (A) Effectiveness of controlling NO_x emissions on NO_y deposition. (B) Effectiveness of controlling NH_3 emissions on NH_x deposition. See Methods for the calculation of effectiveness.

of acidic compounds such as NO_3^- and SO_4^{2-} in precipitation. Control of NH_3 emissions, hence reduction of NH_3 air concentration, would result in decrease of NH_3 in precipitation, according to the vapor-liquid equilibria of the ammonia-water system. As precipitation becomes more acidic, more NH_3 will be partitioned to NH_4^+, thus the amounts of NH_4^+ ions would not decrease linearly as NH_3 emissions decrease.

This "buffering effect" prevents the occurrence of significant reduction of NH_x in wet deposition at the beginning of NH_3 emission abatement. This is similar to the response of NH_4^+ aerosol to NH_3 emission reduction (H. Y. Guo et al., 2018), where the "buffering effect" persists until the aerosol pH is reduced to < 3, with a 60% reduction of NH_3 emission. After that, the amount of NO_3^- and NH_4^+ ions in aerosol dropped sharply due to loss of particle water. This "buffering effect" is responsible for a relatively small change in aerosol pH (0-2) over 15 years (1998-2014) in the U.S. despite an almost 70% decrease of SO_4^{2-} in aerosols (Weber et al., 2016). This also means that the sensitivity of NH_x deposition to NH_3 emission abatement would become weaker under a less acidic environment resulting from decreased NO_x and SO_2 emissions, since additional decrease in the prevailing pH value is needed to reach the effective turning point.

Therefore, significant reductions of NH_x deposition are not likely to emerge in the early stage of the implementation of NH_3 emission control policies. Our modelling results estimate that a 60-80% reduction of NH_x deposition can be achieved per unit of NH_3 emission control, considerably lower than the "full" (100% with ±20% variations due to impacts from meteorological factors) benefits of controlling NO_x emissions on reducing NO_y deposition. It should be noted that we controlled 20% of the anthropogenic emissions in the emission control scenario, as a reasonable amount to attain significant changes, and at the same time an affordable target for emission reduction policy. A recent study in China (M. X. Liu et al., 2019) reported that 50% reduction in NH_3 emission would result in significant changes in $PM_{2.5}$ (11-17%) and NH_x deposition (value not shown). This changed the precipitation pH by about 0.1-1 units, but the lowest pH (~4.4) was still > 3. Therefore, the "buffering effect" may still exist and affect the control effectiveness.

Since the management of NH_x deposition is highly likely to be a focus for many regions in the near future, this "weakened" effectiveness needs to be taken into consideration when

developing control strategies for NH_3 emissions. The results of the present case study for the U.S. are likely applicable to regions with intensive NH_x deposition rates, like India, and regions in which the dominant deposition components are transitioning from NO_y to NH_x, as in Europe, although the specific details, such as the control effectiveness, may differ with local conditions.

CHAPTER 4
SOURCE CONTRIBUTIONS TO SULFUR AND NITROGEN DEPOSITIONS

A version of this chapter was originally published by (J. N. Tan, Fu, Dentener, Sun, Emmons, Tilmes, Flemming, et al., 2018):

Tan, J. N., Fu, J. S., Dentener, F., Sun, J., Emmons, L., Tilmes, S., . . . Keating, T. (2018). Source contributions to sulfur and nitrogen deposition - an HTAP II multi-model study on hemispheric transport. *Atmospheric Chemistry and Physics*, *18*(16), 12223-12240

Statement: JT and JSF designed the study. JT prepared the multi-model ensemble results and analyzed the data with help from JSF, QZ and CEY. FD suggested data analysis. FD and TK coordinated HTAP II. LE and ST provided CAM-Chem model results. JF provided C-IFS_v2 model results. TT provided SPRINTARS model results. HB provided GEOS5 model results. JT wrote the manuscript and JSF edited it with contributions from all co-authors.

4.1 Abstract

With the rising anthropogenic emissions from human activities, elevated concentrations of air pollutants have been detected in the hemispheric air flows in recent years, aggravating the regional air pollution and deposition issues. However, the regional contributions of hemispheric air flows to deposition have been given little attention in the literature. In this light, we assess the impact of hemispheric transport on sulfur (S) and nitrogen (N) deposition for 6 world regions: North America (NA), Europe (EU), South Asia (SA), East Asia (EA), Middle East (ME) and Russia (RU) in 2010, by using the multi-model ensemble results from the second phase of Task Force Hemispheric Transport of Air Pollution (HTAP II) with 20% emission perturbation experiments. About 27-58%, 26-46% and 12-23% of local S, NO_x and NH_3 emissions and oxidation products are transported and removed by deposition outside of the source regions annually, with seasonal variation of 5% more in winter and 5% less in summer. The 20% emission reduction in the source regions could affect 1-10% of deposition in foreign continental regions and 1-14% in foreign coastal regions and the open ocean. Significant influences are found from NA to the North Atlantic Ocean (2-14%), and from EA to the North Pacific Ocean (4-10%) and to western NA (4-6%) (20% emission reduction). The impact on deposition caused by short-distance transport between neighbouring regions (i.e. from EU to RU) occurs throughout the whole year (slightly stronger in

winter), while the long-range transport (i.e. from EA to NA) mainly takes place in spring and fall, which is consistent with the seasonality found for hemispheric transport of air pollutants. Deposition in the emission intensive regions such as US, SA and EA is dominated (~80%) by own region emissions, while deposition in the low emission intensity regions such as RU is almost equally affected by foreign exported emissions (40-60%) and own region emissions. We also find that deposition of the coastal regions or the near-coastal open ocean is twice more sensitive to hemispheric transport than the non-coastal continental regions, especially for regions in the downwind direction of emission sources (i.e. west coast of NA). This study highlights the significant impacts of hemispheric transport of air pollution on the deposition in coastal regions, the open ocean and low emission intensity regions. Further research is proposed to improve the ecosystem and human health, with regards to the enhanced hemispheric air flows.

4.2 Introduction

The increasing consumption of energy by human activities has largely increased the deposition of nitrogen (N) over the terrestrial and marine ecosystem (Duce et al., 2008; Galloway et al., 2008; T. W. Kim et al., 2011). The impact is estimated to continue increasing in the near future (Bleeker et al., 2011; Kanakidou et al., 2016; Lamarque et al., 2013; Lamarque et al., 2005; Paulot et al., 2013). The NO_x emissions have increased by about 10 Tg(N) from 2001 to 2010, due to the large increase in the Asia regions (J. N. Tan, Fu, Dentener, Sun, Emmons, Tilmes, Sudo, et al., 2018), while recent studies have reported year 2011 as the turning point for NO_x emissions from China (M. Li, Liu, et al., 2017; F. Liu et al., 2016). On the other hand, the global sulfur (S) emissions have declined by about 5 Tg(S) from 2000 to 2010 (J. N. Tan, Fu, Dentener, Sun, Emmons, Tilmes, Sudo, et al., 2018). The global amounts of SO_2 emissions from fossil fuel have been decreasing since 1980, owing to the significant decline of emissions from Europe (EU) and U.S. (Chin et al., 2014). The SO_2 emission in China experiences increases from 2000-2005 due to energy consumption and decreases after 2006 thanks to the implementation of the Flue-Gas Desulphurization system on power plants. Deposition supplies the ecosystem with nutrients, but too much deposition could cause various adverse impacts on the environment, including acidification and eutrophication of the forest and waterbody (Bergstrom & Jansson, 2006; A. F.

Bouwman et al., 2002; Dentener et al., 2006; Phoenix et al., 2006), soil acidification which slows down the crop production (J. H. Guo et al., 2010; Janssens et al., 2010) and even destroying the plant biodiversity (Bobbink et al., 2010; Clark & Tilman, 2008). The prevention and control of exceeding deposition have become a growing worldwide concern.

Hemispheric transport of air pollutants is found to aggravate the regional air pollution issues (Fiore et al., 2009; Fu et al., 2012; Sudo & Akimoto, 2007; Wild & Akimoto, 2001) as well as enlarge the local deposition burden (Glotfelty, Zhang, Karamchandani, & Streets, 2014; Sanderson et al., 2008). The mass of aerosols arriving at the coasts of North America (NA) is comparable to that emitted domestically (Yu et al., 2012).Air pollution from Asia contributes to the $PM_{2.5}$ concentration in western U.S. by 1.5 μg m^{-3} (Tao, Yu, & Chin, 2016), the O_3 concentration by 3-10 ppbv (Brown-Steiner & Hess, 2011; Jacob, Logan, & Murti, 1999; Reidmiller et al., 2009; Yienger et al., 2000; L. Zhang et al., 2008; L. Zhang, D. J. Jacob, et al., 2009) and the peroxyacyl nitrate (PAN) concentration by 26 ppbv (Berntsen, Karlsdottir, & Jaffe, 1999) in spring. The long-range transport of air pollution from NA is estimated to contribute by 3-5 ppb (7-11%) to the O_3 concentration in EU annually (Auvray & Bey, 2005; Derwent, Stevenson, Collins, & Johnson, 2004; Guerova et al., 2006; Q. B. Li et al., 2002) and the increment can reach 25-28 ppbv during particular events (Guerova et al., 2006). European outflow affects the surface O_3 concentration in western China by 2-6 ppbv in spring and summer (X. Y. Li et al., 2014) and North Africa by 5-20 ppbv in summer (Duncan & Bey, 2004; Duncan, West, Yoshida, Fiore, & Ziemke, 2008). The study by (Yu et al., 2013) found that the long-range transport contribute by 6-16% and 22-40% to aerosol optional depth and direct radiative forcing in 4 regions including NA, EU, East Asia (EA) and South Asia (SA). Recent studies have reported an increasing trend in the hemispheric transport of air pollution from Asia to NA from mid-1980s to late-2000s. The Asian plume has contributed ~10 ppbv (30%) to the O_3 concentration over western NA from mid-1980s to mid-2000s (Jaffe et al., 2003; Parrish et al., 2004), with an annual increase of 0.34-0.50 ppbv O_3 (Parrish et al., 2009). More recent studies showed that the contribution is about 5-7 ppbv in 2006 with a 1-2 ppb increase from 2000 to 2006 (L. Zhang et al., 2008). The trend agreed well with the rapid growth of Asian emissions (Lu et al., 2010; Richter et al., 2005; van der A et al., 2008; van der A et al., 2006; Q. Zhang et al., 2007).

Compared to the impact of hemispheric transport on air pollution, the impact on deposition hasn't been fully studied. (Arndt & Carmichael, 1995) developed a source-receptor (S-R) relationship for S deposition among the Asia regions in early 1990s. (L. Zhang et al., 2012) found that foreign anthropogenic emissions contribute to 6% and 8% of the oxidized nitrogen (NO_y) and reduced nitrogen (NH_x) deposition in contiguous U.S., respectively. A systematic study by (Sanderson et al., 2008) shed light on the impact of long-range transport on NO_y deposition at global scale. The study used the model ensemble results from HTAP I to calculate the S-R relationship for NO_y deposition in 2001 among four regions: EU, NA, SA and EA. Results showed that about 12-24% of the NO_x emissions were transported and deposited out of the source regions. About 3-10% of the emissions were deposited on the other three regions than the source region and affects their deposition by about 1-3%. However, these studies focused on the emission intensive regions, where the foreign disturbance could be relatively small compared to huge own region emissions. The foreign impact on the low emission intensity regions was not evaluated in the same detail. Furthermore, both the magnitude and spatial distribution of S and N emissions and deposition have been changed considerably during the last ten years (2001-2010) (J. N. Tan, Fu, Dentener, Sun, Emmons, Tilmes, Sudo, et al., 2018). It is necessary to update the S-R relationship for more recent years with regards to these changes.

To explore these questions, this chapter assesses the impact of hemispheric transport of S, NO_x and NH_3 emissions and oxidation products on S and N depositions, with multi-model ensemble results from the HTAP II. Additional to the four regions used in Sanderson's study for HTAP I (NA, EU, SA and EA), we include two new regions in this study: Middle East (ME) and Russia, Belarussia, Ukraine (RU). These two regions are featured with low S and N emissions relative to their areal extent, but located close to the high emission regions such as EU, SA and EA. We calculate the amount of deposition brought by hemispheric transport by comparing model results between the base case and the 20% emission perturbation cases. The experimental design is described in sect. 4.3. We explore the following questions in sect. 4.4:

1) What fractions (percentages) of the S or N emissions are transported and deposited outside of the source regions? What are the fractions of emissions that finally deposited on the other 5 regions and the open ocean? What is the seasonality of the exported fractions?

2) As receptor regions, how much deposition is brought by hemispheric transport? What is the impact on local deposition? Is there any seasonality for this impact?
3) For each region, what are the contributions of hemispheric transport and own region emissions on local deposition? In line with the analysis for other pollutants, to this purpose we evaluate the so-called Response to Extra-Regional Emission Reduction (RERER) metric. We discuss the impacts of hemispheric transport on the coastal regions specifically. The inter-model variations are also illustrated.

Section 4.5 is a summary of the findings in this study and some suggestions for future study.

4.3 Methods

4.3.1 HTAP II and experiment set-up

The HTAP was created in 2004 under the Convention on Long-range Transboundary Air Pollution (CLRTAP). It involves efforts from international scientists aiming at understanding the hemispheric transport of air pollutants and its impact on regional and global air quality, public health and near-term climate change. Until now, two phases of HTAP experiments have been conducted successfully. The HTAP I involved more than twenty models from international modeling groups, with 2001 as the base year for modeling studies. A comprehensive report of the major findings of HTAP I was released in 2010 and could be downloaded from http://www.htap.org/. The HTPA II was launched in 2012, with 2010 as the base simulation year. HTAP II required all models to use the same prescribed anthropogenic emissions instead of using the best estimates of emissions by each modeling group as HTAP I. This facilitates an inter-model comparison between models. In addition, HTAP II had a refined definition for the boundaries of regions, which enabled an update in the S-R relationships among regions.

This study uses the ensemble of eleven global models from HTAP II (including CAM-Chem, CHASER_re1, CHASER_t106, EMEP_rv48, GEMMACH, GEOS5, GEOSCHEMAJOINT, OsloCTM3v.2, GOCARTv5, SPRINTARS and C-IFS_v2). A detailed description of the experimental set-up could be found in (Galmarini et al., 2017). The S deposition

includes SO_2 deposition and SO_4^{2-} deposition. The N deposition is categorized to NO_y deposition and NH_x deposition. The NO_y deposition is a sum of all oxidized N except N_2O, including the deposition of NO_2, HNO_3, NO_3^-, PAN and other organic nitrates than PAN (Orgn). The NH_x deposition includes NH_3 deposition and NH_4^+ deposition. To form the multi-model ensemble, we re-grid all models to a uniformed horizontal resolution of 0.1° × 0.1°. We use the multi-model mean (MMM) of all models to present the ensemble results, a procedure which has been proven previously to have a better agreement with observations than single model result (Dentener et al., 2006). The MMM values of the compositions of S or N deposition are calculated separately and then combined to compute the total S or N deposition. More details can be found in (J. N. Tan, Fu, Dentener, Sun, Emmons, Tilmes, Sudo, et al., 2018).

4.3.2 Simulation scenarios

The base simulation uses anthropogenic emissions in 2010 (Janssens-Maenhout et al., 2015), which is called "base case" in this study. The MMM performance on wet deposition has been evaluated with observations from NADP for NA region, EMEP CCC reports for EU region and EANET for EA region in the previous study of (J. N. Tan, Fu, Dentener, Sun, Emmons, Tilmes, Sudo, et al., 2018). Following are some brief results of the evaluation. Modeled sum of gas phase SO_2 wet deposition and aerosol SO_4^{2-} wet deposition is evaluated with observed SO_4^{2-} wet deposition. 76% of the stations of all networks are predicted within ±50% of observation. Negative model biases (-20%) are found at some East Asian stations. Modeled sum of gas phase HNO_3 wet deposition and aerosol NO_3^- wet deposition is compared with observed NO_3^- wet deposition.

About 83% of the stations of all networks are predicted within ±50% of observation. The European and Southeast Asian stations with high observed NO_3^- wet deposition are somewhat underestimated. Modeled sum of gas phase NH_3 wet deposition and aerosol NH_4^+ wet deposition is compared with observed NH_4^+ deposition. About 81% of modeled NH_4^+ wet deposition at stations of all networks are predicted within ±50% of observation. A general underestimation is found in modeled NH_4^+ wet deposition, especially at East Asian stations.

In terms of dry deposition, due to the lack of directly measured data, we compare the modeled dry deposition with inferential data from CASTNET over U.S. The CASTNET data is calculated with observed aerosol concentration and modeled dry deposition velocity, therefore it might have high uncertainties. Comparison shows that the modeled dry deposition is generally higher than the CASTNET inferential data by a factor of 1-2. This is a common feature of many global and regional models (Aas, 2017). According to the analysis, the model bias for dry deposition mainly comes from the model over-prediction of air pollutant concentration (J. N. Tan, Fu, Dentener, Sun, Emmons, Tilmes, Sudo, et al., 2018).The CASTNET sites are generally located in remote regions with relatively lower air pollutant concentrations than urban regions, but the models fail to represent this characteristic with coarse spatial resolution (J. N. Tan, Fu, Dentener, Sun, Emmons, Tilmes, Sudo, et al., 2018) .

HTAP II defines the boundaries of seventeen regions as shown in Fig. 2.1 of chapter 2. The emission perturbation experiments are conducted separately for six regions (regions with color in Fig. 2.1) with high priority: NA, EU, SA, EA, ME and RU. In the perturbation experiments, the anthropogenic emissions (including NO_X, SO_2, NH_3, VOC, CO and PM) of a specific region are reduced by 20% from the amounts in the base case simulation, while the emissions in other regions keep constant. In addition, a global perturbation experiment referred as "GLO" is conducted with 20% reduction of global anthropogenic emissions. We estimate the impact of hemispheric transport on deposition by comparing the model results under perturbation experiments with those under base case simulation.

In order to validate the quality of model outputs, we check the mass balance between emissions and deposition at global scale. The mass balance check for base case simulation is already shown in sect. 2.3.2 of chapter 2, therefore here we only show the mass balance check for perturbation experiments. The mass balance for perturbation experiments are validated by comparing the global total amounts of changes of deposition (ΔDepo) with changes of emissions (ΔEmis) for all perturbation cases (Table 4.1). Model results are excluded if their global ΔDepo values fall outside the range of ±20% of their global ΔEmis. According to the results, the amounts of ΔDepo are all within the scopes for all perturbation cases except the NH_x deposition under EA case. The ΔDepo of NH_x deposition under EA case is not available due to lack of modeled NH_4^+ wet deposition under 20% emission perturbation in EA.

Table 4. 1 Global changes of emissions (ΔEmis) and depositions (ΔDepo) under emission perturbation experiments from MMM (unit: Tg(S or N) yr^{-1})

		Regions of emission perturbation						
		NA	EU	SA	EA	MD	RU	GLO
S	ΔEmis	-1.2	-0.7	-1.1	-2.9	-0.7	-0.5	-10.5
	ΔDepo	-1.1	-0.6	-1.0	-2.8	-0.6	-0.4	-10.1
NO_y	ΔEmis	-0.9	-0.6	-0.7	-1.8	-0.3	-0.3	-7.0
	ΔDepo	-0.9	-0.6	-0.6	-1.8	-0.3	-0.2	-6.8
NH_x	ΔEmis	-0.7	-0.7	-2.1	-1.6	-0.1	-0.2	-8.0
	ΔDepo	-0.7	-0.7	-2.2	-*	-0.1	-0.2	-8.2

Note: * Lack of modelled NH_4^+ wet deposition under EA emission perturbation experiment.

4.4 Results

4.4.1 Export of S and N emissions from source regions

This section studies the export of S and N emissions and oxidation products from the source regions. Table 4.2 shows the S-R relationship of S and N depositions among the six regions. The numbers are the sensitivity ($SEN_{r\rightarrow s}$) of deposition in the receptor/source regions to emission changes in the source regions (Sanderson et al., 2008). The metric is calculated as ΔDepo in the receptor/source regions divided by ΔEmis in the source regions following Eq. *(4-1)*.

$$SEN_{r\rightarrow s} = \frac{\Delta\, Depo\ (r/s)}{\Delta\, Emis\ (s)} \times 100\% \qquad (4\text{-}1)$$

where s is the source region and r is the receptor region. ΔDepo(r/s) is the deposition change in the receptor/source regions, ΔEmis(s) is the emission change in the source regions. The metric indicates the percentages of emissions of the source regions that are deposited locally or exported to foreign regions.

The numbers outside of the parenthesis in Table 4.2 are for coastal and non-coastal regions together and the numbers in the parenthesis are specifically for coastal regions (defined in Fig. 2.1). "Others" means the other regions in the world than the six regions (white color in Fig. 2.1). The NA region has 69% of its S emissions deposited within itself, including 9% deposited on its coastal region. The remaining 31% is exported to the other regions, mostly to the "Others" and less than 3% is deposited on the other five regions (EU, SA, EA, ME and RU). A relatively large fraction (14%) of European S emissions are exported to RU region. Other major pathways of export of S emissions/reaction products are from SA to EA (9%), from EA to RU (5%) and from RU to EU (7%) and EA (5%). ME has considerable high percentages of S emissions exported to its nearby regions such as SA (8%), EA (5%) and RU (5%). The S-R relationship of NO_y deposition is similar to that of S deposition, except that EU and ME have 66% and 54% of NO_x emissions deposited within the source region, which are 6% and 12% higher than those of S emissions, likely due to somewhat longer lifetimes of S emissions compared to NO_x emissions and the high emission altitude of S emissions. In terms of NH_x deposition, about 20% more NH_3 emissions are deposited within the source regions (except ME) compared with S and NO_x emissions, due to its short lifetime in the atmosphere.

Table 4. 2 Source-receptor relationships of S, NO_y and NH_x depositions (%) for six regions (including continental coastal and non-coastal regions). The values in the parentheses are for coastal regions as a subset of the total.

	Receptor Regions	Source Regions					
		NA	EU	SA	EA	ME	RU
S Deposition	NA	68.9 (8.9)	0.2 (0.1)	0.2 (0.0)	1.5 (0.6)	0.3 (0.1)	1.2 (0.6)
	EU	1.1 (0.6)	60.4 (14.4)	0.0 (0.0)	0.2 (0.1)	2.1 (0.2)	6.9 (2.5)
	SA	0.5 (0.1)	1.2 (0.3)	66.4 (10.0)	0.9 (0.4)	7.9 (1.6)	0.3 (0.1)
	EA	0.6 (0.2)	1.8 (0.4)	8.8 (1.3)	73.4 (11.5)	4.6 (0.8)	5.2 (1.4)
	ME	0.0 (0.0)	2.6 (0.6)	0.6 (0.3)	0.0 (0.0)	42.4 (8.2)	0.8 (0.2)
	RU	0.4 (0.1)	13.6 (2.2)	0.1 (0.1)	5.1 (2.2)	5.0 (1.1)	62.2 (4.4)
	Others	28.5	20.1	23.8	19.1	37.7	23.4
NO_y Deposition	NA	71.5 (7.8)	0.8 (0.2)	0.5 (0.1)	1.0 (0.3)	0.5 (0.1)	1.0 (0.3)
	EU	1.3 (0.6)	66.2 (17.5)	0.2 (0.1)	0.3 (0.1)	3.5 (0.9)	9.8 (2.9)
	SA	0.2 (0.0)	0.2 (0.0)	66.2 (8.6)	0.5 (0.2)	7.9 (1.3)	0.2 (0.0)
	EA	0.6 (0.1)	1.2 (0.2)	6.2 (0.7)	74.4 (14.3)	2.4 (0.3)	4.3 (0.9)
	ME	0.4 (0.1)	1.6 (0.3)	0.9 (0.4)	0.1 (0.0)	54.4 (8.0)	0.8 (0.2)
	RU	0.6 (0.1)	10.3 (1.3)	0.1 (0.0)	5.1 (2.2)	4.9 (1.3)	61.4 (3.1)
	Others	25.6	19.7	25.8	18.6	26.4	22.5
NH_x Deposition	NA	88.4 (5.6)	0.2 (0.1)	0.3 (0.1)	-*	0.7 (0.3)	0.4 (0.2)
	EU	0.6 (0.3)	83.2 (17.8)	0.0 (0.0)	-*	4.6 (1.2)	11.9 (3.1)
	SA	0.0 (0.0)	0.1 (0.0)	85.1 (7.6)	-*	8.6 (2.4)	0.0 (0.0)
	EA	0.0 (0.0)	0.4 (0.1)	4.2 (0.3)	-*	2.6 (0.5)	3.8 (1.0)
	ME	0.1 (0.0)	1.3 (0.3)	0.4 (0.2)	-*	49.4 (5.9)	1.5 (0.4)
	RU	0.4 (0.1)	10.3 (1.3)	0.1 (0.0)	-*	7.3 (1.5)	76.9 (4.1)
	Others	10.5	4.4	9.7	-*	26.9	5.7

* Lack of NH_4^+ wet deposition under EA emission perturbation experiment from all models.

The seasonal variations of the export of S and N emissions from source regions are shown in Fig. 4.1. In terms of S emissions, there are 5-10% seasonal differences around the annual average export fractions for all regions except SA. SA exports almost half of its S emissions in spring, which is twice the numbers in summer (20%) and fall (25%), related to the specific dry period and monsoon circulation. The seasonal export fractions of NO_x and NH_3 emissions are similar to that of S emissions in the pattern, but generally lower in values in all seasons. Generally, the source regions export the highest percentage of their emissions in winter and spring and lowest in summer. More proficient oxidation chemistry in summer results in more soluble component, and local weather systems, especially the episodic of precipitation has large influence on this seasonality. For most continental regions, the wet deposition accounts for 50-70% of total deposition (J. N. Tan, Fu, Dentener, Sun, Emmons, Tilmes, Sudo, et al., 2018). Therefore, local precipitation plays an important role in the removal process of local pollution. On the other hand, for regions with low local precipitation like ME, the percentage of emissions removed within own region would be lower than the other regions. In addition, the strong westerly winds in winter and spring favor the hemispheric transport in the mid-latitudes of the North Hemisphere. While the rapid vertical convections in summer slowdown the zonal transport of air flows and accelerates the local removal process.

A comparison is conducted with previous studies. About 70% of the emitted NO_x from Asia is reported to be lost within its boundary by HNO_3 deposition in spring (Bey et al., 2001). The estimations in our study are 70% for EA and 61% for SA, close to the literature. About 20% of anthropogenic NO_x emitted by NA is deposited out of its boundary (about 1000 km offshore) (Q. B. Li, Jacob, Munger, Yantosca, & Parrish, 2004). Another study reported that 9-22% of surface NO_x emissions are exported out of the boundary of NA (Stohl, Trainer, Ryerson, Holloway, & Parrish, 2002). Our estimation is about 30%, higher than the literatures. The HTAP I study in 2001 developed a SR relationship for NO_y deposition among NA, EU, SA and EA (Sanderson et al., 2008). About 12-24% of the emitted NO_x is deposited out of the source regions. This study of HTAP II finds a higher percentage of export (26-34%). It should be noted that the estimations of different studies are not fully comparable since they are influenced by several factors: (1) definition of the boundaries of the source and receptor regions. For instance, we use the continental boundaries defined by HTAP II, while some studies use domains to define the

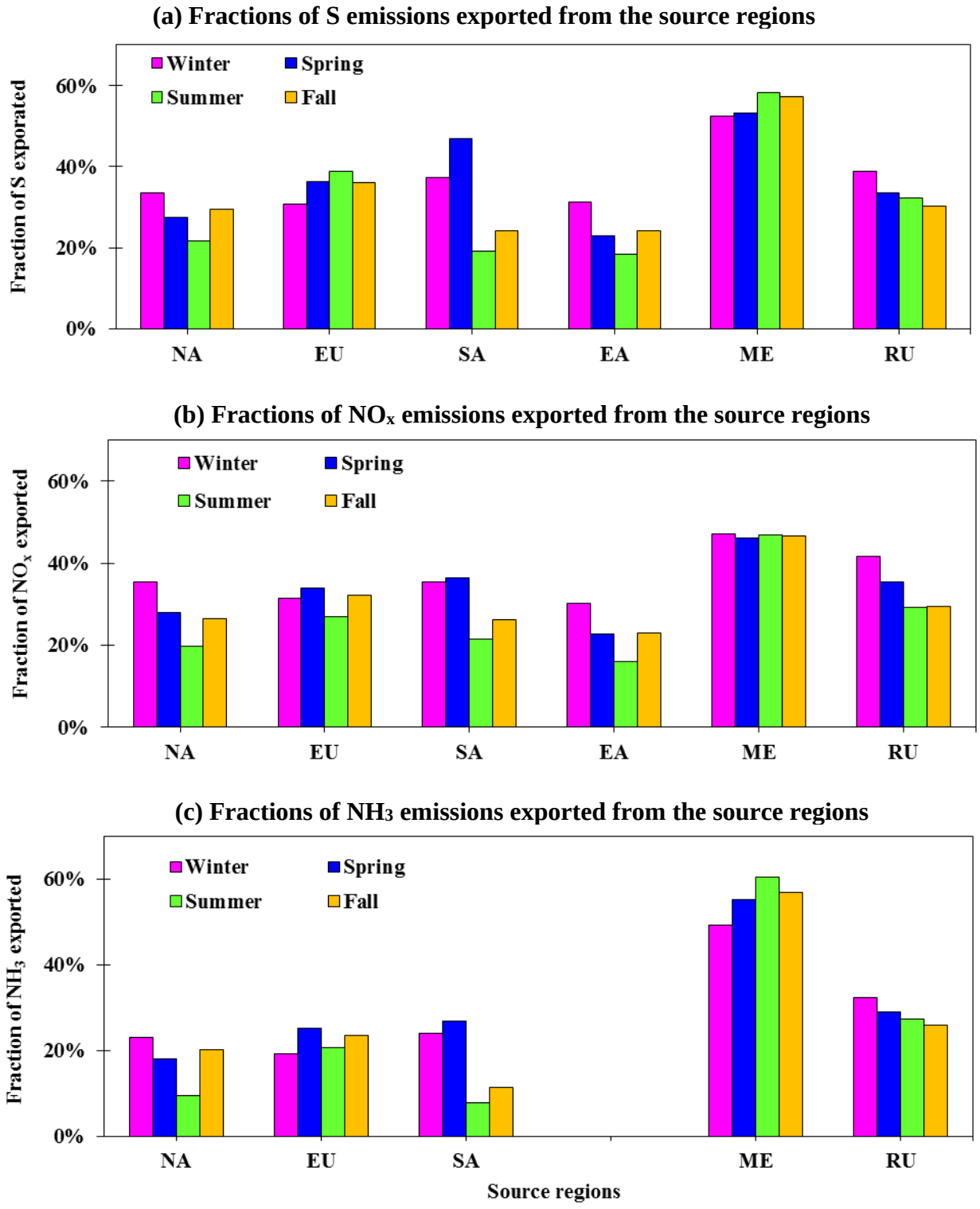

Figure 4. 1 Fractions of S, NO_x and NH_3 emissions exported from the source regions in four seasons.

boundary, such as a squared domain with 65-130°W in east-west direction and 25-55°N in north-south direction (Q. B. Li et al., 2004). There are also changes in the boundaries of regions from HTAP I to HTAP II. For instance, the Mexico and Central America are included in NA in HTAP I, but they are defined as a separate region in HTAP II (region 12 in Fig. 2.1). The boundary of EU is also changed in HTAP II; (2) design of the perturbation simulations. The perturbation simulations in HTAP I only change the NO_x emissions, but HTAP II simulations also reduce the other anthropogenic emissions, including SO_2 and PM. The joint effects of controlling multiple species may result in more reduction in NO_y deposition, but it is hard to estimate the influence in this study.

4.4.2 Impacts of hemispheric transport on local deposition

This section investigates the impacts of hemispheric transport on deposition in the receptor regions. Figure 4.2 shows the annual response of S deposition to 20% emission reduction in the source regions calculated as Eq. *(4-2)*.

$$Response = \frac{\Delta\, Depo\ (perturbation)}{Depo\ (base)} \times 100\% \qquad (4\text{-}2)$$

where ΔDepo (perturbation) is the ΔDepo between perturbation case and base case. Depo (base) is the deposition under base case. The negative values mean that the deposition decreases with reduction in emissions.

Figure 4.2(a) shows the global response of S deposition to 20% emission reduction in NA. The largest deposition change is found in the source region (NA), with a 4-20% decrease in S deposition in the non-coastal region and 14-16% decrease around the east coast. The impact on the North Atlantic Ocean declines gradually from the near coastal region (12-14%) to the open ocean (2-12%) and Eurasia (<1%). Figure 4.2(b) shows the global response of S deposition to 20% emission reduction in EU. Although the impact on continental non-coastal regions is also high (6-18%), the impact on the coastal regions is generally less than 6%, much lower than NA's impact on its east coast (14-16%). The deposition in North Africa, central Asia and western RU is affected by 2-6%. The 20% emission reduction in SA (Fig. 4.2(c)) shows large influences over its

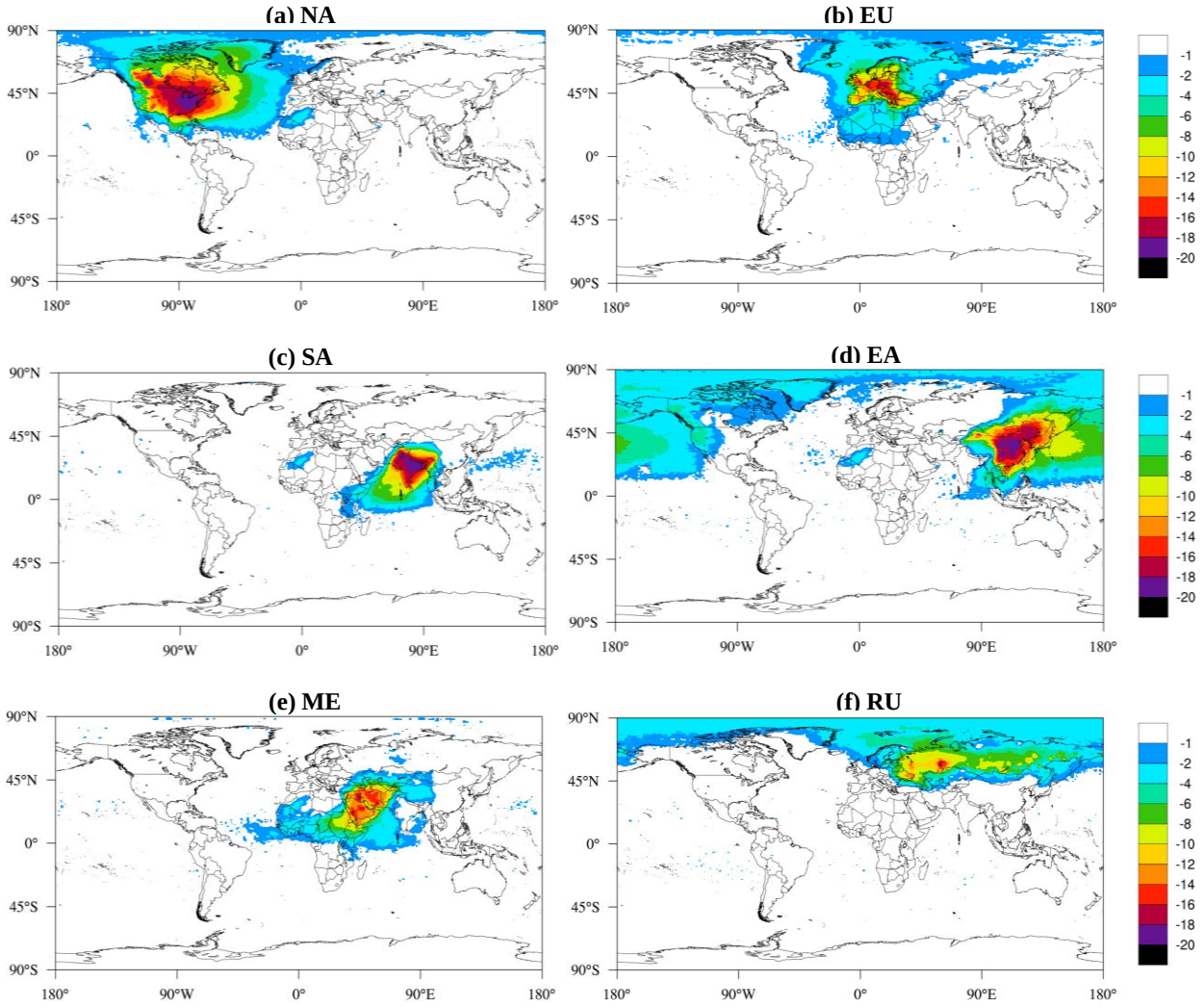

Figure 4. 2 The responses of S depositions to 20% emission reductions in the source regions. The values are the percentage changes (%) in depositions calculated as (changes in deposition with 20% emission reduction) / (base case deposition) ×100%. The unit is (% per 0.1×0.1° grid box).

south-west coast and the Arabian Sea (4-12%). The SA's outflow affects the deposition in south-eastern ME and eastern Sub Saharan Africa by 1-4% and western EA and Southeast Asia (mainly Bangladesh) by 2-6%. Figure 4.2(d) shows the impact on S deposition from 20% emission reduction in EA. On one hand, the impact is strong on the east coast of China (12-16%) and decreases gradually over the North Pacific Ocean (4-10%). Although the majority of S emissions are deposited on the North Pacific Ocean, the influence on western NA can still reach 4-6%. On the other hand, the impacts on Southeast Asia and SA are much lower (2-5% and <1%), due to the block of air flows by the Himalaya Mountains (Fig. S4.13 in the Appendix). The 20% emission reduction in ME mainly affects the S deposition in Africa by 2-10% and western EA by 2-4%. Figure 4.2(f) shows the change of S deposition with 20% emission reduction in RU. The regions of impact are mainly located at high latitudes of the North Hemisphere, including northern EU (2-6%) and western Arctic Circle (1-4%). The Russian flow enters the Arctic in the lower troposphere in winter season (Stohl, 2006).

Figure 4.3 shows the impacts of reducing NO_x emissions on NO_y deposition. The overall impact is qualitatively similar to that of S emissions in the spatial pattern, with some differences in the values. Some regions receive lower impact on NO_y deposition than S deposition. For instance, SA's impact on eastern Africa is about 1-4% on S deposition, but is <1% on NO_y deposition. ME's impact on the western Africa and Gulf of Guinea is about 2-4% on S deposition, but is <1% on NO_y deposition. These smaller sensitivities reflect differences in lifetimes, and the lower formation of aerosol NO_3^- under warm conditions in tropical regions. Under the NA perturbation case (Fig. 4.3(a)), an 8-12% change of NO_y deposition is found on the west coast of California, due to high NO_x emissions in California from mobile source, which is not seen in S deposition. The impacts of emission reduction in EU and EA on their coastal regions are generally 2-4% higher for NO_y deposition than S deposition (Fig. 4.3(b) and (d)). The impact on NH_x deposition is similar to that on NO_y deposition (Fig. 4.4). It should be noted that this is the result from 20% emission reduction in the source regions, therefore the actual impact (100% emission reduction) could be five times higher when assuming a linear relationship between 20% and 100% emission reduction on deposition.

The amount of deposition carried by hemispheric transport is quantified with seasonal variations. Figure 4.5 shows the monthly changes of S deposition for 20% emission reductions in

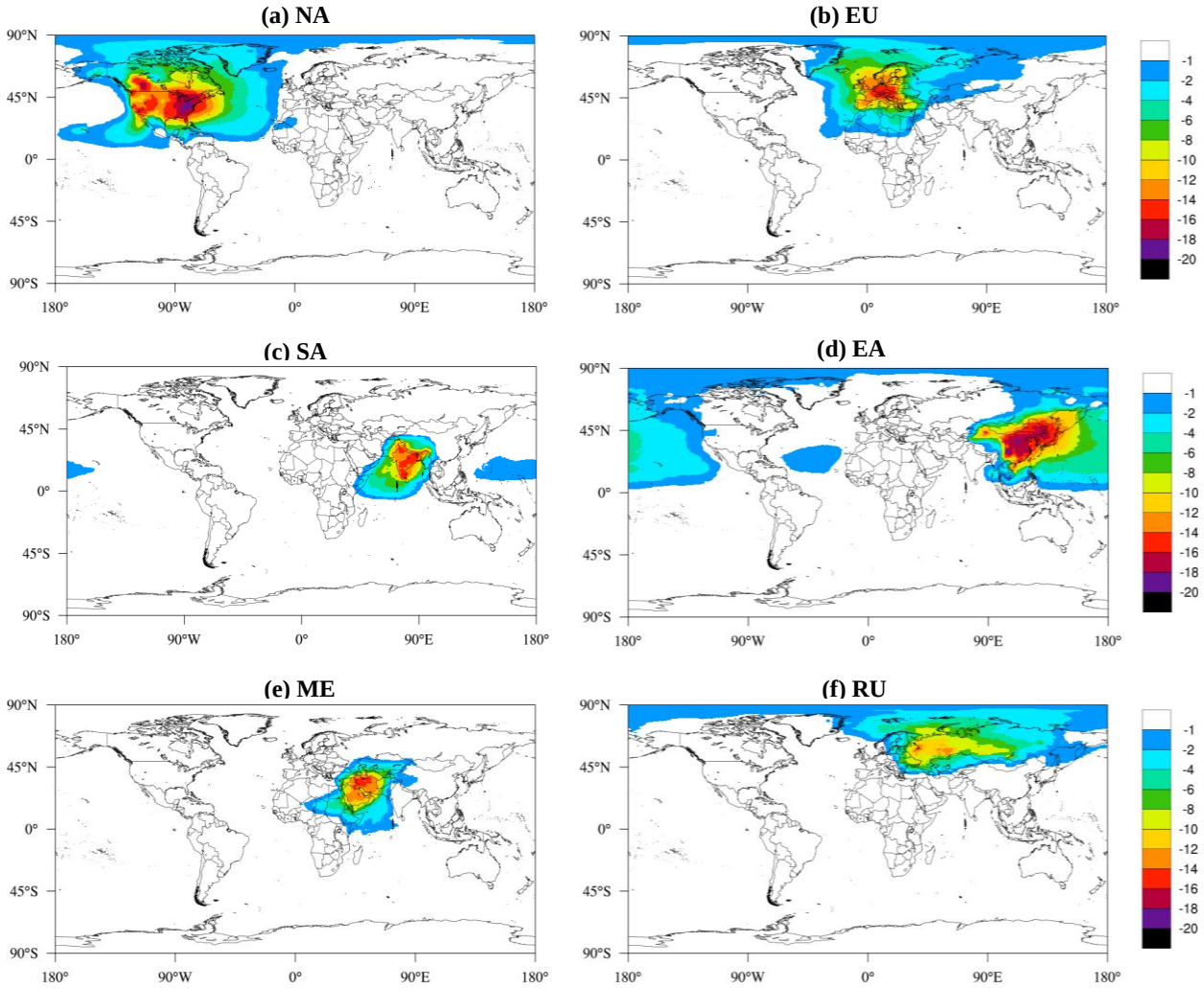

Figure 4. 3 Same as Fig. 4. 2 but for NO_y depositions. The unit is (% per 0.1×0.1° grid box).

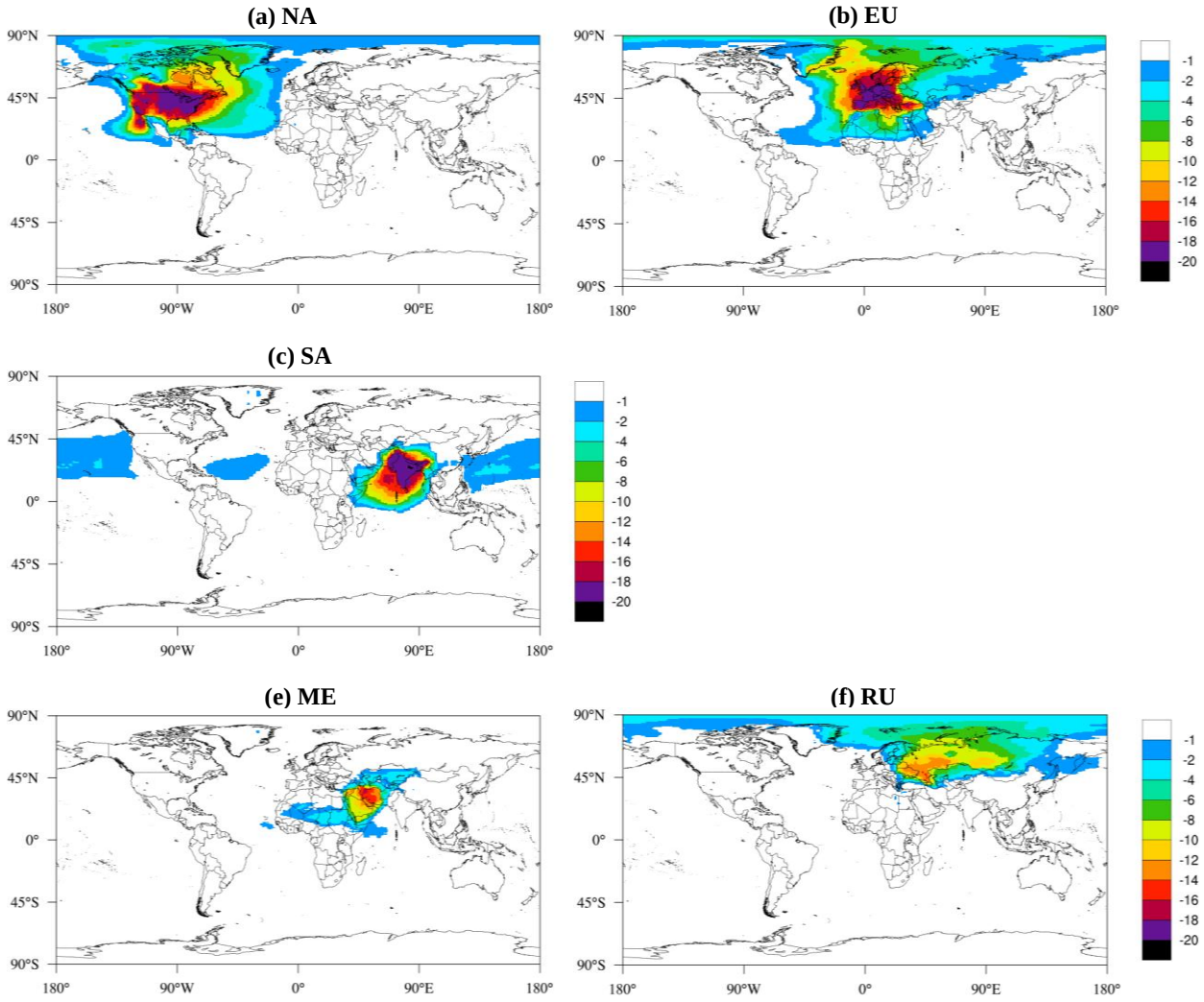

Figure 4. 4 Same as Fig. 4. 2 but for NH_x depositions. The unit is (% per 0.1×0.1° grid box).

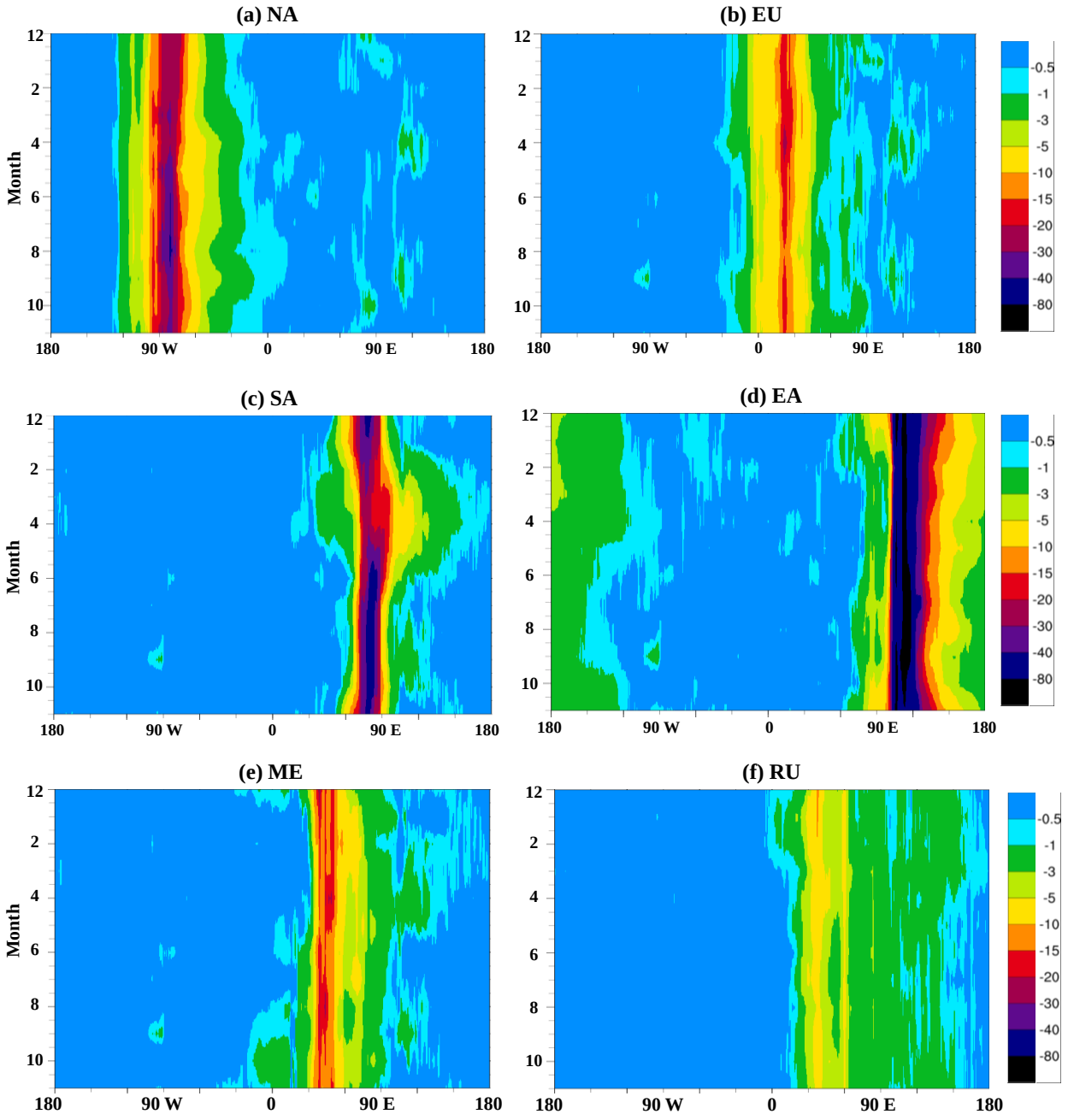

Figure 4. 5 The monthly changes of S depositions with 20% emission reductions in the source regions. The x-axis values are meridional total values versus time (y-axis) with a west-east resolution of 0.1°. The unit is ($\times 10^4$ kg(S) month^{-1} per 0.1° longitude). Negative values indicate declines in depositions with reductions in emissions.

the source regions. The values are meridional sum with a west-east resolution of 0.1 degree. The figure displays well the locations of the source regions. The negative values indicate the amounts of pollutants transported from the source regions to the receptor regions. According to Fig 4.5(a), NA has about (1-10) $\times 10^4$ kg(S) $month^{-1}$ per 0.1° longitude of its S emissions transported and deposited over the North Atlantic Ocean (15-75°W) throughout the whole year. About (1-3) $\times 10^4$ kg(S) $month^{-1}$ per 0.1° longitude decrease of S deposition at about 90°E and 120°E in spring and fall, which gives evidence to NA's influence on Eurasia via the transatlantic flow, although this amount accounts for less than 1% of local S deposition (white in Eurasia in Fig. 4.2(a)).

Figure 4.5(b) shows that about (1-3) $\times 10^4$ kg(S) $month^{-1}$ per 0.1° longitude of EU's emissions is transported and deposited at 30-60°E in RU throughout the whole year and at 100-120°E in EA in spring and fall. According to Fig. 4.5(c), SA exports its S emissions to 30-60°E in ME and eastern Africa in early spring and to 90°E-180° in EA and the North Pacific Ocean from late spring until fall. In particular, the influence on EA can reach (5-10) $\times 10^4$ kg(S) $month^{-1}$ per 0.1° longitude in mid-spring. According to Fig. 4.5(d), EA's S emissions are widely transported and deposited over the North Pacific Ocean throughout the whole year. The Asian outflow arrives at the west coast of NA (~130°W) in all seasons except summer, but only reaches far in western NA (~90°W) in spring and brings about 1 $\times 10^4$ kg(S) $month^{-1}$ per 0.1° longitude of S deposition. The export to SA is only found during the Asia winter monsoon.

Figure 4.6 shows the monthly changes of NO_y deposition with perturbation experiments. Compared to S deposition, the changes in NO_y deposition by hemispheric transport are generally smaller. For instance, the NA's impact on Eurasia is (1-3) $\times 10^4$ kg(S) $month^{-1}$ per 0.1° longitude for S deposition, but is less than 0.5 $\times 10^4$ kg(N) $month^{-1}$ per 0.1° longitude for NO_y deposition. The SA's impact on EA (90-120°E) can reach (5-10) $\times$ 10^4 kg(S) $month^{-1}$ per 0.1° longitude for S deposition, but the amount is four times lower for NO_y deposition. This result is in accordance with the S-R results in sect. 4.4.1 that more S emissions are transported out of the source regions than N emissions, probably due to longer chemical lifetimes and higher emission altitudes. Patterns similar to NO_y deposition are found in the monthly changes of NH_x deposition (Fig. 4.7).

The deposition changes due to transport between neighboring regions are found throughout the whole year and are slightly stronger in winter, such as between EU and RU (~30°E) (Fig. 4.6(b)

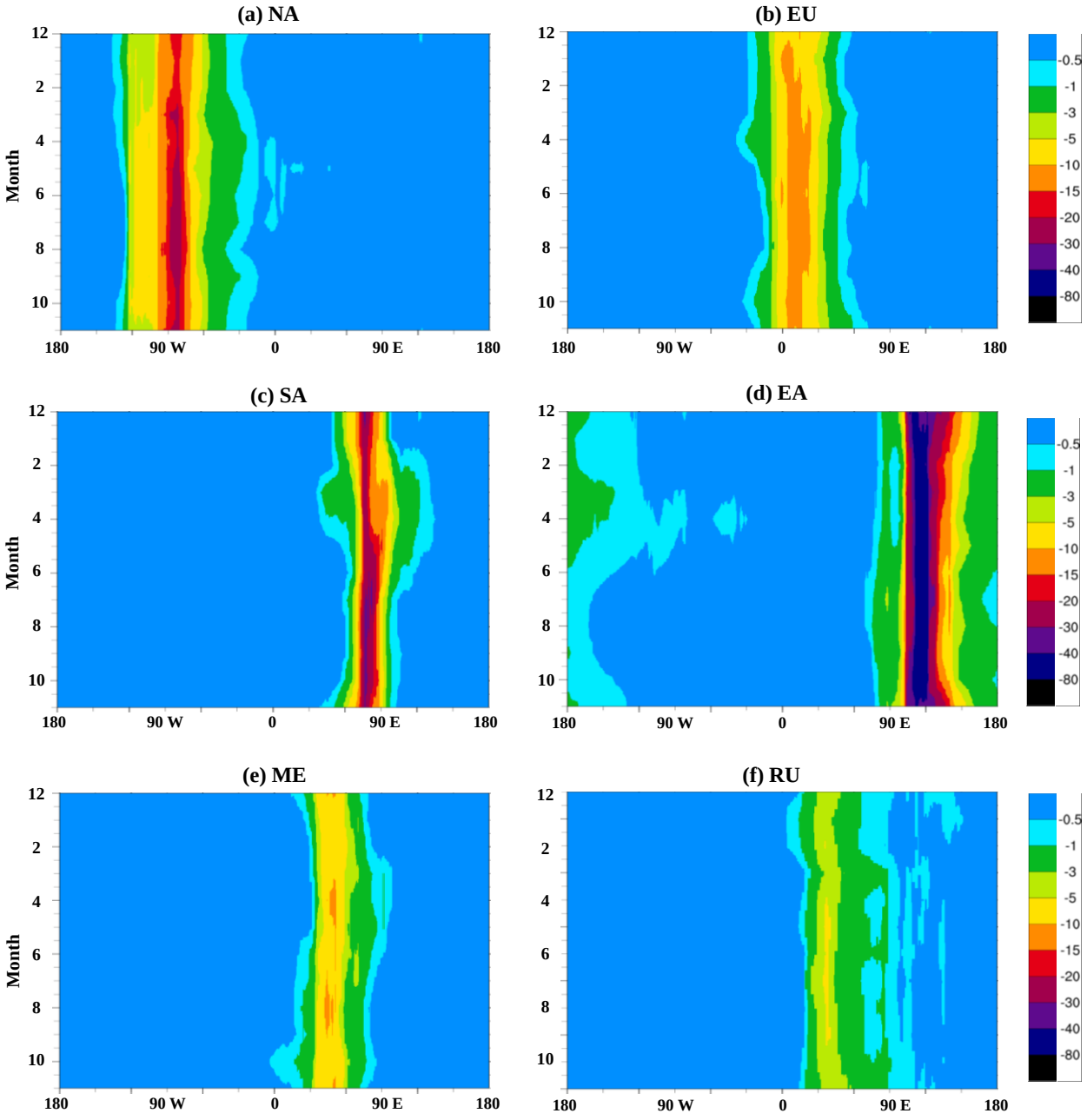

Figure 4. 6 Same as Fig. 4.5 but for NO_y depositions. The unit is ($\times 10^4$ kg(N) $month^{-1}$ per 0.1° longitude).

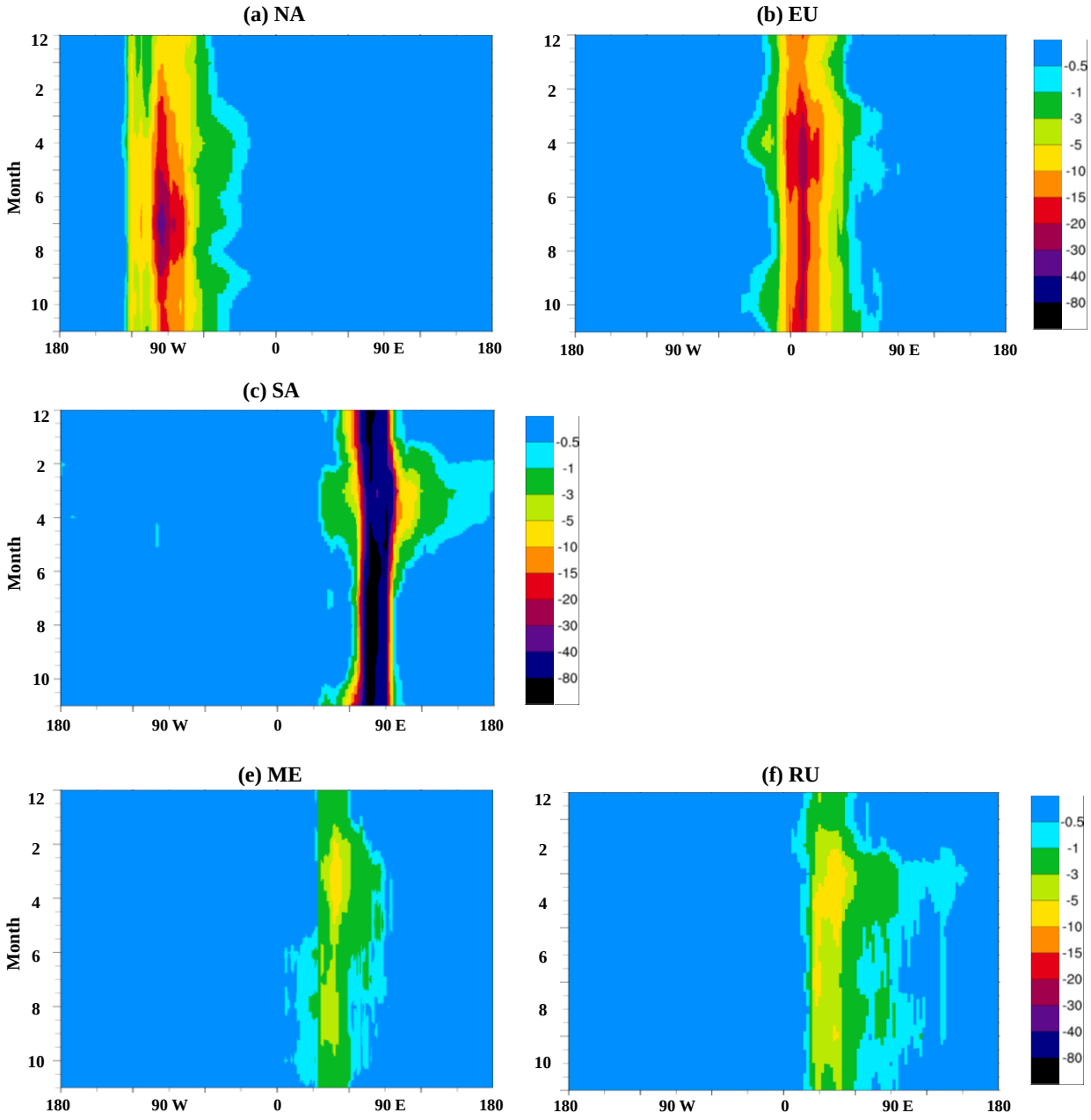

Figure 4. 7 Same as Fig. 4.5 but for NH_x depositions. The unit is ($\times 10^4$ kg(N) month^{-1} per 0.1° longitude).

and (f)) and from EA to the North Pacific Ocean (~130°E) (Fig. 4.6(d)). This is consistent with the seasonality found for the export of emissions from source regions in sect. 4.4.1. In addition, most source regions reduce more S and NO_x emissions in winter than the other seasons (Table S4.1), thus more emissions are exported abroad in this season. On the contrary, the deposition change by transport over long distance mainly occurs in spring and fall, especially the hemispheric transport from NA to EU, from EU to EA and from EA to NA.

The seasonality of long-range transport for NA, EU and EA well fits the characteristic of westerlies, which is the prevailing winds in the mid-latitude of the North Hemisphere. This agrees with the seasonality of the transpacific, transatlantic and trans-Eurasia flows of air pollutants that spring is the most efficient season for long-range transport in the mid-latitudes (Auvray & Bey, 2005; Brown-Steiner & Hess, 2011; Holzer, Hall, & Stull, 2005; X. Y. Li et al., 2014; Q. Liang et al., 2004; H. Y. Liu et al., 2003; J. F. Liu, Mauzerall, & Horowitz, 2005; Wild, Pochanart, & Akimoto, 2004). Although the westerlies are also strong in winter, the concentrations of air pollutants in the air flows are lower than spring. The formations of secondary species like PAN are suppressed by slow oxidation in the cold environment (Berntsen et al., 1999; Deolal et al., 2013; Moxim et al., 1996), which plays an important role as a reservoir for NO_x in the long-range transport of air plumes (Hudman et al., 2004; Lin, Holloway, Carmichael, & Fiore, 2010).

4.4.3 Own region and foreign contributions on deposition

This section compares the contributions of hemispheric transport and own region emission control on local deposition. A metric called RERER is calculated by dividing the ΔDepo due to foreign emission reduction by ΔDepo due to global (foreign + own region) emission control following Eq. *(4-3)*.

$$RERER_i = \frac{\Delta\, Depo_i\,(foreign)}{\Delta\, Depo_i\,(global)} \qquad (4\text{-}3)$$

where i is the region of focus. $\Delta Depo_i$ (foreign) is the ΔDepo in region i due to 20% foreign emission reduction. It is calculated by subtracting the ΔDepo due to 20% own region emission control from ΔDepo due to 20% global emission reduction. $\Delta Depo_i$ (global) is the ΔDepo in region

i due to 20% global emission reduction. This metric indicates the importance of foreign/local emissions on local deposition. A low RERER value (close to 0) indicates a predominant effect of own region emissions on local deposition, while a high RERER value (close to 1) means strong impacts from hemispheric transport.

Table 4.3 shows the RERER values for total (include both non-coastal and coastal regions), non-coastal and coastal regions. For both non-coastal and coastal regions, the own region impact includes control of both its coastal and non-coastal regions, and the foreign impact comes from emission reduction of both foreign coastal and non-coastal regions. NA (0.07, 0.17, and 0.17), SA (0.04, 0.17, and 0.18) and EA (0.16 and 0.16) regions have relatively low RERER values, due to large local emissions compared to the foreign contributions. EU (0.12, 0.34 and 0.36) and ME (0.32, 0.32 and 0.42) have relatively higher RERER values. RU is the only region with all RERER value (0.55, 0.59 and 0.61) higher than 0.5, which means its deposition is almost equally sensitive to the foreign exported air pollution and own region control. The RERER values of NO_y deposition are of similar magnitudes to those of S deposition, while the RERER values of NH_x deposition are 0.1 lower than those two, probably due to the lack of data for the EA perturbation case, so that the contributions from EA are not included.

The RERER values of coastal regions are generally 0.1-0.3 higher than those of non-coastal regions. Even regions with low non-coastal RERER values such as NA and SA have high RERER values in coastal regions. For instance, the RERER values of NA reaches 0.3-0.4 for its coastal region, more than double of the RERER values in its non-coastal regions (0.05-0.12). Coastal regions receive high proportions of deposition from the hemispheric transport. Except large scale circulation like prevailing westerlies, the coastal regions are featured with complex small-scale circulations. For instance, the low-level jet (zonal winds with high speed) contributes to the rainfall in coastal regions in Asia (Xavier, Kottayil, Mohanakumar, & Xavier, 2018). The orographic effects enhance the precipitation over coastal mountain regions such as the west coast of NA and EU, and the southeast coast of RU (James & Houze, 2005). According to Table 4.3, EA exports 5% of its S and N emissions to RU, almost half of which are deposited on RU's coastal regions. RU exports 7-12% of S and N emissions to EU, 30% of which are deposited on EU's coastal regions.

Table 4. 3 Extra-regional emission reduction (RERER) values of S, NO_y and NH_x depositions for continent non-coastal and coastal regions. The RERER values are calculated by dividing the ΔDepo due to foreign emission reductions by ΔDepo due to global (foreign + own region) emission control. Total column gives the RERER for coastal and non-coastal together.

Regions	S deposition			NO_y deposition			NH_x deposition		
	Total	Non-coastal	Coastal	Total	Non-coastal	Coastal	Total	Non-coastal	Coastal
NA	0.17	0.12	0.40	0.17	0.12	0.43	0.07	0.05	0.31
EU	0.36	0.27	0.53	0.34	0.27	0.48	0.12	0.09	0.22
SA	0.18	0.14	0.35	0.17	0.12	0.37	0.04	0.03	0.17
EA	0.16	0.14	0.28	0.16	0.12	0.27	-	-	-
ME	0.32	0.27	0.46	0.32	0.27	0.50	0.42	0.36	0.67
RU	0.61	0.56	0.84	0.59	0.52	0.90	0.55	0.49	0.85

The impact of hemispheric transport is identical or even larger than the effect of controlling own region emissions for some coastal or near coastal regions. According to Fig. 4.2, 20% emission reduction in EA can reduce 2-6% of S deposition in the west coast of NA. This effect is even larger than 20% emission reduction in its own region (<1%). Similarly, 20% emission reduction in NA can change 2-5% of S deposition in the west coast of EU, which is almost identical to the effect of 20% emission control in EU. On one hand, the emissions in western NA and western EU are relatively low, thus the effect of own region control is not significant. On the other hand, these coastal regions are in the downwind directions of eastern EA and eastern NA, which are the main source regions of S and N emissions. Coastal regions serve as transit places for air-sea exchanges with vulnerable ecosystems (T. Jickells, 2006; T. D. Jickells et al., 2017). The over-richness of deposition in coastal water and ecosystems can evoke a number of environmental issues, of which some are specifically for coastal regions such as threats to coastal benthic and planktonic system and sustainability of fishery (Doney et al., 2007; Paerl, 2002).

Figure 4.8 shows the source concentrations of deposition from hemispheric transport and own region emissions. Other (OTH, pattern fill in the figure) is calculated as $\Delta Depo_{(GLO)} - \sum \Delta Depo_{(case)}$ (case = 6, including NA, EU, SA, EA, ME and RU). It indicates the deposition change due to other reasons than the total effects of separate emission reduction in the six regions. It could come from the emission reduction in the rest of the world, especially nearby regions such as from Central Asia and North Africa to EU and ME. It could also come from the joint effects of emission control in multiple source regions, which possibly change the oxidant chemistry, atmospheric mixing and lifetimes of reactive pollutants. However, the model simulations do not allow to separate these contributions in this study. For regions with low RERER values (NA, SA and EA), the own region emissions dominate the local deposition by more than 80%. For these regions, determined by vicinity and transport patterns, the foreign impact is somewhat dominated by certain source regions, such as from EA to NA (2-4% out of 4-5%), from ME to SA (5-6% out of 7-11%) and from SA to EA (3-4% out of 4-7%). For regions with higher RERER values (i.e. EU and ME), there is about 20% contribution from "OTH". Beside this, RU contributes 4-5% to EU's deposition and EU contributes 5% to ME's deposition. The high RERER region (i.e. RU) has a different pattern than the other regions. The contributions of hemispheric transport from the other 5 regions (23-45%) are almost equivalent to its own region emission control (39-45%), with significant impacts from EA (20-24%) and EU (13-15%).

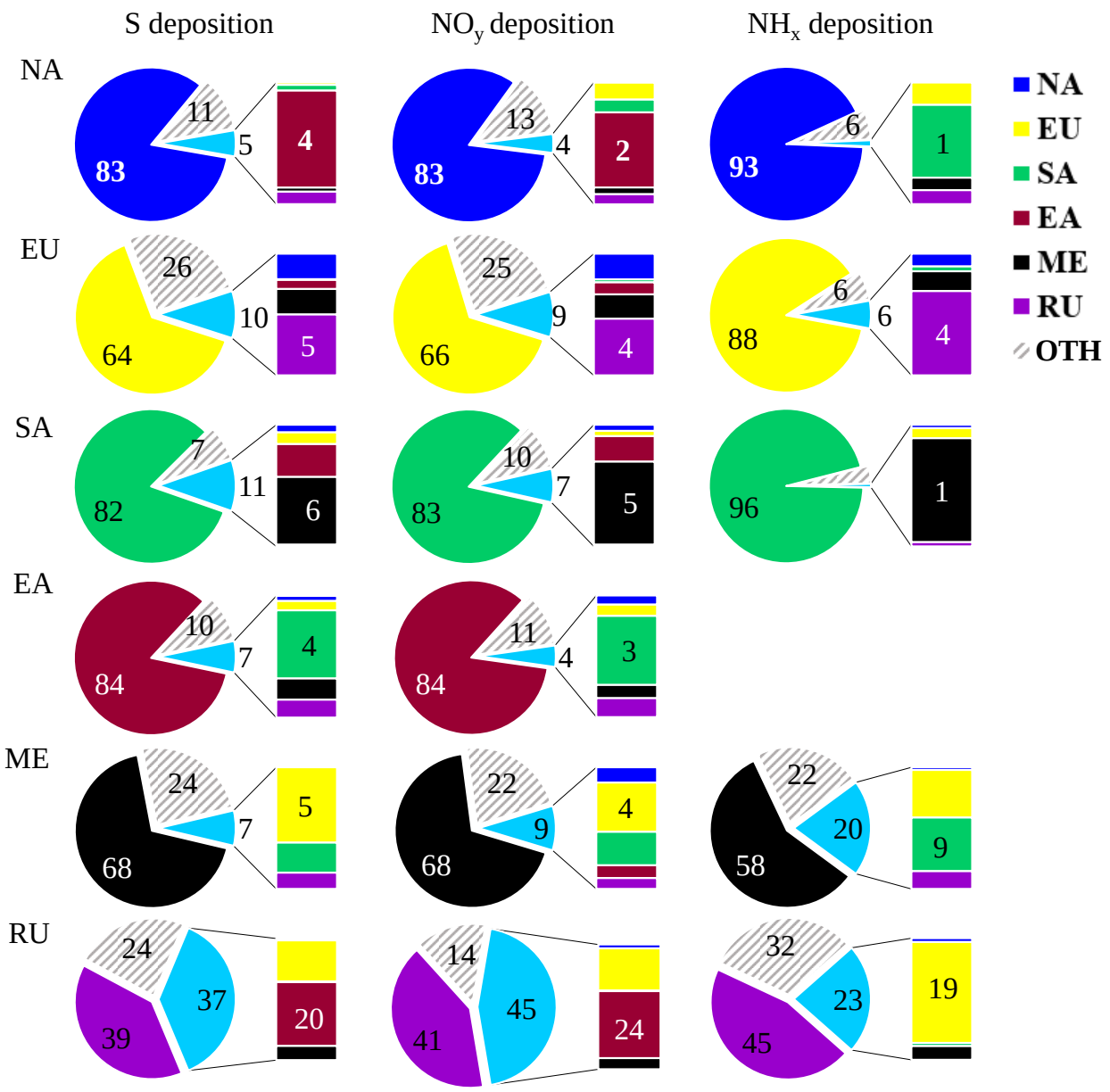

Figure 4. 8 Source contributions to S and N depositions from the hemispheric transport from foreign regions and from own region emissions. Other (OTH, pattern fill) is the contribution by other reasons than the total effects of separate emission reductions of the six regions (see manuscript for details).

4.4.4 Inter-model variations

Figure 4.9 shows the differences among models on simulating the ΔDepo of S, NO_y and NH_x deposition under emission perturbation cases, separately for wet and dry deposition. The values are global integrated changes in the components of deposition between base case and perturbation experiments from MMM results, with error bars showing the maximum and minimum values of models. The figure only shows the main compositions of S and N depositions, which together account for more than 95% of total deposition.

In terms of S deposition (Fig. 4.9(a)), the modelled ΔDepo by multiple models, defined as (maximum value of multi-model – minimum value of multi-model), ranges (0.06-0.23) Tg(N) yr^{-1} and (0.01-0.22) Tg(N) yr^{-1} for SO_2 dry and wet deposition, and (0.01-0.03) Tg(N) yr^{-1} and (0.009-0.17) Tg(N) yr^{-1} for SO_4^{2-} dry and wet deposition, respectively (ranges are for different cases). High uncertainty is found in EA perturbation case, where the model divergence are mainly from SO_2 wet and dry deposition and SO_4^{2-} wet deposition.

In terms of NO_y deposition (Fig. 4.9(b)), the differences among models range (0.003-0.07) Tg(N) yr^{-1} for NO_2 dry deposition, and (0.07-0.55) Tg(N) yr^{-1} and (0.03-0.75) Tg(N) yr^{-1} for NO_3^- dry and wet deposition, respectively. The EA perturbation case also has the largest inter-model variation, with high uncertainties in simulating both the NO_3^- wet and dry deposition. In terms of NH_x deposition (Fig. 4.9(c)), the differences among models range (0.04-0.09) Tg(N) yr^{-1} for NH_3 dry deposition, and (0.008-0.15) Tg(N) yr^{-1} and (0.002-0.11) Tg(N) yr^{-1} for NH_4^+ dry and wet deposition, respectively. Both EA and SA perturbation cases have relatively high uncertainties on NH_4^+ dry deposition.

Overall, the inter-model variations are considerably high under emission perturbation in Asian regions, especially EA. On one hand, the EA perturbation case assumes the largest amounts of emission reduction among all perturbation cases (Table S4.1 in the Appendix). On the other hand, model evaluation reported high model bias in simulating the deposition in this region (J. N. Tan, Fu, Dentener, Sun, Emmons, Tilmes, Sudo, et al., 2018), and suggested an incomplete knowledge from the combined picture provided by observations and models.

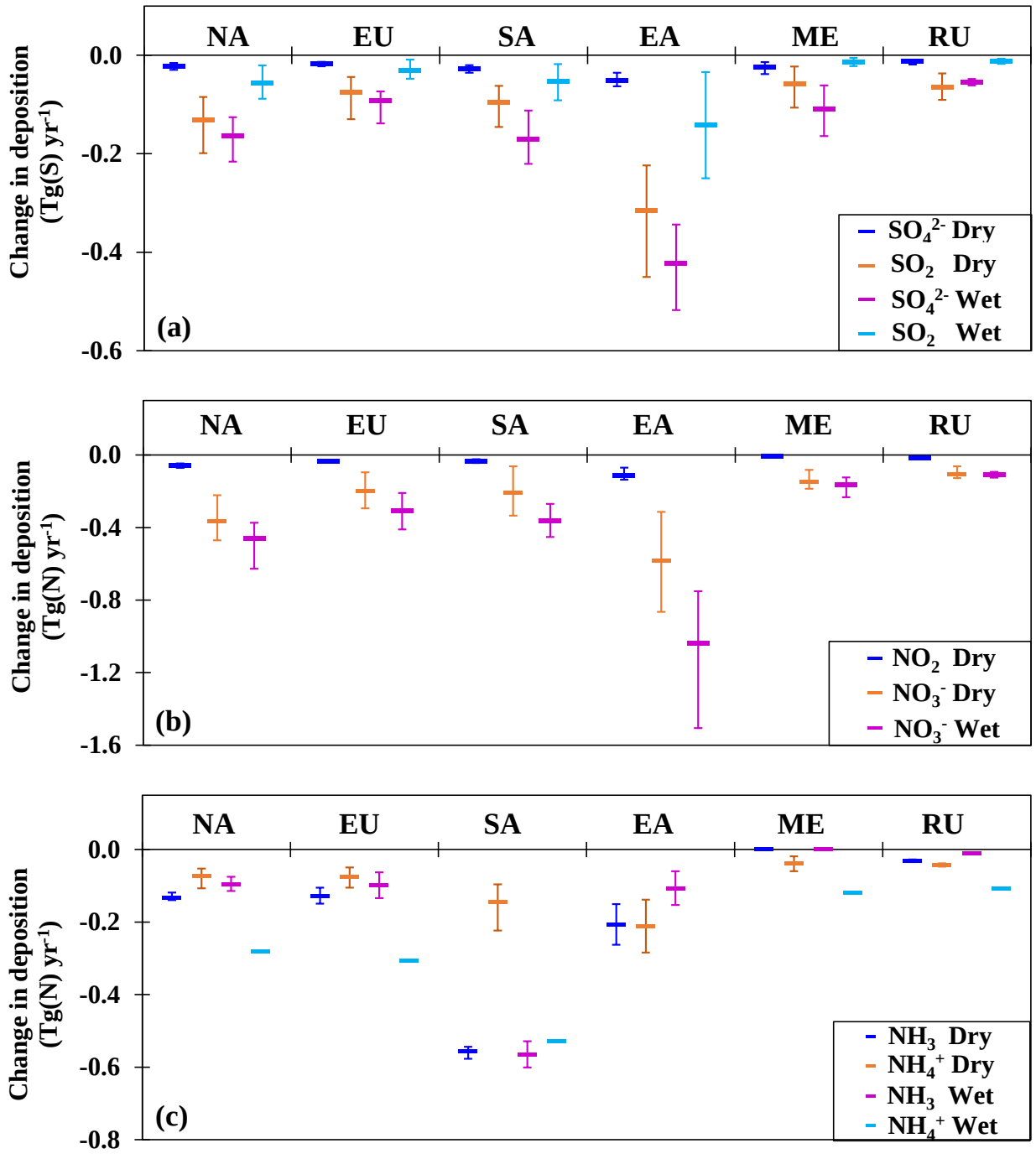

Figure 4. 9 Inter-model variations in the change of wet and dry depositions (unit: Tg(S or N) yr^{-1}) under emission perturbation experiments. The values are global integrated changes in the components of S and N depositions between the base case and the perturbation experiments from MMM results. The error bars are the max and min values among all models. Species without error bars are derived from the results of individual models.

4.5 Conclusion

This study assesses the impact of hemispheric transport on S and N depositions for six regions: North America (NA), Europe (EU), South Asia (SA), East Asia (EA), Russia (RU) and Middle East (ME), by using multi-model ensemble results from eleven models of HTAP II, with simulations under base case and 20% emission perturbation scenario for each region.

The exports of S and N emissions and oxidation products are quantified for the source regions. Results show that about 27-58%, 26-46% and 12-23% of the emitted S, NO_x and NH_3 emissions are deposited outside of the source regions (ranges are for different source regions). The most significant exports of emissions are: (1) transport between EU and RU. 10-14% of EU's emissions are transported to RU and 7-12% of RU's emissions are transport to EU; (2) transport between EA and RU. 5% of EA's emissions are transported to RU and 4-5% of RU's emissions are transported to EA; (3) transport from SA to EA (4-9%). Most regions export 5-10% more emissions in winter than summer, which is highly influenced by chemistry, precipitation amount and frequency, atmospheric mixing and transport patterns.

The impacts of hemispheric transport on deposition are studied for the receptor regions. Overall, 20% emission reduction in the source regions could affect 1-10% of deposition in foreign continental regions and 1-14% in foreign coastal regions and the open ocean. The most significant impacts are from NA to the North Atlantic Ocean (2-14%), and from EA to the North Pacific Ocean (2-12%) and to western NA (4-6%). The amounts of deposition brought by hemispheric transport range 10^4 - 10^5 kg(S or N) $month^{-1}$ per 0.1° longitude (meridional sum). The impacts via short-distance transport between neighbouring regions (i.e. EU to RU) are found throughout the whole year and slightly stronger in winter, while those by long-range transport (i.e. from EA to NA) are mainly found in spring and fall.

The contributions of hemispheric transport on local deposition are compared with those of own region emissions. The deposition in NA, SA and EA is dominated (~80%) by their own region emissions, while EU, ME and RU receive 40-60% of deposition from hemispheric transport. In particular, Russian deposition is almost equally contributed by foreign inputs and own region emissions, with high contributions from two neighbouring source regions: EA (~20%) and EU

(~15%). For some regions, upmost half of the exported emissions from foreign regions are deposited over their coastal regions. Deposition in coastal regions or the near-coastal open ocean is found twice more sensitive to long-range transport than non-coastal regions. For some coastal regions such as west coast of NA and west coast of EU, the impacts of hemispheric transport are identical or even larger than controlling own region emissions.

This study highlights the impact of hemispheric transport on aggravating the deposition burden, especially in coastal regions and the open ocean, which hasn't been fully studied in the literatures. It is suggested to conduct further research on the impact on the mitigation of coastal and oceanic ecosystem, with regards to the increasing air pollutants in the hemispheric outflow. Significant impacts of hemispheric transport on deposition are also found in relatively low emission intensity regions such as RU. Meanwhile, there is still a portion of foreign impacts that haven't been attributed in this study. For instance, at least four regions (NA, EU, SA and ME) have shown considerable impacts (2-10%) on the S and N depositions in North Africa. But since North Africa is not included as a receptor/source region in the perturbation experiments, it is hard to quantify the amount. Meanwhile, Southeast Asia is regarded as a big emission contributor in Asia. It is important to establish an S-R relationship with other Asian regions. It is suggested to include these regions in the perturbation experiments in future studies.

CHAPTER 5
EXCEEDANCE OF CRITICAL LOADS OF ATMOSPHERIC DEPOSITION

This article hasn't been published anywhere, nor will it be before I turn in the final version of my ETD, so I didn't include a publication statement.

5.1 Abstract

Critical load (CL), which is the threshold to describe the maximum burden of deposition that the ecosystem can bear before the occurrence of significant changes on the sensitivity compounds of the ecosystem, has been used to assess the exceedance of S and N depositions. Three commonly used methods to calculate CLs are introduced: Empirical CLs, Simple Mass Balance (SMB) model and Dynamic model. This study collects the available datasets for empirical and SMB CLs over U.S., EU and China from publications and assesses the exceedance of these CLs with modelled S and N depositions over U.S. and EU in 2001 and 2010. Changes in the status between exceeding CLs and no exceedance is trivial (0-5% changes) during ten years over U.S. for most ecosystems in this study, but we found large decreases in the magnitude of exceedance over Northeast U.S. and significant increases in the magnitude of exceedance in Southwest U.S., especially California. Study over EU, otherwise, found significant changes (up to 10% change) in the exceedance status in Western Ireland, Northern England, South Norway and South Sweden (from exceeding CLs to no exceedance), and decreases in the magnitude of exceedance over many regions in central EU.

5.2 Introduction

Nature gives response when the loading of N deposition has exceeded certain thresholds. The term "critical load (CL)" is used to quantify such threshold, which is described as the maximum burden of deposition that the ecosystem can bear before the occurrence of significant changes on the sensitivity compounds of the ecosystem. A formal definition of CL is "the highest load that will not cause chemical changes leading to long-term harmful effects on most sensitive ecological systems" (Nilsson, 1988).

The CLs have been widely used to assess the exceedance of atmospheric deposition. About 7-17% and 7-18% of the global ecosystems have exceeded the CLs for acidification (S and N depositions) and eutrophication (N deposition) in 1992 (A. F. Bouwman et al., 2002). The risks were high in the industry-intensive regions in U.S., EU, RU, Asia and parts of South America and Africa. Regional studies were also conducted. For NA, about 24 of the 45 national parks in U.S. received exceeded N deposition in 2006 (Ellis et al., 2013). And another 14 parks were located close to the regions (~50 km) that exceeded the crucial loads (Ellis et al., 2013). For EU, about 5% of the forest regions in Galicia, Spain has exceeded the CLs for acid S and N depositions (Rodriguez-Lado & Macias, 2006). About 54% of ecosystems have exceeded N and S depositions in 2000, especially in Germany and Poland and southern EU (Posch et al., 2015). For Asia, about 50% of the ecosystems have exceeded the N and S deposition in 2000 in China, especially in eastern and south-central China, where intensive industries were located (Posch et al., 2015). A study in China calculated the sensitivity of CLs exceedance to acidity, S deposition and N deposition separately, and found that southeast China was sensitive to acid deposition and northwest China was more affected by CLs for N deposition (Duan et al., 2001).

Among these studies, most of CLs were developed on country-scale or regional-scale, probably due to the requirement for site-specific variables and expertise knowledge. This study collects the available CLs over U.S., EU and China from publications and reports and compares the data inputs and processes used to calculate the CLs by different studies (sect. 5.4.1). Then we map the CLs over U.S. and EU with ArcGIS, with a comparison of studies on the same object (sect. 5.4.2). Finally, we assess the exceedance of CLs with the S and N depositions created in Chapter 2 (sect. 5.4.3). We compare the exceedance of CLs in 2001 and 2010 to investigate the changes in the last decade.

5.3 Methods

The impacts of pollutants on ecosystems is classified into critical limit and CL. Critical limit is the impact on the above-ground part of vegetation, such as the exposure to SO_2, NO_x, O_3 and other air pollutants, and is also recognized as “direct” impact since it can be easily observed. CL is

associated with the impacts on the ground soil-mediated part, which is mainly associated with changes in the chemical and biological characteristics of soils. The changes involve multiple factors including the pH value, alkalinity, N and mineral nutrients, concentration of soluble aluminum, and the mobilization of potentially toxic cations such as aluminum and heavy metals. The pH value and alkalinity are related to the acidification effects of S and N depositions. CL is known as "indirect effect" of excessive deposition. The studies are conducted separately on terrestrial ecosystems and aquatic ecosystems. This study focuses on exceedance of CLs on terrestrial ecosystems. Three types of methods are commonly used in recent studies to calculate the CL according to the research goals and data availability: Empirical CLs, Steady-State Mass Balance model (SSMB) or Simple Mass Balance model (SMB) and Dynamic Model. Following are methods to calculate CLs:

5.3.1 Empirical CLs

Empirical CLs are derived from the responses of the ecosystems/receptors to different deposition levels from site observations or laboratorial experiments. The common negative responses are changes related to the abundance of species (such as decrease in specie growth or richness), structure of ecosystems (such as change in community composition and reduction in the diversity of species) and functioning (such as decomposition or mineralization rate) (Bobbink et al., 2015).

Methods. The most widely used ways to attain data include long-time field addition experiments, N deposition gradient studies and long-term monitoring studies (Bobbink et al., 2015). The field addition experiment increases the N deposition artificially by adding inorganic N into the ecosystem. Then it detects the time for occurrence of significant changes in different components of the ecosystem. The most common problem lays in the determination of the background level. It is recommended to set-up experiment areas with low-background N concentration to help identifying significant changes. The N deposition gradient study is field survey in sites with gradient distributions of N deposition (such as sites nearby to intensive emission sources). It is recommended to carry out study in regions rich with common structural and functional species, but it is not applicable for rare species. Long-term monitoring studies use large and long-term observation datasets, thus the coverage of study can be much wider than the previous two. But it

is hard to tell the contribution of specific components of deposition (such as NO_y or NH_x deposition) to the changes in the ecosystem since other factors such as changes in land use and management may also contribute.

Reliability/uncertainty. (Unece, 2004) checked the uncertainty of empirical CLs by checking the comparability of the results among different studies for the same ecosystems. The uncertainties are classified to (1) reliable: when the results are comparable among several studies, (2) quite reliable: when some studies are comparable and (3) expert judgement: no other studies available for comparison and the uncertainty is depend on expert judgement.

5.3.2 SMB model

The SMB model calculates the CLs according to the mass balance of the soil factors. Depending on the harmful effects, CLs can be classified into three categories: eutrophication CLs (CL_{nut}), acidification CLs (CL_{acd}) and mental accumulation. This study includes the first two categories of CLs. CL_{nut} is related to over-richness in nutrient, and current studies only include N deposition. Another essential nutrient for organism is bioavailable P. It has already raised public attention due to increased N:P ratio in many regions under human perturbation in recent years (Elser et al., 2009). See more information and discussion in Chapter 6. CL_{acd} is caused by the acidic components in depositions, thus it is associated with the amounts of both S and N depositions

Uncertainty: The SMB model requires average data from long-term observation. Therefore, short-term values are not recommended for application regarding the possibility of natural perturbation (rotation of forest) and anthropogenic perturbations (i.e. harvesting). Furthermore, the SMB model considers the whole soil system as a single and homogeneous layer, thus it ignores the biochemical processors inside the soil system.

Calculation of CL_{nut}. The development of CL_{nut} is based on the mass balance assumption in Eq. *(5-1)*. After ignored the time-dependent variables (such as N_{ad}) and relatively small-value variables (such as N_{eros}), the model is simplified to Eq. *(5-2)*. Assuming that CL_{nut} is equal to N_{dep} at the critical point, CL_{nut} is calculated as Eq. *(5-3)*.

$$N_{dep} + N_{fix} = N_{ad} + N_i + N_u + N_{de} + N_{eros} + N_{fire} + N_{vol} + N_{le,acc} \quad (5\text{-}1)$$

$$N_{dep} = N_i + N_u + N_{de} + N_{le} \quad (5\text{-}2)$$

$$CL_{nut}(N) = N_i + N_u + N_{de} + N_{le,acc} \quad (5\text{-}3)$$

where:

N_{dep}	Input of N by total N deposition
N_{fix}	Input of N by biological fixation of N from atmosphere. The value is negligible in forest ecosystems for non-N fixing species
N_{ad}	Adsorption of N, such as NH_4 adsorbed by clay minerals, which accounts as N accumulated in soil. Ignored at steady state
N_i	Loss of N due to immobilization
N_u	Loss of N due to harvesting vegetation and animals
N_{de}	Loss of N by denitrification. Release of N to the atmosphere
N_{eros}	Loss of N by erosion, relatively small value
N_{fire}	Loss of N by fire, relatively small value
N_{vol}	Loss of N by NH_3 volatilization
N_{le}	Loss of N due to leaching
$N_{le,acc}$	Value of N_{le} at the critical point

Calculation of CL_{acd}. CL_{acd} is established base on the balance of ions in the leaching of soils according to Eq. *(5-4)*. The leaching of Acid Neutralising Capacity (ANC) is defined as Eq. *(5-5)*. The leaching of species is associated with atmospheric deposition and other factors (Eqs. *(5-6)* - *(5-10)*).

$$H_{le} + Al_{le} + BC_{le} + NH_{4,le} = SO_{4,le} + NO_{3,le} + Cl_{le} + HCO_{3,le} + Org_{le} \quad (5\text{-}4)$$

$$ANC_{le} = -H_{le} - AL_{le} + HCO_{3,le} + Org_{le} \quad (5\text{-}5)$$

$$Cl_{le} = Cl_{dep} \quad (5\text{-}6)$$

$$BC_{le} = BC_{dep} + BC_w - BC_u \quad (5\text{-}7)$$

$$S_{le} = S_{dep} - S_{ad} - S_i - S_u - S_{re} - S_{pr} \quad (5\text{-}8)$$

$$NO_{3,le} = N_{dep} - N_i - N_u - N_{de} \quad (5\text{-}9)$$

$$NO_{4,le} = 0 \quad (5\text{-}10)$$

where:

Al	Positive changed aluminum
BC	Sum of base cations (*BC*), sum of *Ca, Mg, K* and *Na*
Org	Organic anions
Subscript *le*	Leaching
Subscript *w*	Weathering

Subscript *u*	Net growth uptake
Subscript *ad*	Adsorption
Subscript *i*	Immobilization
Subscript *re*	Reduction
Subscript *pr*	Precipitation
Subscript *de*	Denitrification

The S_{ad}, S_i, S_u, S_{re} and S_{pr} are ignored since the values are insignificant in the S cycle. After simplification, Eq. *(5-4)* is changed to Eq. *(5-11)*. Again, we assume the CL of N (*CL(N)*) and CL of S (*CL(S)*) are equal to N_{dep} and S_{dep} at the critical point (Eq. (*5-12*)). Finally, CL_{acd} is calculated by Eqs. *(5-13)– (5-15)*.

$$N_{dep} + S_{dep} = BC_{dep} + BC_w - BC_u + N_i + N_u + N_{de} - Cl_{dep} - ANC_{le} \quad (5\text{-}11)$$

$$CL(N) + CL(S) = BC_{dep} + BC_w - BC_u + N_i + N_u + N_{de} - Cl_{dep} - ANC_{le} \quad (5\text{-}12)$$

$$CL_{max}S = BC_{dep} - Cl_{dep} + BC_w - BC_u - ANC_{le,crit} \quad (5\text{-}13)$$

$$CL_{min}N = N_i + N_u + N_{de} \quad (5\text{-}14)$$

$$CL_{max}N = CL_{min}N + CL_{max}S \quad (5\text{-}15)$$

Exceedance of CLs. The exceedance of CL_{nut} (Ex_{nut}) is calculated by Eq. *(5-16)*.

$$Ex_{nut}\ (N\ depo) = N_{dep} - CL_{nut}(N) \qquad N_{dep} > CL_{nut}(N)$$
$$= 0 \qquad N_{dep} \leq CL_{nut}(N) \quad (5\text{-}16)$$

The exceedance of CL_{acd} (Ex_{acd}) involves both N and S depositions and is assessed by the following procedures. First, the values of S and N depositions are changed to equivalent CLs following Eqs. *(5-17)* and *(5-18)*, which refer to molar equivalent of potential acidity resulting from S, N and BC. The calculation is based on the ion charge. NO_y and NH_x are referred as NO_3^- and NH_4^+, with valency of 1, and the prevalent form of S is SO_4^{2-}, with charge of 2.

$$1 \text{ eq N ha}^{-1}\text{ yr}^{-1} = 14 / 1000 \text{ Kg N ha}^{-1}\text{ yr}^{-1} \quad (5\text{-}17)$$

$$1 \text{ eq S ha}^{-1}\text{ yr}^{-1} = 32 / (2 \times 1000) \text{ Kg S ha}^{-1}\text{ yr}^{-1} = 16 / 1000 \text{ Kg S ha}^{-1}\text{ yr}^{-1} \quad (5\text{-}18)$$

Then, Ex_{acd} is calculated by Eq. *(5-19)*. Five different equations are applied to the "Regions" in Fig. 5.1.

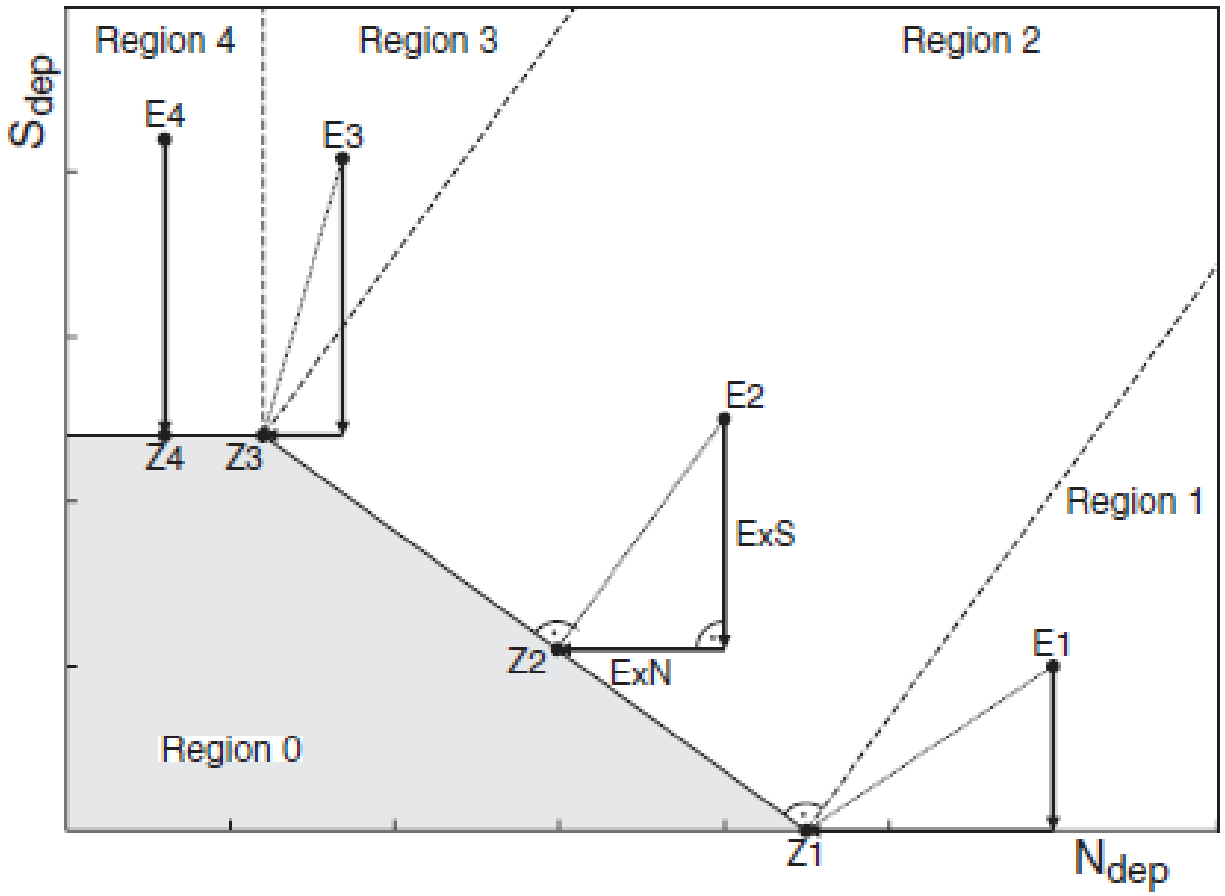

Figure 5. 1 Calculation of the exceedance at different conditions (adopted from (*Critical Loads and Dynamic Risk Assessments*, 2015)).

$$
\begin{aligned}
Ex_{acd} &= 0 \; or \; E_0 && \text{(Region 0)} \\
&= N_{dep} - CL_{\max}(N) + S_{dep} && \text{(Region 1)} \\
&= N_{dep} - N_0 + S_{dep} - S_0 && \text{(Region 2)} \\
&= N_{dep} - CL_{\min}(N) + S_{dep} - CL_{\max}(S) && \text{(Region 3)} \\
&= S_{dep} - CL_{\max}(S) && \text{(Region 4)} \qquad \textit{(5-19)}
\end{aligned}
$$

$$N_0 = \frac{N_{dep} + mS_{dep} + m^2 CL_{\max}(N)}{1+m^2} \qquad \textit{(5-20)}$$

$$S_0 = m(N_0 - CL_{\max}(N)) \qquad \textit{(5-21)}$$

$$m = \frac{CL_{\max}(S)}{CL_{\min}(N) - CL_{\max}(N)} \qquad \textit{(5-22)}$$

$$
\begin{aligned}
E_0 &= S_{dep} - CL_{max}(S) && N_{dep} \le CL_{min}(N) \\
&= S_{dep} - mN_{dep} - CL_{max}(N) && CL_{min}(N) < N_{dep} \le CL_{max}(N) \qquad \textit{(5-23)}
\end{aligned}
$$

where S_0 and N_0 are calculated by Eqs. *(5-20)* - (*5-22)*. Study by (Makar et al., 2018) calculated the E_0 value with Eqs *(5-23)*, which is a negative value to define the distance from the current deposition level to exceed CL_{acd}.

5.3.3 Dynamic model

Dynamic models are biogeochemical models that simulate the biogeochemical response of the ecosystems to changes in the environment. Figure 5.2 shows the chemical responses and changes of acid deposition in five stages in dynamic models: Stage 1: When the acid deposition is below CLs, no significant chemical changes are found. Stage 2: When the acid deposition increases to above CLs, the chemical response, although increases with time, is delayed because of the damage buffer effect. No significant chemical changes are shown during this Damage Delay Time (DDT). Stage 3: After DDT, the chemical responses become significant. Stage 4: The acid deposition drops to level below CLs, but the chemical criterion is still under coverage. This time zone is called Recovery Delay Time (RDT). Stage 5: After RDT, the influences on the ecosystem are fully recovered. This diagram assumes the damages are recoverable, which may not be the reality in some cases. Compared to empirical CLs, dynamic model can both tell when the significant changes occur and identify which specific components of deposition are responsible for the changes.

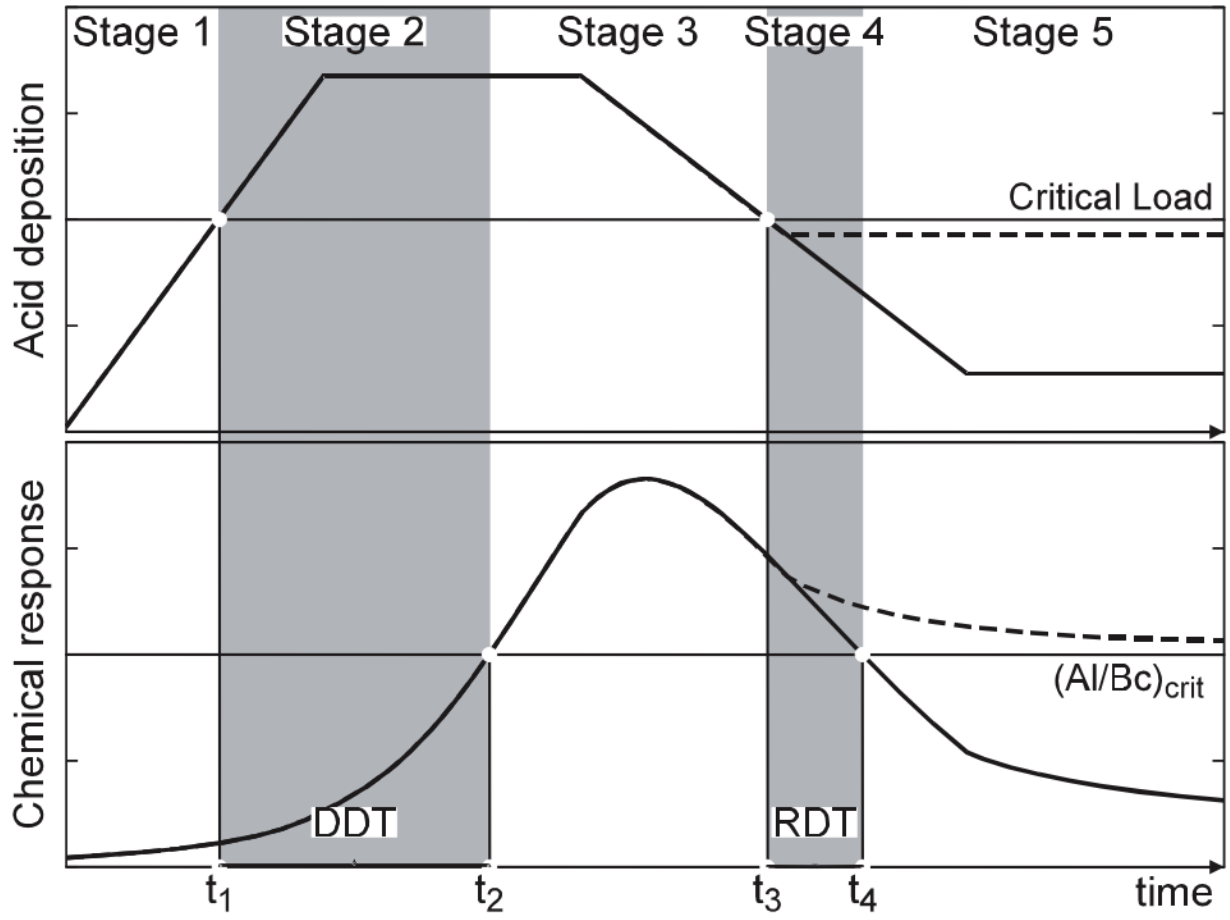

Figure 5. 2 The chemical responses to acid deposition changes at five stages (adopted from (*Critical Loads and Dynamic Risk Assessments*, 2015)).

Compared to SMB model which does not involve temporal changes, dynamic model considers the leg effect between the exceedance of CLs and the occurrence of significant changes in the ecosystems. This helps to answer the time-dependent questions, such as when the adverse impacts will show up after CLs are exceeded and when adverse impacts on the ecosystem would be fully removed after the acid deposition is reduced to level below CLs, which are important references for developing control strategies.

5.4 Results

5.4.1 Collection of CLs over different ecosystems.

The CLs are generally developed on country-scale or region-scale, probably due to the requirement for site-specific variables and expertise knowledge. There is no global-scale CLs dataset based on our review of available literature. In this section, we collect and introduce available CLs over different regions from publications and reports (Table 5.1).

Dataset 1. The National Critical Loads Database (NCLD, version 3.0) was released by NADP Critical Loads of Atmospheric Deposition (CLAD) Science Committee of US in 2017. The package is available for download at: http://nadp.slh.wisc.edu/ committees/clad/db/. It compiled CLs datasets published in peer-reviewed journals or federal and institutional reports over U.S. This study uses the results of seven terrestrial ecosystems, including empirical CLs for Herbaceous Plant (HP) community (Pardo et al., 2011; Simkin et al., 2016), Lichen community (Geiser, Jovan, Glavich, & Porter, 2010; Pardo et al., 2011; Root, Geiser, Jovan, & Neitlich, 2015), Fungi community, nitrate leaching and forest-tree health (Pardo et al., 2011) and CL_{acd} derived from the SMB model (Duarte, Pardo, & Robin-Abbott, 2013; McNulty et al., 2007; Phelan et al., 2014). All data are prepared in the E00 format and are easy to read by ArcGIS. We map these CLs in sect. 5.4.2. For empirical CLs, the values derived from limited site experiments are applied to the same ecoregions (Fig. S5.1 in Appendix). For those ecosystems with more than one study, such as the studies on HP community from (Pardo et al., 2011) and (Simkin et al., 2016), we compare the studies in sect. 5.4.2 and use the one that is more applicable to this study in sect. 5.4.3. For SMB

Table 5. 1 Available datasets for CLs

Datasets.	Region	Ecosystem for application	Harmful effects	Species	Spatial Resolution	Method	Reference	Data Format
1	US	Terrestrial ecosystem	Acidification	N and S depositions	Points	SMB model	(Blett et al., 2014; Clark et al., 2018)	E00
		Aquatic ecosystem						
		Forest-Tree Health	Nutrient	N deposition	Level 1 ecoregion, polygon	Empirical		
		NO_3^- Leaching						
		Fungi						
		Lichen						
		HP						Table
2		Different Ecoregions					(*Critical Loads and Dynamic Risk Assessments*, 2015)	Table 5.1, page 134-141
3	UK	Acid grassland, calcareous grassland, dwarf shrub heath, bog, montane, unmanaged woodland, dune grasslands, saltmarsh	Nutrient	N	1×1 km	Empirical	(Hall, 2018)	Excel
		Managed woodland				SMB		
		Acid grassland, calcareous grassland, dwarf shrub heath, bog, montane, and unmanaged woodland	Acidification	N and S	1×1 km	Base on mineralogy and soil chemistry, with habitat-specific data		
		Managed woodland	Acidification	N and S	1×1 km	SMB		
		1752 surface water	Acidification	-	-	Catchment-based First-order Acidity Balance (FAB) model		
2	Europe	Different Ecoregions	Nutrient	N deposition	European Habitat	Empirical	(*Critical Loads and Dynamic Risk Assessments*, 2015)	Table 4.1 page 91-95
4	Europe and China	Forest and (semi-) natural vegetation	Nutrient	N	0.5°×0.5°	SMB	(Posch et al., 2015)	Figure (color)
			Acidification	N and S				
5	Europe and North Asia	Terrestrial ecosystem	Acidification	N and S	50×50 km	SMB	(Reinds, Posch, De Vries, Slootweg, & Hettelingh, 2008)	Figure (black &white)
6	China	All	Acidification and Nutrient	N and S	1°×1°	SMB	(Duan et al., 2001)	Figure (black &white)
7		Five forest catchments	-	N	Site specific	Extend S-N-BC CL function base on SMB	(Zhao, Duan, Larssen, Hu, & Hao, 2007; Zhao, Duan, Larssen, Mulder, et al., 2007)	Table

model CLs, only the study by (McNulty et al., 2007) covers the whole CONUS, whereas the other studies by (Phelan et al., 2014) and (Duarte et al., 2013) were conducted on small areas (Pennsylvania in Phelan's study and Northeastern U.S. in Duarte's study). Therefore, we only use McNulty's results in the following study.

Dataset 2. (*Critical Loads and Dynamic Risk Assessments*, 2015) collected empirical CLs from literatures for different ecosystems over U.S. (Table 5.1 of the reference, page 134-141) and Europe (Table 4.1 of the reference, page 91-95). We map the empirical CLs from these datasets on the spatial maps of ecosystems over EU in sect. 5.4.2 (since dataset 1 already includes a detailed dataset for empirical CLs over U.S.). The spatial map of the European habitat is downloaded in from European Environment Agency (https://www.eea.europa.eu/data-and-maps/data/ecosystem-types-of-europe/level-1/1km) (Fig. S5.2 in Appendix). Then, we attribute the empirical CLs to the corresponding ecosystems in ArcGIS.

Dataset 3. (Hall, 2018) developed CL_{nut} and CL_{acd} for UK habitats. The spatial resolution of the CLs map is 1km. It used the distribution of habitats from Land Cover Map 2000 (LCM2000) at 10km resolution. Results are recorded in excel files and can be downloaded from Environmental Information Platform at: https://doi.org/10.5285/299e2779-0787-46bb-9482-03ad474eae27. Since the geographical information is not available, we do not use this dataset in the following study, but we will consider it in future study.

Datasets 4-7. Datasets 4-7 calculated CLs with SMB model. We compare the input data of these studies in Table 5.2. The main parameters required to calculate SMB CLs are land cover type, soil parameters (includes soil type, soil texture, parent material class and drainage class), BC deposition and weathering, net nutrient uptake, N immobilization, denitrification and meteorological and hydrological parameters. BC deposition data were either derived from observation network or dispersion model. Studies for U.S. and EU calculated the BC weathering rates as a function of soil parameters, and studies for China used the PROFILE model

Table 5. 2 Comparison of the parameters used to calculate SMB CLs in different datasets

Datasets in Table 5.1	Region	Land cover	Soil parameters	BC deposition	BC weathering	Net nutrient uptake	N immobilization	Denitrification	Meteorology and hydrology
1	U.S.	USGS + USDA, 1km resolution	STATSGO data set	NADP observation	Calculated as a function of soil parent material class and texture material, adjusted with temperature	Estimated by annual average growth of major vegetation types and the element contents of BC and N in these compartments	42.86 eq N ha^{-1} yr^{-1}	Set as 0	Local runoff map
4	EU	Global Land Cover 2000, 1km resolution	The European Soil Database v2 map	Dispersion model			71.4 eq N ha^{-1} yr^{-1}	Denitrification flux estimated as a function of soil drainage status	Long-term temperature and precipitation were observation from European database; Evaporation and runoff were from IMAGE model
	China	Vegetation map from literature, 95 types	Soil map from literature, 43 soil types	Calculated by estimated emission and dynamic Eulerian model simulation	Calculated with the PROFILE model		Total amount of soil N divided by the period of soil formation	-	Local runoff map
5	EU	Harmonized land cover map by Coordination Center for Effects (CCE) and Stockholm Environment Institute (SEI) and Global Land Cover 2000	The European Soil Database v2 map	EMEP monitoring and modelling	Same as the method of dataset 1		71.4 eq N ha^{-1} yr^{-1}	Denitrification flux estimated as a function of soil drainage status	Long-term temperature and precipitation were observation from European database; Evaporation and runoff were from IMAGE model
6	China	86 vegetation types	46 soil groups	National monitoring network	Calculated with the PROFILE model		-	-	-

(Warfvinge & Sverdrup, 1992), which also calculated the weathering rate with soil data. Eq. *(5-24)* shows the calculation of weathering rate by (McNulty et al., 2007):

$$\begin{aligned} W &= (56.7 \times \%clay) - (0.32 \times \%clay^2) && \text{Acid substrate} \\ &= 500 + (53.6 \times \%clay) - (0.18 \times \%clay^2) && \text{Intermediate substrate} \\ &= 500 + (59.2 \times \%clay) && \text{Basic substrate} \end{aligned} \quad (5\text{-}24)$$

where *W* is the weathering rate; *%clay* is the percentage of clay in soils.

Net nutrient uptake is the amount of BC and N removed from soils by harvesting. All studies used the same method by using the annual average growth of major local vegetation and the content of BC and N in vegetation. N immobilization is the process that micro-organisms covert inorganic N to organic N (see sect. 1.1 in Chapter 1 for details). (McNulty et al., 2007) showed a range of this rate from 14.3 to 35.7 eq N ha^{-1} yr^{-1} for cold climates and 71.4 eq N ha^{-1} yr^{-1} for warm climates. Studies for EU adopted the upper end of this range and studies for U.S. used a value between cold and warm environments. Denitrification is the process to convert NO_3^- to N_2 gas as a loss of soil N. Although it was set as zero in the study for U.S., but would be assigned with values in future studies due to its importance in wetland (McNulty et al., 2007).

5.4.2 Empirical and SMB CLs over U.S. and EU

This section plots the spatial distributions of CLs over U.S. (dataset 1 in Table 5.1) and EU (dataset. 2 in Table 5.1) with ArcGIS.

Empirical CLs for HP community over U.S. (Simkin et al., 2016) and (Pardo et al., 2011) developed empirical CLs for HP community. The exceedance of CLs would result in reduction of community richness. Simkin's results are applied to Ecoregion Levels I-IV (Fig. S5.1 in Appendix). Figure 5.3 shows the mapping on the finest land cover classification (Ecoregion Level IV). Pardo's work developed CLs on a coarse land cover map (Ecoregion Level I) (Fig. 5.4(a, c)). We compare the results of these two studies in Fig. 5.4. Both studies lack studies for ecoregion-7 marine west coast forest, ecoregion-12 southern semiarid highlands and ecoregion-15 tropical wet forests. Pardo's work has large ranges between minimum CLs (CL_{min}) and maximum CLs (CL_{max}),

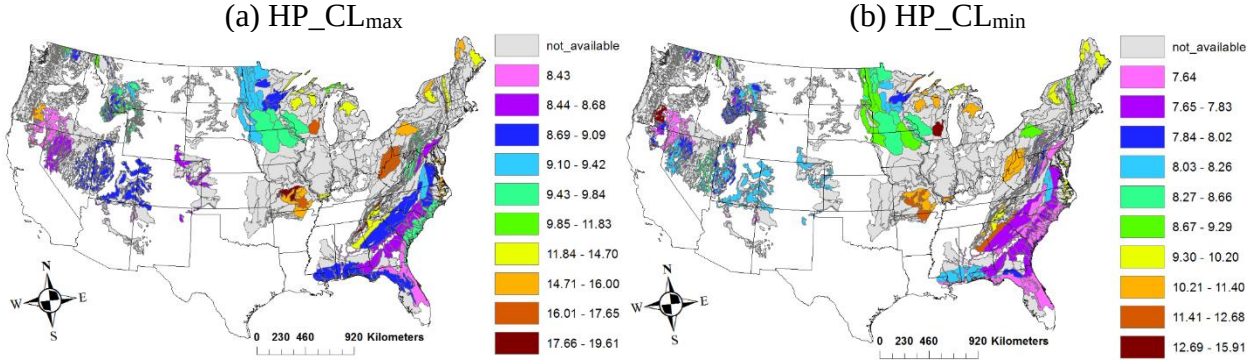

Figure 5. 3 Empirical *CL*$_{max}$ and *CL*$_{min}$ for HP community on Ecoregion IV developed by (Simkin et al., 2016). Unit: Kg (N) ha^{-1} yr^{-1}.

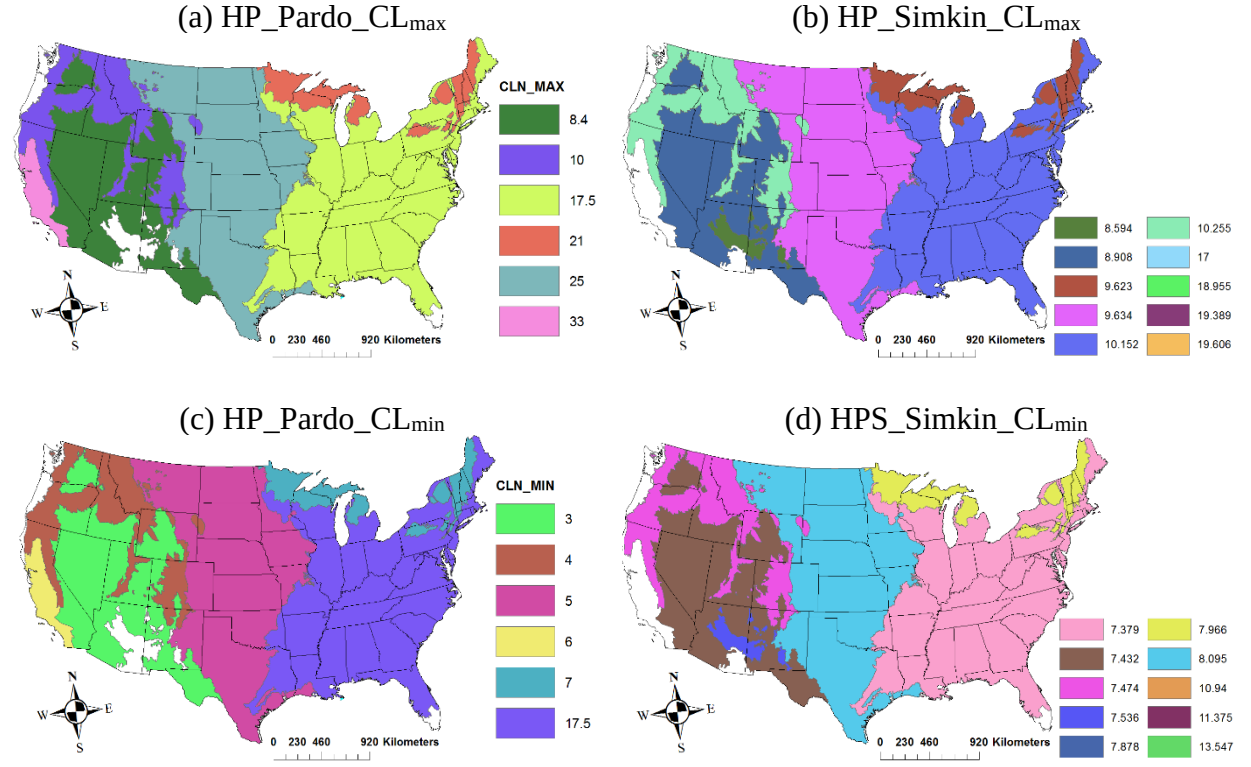

Figure 5. 4 Empirical *CL*$_{max}$ and *CL*$_{min}$ for HP community on ecoregion I by (Pardo et al., 2011) and (Simkin et al., 2016). Unit: Kg (N) ha^{-1} yr^{-1}.

while the ranges in Simkin's work are relatively smaller.

As for CL_{max} (Fig. 5.4 (a, b)), two studies are consistent on ecoregion-6 northwestern forested mountains (CL_{max} around 10 kg N ha^{-1} yr^{-1}) and ecoregion-10 North American Deserts (CL_{max} around 8.5 kg N ha^{-1} yr^{-1}). Large discrepancies between two studies are found in ecoregion-9 Great Plains, where Pardo's work (25 kg N ha^{-1} yr^{-1}) is much higher than Simkin's work (9.6 kg N ha^{-1} yr^{-1}); ecoregions-5 Northern forests, where Pardo's result (21 kg N ha^{-1} yr^{-1}) is much higher than Simkin's result (9.6 kg N ha^{-1} yr^{-1}); ecoregion-8 Eastern temperate forest, where Pardo's value (17.5 kg N ha^{-1} yr^{-1}) is higher than Simkin's value (10.2 kg N ha^{-1} yr^{-1}). As for CL_{min} (Fig. 5.4 (c,d)), two studies are consistent for most ecoregions (differences < 3 Kg N ha^{-1} yr^{-1}) except ecoregion-8 Eastern temperate forest, where Pardo's result (17.5 kg N ha^{-1} yr^{-1}) is much higher than Simkin's result (7.4 kg N ha^{-1} yr^{-1}). Overall, the comparison between the two studies indicates relatively high uncertainty on ecoregion-8 Eastern temperate forest, followed by ecoregion-9 Great Plains and ecoregion-5 Northern forests. We use Simkin's results in the following study because it provides results on finer ecoregion classification (Fig. 5.3). But since Simkin's CLs is generally lower than Pardo's results, it is likely that using Simkin's results may overestimate CLs exceedance.

Empirical CLs for Lichen ecosystem over US. (Pardo et al., 2011) developed the empirical CLs for lichen community and mapped them on Ecoregion Level I (Fig. 5.5 (a,c)). (Geiser et al., 2010) and (Root et al., 2015) also studied CLs for lichen (the two studies were combined and is referred as GeiserRoot in the following study), but the study regions only included Western Oregon and Washington Forest (Fig. 5.5 (b,d)). We compare the results between the two studies in Fig 5.5. As for CL_{max}, the two studies are consistent in ecoregion-5 northern forest and ecoregion-15 Marine west coast forest, but are different in ecoregion-13 Northwestern forested mountains, where Pardo's study (7.1 Kg N ha^{-1} yr^{-1}) is slightly higher than GeserRoot's study (2.5-6 Kg N ha^{-1} yr^{-1}). As for CL_{min}, big differences between two studies are found in ecoregion-7 Marine west coast forest, where GeiserRoot's study attributes higher CLs (4-10 Kg N ha^{-1} yr^{-1}) than Pardo's study (2.7 Kg N ha^{-1} yr^{-1}).

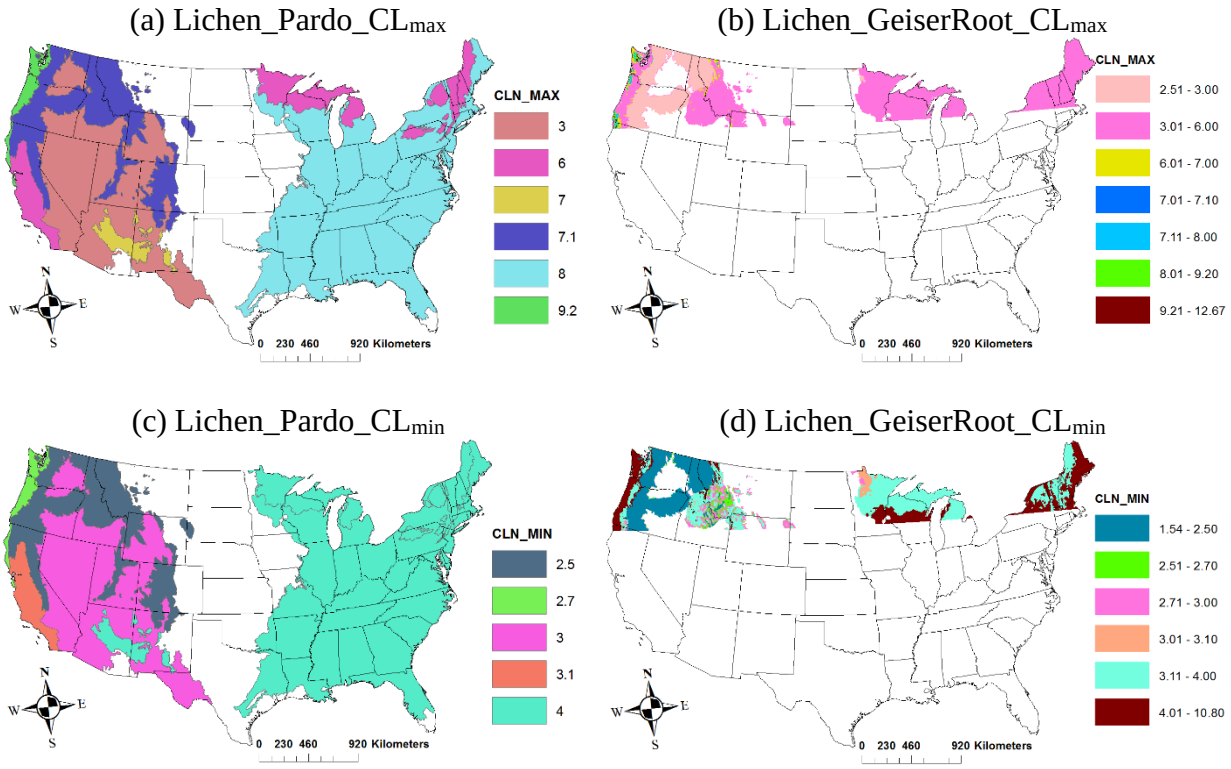

Figure 5. 5 Empirical *CL$_{max}$* and *CL$_{min}$* for Lichen community. Unit: Kg (N) ha^{-1} yr^{-1}.

Empirical CLs for fungi, nitrate leaching and forest-tree health over US. Figure 5.6 plot the CL_{max} and CL_{min} for fungi community, nitrate leaching and forest-tree health developed by (Pardo et al., 2011). Only one study is collected for each ecosystem.

SMB CLs for soil acidity over US. Figure 5.7 shows the CL_{acd} for soil acidity developed by (McNulty et al., 2007). It includes CL_{min} and CL_{min} for N deposition and CL_{max} for S deposition. All three values are used to assess the exceedance of CL_{acd}.

Empirical CLs for different terrestrial ecosystems over EU. Table 5.3 lists the empirical CLs for four types of terrestrial ecosystems over EU used in this study. The values are derived from dataset 2 in Table 5.1. The classification of the habitat types is based on the European Nature Information System (EUNIS).

5.4.3 Exceedance of CLs in 2001 and 2010 over U.S. and EU

This section assesses the exceedance of CLs over U.S. and EU in 2001 and 2010 by comparing the CLs datasets in sect. 5.4.2 with the S and N depositions developed in Chapter 2. For empirical CLs, the exceedance is calculated by subtracting CLs from N deposition. For SMB model CLs, the exceedance is calculated following Eq. *(5-19)* in sect. 5.3.2. The positive values indicate the amounts of N and/or S depositions that have exceeded the CLs. The negative values denote the distance from the current deposition level to exceed the CLs.

Exceedance of CLs over U.S. Figures 5.8-5.12 show the exceedance of CL_{max} and CL_{min} for HP community, Lichen community, fungi, nitrate leaching and forest-tree health in 2010 (HTAP-II) and 2001 (HTAP-I). Table 5.4 summarizes the regions exceeded CL_{max} and CL_{min} in 2001 and 2010. Since the calculated CLs do not cover the whole CONUS for most ecosystems, we calculate the percentage of regions exceeding the CLs, which is calculated by dividing the areas exceeding the CLs by the total areas covered in this study, to enable comparison with other studies

For lichen community and nitrate leaching, the percentage areas exceeding the CL_{min} have increased by 2% from 2001 to 2010, but the percentage areas exceeding the CL_{max} have decreased

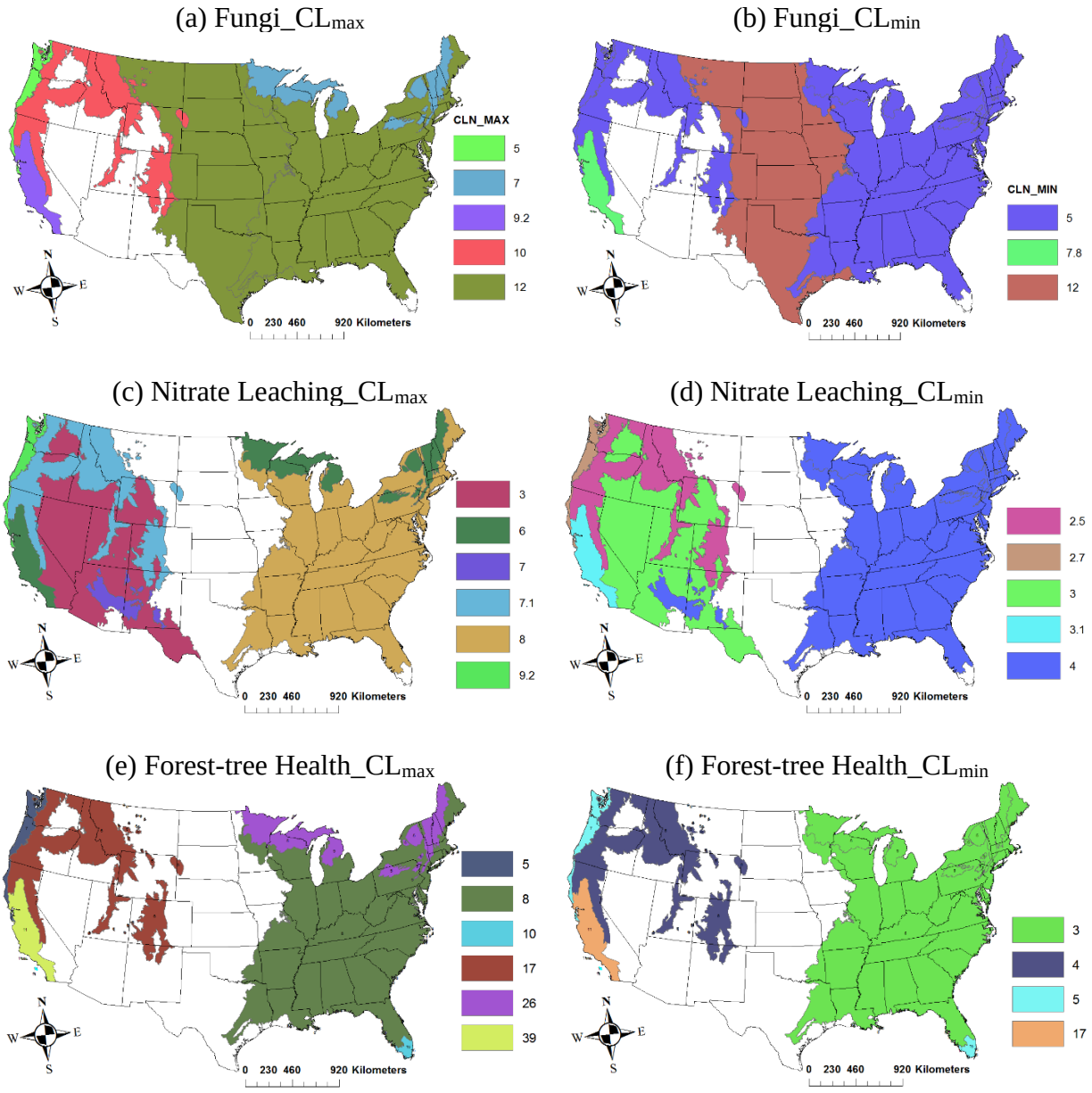

Figure 5. 6 Empirical maximum and minimum CLs for fungi, nitrate leaching and forest-tree health. Unit: Kg (N) ha^{-1} yr^{-1}.

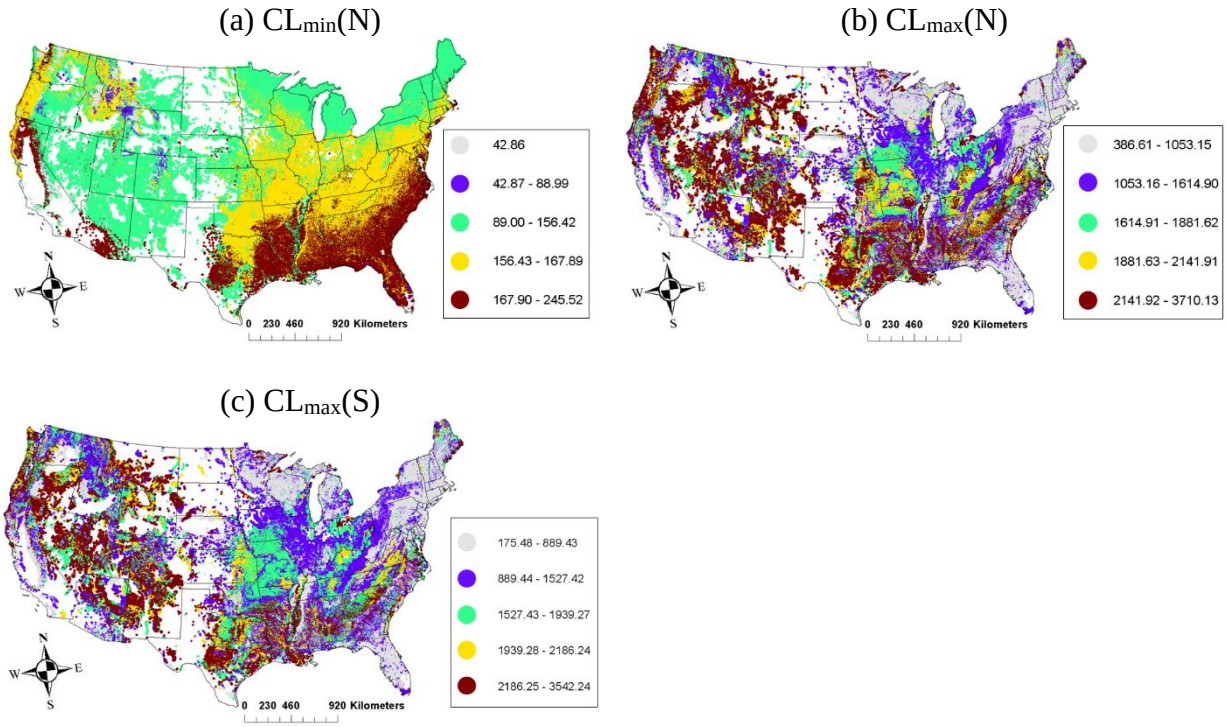

Figure 5. 7 The *CL*$_{max}$*(S)*, *CL*$_{max}$*(N)* and *CL*$_{min}$*(N)* for soil acidification. Unit: Eq (N or S) ha^{-1} yr^{-1}.

Table 5. 3 Empirical *CL*$_{min}$ and *CL*$_{max}$ for different terrestrial ecosystems over EU (kg N ha^{-1} yr^{-1}).

Ecosystem types (EUNIS class)	Habitat types in Fig. S5.2 in Appendix	*CL*$_{min}$	*CL*$_{max}$
Mires, bogs and fens (D)	4	5	30
Grasslands and lands dominated by forbs, mosses or lichens (E)	5	5	30
Heathland, scrub and tundra (F)	6	3	30
Woodland, forest and other wooded land (G)	7	5	20

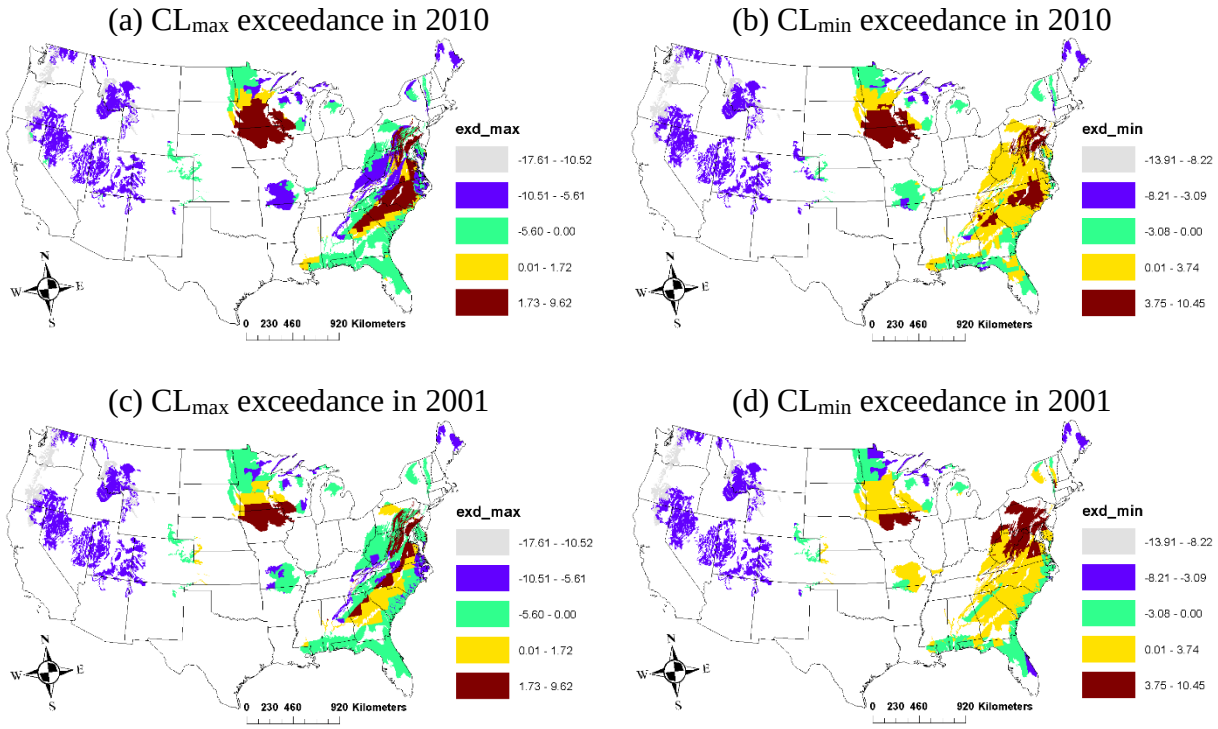

Figure 5. 8 Exceedance of N CL_{max} and CL_{min} for HP community in 2010 and 2001. Unit: Kg (N) ha^{-1} yr^{-1}.

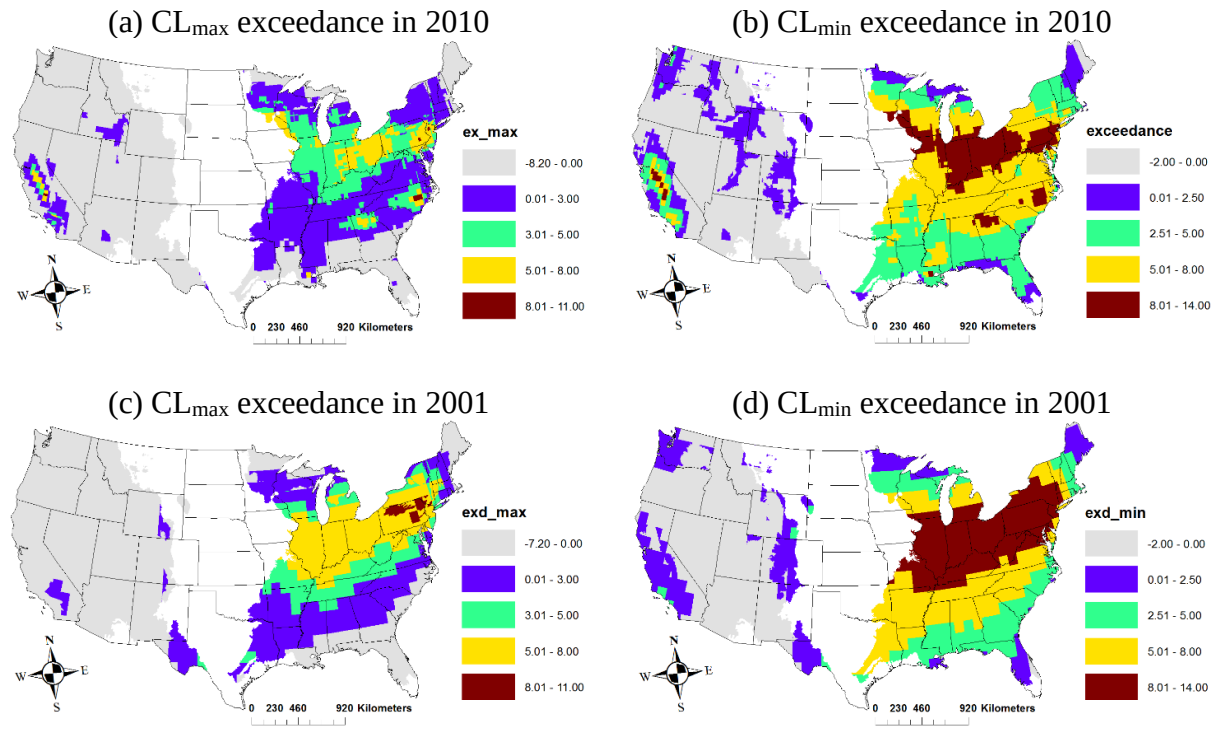

Figure 5. 9 Same as Fig 5.8 but for lichen community.

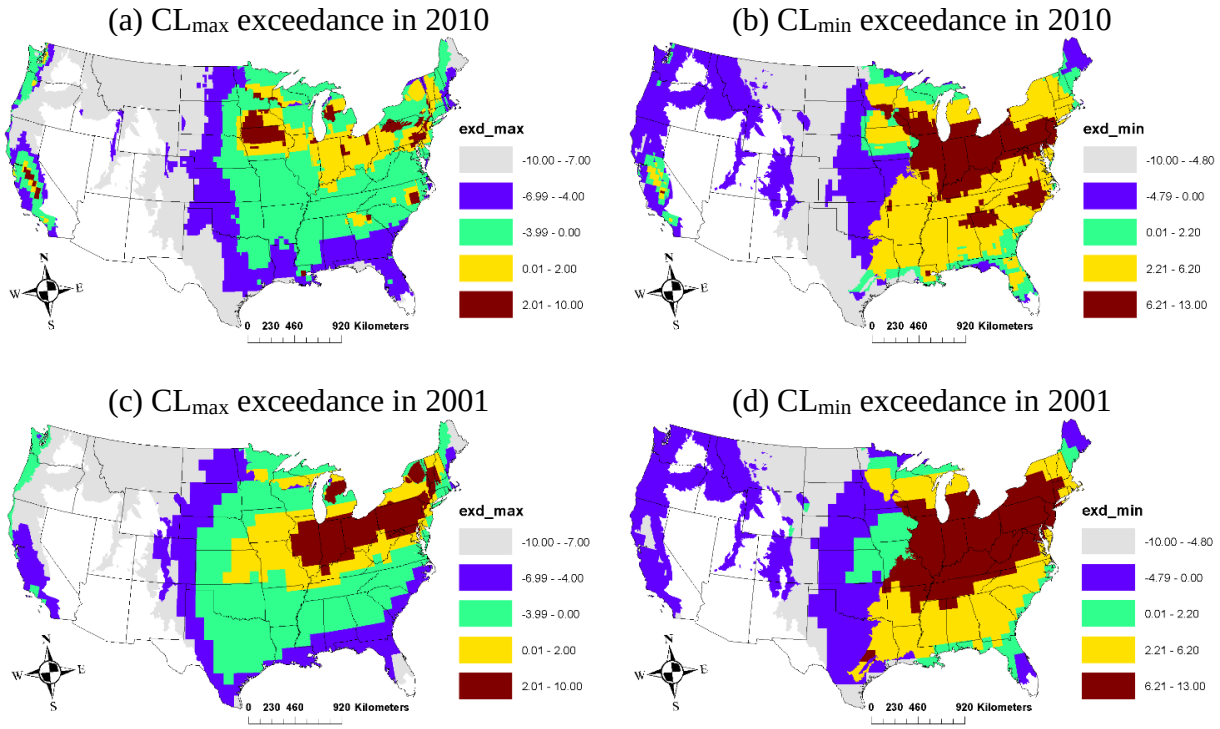

Figure 5. 10 Same as Fig. 5.8 but for fungi community.

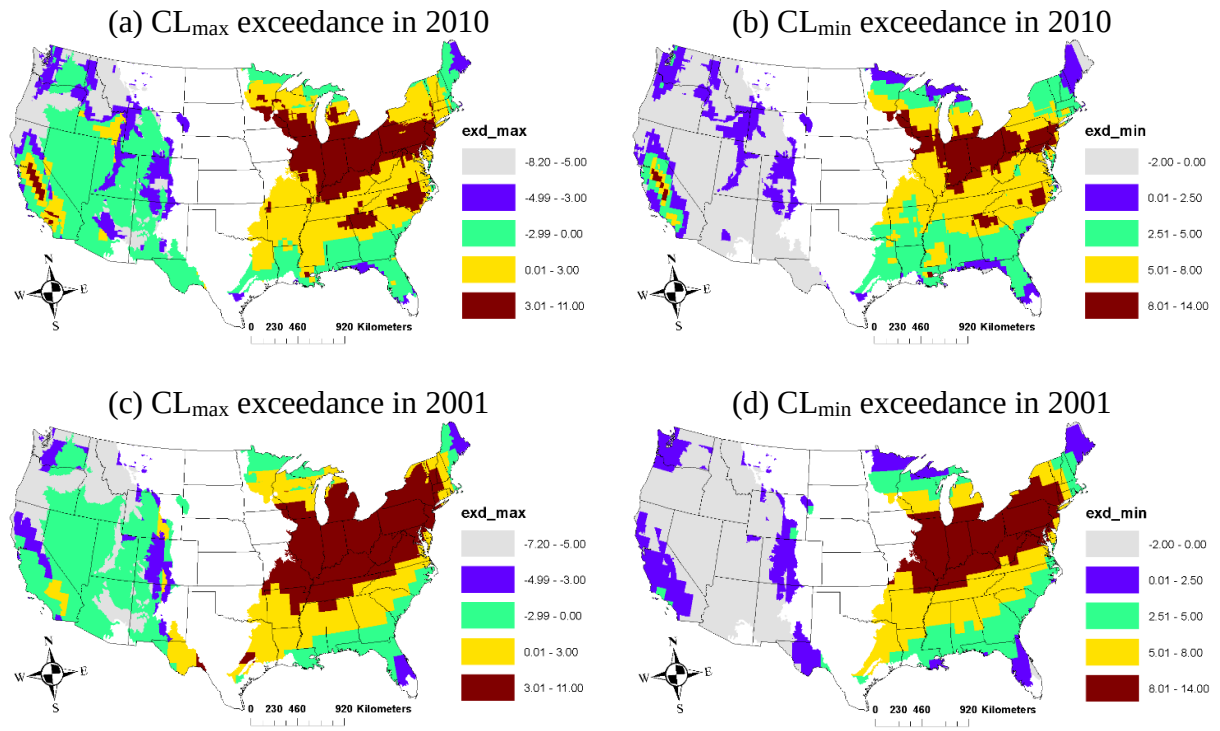

Figure 5. 11 Same as Fig. 5.8 but for nitrate leaching.

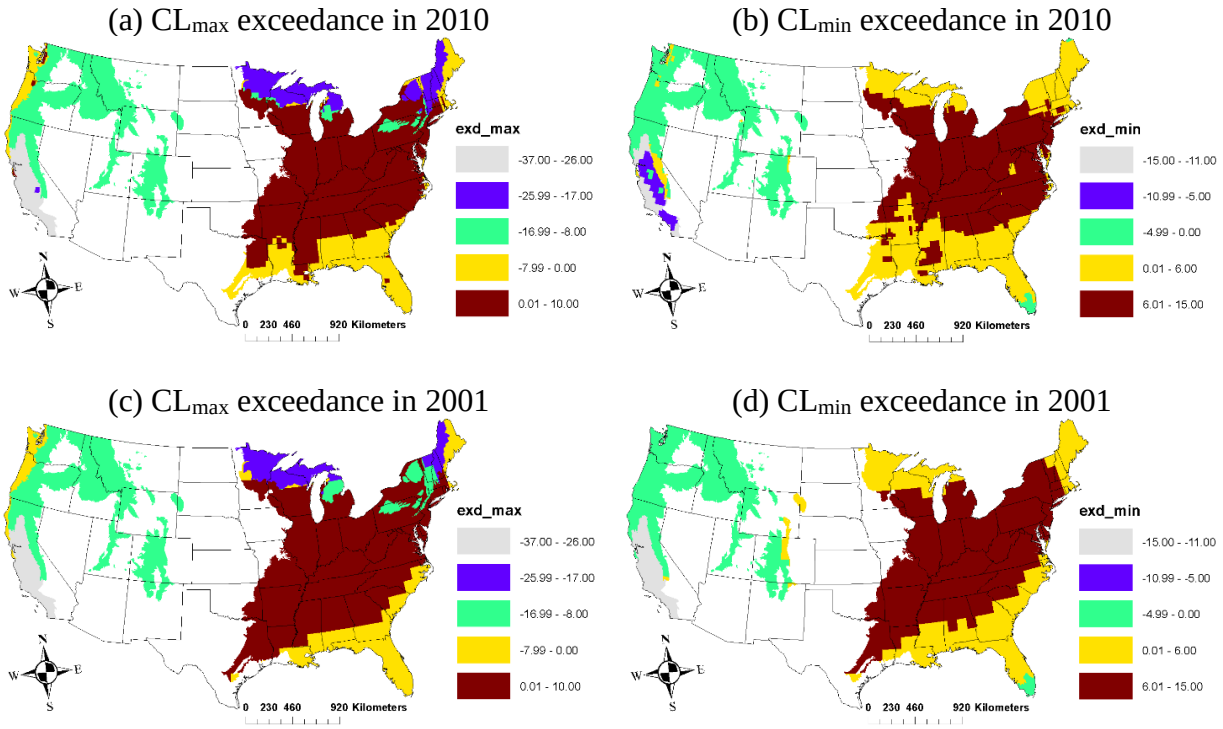

Figure 5. 12 Same as Fig. 5.8 but for forest-tree health.

Table 5. 4 Areas exceeding the CL_{max} and CL_{min} in different ecosystems in 2010 (HTAP II) and 2001 (HTAP I) over United States.

Ecosystems	Study Year	Area Exceeding CL_{max}		Area Exceeding CL_{min}	
		Million km^2	Percentage area %[1]	Million km^2	Percentage area %[1]
Lichen	2001	2.47	45.20	3.46	63.41
	2010	2.39	43.74	3.56	65.20
HP	2001	0.42	19.94	0.93	43.63
	2010	0.47	22.12	1.01	47.27
Fungi	2001	1.39	22.51	3.04	49.29
	2010	0.90	14.61	3.03	49.08
Nitrate Leaching	2001	2.47	45.20	3.46	63.41
	2010	2.39	43.74	3.56	65.20
Forest-Tree Health	2001	2.07	52.24	2.91	73.54
	2010	1.97	49.68	2.91	73.56

Note:
[1] Calculated by dividing the areas exceeding the CLs by the total areas covered in this study.

by 2%. For lichen community, N deposition levels in several areas in Southwest U.S. changed from below CL_{min} in 2001 to 0-2.5 kg(N) $ha^{-1}yr^{-1}$ exceedance of CL_{min} in 2010 (Fig. 5.9). Especially in California, the magnitude of CL_{min} exceedance increased from 0-2.5 to 2.5-14 kg(N) $ha^{-1}yr^{-1}$ and the amount of CL_{max} exceedance increased from 0 to 5-8 kg(N) $ha^{-1}yr^{-1}$. On the other hand, large extended regions in Northeast U.S. have decreased the magnitudes of both CL_{min} and CL_{max} exceedances. Similar condition occurred for nitrate leaching (Fig. 5.11). For HP community, both the percentage areas exceeding the CL_{min} and CL_{max} have increased by 2-3%. Minnesota, Missouri and North Carolina states have large increases in the magnitudes of CLs exceedances (Fig. 5.8). For fungi community and forest-tree health (Figs. 5.10 and 5.12), there are no significant changes in the percentage areas exceeding the CL_{min}, and 3-8% decreases in the percentage areas exceeding the CL_{max}, mainly occurred in South and Midwest U.S. But the exceedances of both CL_{min} and CL_{max} have somewhat increased in California.

Figure 5.13 shows the areas exceeding the SMB CL_{acd} in 2001 and 2010 over U.S. The % values in the grey squares indicate the percentage areas in five Regions defined in Fig. 5.1. The arrows between the two squares indicate the changes in the distribution from 2001 to 2010. Changes from Region 0 to other regions indicate aggregation in the exceedance of CLs caused by different deposition components. For instance, change from Region 0 to Region 4 is caused by increased S deposition, since N deposition in this region is totally below CL_{min}. Change from Region 0 to Region 2 or Region 3 is more likely a joint effect of increased S and N depositions. Change from Region 0 to Region 1 is mostly contributed by elevated N deposition, because the N deposition in this region changes from below CL_{max} to exceeded CL_{max}. About 76% of the research regions were in Region 0 in 2001, of which 75% remained in Region 0 in 2010 and 1% changed to Region 2. About 22% of the regions are in Region 2 in 2001, of which 5% changed to Region 0 in 2010 and others remained in Region 2.

Comparison with other studies. We compare the results with study by (Clark et al., 2018) in Table 5.5. (Clark et al., 2018) used the modelled deposition from the Community Multiscale Air Quality (CMAQ) model at spatial resolution of 12km from 2002 to 2011. Both that study and this study used the NEI emission inventory from U.S. EPA as model inputs. The calculated areas

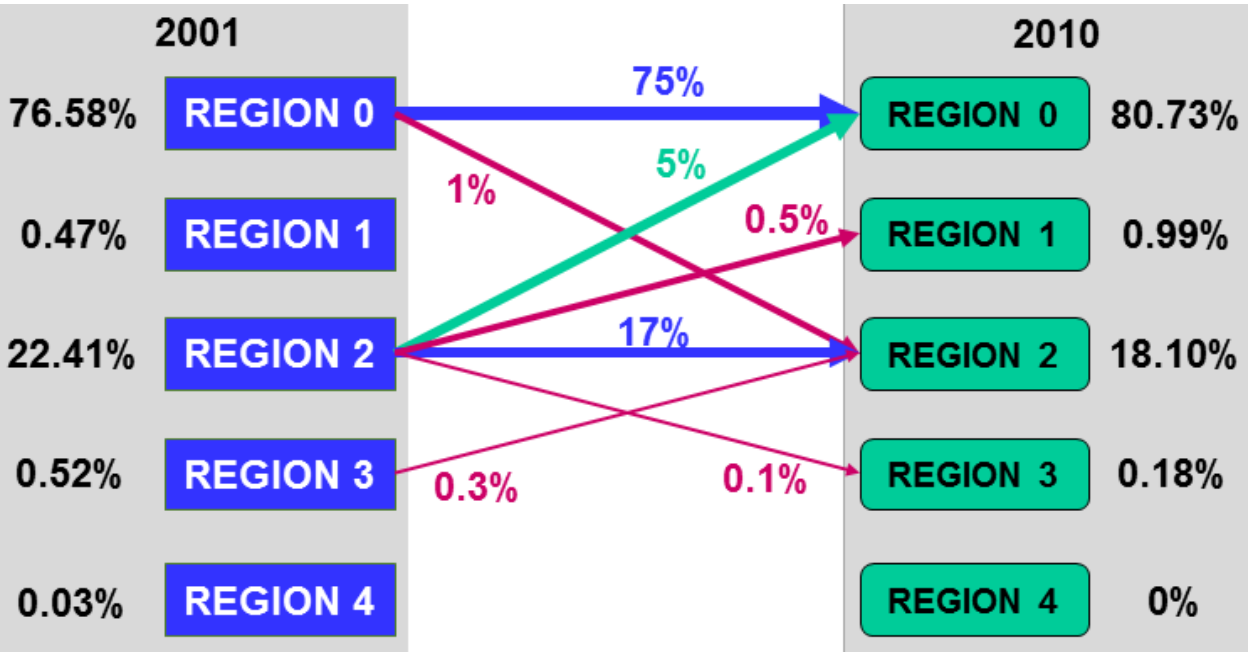

Figure 5. 13 Percentage of areas exceeding CL_{acd} over U.S. and changes from 2001 to 2010.

Table 5. 5 Comparison of this study with (Clark et al., 2018) in the CL exceedance over US.

Ecosystems	Study Year	Area exceeding CL_{min} (million km^2)	
		This study	Clark et al[1]
Lichen	2001	3.46	3.5
	2010	3.56	3.4
HP	2001	0.93	2.8
	2010	1.01	2.3
Fungi	2001	3.04	-
	2010	3.03	-
Nitrate Leaching	2001	3.46	3.3
	2010	3.56	2.9
Forest-Tree Health	2001	2.91	3.0
	2010	2.91	3.0
Acidification	2001	Not available[2]	2.5
	2010	Not available[2]	2.0

Note
[1] Derived from figure 5 of (Clark et al., 2018)
[2] The CLs are presented as points in ArcGIS, so we don't calculate the areas of exceedance.

exceeding CL_{min} are similar between the two studies for lichen community, nitrate leaching and forest-tree health. The large differences for HP community is because this study uses the CLs on Ecoregion Level IV by (Simkin et al., 2016) (Fig. 5.4), while (Clark et al., 2018) used the CLs on Ecoregion Level I by (Pardo et al., 2015) (Fig. 5.5). The application of CLs on different maps of land type classification could result in large differences in the exceedance of CLs.

Exceedance of CLs over EU. Figures 5.14-5.17 show the exceedance of CL_{max} and CL_{min} for four types of habitats over EU in 2010 (HTAP-II) and 2001 (HTAP-I). Since the EU habitat type is provided in the shape of points (Fig. S5.2), the CLs map we developed for EU is also in points. We calculate the percentage of units (points) exceeding the CLs in Table 5.6 instead of areas exceeding the CLs. For all habitat types, there is almost no exceedance of CL_{max} in both 2001 and 2010 (Table 5.6). According to Figs. 5.14-5.17, no regions have exceeded CL_{max} for habitat type 4 and 5. For habitat type 6, there is exceedance in Netherlands in both 2001 and 2010. The exceedance of CL_{max} in Northwest Germany in 2001 still exists in 2010, but the areas of exceedance have diminished. The exceedance of CL_{max} in North Italy in 2001 is no longer found in 2010. For habitat type 7, North Italy has no exceedance of CL_{max} in 2001, but is found with exceedance in 2010. The area exceeding the CL_{max} in Netherlands and North-west in 2001 remain the same in 2010.

There are significant decreases in the percentage of areas exceeding the CL_{min} from 2001 and 2010 (Table 5.6). The differences are about 10% for habitat type 4 and 7 and about 5% for habitat type 5 and 6. We check the change of the exceedance status, in this case change from exceeding CL_{min} (positive value) to no exceedance (0 or negative value). We found that Western Ireland (all types of habitats), Northern England (habitats type 5-7), Southern Norway and Southern Sweden (all types of habitats) all have somewhat changes in the exceedance status from 2001 and 2010. Besides, many regions in center EU (mainly France, Germany, Italy and Poland) have significant decreases in the magnitude of CL_{min} exceedance from 2001 to 2010, but the changes are not big enough to change their exceedance status.

(a) CL_{max} exceedance in 2010

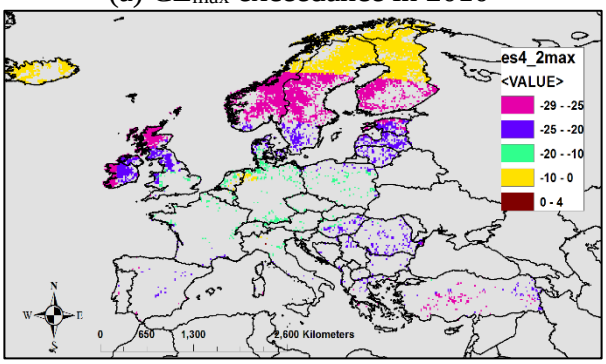

(b) CL_{min} exceedance in 2010

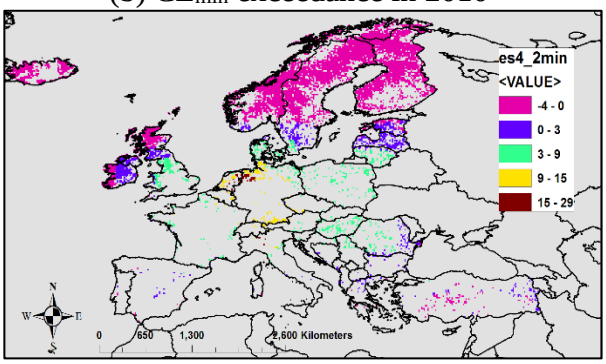

(c) CL_{max} exceedance in 2001

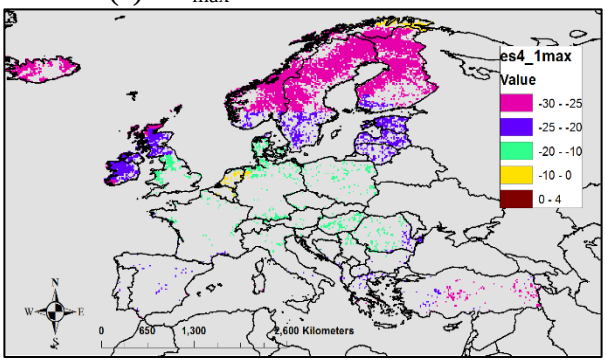

(d) CL_{min} exceedance in 2001

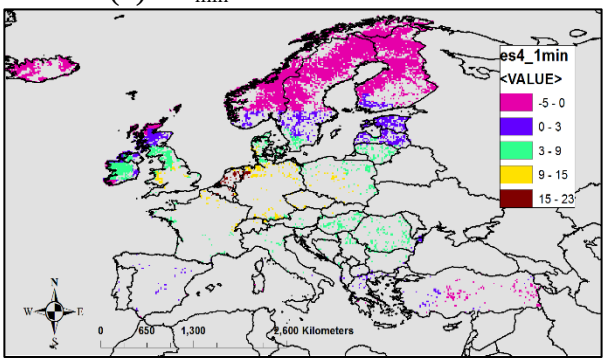

Figure 5. 14 Exceedance of N *CL_{max}* and *CL_{min}* for habitat type 4 - mires, bogs and fens in 2010 and 2001 over EU. Unit: Kg (N) ha^{-1} yr^{-1}.

(a) CL_{max} exceedance in 2010

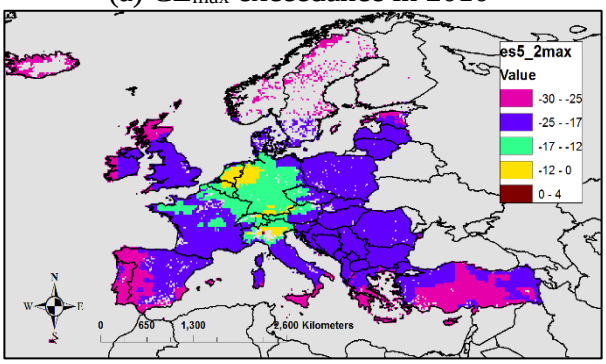

(b) CL_{min} exceedance in 2010

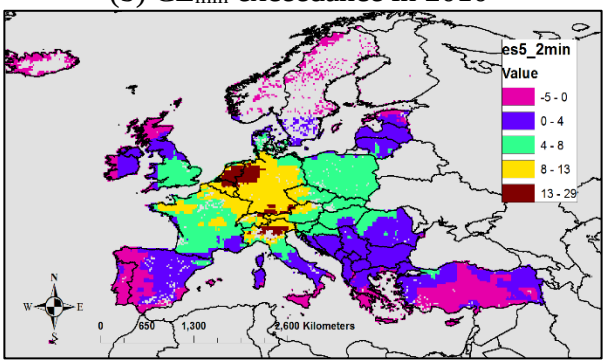

(c) CL_{max} exceedance in 2001

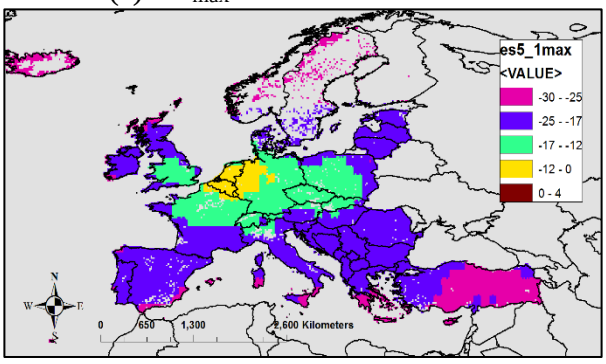

(d) CL_{min} exceedance in 2001

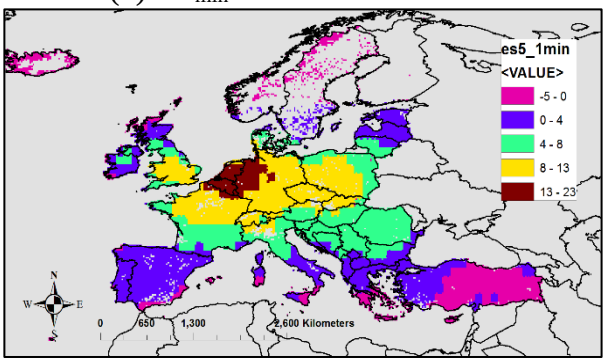

Figure 5. 15 Same as Fig. 5.14 but for habitat type 5 – grasslands.

(a) CL_{max} exceedance in 2010

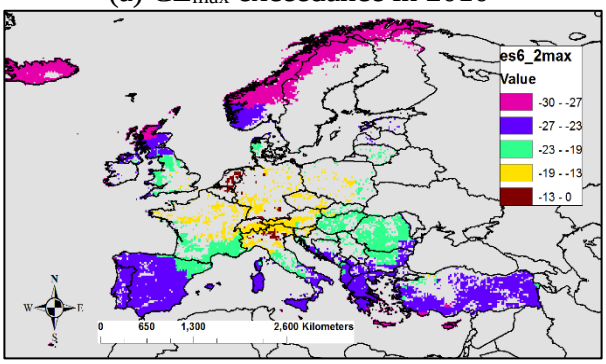

(b) CL_{min} exceedance in 2010

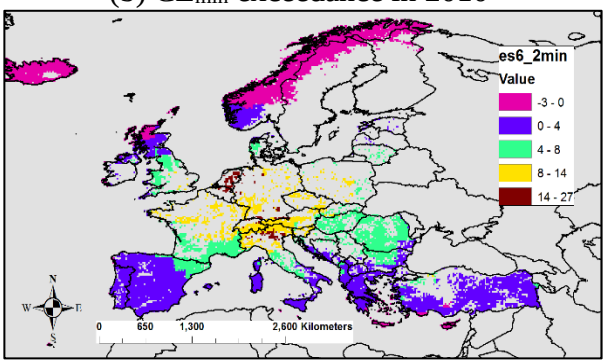

(c) CL_{max} exceedance in 2001

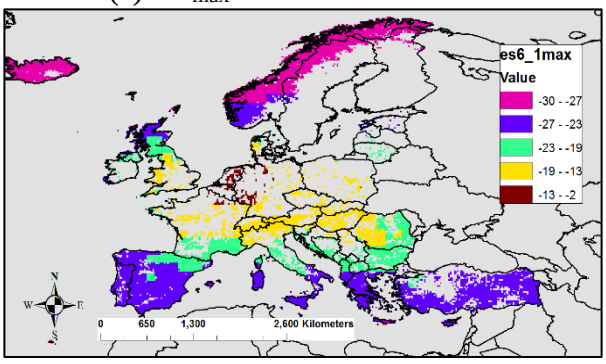

(d) CL_{min} exceedance in 2001

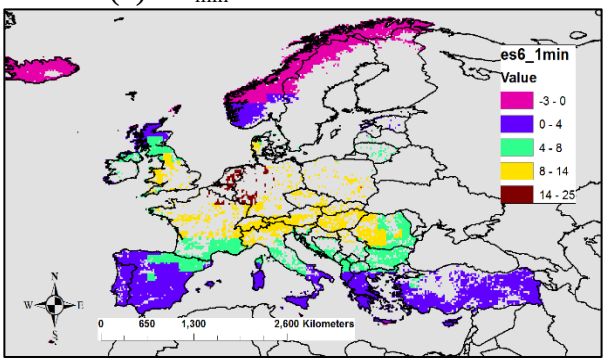

Figure 5. 16 Same as Fig. 5.14 but for Habitat Type 6 - heathland, scrub and tundra.

(a) CL_{max} exceedance in 2010

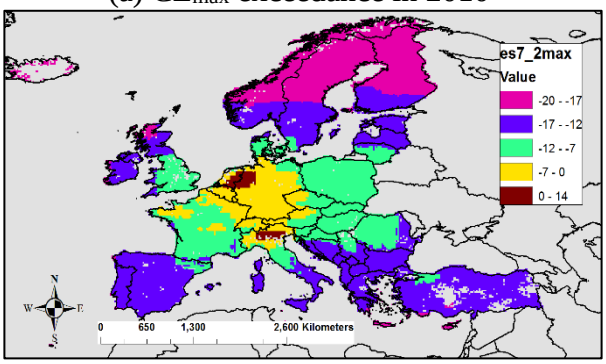

(b) CL_{min} exceedance in 2010

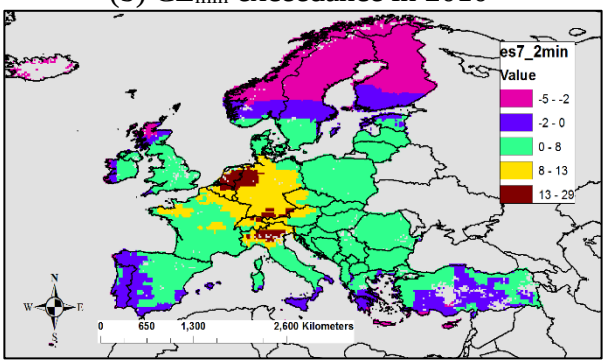

(c) CL_{max} exceedance in 2001

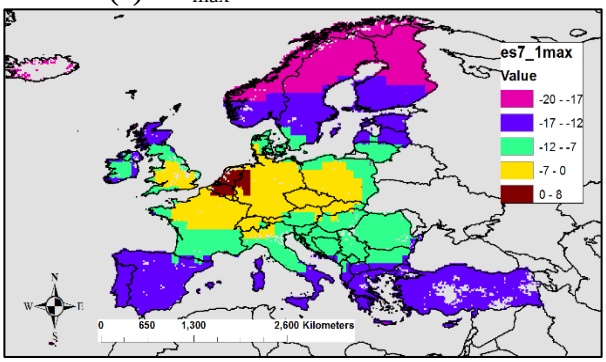

(d) CL_{min} exceedance in 2001

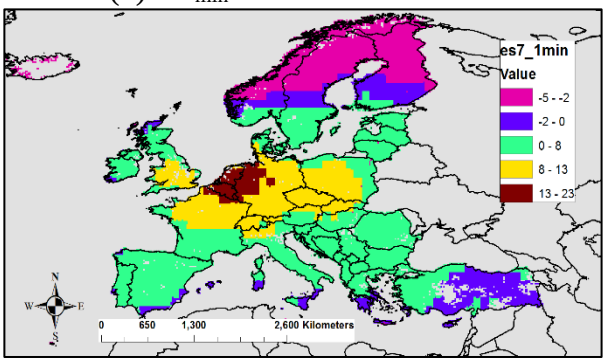

Figure 5. 17 Same as Fig. 5.15 but for Habitat Type 7 woodland, forest and other wooded land.

Table 5. 6 Percentage of areas exceeding the *CL*$_{max}$ and *CL*$_{min}$ in different ecosystems in 2010 (HTAP II) and 2001 (HTAP I) over Europe

Habitat types	Study year	*CL*$_{max}$ Exceedance	*CL*$_{min}$ Exceedance
4	2001	0	28.8
	2010	0	18.9
5	2001	0	81.8
	2010	0	75.1
6	2001	0	64.8
	2010	0	60.1
7	2001	0	28.8
	2010	0	18.9

5.5 Preliminary conclusion and discussion

We illustrate the calculation of the three most commonly used methods for developing CLs: Empirical CLs, SMB model and dynamic model, focusing on the first two methods. From the perspective of data reliability, empirical CLs have relatively high reliability since they come from direct observation. And the uncertainty can be assessed by comparing the values among similar studies. However, the application of data on coarse land cover classification in present datasets (such as on Ecoregion Level I over U.S.) may cause uncertainty to further studies, since the empirical CLs values are derived from site experiments with more detailed speciation of ecosystems. And the uncertainty brought by this issue has not been fully assessed. The SMB model is developed on the conception of mass balance, and the uncertainty come from both the model itself and data inputs for model calculation. The inputs are required to be long-term observation free of anthropogenic and natural perturbation, which is hard to avoid and there still lacks a method to assess the uncertainty. In addition, the SMB model ignores the "lag effect" between the exceedance of CLs and the occurrence of damage in ecosystems. From the perspective of data availability, we find multiple datasets for empirical CLs over U.S., Europe and China and SMB model results over U.S., U.K. and China. Both methods have detailed documentation and most studies are following the similar procedures, with slight differences in model inputs for SMB model due to data availability.

We compare the empirical CLs and SMB model CLs with modelled deposition over U.S. and EU to investigate the exceedance of CLs in 2001 and 2010. For U.S. there is slight changes (0-2% changes for Lichen, HP, nitrate-leaching and forest tree-health, 8% for fungi and 5% for soil acidification) in the percentage areas exceeding the empirical CLs over ten years. However, we found that Northeast U.S. have large decreases in the magnitude of exceedance, although the changes are not large enough to change their exceedance status (exceedance or no exceedance). And regions in Southwest U.S., especially California, have significant increases in the amount of exceedance and require attention. As for CLs of acidification, about 5% of CONUS regions changed from exceeding CL_{acd} to non-exceedance, probably due to the joint effects of reduction of S and N depositions. Study over EU, otherwise, shows significant changes (up to 10%) in the percentage of areas exceeding the empirical CLs over ten years. The changes main occurred in Western Ireland, Northern England, Southern Norway and Southern Sweden, where many areas

have changed from exceedance to non-exceedance. Besides, central EU have significant decreases in the amount of CLs exceedance.

However, we should be cautious to draw any conclusion related to the exceedance status of regions, owing to the high uncertainty in both the modelled deposition fields (see detail in Chapter 2) and the CLs. We find the following the issues when applying the CLs: (1) the inconsistency between similar studies (for example, the comparison of the empirical CLs for HP community between Simikin's and Pardo's study in sect. 5.4.2); (2) the application of empirical CLs on spatial maps with coarse land cover classification; (3) the empirical CLs are commonly presented in the unit of kg (N) ha^{-1} yr^{-1}, with an order of magnitude of ten. One-unit increase/decrease in the CL values could result in very significant changes in the exceedance status.

CHAPTER 6
STUDY ON PHOSPHEROUS DEPOSITION

This article hasn't been published anywhere, nor will it be before I turn in the final version of my ETD, so I didn't include a publication statement.

6.1 Abstract

As the essential nutrients to organisms, the bioavailability of N and P determine the productivity of the ecosystem. Human activities have been alerting the natural N and P cycles and have resulted in shifts in the nutrient limitation patterns. To keep track of the changes, we need to update our understanding of the N and P budgets. Compared to the long-term measurement and modelling studies on N species and N depositions, much less attention has been given to the P budgets. The mapping of the distribution of P and the estimation of the P budget are much harder than N, since P neither a regular species in observation networks nor an element in most chemical transport models. This chapter summarizes our understanding on the P budget from previous studies via both measurement and modelling approaches. We collect the observation data of P depositions from 1980s to 2010s from literatures and compile them into a database with 282 records of total P depositions, 45 records of dissolved P depositions, 149 records of dissolved inorganic P depositions. Then we illustrate the main studies about the numerical simulations of P, focusing on the methodologies to estimate the P emissions from different sources. Based on the information, we summarize our understanding on the global P budget, emphasizing on the transport of P among the four earth cycles: atmosphere, ocean, biosphere and lithosphere. Finally, we discuss the uncertainties and problems found in previous studies and the future works.

6.2 Introduction

The bioavailability of N and P nutrients determines the productivity of the ecosystems. Alfred Redfield discovered that the ratio of C:N:P is a nearly constant ratio (106:16:1, by molecular weight) throughout the world's ocean. Therefore, the "Redfield ratio", also called N:P ratio, is used to determine the requirement of N and P nutrients by the ecosystems. Human activities have been altering the N and P cycles and even changing the nutrient limitation patterns of many

ecosystems. And the atmospheric deposition was found with significate contributions on these changes. (Elser et al., 2009) studied the nutrient limitation for more than two-thousand lakes in Norway, Sweden and US, and found shifts in the nutrient limitations for the phytoplankton due to the large increases in atmospheric N deposition. (Camarero & Catalan, 2012) observed decreases in the N:P ratios in the Pyrenean lake in Europe, due to human-induced P deposition contributed by dust transported from North Africa.

These studies pointed out the importance of increasing our understanding in the budgets of N and P in the ecosystem, under a fast-changing environment with increasing impacts from human activities. The liabilities of the studies depend largely on the accuracy in the estimations of N and P concentrations and depositions. Several national observation networks, such as the NADP and CASTNET networks over US, the EMEP networks over EU and the EANET networks over EA, have been detecting the air concentrations of NO_x and wet and dry depositions of N continuously. In addition, modelling studies have been conducted to understand the decadal budgets of N depositions at both global and region scales (Dentener et al., 2006; Kanakidou et al., 2016; Lamarque et al., 2013; J. N. Tan, Fu, Dentener, Sun, Emmons, Tilmes, Sudo, et al., 2018; Vet et al., 2014). But the P budget remains unclear compared to the long-term measurement and modelling studies on understanding the N budget. P is not the regular detected specie in current observation networks. It is also not a variable in the CTMs and most earth system models (ESMs) projects (Y. Sun et al., 2017), which makes the mapping of P deposition more difficult than N deposition. Furthermore, studies also found that many ecosystems were more sensitive to the changes in available P than N. Study by (Brahney, Mahowald, Ward, Ballantyne, & Neff, 2015) found that the P deposition could induced sixteen times more impact on nature primary productivity than that of N deposition. The availability of P nutrient may limit the carbon uptake of atmospheric CO_2 (Y. Sun et al., 2017).

This chapter is a summary on our understanding on the P budget from previous studies via both measurement and modelling approaches. Sect. 6.3.1 lists the measurement data on the atmospheric P deposition from literatures. We compile these data to a uniformed dataset for the further studies on the characteristics of P and for the evaluation and improvement of model simulations. Sect. 6.3.2 reviews the current status on simulating the emission source, transfer and deposition of P. We focus on introducing the different methodologies to form the emission

inventory of P (i.e. identification of emission sources and determination of P solubility). Sect. 6.3.3 summarizes the understanding on P and gives estimations on P budget based on these literatures. Sect. 6.4 discusses the uncertainties and problems found in previous studies and the future works.

6.3 Results

6.3.1 Measurement datasets on P depositions

Total P (TP) can be classified into inorganic P (IP) and organic P (OP) according to the presence of carbon element. It is also classified into dissolved P (DP) and particulate P (PP) according to the solubility. As for the measurement of P, generally two forms of P are recorded: total P (TP) and dissolved inorganic P (DIP). TP measurement is the sum of all forms of P that can be detected in the sample. To measure TP, all forms of P are converted to PO_4^{3-} with chemical and physical treatments. DIP, also referred as soluble reactive P (SRP) and filtered P, is the soluble and inorganic fraction of TP. The value of DIP is generally equivalent to PO_4^{3-}. It is denoted as the bioavailable part of TP for the ecosystem.

This section introduces the measurement datasets of P depositions over difference continents and oceans. The collection includes five studies that collect the observations from different reports and literatures, and two single studies that report the measured data from site experiments. Following are the main datasets used in this study:

- Dataset 1: (Tipping et al., 2014) collected the measured P deposition from literatures (147 sites) and unpublished data (97 sites in UK and Germany) for 250 sites from 1954 to 2012. This dataset included the geographical locations of measurement sites, measurement years (annual average data) and separate records of TP and IP depositions. Most of the records were located in Europe (153 sites, mainly in UK and Germany) and North America (42 sites in U.S. and 12 sites in Canada), with small numbers of sites in Africa, Asia, Oceania and South and Central America.
- Dataset 2: (Brahney et al., 2015) developed a collection for measured P deposition with corresponding observed N deposition for 33 sites over Europe (19), India (1), Canada (1), U.S.

(6), South and Central America (6). The experiment time ranged from 1972 to 2010. The observation of P depositions was coupled with N depositions, which enabled the calculation of N:P ratio.

- Dataset 3: (N. Mahowald et al., 2008) summarized the P deposition from literatures for 40 sites over North America, 36 sites over Europe, three sites over Africa, two sites over South America, two site over Asia and three sites over Oceania. Some data were measured from cruise campaigns and were good references for marine study. The sampling time mainly ranged from 1970s to 1990s.
- Dataset 4: (Vet et al., 2014) collected the depositions of TP, DP and DIP for fifteen sites, including nine sites with monthly sampling from 2001 to 2003, one Canadian sites with weekly sampling from 2000 to 2005, three Canadian sites with variable sampling periods from 2003 to 2007 and two sites with event sampling.
- Dataset 5: (Zhu et al., 2016) collected the wet deposition of P from 41 sites from the Chinese Ecosystem Research Network (CERN) over China. The sampling frequency was 3-5 times every month of 2013. The lack of observation data in China has been reported by several studies, since the EANET sites were mainly located in Japan, Korean and Southeast Asia. And this dataset provided a relatively comprehensive observation over China with a good coverage over eastern China.
- Single study 1: (W. Wang, Liu, Xu, Dore, & Xu, 2018) measured the DP deposition at one site in Nyingchi city and one site in Sejila Mountain near the Qinghai-Tibet plateau. The observation was carried out during March-October of 2017. We predicted the annual value based on the eight-month data. The study showed significant monthly variations in the DP deposition, with low values in spring and fall and high values in summer.
- Single study 2: (J. Luo et al., 2011) reported the observed concentrations of P over the northern part of Lake Taihu in 2003. Six samples were collected for four months of 2003. The study used three methods to calculate total P: (1) oxidation with persulfate and autoclaved at 120°C for 30 minutes; (2) ashed at 550°C for 1 hour; (3) digestion with HNO_3 and HF. We anticipated the annual value based on the four-month data and calculated the average value of the three methods.

We compile these data into a database, by deleting the duplicated records, unifying the names and units of species and adding remarks. Figure 6.1 maps the observations of TP, DP and PO_4 depositions on global map with ArcGIS. Table 6.1 lists the numbers of observation records over different continents for the three species. The detailed information about the observations are listed Tables S6.1-S6.6 in supplementary material for Chapter 6. According to Fig. 6.1, this database has well covered NA, EU and EA. The experimental times in NA and EU mainly lay on the 1980s-2010s, with limited observations after 2010. While the observations in EA are mainly after 2010, thanks to the contribution by (Zhu et al., 2016). The numbers of DP and PO_4 observations are less than those of TP in all continents except EU. According to the limited number of observations, the concentrations of P deposition are at the same magnitudes in NA, EU and EA, but are relatively higher at some African sites. The high P deposition in Africa may due to the mineral dust from the Sahara Desert. However, the P depositions at the Asian sites near the Gobi Desert seem to be identical to the other sites.

6.3.2 Modelling study on P budgets

Study by (Graham & Duce, 1979). This study estimated the P deposition rate (amount of deposition per unit area) in the 1970s with measured P concentration and deposition rate. The P deposition rate was calculated by multiplying the atmospheric concentrations of P with the depositions velocity derived from site measurements and literatures. Then the site measurements were interpolated into the whole study field. As an early attempt to quantify the P budget, this study has many uncertainties due to limited measurement data and technology: (1) the uncertainty depended largely on the intensities and locations of the measurement sites, the representability of the site (the author do mention most of the continental sites were located in urban regions) and the methodology for interpolation; (2) there was worry about the quality of the measurement data. The sampling intervals varied from days to months. The monthly sample was too long to prevent the incidental contamination of samples; (3) the study applied many assumed values for regions that lack localized data. According to (Graham & Duce, 1979), the total uncertainty was about 2~3 times of the true values.

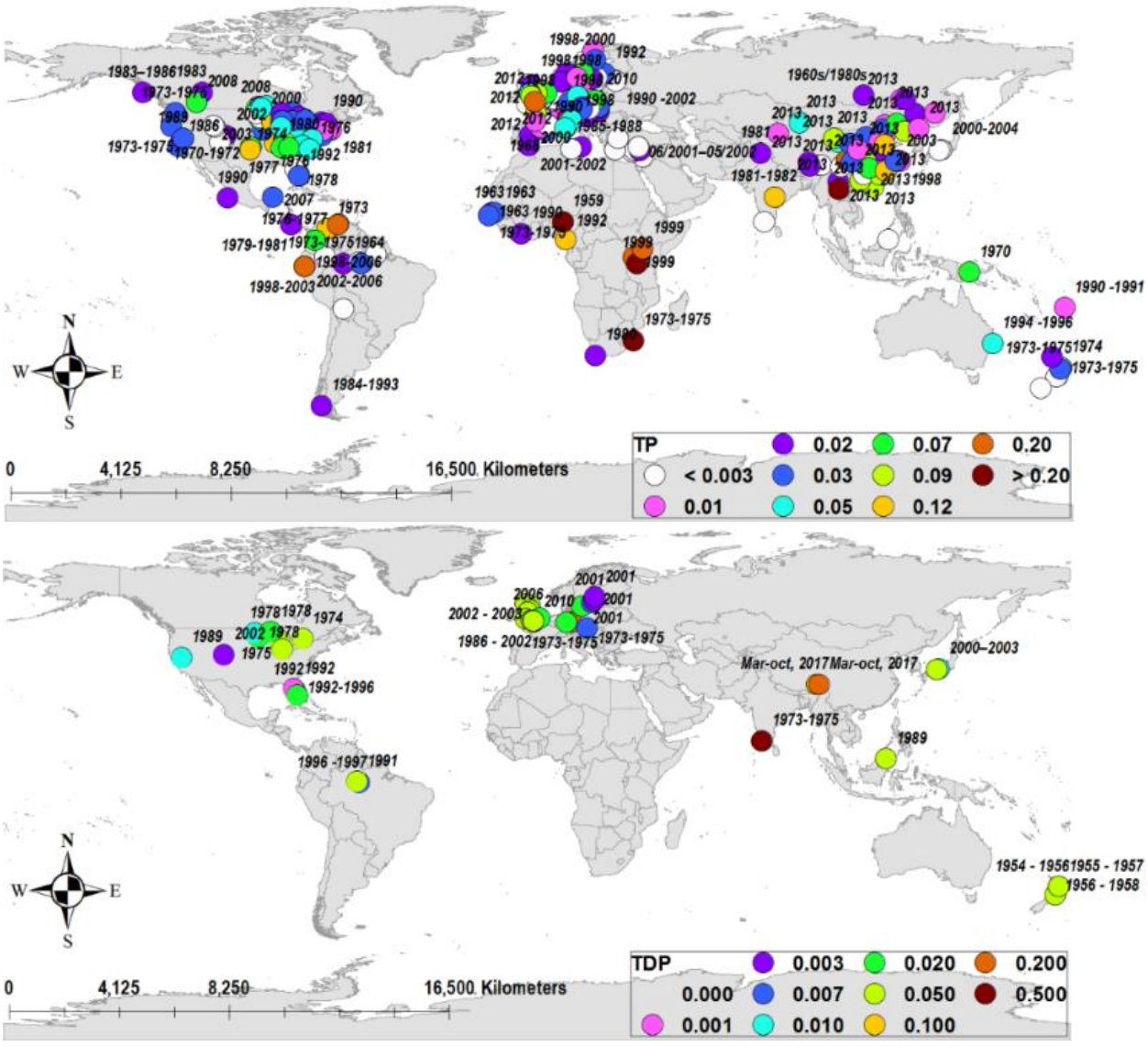

Figure 6. 1 Observations P depositions and the experimental times from literatures (top: TP; middle: DP; bottom: PO_4). The values were annual accumulated deposition rates (g m^{-2} a^{-1}).

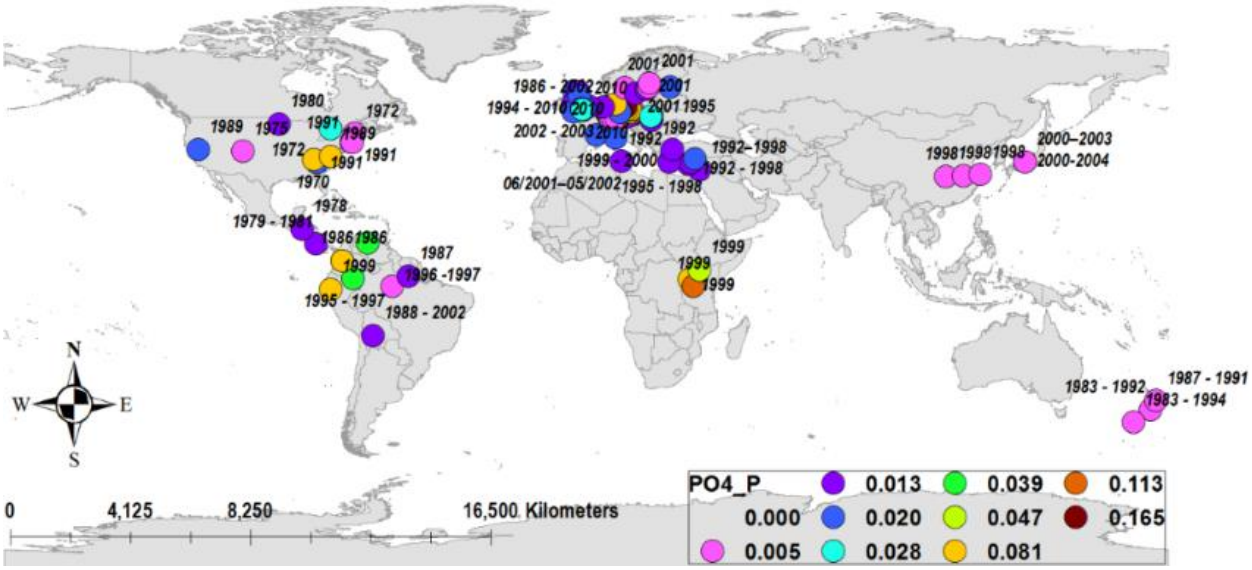

Figure 6. 1 Continued.

Table 6. 1 Numbers of observation records over different continents for TP, DP and PO_4

Regions/Species	TP	DP	PO_4
North America	85	11	11
South & Central America	14	2	10
Europe	116	23	116
Asia	46	6	6
Africa	13	0	3
Oceania	8	3	3
Total	**282**	**45**	**149**

Study by (N. Mahowald et al., 2008). This study estimated the global distribution of P in 2000 with both measurement and modelling approach. The study tried to identify the emission sources of P by analyzing the measurement data with Principal Component Analysis (PCA). It defined several signature elements as the indicators of certain emission sources. For instance, Al, Fe, Ca and Si were used to identify mineral sources; black carbon, S, V, SO_4, NO_3 were used to identify combustion source; K and Mg were used to identify primary biogenic aerosol particles (PBAPs); Na and Cl were used to identify marine sources. Then it developed the relationships between P and these elements for individual sites. For sites with significant statistical correlations (≥ 95%), the slopes between P and the signature elements were used to calculate the percentages of P from the corresponding emission sources.

This study was one of early attempts to simulate the concentration and deposition of P via modeling approach. It used the Model of Atmospheric Transport and Chemistry (MATCH) with a horizontal resolution of 1.8° × 1.8° and a vertical resolution of 28 layers. For the physical and chemical processes of P in models, P was considered to fully convert to PO_4^{3-} once it was emitted from the emission sources and contacted the air. Thus, no further chemical reaction was considered during the horizontal transport and the wet and dry deposition processes. To estimate the amount of wet deposition, a unified solubility was adopted that 10% of P from dust emission and 50% of P from other sources were soluble. But the study also mentioned that the measured solubility ranged from 7 to 100% according to different literatures. Following are the main assumptions to prepare the model inputs of P emissions from different emission sources:

- For dust source, the Dust Entrainment and Deposition model was used to simulate the amount and distribution of mineral dust. A four-size-bin distribution was applied with 10% in 0.1-1 μm, 30% each in 1-2.5, 2.5-5.0 and 5.0-10 μm. And for the P content in dust, the study used a uniformed 720 ppm concentration for all global regions, which was the average value from site experiments in North Africa. Studies over other regions showed the P content can range from 700 ppm to 1300 ppm, giving about 30% uncertainty to this estimation. But sensitivity studies showed that the impact on results was minor because the dominating contribution of dust emission in total emission.
- For combustion emission, the study calculated the particle emissions from combustion with the Speciated Particulate Emission Wizard (SPEW) program. The program calculated the

emission with activity data (consumption of fuels) and emission factor, which was a traditional bottom-down method for calculating emissions. Then the study estimated the P emission by applying the P content in particles. The PM emission contained 0.3-1.5% emissions of fine-mode P and 0.2-1.95% of coarse-mode P.

- For biomass burning source, the fine and coarse mode of P emissions were calculated and treated separately. The study retried the biomass burning data from satellite to estimate the emission of fine-mode P. Then it assumed the source of coarse-mode P was about 20% of that of fine-mode P. The fine-mode P was treated as hydrophobic aerosols during the atmospheric transport process as BC initially, which was not soluble in water, thus wouldn't be removed by precipitation. It turned to hydrophilic aerosol after 1.2 days in simulation. By this setting, it assumed a residence time of 1.2 days for fine-mode P, which is close to the 90 hours reported by (Ruttenberg, 2003). The coarse-mode P transported as dust aerosols in the model.
- For primary biogenic aerosols, it calculated the area of above-ground biomass (aboveground C m^{-2}) and used the emission factor of 8.9×10^{-18} g P g aboveground C^{-1} s^{-1}. This parameter was derived from site experiments in tropical regions and may not be applicable in other regions. It also assumed equal split of primary biogenic aerosols into fine and coarse modes.
- For marine source, it calculated the sea salt aerosols with the Community Atmosphere Model (CAM3) with resolution of 2.8° × 2.8° and then interpolated the results to match the resolution of the MATCH model. It also used the mapping of PO_4 concentration from National Oceanic and Atmospheric Administration's Oceanographic Data Center (NODC) as the concentration for DIP.

A comparison of the model results with available observations of PO_4 showed that the model could well simulate the sites with observed PO_4 concentration lower than 10 ng m^{-3}, but underestimated the sites with higher PO_4 concentrations over the Mediterranean Sea, North Atlantic and North Pacific. These regions were all in the downwind direction of largest dust sources: Sahara Desert and Gobi Desert. The major reasons for the model bias might be the insufficient and sparse observation of P, which made it difficult to determine some important parameters in the model, such as the solubility and size distribution of P from different emission sources. Another important reason was the failure to include some important emission sources

such as fertilizer production and fugitive dust emission, because no emission information was available at that time.

Follow-up study to accurate the emissions. (Brahney et al., 2015) estimated the P budgets with improvements on the work by (N. Mahowald et al., 2008). For dust emission, it still used the 720 ppm concentration but changed the size distribution of P in dust emission. The updated size distributions for 0.1-1, 1-2.5, 2.5-5.0 and 5.0-10 μm were 1%, 11%, 17% and 69%. Compared to the old distribution, this study split more P to the coarse mode. For combustion emission, it used the Global Fire Emission Database (GFED) v3 to calculate the biomass burning emission and used the observation to tune the amount of emission. For PBAPs, it updated the estimation of above ground biomass with the leaf area indices (LAI) retried from satellite data. For the physical transport of P, it assumed that only P size <10 μm would transport to other grids in the model. Otherwise, it deposited within the same grid of emission.

(Myriokefalitakis, Nenes, Baker, Mihalopoulos, & Kanakidou, 2016) simulated the global P budget with the Tracer Model 4 of the Environmental Chemical Processes Laboratory (TM4-ECPL) model with a spatial resolution of 3° × 2°, vertical structure of 34 layers and a 30-minute time step. It assumed 880 ppm P content in the mineral dust emission. Compared to the 720 ppm P content used in (N. Mahowald et al., 2008), it changed the concentration according to the measurement data in the Sahara Desert, but still used a constant value for all study regions. It mentioned the plan to use different content of P in dust sources in different locations, but was unable to apply this method due to lack of information for sources at that time. Another important update was about the solubility of dust emission. It still used the 10% solubility for the initial emission of P from mineral dust, but considered the solubility of P in the acidity condition by developing a mechanism to change the solubility according to environmental parameters such as pH of the atmospheric water and temperature. It also used more complicated method to calculate the PBAP emission, with detailed information of land use type and specific emission rates from different types of vegetation.

The study by (R. Wang et al., 2015) used a new method to calculate the P emission from combustion. It collected the P content in 31 types of fuels, including hard coal, municipal waste,

biomass and crop residues. Then it calculated the amount of P released into the air by assuming the percentages of P released in fly ash, stayed in residual ash (the material that stayed in the boilers) and removed by control devices. It pointed out that the method used by (N. Mahowald et al., 2008), which calculated the particle emissions from combustion and the P content in particles, might have ignored the P released as gas phase into the atmosphere. Therefore, this study reported much higher P emission from combustion (1.1 Tg a^{-1}) than (N. Mahowald et al., 2008)'s study and other studies that have adopted (N. Mahowald et al., 2008)'s method (around 0.06 Tg a^{-1}). However, the study declared that the actual amount of volatile status P has not been quantified by experiment, thus further study was required to confirm if this can explain the difference with (N. Mahowald et al., 2008).

According to these studies, the updates in emissions have been focused on two directions: (1) accurate the estimation by using more complicated methods or more detailed information; (2) improve the estimation by adopting more "reliable" parameters, especially the size distribution of P and the solubility of P. These two parameters have been recognized as the most important parameters in simulating the P deposition. The size distribution of P mainly affects the physical processes of P in models, such as spatial transport and deposition velocity of P. The solubility of P affects the biochemical processes of P, which determines the amount of bioavailable P. Although some studies (Brahney et al., 2015) tried to make some comparison with others (R. Wang et al., 2015), it is hard to tell which results/methods are more reasonable, due to insufficient observation data for a comprehensive model evaluation.

6.3.3 Estimation on P budget

Table 6.2 summarizes the amounts of P emissions from main emission sources. The numbers are derived from five studies (Graham & Duce, 1979; Kanakidou, Myriokefalitakis, & Tsigaridis, 2018; N. Mahowald et al., 2008; Myriokefalitakis et al., 2016; R. Wang et al., 2015), which cover the major emission sources, and some studies (L. Bouwman et al., 2013; Kanakidou et al., 2012; X. Liu et al., 2016) focusing on specific emission sectors or regions. We calculate the proportions of the emission sources in the total emission when both values are reported in the same study.

Table 6. 2 Global and regional P emissions from literatures

Emission Sources	Study year	Region Unit	TP 10^{10} g a^{-1}	PO_4-P 10^{10} g a^{-1}	Reference	Remarks	Contribution %
Total Emission	1973-1976	Global	459	-	(Graham & Duce, 1979)	-	100
	2000	Global	139	24	(N. Mahowald et al., 2008)	Table 4	100
	1960-2007	Global	350 (90-780)	-	(R. Wang et al., 2015)	Table 1	100
	2008	Global	133 (129,133,130)	-	(Myriokefalitakis et al., 2016)	2008 (1850,2008,2100	100
	1977-2008[1]	Global	54 (OP)	-	(Kanakidou et al., 2012)	OP	-
	-	Global	138 (50-950)	-	(Kanakidou et al., 2018)	Review paper, table 1	100
	2000[2]	Global	270, 190	-	(Brahney et al., 2015)	Current, preindustrial, table 2	100
Mineral dust and weathering	1973-1976	Global	400	-	(Graham & Duce, 1979)	Soil particle nature + fertilizer	87
	2000	Global	115	11.5	(N. Mahowald et al., 2008)	Table 4, dust	83
	1960-2007	Global	93 (23-210)	-	(R. Wang et al., 2015)	Table 1, mineral dust	27
	2008	Global	109.7	-	(Myriokefalitakis et al., 2016)	Soils, 1850, 2008, 2100 stable value	82
	-	Global	110 (23 - 380)	-	(Kanakidou et al., 2018)	Review paper, table 1, desert dust	80
	1960-2012	China	24	-	(X. Liu et al., 2016)	Wind erosion; same value in 1960, 1990, 2012, Fig 1	-
	2000[2]	Global	240, 170	-	(Brahney et al., 2015)	Current, preindustrial, table 2	89, 89
Sea-salt	1973-1976	Global	33	-	(Graham & Duce, 1979)	-	7.2
	2000	Global	0.49	0.49	(N. Mahowald et al., 2008)	Table 4	0.4
	1960-2007	Global	16 (0.49 - 33)	-	(R. Wang et al., 2015)	Table 1	4.6
	2008	Global	0.8	-	(Myriokefalitakis et al., 2016)	1850, 2008, 2100 stable value, Table 1	0.6
	-	Global	1 (0.5 - 271)	-	(Kanakidou et al., 2018)	Review paper, table 1	0.7
	1960-2012	China	0.4	-	(X. Liu et al., 2016)	Same value in 1960, 1990, 2012, fig 1	-
	2000[2]	Global	0.046, 0.046	-	(Brahney et al., 2015)	Current, preindustrial, table 2	0.02, 0.02
Primary biogenic aerosol particles (PBAPS)	2000	Global	16.4	8.2	(N. Mahowald et al., 2008)	Table 4	12
	1960-2007	Global	58 (16-100)	-	(R. Wang et al., 2015)	Table 1	17
	2008	Global	15.6	-	(Myriokefalitakis et al., 2016)	1850, 2008, 2100 stable value, Table 1	12
	-	Global	15.6 (0.2 - 213)	-	(Kanakidou et al., 2018)	Review paper, table 1	11
	2000[2]	Global	18, 18	-	(Brahney et al., 2015)	Current, preindustrial, table 2	6.7, 9.5
Volcanoes	2000	Global	0.6	0.3	(N. Mahowald et al., 2008)	Table 4	0.4
	1960-2007	Global	0.6 (0.3-0.9)	-	(R. Wang et al., 2015)	Table 1	0.2
	2008	Global	0.6	-	(Myriokefalitakis et al., 2016)	1850, 2008, 2100 stable value, Table 1	0.5
	-	Global	1 (0.6 - 21.8)	-	(Kanakidou et al., 2018)	Review paper, table 1	0.7
	2000[2]	Global	1.1, 1.1	-	(Brahney et al., 2015)	Current, preindustrial, table 2	0.5, 0.6

Table 6.2 continued

Emission Sources	Study year	Region	TP 10^{10} g a^{-1}	PO_4-P 10^{10} g a^{-1}	Reference	Remarks	Contribution %
Combustion	1973-1976	Global	7.3	-	(Graham & Duce, 1979)	Combustion	1.6
			0.6	-	(Graham & Duce, 1979)	Wildfires	0.1
	1960-2007	Global	110 (30-310)	-	(R. Wang et al., 2015)	Human combustion	31
			70 (20-130)	-		Natural combustion	20
	2008	Global	4.3 (0.8,4.3,0.9)	-	(Myriokefalitakis et al., 2016)	2008 (1850,2008,2100), anthropogenic combustion, Table1	3.2
	2008	Global	1.8 (1.4,1.8,2.2)	-	(Myriokefalitakis et al., 2016)	2008 (1850,2008,2100) Biomass burning, Table 1	1.4
	2000	Global	2.4	1.2	(N. Mahowald et al., 2008)	Table 4, Fossil fuels	1.7
			2.1	1		Table 4, Biofuels	1.5
			2.5	1.2		Table 4, Biomass burning	1.8
	2008	Global	10 (7.1 - 250)	-	(Kanakidou et al., 2018)	Review paper, Biomass burning, table 1	7.2
	2000[2]	Global	2.4, 0.48	-	(Brahney et al., 2015)	Fossil fuels, Current, preindustrial, table 2	0.9, 0.3
			1.1, 0.56	-		Biofuels, Current, preindustrial, table 2	0.4, 0.3
			2.9, 2.1	-		Fires, Current, preindustrial, table 2	1.1, 1.1
Phosphate industry	1973-1976	Global	16	-	(Graham & Duce, 1979)	-	3.5
Fertilizer	2000	Global	1400 (0,300,1400)	-	(L. Bouwman et al., 2013)	2000 (1900,1950,2000)	-
	1960-2012	China	755 (11,226 ,755)	-	(X. Liu et al., 2016)	2012 (1960,1990,2012), fig 1	-

Note:
1. The study did not mention the experimental year. The time is referred according to the measurement data used to develop the emission.
2. The study mentioned the study year as “current” in (Lamarque et al., 2010).

Note that the amounts of emissions from different studies are not totally comparable. Some studies were conducted for specific years, such as the study by (Graham & Duce, 1979). While other studies did not have a specific study time, because the emissions were calculated with measurement data collected for different years. For instance, the OP emission by (Kanakidou et al., 2012) were developed with a series of incontinuous observations from 1977 to 2008.

Mineral dust accounts for 80-90% of total P emissions. It is the largest emission source according to most studies except (R. Wang et al., 2015) (27%), which claims more contribution to combustion emission. The second biggest emission source is PBAPs, which accounts for 7-17% of total P emissions. Most studies estimated an annual emission of 0.16-0.18 Tg, while (R. Wang et al., 2015) gave a higher estimation (0.58 Tg a^{-1}). The third biggest emission source is combustion (including biomass burning). Its contributions to total P emission are about 1.2-7.2% and the annual emissions are about 0.057-0.1 Tg in all study except (R. Wang et al., 2015), which argues a contribution of 51% and emission of 1.8 Tg a^{-1}. The global total P emission, including natural and anthropogenic sources, is estimated to be 1.33-4.59 Tg a^{-1}. The three studies for the 2000s estimated similar amounts of TP emissions (1.39, 1.33 and 1.38 Tg a^{-1}, respectively). (Myriokefalitakis et al., 2016) estimated the P emissions in 1850, 2008 and 2100 to be 1.29, 1.33 and 1.30 Tg a^{-1}, which indicated very small changes in the amount in 350 years.

Most of the studies have reached high agreements on the amounts and contributions of individual emission sources. But this does not indicate low uncertainty in the estimation, since most studies adopt similar methods to calculate the emissions, with slight modifications on some parameters (sect. 6.3.2). The study by (R. Wang et al., 2015) is an exception, which predicts significantly different combustion emission by using a different methodology. In addition, most studies have ignored the agricultural sources: fertilizer application and manure, probably due to focusing on simulating the transport of P between the atmosphere and the earth surface. According to the study by (L. Bouwman et al., 2013), the application of fertilizer and manure input 14 Tg and 17 Tg of P into the agriculture fields every year, respectively (Table 6.2). And about 4 Tg a^{-1} of P was transported to ocean by runoff. According to the specific study in China by (X. Liu et al., 2016), about 7.55 Tg a^{-1} of P-fertilizer was applied to agriculture and 1.57 Tg a^{-1} of P was released to rivers via run off. Therefore, the agricultural emission could be an important source when considering the P budget in the biosphere.

Table 6.3 summarizes the TP deposition and deposition velocity over different continents and oceans collected from literatures. The global total amounts of TP depositions range from 300 to 456 among different models. The estimations on continental deposition are consistent among the four studies, ranging from 2.7 to 3.21 Tg a^{-1}, despite that the values are calculated via different approaches (modelling and measurement studies). The estimations on oceanic deposition range from 0.56 to 1.35 Tg a^{-1}. The uncertainties on oceans are slightly higher than inland regions. Deposition is the main pathway for the sink of P in current modelling studies, since the transport of P along the earth surface, such as runoff, manure and leaching, has not been included in most modelling studies. As a result, model results show almost equal values between emission (model inputs) and deposition (model outputs). According to (Graham & Duce, 1979), the global total amount of deposition (4.56 Tg a^{-1}) was comparable to the amount of emission (4.59 Tg a^{-1}). (R. Wang et al., 2015)'s study also predicted almost equal values of emission and deposition of TP (3.5×10^{10} g a^{-1}).

Figure 6.2 summarizes all the information on the P budgets. The annul fluxes of the processes are derived from the literatures listed in sect. 6.3.2., (Ahlstrom & Cornell, 2018), (Smil, 2000) and (Ruttenberg, 2003). The estimations on the annual fluxes among different earth cycles (i.e. L->A) and the predicted fluxes of individual processes (i.e. mining) come from different literatures, thus the values are not totally comparable. The figure emphasizes on the transport of P among the four earth cycles: atmosphere, ocean, biosphere and lithosphere. The P is released from the lithosphere to the atmosphere mainly through weathering (natural process) and mining (human activity). The annual fluxes from the lithosphere to the atmosphere and biosphere are about 1.4 Tg and 45 Tg, respectively. The annual P emission from mineral dust is about 0.93-2.4 Tg a^{-1}. P can stay in the air for about 80 hours before removed by wet and dry depositions. The annual P deposition on ocean is about 0.56-1.35 Tg, which is within the estimation on the transport from atmosphere to ocean (A->O = 0.6 Tg). The only oceanic emission that has been considered in the emission inventory is the sea-salt emission. The amount (0.0049-0.33 Tg) is slightly lower than the deposition. The rest P in the ocean sinks to the seabed and gets uplifted after 10^7-10^8 years. The residence time of P is shorter on ocean surface (2-4 years) and in ocean biota (16-78 days), and much longer in the deep ocean (1,500 years). The annual accumulated P deposition on land is about 2.7-3.2 Tg, which is slightly higher than the total emissions from the biosphere to the atmosphere in the model (0.22-2.38 Tg as sum of bioaerosol, fire and combustion). The residence

Table 6. 3 TP depositions and deposition velocities over different continents and oceans from literatures

	Regions	Deposition rate	Total deposition	Reference	Remark
	unit	μg cm^{-2} a^{-1}	10^{10} g a^{-1}		
North America	North America	3	50	(Graham & Duce, 1979)	Table 6, not include north of 60°N
	Wind River Range of Wyoming, US	1.06 - 3.34	-	(Brahney et al., 2014)	Depo rate of dust, Study for summer of 2009 and 2010
Europe	Europe	5	37	(Graham & Duce, 1979)	Table 6, not include north of 60°N
	Mediterranean coast of Israel	0.8 - 0.9	-	(Herut, Krom, Pan, & Mortimer, 1999)	DIP only
	Mediterranean	0.14	-	(Richon, Dutay, Dulac, Wang, & Balkanski, 2018)	1997-2012; model source apportionment
Other continents	Other continental than NA and EU	2.5	234	(Graham & Duce, 1979)	Table 6, not include north of 60°N and Antarctica
	Lake Taihu, China	8.4	-	(Zhai, Yang, & Hu, 2009)	2007, period of optimal algal growth
	Four Sampling sites at Amazon	1.6	-	(N. M. Mahowald et al., 2005)	Average of 2.6, 1, 0.8, 2.0
	China	150 (42,78,150)	-	(X. Liu et al., 2016)	2012 (1960,1990,2012)
Total continental		-	321	(Graham & Duce, 1979)	Table 6, based on measurement
		-	300	(Yuan et al., 2018)	Fig 1, review
		-	270	(R. Wang et al., 2015)	Table 1, based on simulation
		-	315	(Tipping et al., 2014)	Table 1, based on measurement
North Atlantic		0.4	73	(Graham & Duce, 1979)	Table 6
		-	19	(N. Mahowald et al., 2008)	Table 5
		-	20	(Prospero et al., 1996)	Calculate from Mineral dust: 170 Tg a^{-1}
Other oceanic		0.2	62	(Graham & Duce, 1979)	Table 6
		-	36.8	(N. Mahowald et al., 2008)	Table 5
Total oceanic		-	135	(Graham & Duce, 1979)	Table 6, based on measurement
		-	56	(N. Mahowald et al., 2008)	Table 5, based on modelling
		-	80	(R. Wang et al., 2015)	Table 1, based on modelling
		-	56	(Tipping et al., 2014)	Table 1, based on measurement
		-	43 (OP), 35 (DOP)	(Kanakidou et al., 2012)	OP
Total global		-	456	(Graham & Duce, 1979)	Table 6
		-	300-400	(Smil, 2000)	
		-	350	(R. Wang et al., 2015)	Table 1
		-	370	(Tipping et al., 2014)	Table 1
		-	54 (OP), 41 (soluble OP)	(Kanakidou et al., 2012)	Table 4
		1.65 ± 0.6 (TP); 1.35 ± 0.5 (TIP); 0.3 ± 0.15 (OP)	-	(Chen, Hung, Fang, & Gong, 2008)	

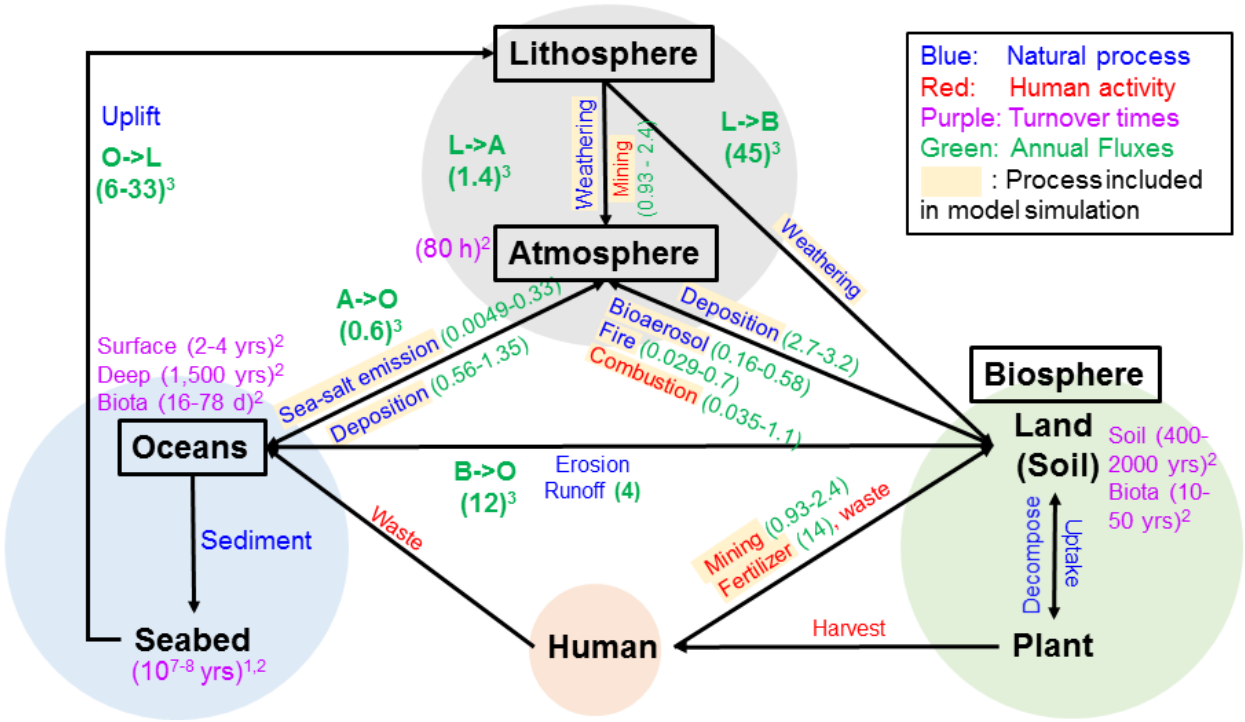

Figure 6. 2 The P budge developed from literatures. The blue and red colors indicate the natural and anthropogenic processes of P among different cycles. The processes covered with yellow shade are the ones have been included in the numerical modelling in sect. 6.3.2. The purple color indicates the residence time of P in the earth cycles. The green color shows the annual fluxes of different processes (unit Tg P a^{-1}).

Note: Reference 1:(Smil, 2000); Reference 2: (Ruttenberg, 2003); Reference 3: (Ahlstrom & Cornell, 2018). See more details in Table S6.7 in the supporting materials of chapter 6.

time of P in the biosphere was about 400-2000 years in soil and 10-50 years in living organisms. Erosion and runoff are the main pathway for the transport the between the biosphere and oceans (12 Tg a^{-1}). Human waste is another important pathway for the transport of P between these two earth cycles, but the annual flux is still unclear.

6.4 Future Prospects

We illustrate the main studies about the numerical simulations of P, focusing on the methodologies to estimate emissions. The work by (Graham & Duce, 1979) and (N. Mahowald et al., 2008) have established a framework to develop the emission inventory of P. On one hand, we see continuous efforts in recent years to accurate the amounts of emissions from different sources with advancing methods. Most works agree well with each other, but some studies like the work by (R. Wang et al., 2015) argue the inconsistent results. Such efforts are making significant contributions to perfect the P budget. On the other hand, we see very limited study on the missing sources reported in (N. Mahowald et al., 2008), such as fertilizer production and application, runoff and erosion, probably due to lacking information. Some processes such as fertilizer application are not applicable in most of the current modelling studies using CTMs. But as our study extended to the impacts on the ecosystem, they could be very important elements in the earth-system modelling.

About modelling of the transport of P. Currently, only the physical transport of P has been considered in model simulation. The accuracy depends largely on the choice of parameters. According to the previous studies, the most important variables are size distribution of P and solubility of P. These two values could be highly spatiotemporal different because of emission sources, but most studies are still applying uniformed parameters to all study regions. On the other hand, we may start to consider the chemical and biogenic changes of P in further study.

About the lack of observation data to constrain and evaluate the model performance. The observation of P is poorer than N both in the spatiotemporal coverages of records and the qualities of site sampling. P is not in the regular routine for monitoring networks, thus no public platform is collecting the measurements. That is the motivation to collect and compile the data reported in literatures and reports, especially for regions with limited data. Although such kind of studies have

been reported several times, there is still no documentation on the format of records and not confirmation in the continuation of these works.

CHAPTER 7
CONCLUSION AND FUTURE WORK

This study investigates several issues about N deposition. We start by building a basic understanding of the characteristics of N deposition at global scale. By using the multiple model ensemble results of HTAP-II, which is an international cooperation of observational and modelling studies on global pollution issues, we map the global distributions of S and N depositions in 2010. The approach of multi-model ensemble helps to eliminate the risk of "random error" by single model. We evaluate the model performance over North America, Europe and East Asia with regional monitoring network, and find the model accuracies on predicting atmospheric deposition have been improved slightly over North America and East Asia and significantly over Europe, compared to similar multi-model studies in early 2000s. But model underestimation of NH_4^+ wet deposition over all three regions remains a problem, probably due to the poorly developed NH_3 emission inventory. In addition, we are still unclear about the model performances in measurement-poor regions, some of which are the most heavily polluted regions in the world such as China and India. A comparison of this study with the deposition in 2000 indicates significant changes of global S and N budgets in recent years, with aggregated pollution in Asia regions and alleviated stress in North America and Europe, and the trends agree well with the changes in anthropogenic emissions.

Then, we investigate the two predominant drivers of future N deposition: anthropogenic emissions and climate changes. We conduct a case study in the United States to examine the impacts of emission control on reducing N deposition. Control on NO_x emissions has been reported as a big success on reducing NO_2 air concentration levels. It is also effective on decreasing NO_y deposition according to this study. However, we find it difficult to develop a similar relationship between NH_3 emission and NH_x deposition. We find that a "buffering effect", which increases the partitioning of NH_3 to NH_4^+ as the precipitation gets more acidic, would persist the reduction of NH_x deposition at the early stages of NH_3 emission abatement. Therefore, the benefit of controlling NH_3 emission on NH_x deposition would be up to 40% lower than that of controlling NO_x emission on NO_y deposition. This is an important issue that the policy makers need to take into consideration when developing control strategies, under the circumstance that many regions (i.e. United States and Europe) are suffering more and more by the increasing NH_x deposition.

We examine the impacts of another important driver, climate changes, on N deposition. This study focuses on the impacts of long-range transport of air pollutants on regional deposition. Many recent studies have demonstrated significant contributions of continental outflow to the air pollution issues (i.e. O_3 and PM) on its downwind continents, but seldom study has paid attention to the influences on deposition according to our review of literature. Our study finds that for low emission intensity regions, such as Russia, the amounts of atmospheric deposition brought by long-range transport is almost equivalent (40-60% for Russia in this study) to the amounts contributed by their own-region emissions. Meanwhile, long-range transport of air pollutants increases the N burden on coastal regions and Open Ocean, especially on those in the downwind regions of intensive emission sources. Whether this extra supply of N leads to adverse impacts (i.e. coastal eutrophication) or benefit (i.e. favor vegetation growth in wetlands and increase carbon sequestration) requires further study.

Then, we connect our study on the characteristics of N deposition to the ecosystems. We investigate the impacts of excessive N deposition on terrestrial ecosystems. Although the concept of CLs was developed as early as 1980s, the studies on CLs are conducted over limited numbers of regions (mostly on United States, Europe and China according to our review of literature), probably due to the expert knowledge needed to develop the CLs. Empirical CLs requires site experiments and thus is not possible for regions with no records. While the modelling approach (i.e. simple mass balance (SMB) model and dynamic model), which use environmental parameters in soils to calculate the CLs, makes it possible for developing a CLs dataset at global scale. We collect the available SMB CLs over the United States, Europe and China from publications and compare the procedures/data used for CLs calculation. Most studies are following the same procedures, and use substitutions when some parameters are not available (i.e. use modelled base cations deposition where monitoring data are not available). However, after applying these datasets to assess the exceedance of CLs, we find these CLs are still subject to large uncertainties associated with the spatial distribution of data and land type classification. We shall be cautious to interpolate the results and draw conclusions merely based on the present work.

In the last chapter, we pay attention to the deposition of P, which together with N are the two essential nutrients that determine the productivity of ecosystems. The N emitted by human activity has largely disturbed the natural N cycle and altered the balance between N and P. There

is evidence from observations that many ecosystems have switched their nutrient limitation patterns from N-limited to P-limited. However, compared to the long-term measurement and modelling studies on N species and N depositions, much less attention has been given to the P budgets, owing to the fact that P is neither a regular detected specie in current observation networks nor a variable in the earth system models. Motivated by the needs in study about P, we conduct a review on the previous studies on P deposition and summarize the following information for further study on P deposition: (1) a dataset with collected measurement of P deposition (2) a collection of different methods to form the emission inventory of P for model inputs and the important parameters (i.e. solubility of P) for numerical modelling.

REFERENCES

Aas, W., R. Artz, V. Bowersox, G. Carmichael, A. Cole, F. Dentener, H. Fagerli, D. Gay, J. Geddes, C. Hogrefe, F. O'Connor, J. Pienaar, A. Stein, AND Johnt Walker. . (2017). *Global Atmopshere Watch Workshop on Measurement-Model Fusion for Global Total Atmospheric Deposition (MMF-GTAD).* Retrieved from World Meteorological Organization, Geneva, Switzerland.:

Ahlstrom, H., & Cornell, S. E. (2018). Governance, polycentricity and the global nitrogen and phosphorus cycles. *Environmental Science & Policy, 79*, 54-65. doi:10.1016/j.envsci.2017.10.005

Arndt, R. L., & Carmichael, G. R. (1995). Long-range transport and deposition of sulfur in Asia. *Water Air and Soil Pollution, 85*(4), 2283-2288.

Auvray, M., & Bey, I. (2005). Long-range transport to Europe: Seasonal variations and implications for the European ozone budget. *Journal of Geophysical Research-Atmospheres, 110*(D11).

Baker, A. R., Lesworth, T., Adams, C., Jickells, T. D., & Ganzeveld, L. (2010). Estimation of atmospheric nutrient inputs to the Atlantic Ocean from 50 degrees N to 50 degrees S based on large-scale field sampling: Fixed nitrogen and dry deposition of phosphorus. *Global Biogeochemical Cycles, 24*. doi:10.1029/2009gb003634

Bergstrom, A. K., & Jansson, M. (2006). Atmospheric nitrogen deposition has caused nitrogen enrichment and eutrophication of lakes in the northern hemisphere. *Global Change Biology, 12*(4), 635-643. doi:10.1111/j.1365-2486.2006.01129.x

Berntsen, T. K., Karlsdottir, S., & Jaffe, D. A. (1999). Influence of Asian emissions on the composition of air reaching the North Western United States. *Geophysical Research Letters, 26*(14), 2171-2174.

Bey, I., Jacob, D. J., Logan, J. A., & Yantosca, R. M. (2001). Asian chemical outflow to the Pacific in spring: Origins, pathways, and budgets. *Journal of Geophysical Research-Atmospheres, 106*(D19), 23097-23113. doi:10.1029/2001jd000806

Bian, H. S., Chin, M., Hauglustaine, D. A., Schulz, M., Myhre, G., Bauer, S. E., . . . Tsyro, S. G. (2017). Investigation of global particulate nitrate from the AeroCom phase III experiment. *Atmospheric Chemistry and Physics, 17*(21), 12911-12940.

Bleeker, A., Hicks, W. K., Dentener, E., Galloway, J., & Erisman, J. W. (2011). N deposition as a threat to the World's protected areas under the Convention on Biological Diversity. *Environmental Pollution, 159*(10), 2280-2288.

Blett, T. F., Lynch, J. A., Pardo, L. H., Huber, C., Haeuber, R., & Pouyat, R. (2014). FOCUS: A pilot study for national-scale critical loads development in the United States. *Environmental Science & Policy, 38*, 225-236.

Bobbink, R., Hicks, K., Galloway, J., Spranger, T., Alkemade, R., Ashmore, M., . . . De Vries, W. (2010). Global assessment of nitrogen deposition effects on terrestrial plant diversity: a synthesis. *Ecological Applications, 20*(1), 30-59. doi:10.1890/08-1140.1

Bobbink, R., Tomassen, H., Weijters, M., van den Berg, L., Strengbom, J., Braun, S., . . . Hettelingh, J. P. (2015). *Effects and Empirical Critical Loads of Nitrogen for Europe* (Vol. 25).

Bouwman, A. F., Van Vuuren, D. P., Derwent, R. G., & Posch, M. (2002). A global analysis of acidification and eutrophication of terrestrial ecosystems. *Water Air and Soil Pollution, 141*(1-4), 349-382. doi:10.1023/a:1021398008726

Bouwman, L., Goldewijk, K. K., Van Der Hoek, K. W., Beusen, A. H. W., Van Vuuren, D. P., Willems, J., . . . Stehfest, E. (2013). Exploring global changes in nitrogen and phosphorus cycles in agriculture induced by livestock production over the 1900-2050 period. *Proceedings of the National Academy of Sciences of the United States of America, 110*(52), 20882-20887. doi:10.1073/pnas.1012878108

Brahney, J., Ballantyne, A. P., Kociolek, P., Spaulding, S., Otu, M., Porwoll, T., & Neff, J. C. (2014). Dust mediated transfer of phosphorus to alpine lake ecosystems of the Wind River Range, Wyoming, USA. *Biogeochemistry, 120*(1-3), 259-278.

Brahney, J., Mahowald, N., Ward, D. S., Ballantyne, A. P., & Neff, J. C. (2015). Is atmospheric phosphorus pollution altering global alpine Lake stoichiometry? *Global Biogeochemical Cycles, 29*(9), 1369-1383.

Brown-Steiner, B., & Hess, P. (2011). Asian influence on surface ozone in the United States: A comparison of chemistry, seasonality, and transport mechanisms. *Journal of Geophysical Research-Atmospheres, 116*. doi:10.1029/2011jd015846

Camarero, L., & Catalan, J. (2012). Atmospheric phosphorus deposition may cause lakes to revert from phosphorus limitation back to nitrogen limitation. *Nature Communications, 3*.

Cao, J., Garbaccio, R., & Ho, M. S. (2009). China's 11th Five-Year Plan and the Environment: Reducing SO2 Emissions. *Review of Environmental Economics and Policy, 3*(2), 231-250. doi:10.1093/reep/rep006

Chen, H. Y., Hung, C. C., Fang, T. H., & Gong, G. C. (2008). Dry deposition and particle-size distribution of phosphorus in the marine atmosphere over the northeastern coast of Taiwan. *Continental Shelf Research, 28*(6), 756-766. doi:10.1016/j.csr.2007.12.008

Chin, M., Diehl, T., Tan, Q., Prospero, J. M., Kahn, R. A., Remer, L. A., . . . Zhao, X. P. (2014). Multi-decadal aerosol variations from 1980 to 2009: a perspective from observations and a global model. *Atmospheric Chemistry and Physics, 14*(7), 3657-3690.

Clark, C. M., Phelan, J., Doraiswamy, P., Buckley, J., Cajka, J. C., Dennis, R. L., . . . Spero, T. L. (2018). Atmospheric deposition and exceedances of critical loads from 1800-2025 for the conterminous United States. *Ecological Applications, 28*(4), 978-1002.

Clark, C. M., & Tilman, D. (2008). Loss of plant species after chronic low-level nitrogen deposition to prairie grasslands. *Nature, 451*(7179), 712-715.

Crippa, M., Guizzardi, D., Muntean, M., Schaaf, E., Dentener, F., van Aardenne, J. A., . . . Janssens-Maenhout, G. (2018). Gridded emissions of air pollutants for the period 1970-2012 within EDGAR v4.3.2. *Earth System Science Data, 10*(4), 1987-2013.

Critical Loads and Dynamic Risk Assessments. (2015). (J.-P. H. Wim de Vries, Maximilian Posch, Ed.): Springer.

de Vries, W., & Posch, M. (2011). Modelling the impact of nitrogen deposition, climate change and nutrient limitations on tree carbon sequestration in Europe for the period 1900–2050. *Environmental Pollution, 159*(10), 2289-2299. doi:https://doi.org/10.1016/j.envpol.2010.11.023

Dentener, F., Drevet, J., Lamarque, J. F., Bey, I., Eickhout, B., Fiore, A. M., . . . Wild, O. (2006). Nitrogen and sulfur deposition on regional and global scales: A multimodel evaluation. *Global Biogeochemical Cycles, 20*(4), 21. doi:10.1029/2005gb002672

Deolal, S. P., Staehelin, J., Brunner, D., Cui, J. B., Steinbacher, M., Zellweger, C., . . . Vollmer, M. K. (2013). Transport of PAN and NOy from different source regions to the Swiss high alpine site Jungfraujoch. *Atmospheric Environment, 64*, 103-115. doi:10.1016/j.atmosenv.2012.08.021

Derwent, R. G., Stevenson, D. S., Collins, W. J., & Johnson, C. E. (2004). Intercontinental transport and the origins of the ozone observed at surface sites in Europe. *Atmospheric Environment, 38*(13), 1891-1901. doi:10.1016/j.atmosenv.2004.01.008

Doney, S. C., Mahowald, N., Lima, I., Feely, R. A., Mackenzie, F. T., Lamarque, J. F., & Rasch, P. J. (2007). Impact of anthropogenic atmospheric nitrogen and sulfur deposition on ocean acidification and the inorganic carbon system. *Proceedings of the National Academy of Sciences of the United States of America, 104*(37), 14580-14585. doi:10.1073/pnas.0702218104

Dong, X., Fu, J. S., Zhu, Q., Sun, J., Tan, J., Keating, T., . . . Huang, K. (2018). Long-range Transport Impacts on Surface Aerosol Concentrations and the Contributions to Haze Events in China: an HTAP2 Multi-Model Study. *Atmos. Chem. Phys. Discuss., 2018*, 1-33. doi:10.5194/acp-2018-91

Du, E. Z., de Vries, W., Galloway, J. N., Hu, X. Y., & Fang, J. Y. (2014). Changes in wet nitrogen deposition in the United States between 1985 and 2012. *Environmental Research Letters, 9*(9).

Duan, L., Xie, S. D., Zhou, Z. P., Ye, X. M., & Hao, J. M. (2001). Calculation and mapping of critical loads for S, N and acidity in China. *Water Air and Soil Pollution, 130*(1-4), 1199-1204. doi:10.1023/a:1013908629150

Duarte, N., Pardo, L. H., & Robin-Abbott, M. J. (2013). Susceptibility of Forests in the Northeastern USA to Nitrogen and Sulfur Deposition: Critical Load Exceedance and Forest Health. *Water Air and Soil Pollution, 224*(2).

Duce, R. A., LaRoche, J., Altieri, K., Arrigo, K. R., Baker, A. R., Capone, D. G., . . . Zamora, L. (2008). Impacts of atmospheric anthropogenic nitrogen on the open ocean. *Science, 320*(5878), 893-897. doi:10.1126/science.1150369

Duncan, B. N., & Bey, I. (2004). A modeling study of the export pathways of pollution from Europe: Seasonal and interannual variations (1987-1997). *Journal of Geophysical Research-Atmospheres, 109*(D8).

Duncan, B. N., West, J. J., Yoshida, Y., Fiore, A. M., & Ziemke, J. R. (2008). The influence of European pollution on ozone in the Near East and northern Africa. *Atmospheric Chemistry and Physics, 8*(8), 2267-2283.

Ellis, R. A., Jacob, D. J., Sulprizio, M. P., Zhang, L., Holmes, C. D., Schichtel, B. A., . . . Lynch, J. A. (2013). Present and future nitrogen deposition to national parks in the United States: critical load exceedances. *Atmospheric Chemistry and Physics, 13*(17), 9083-9095.

Elser, J. J., Andersen, T., Baron, J. S., Bergstrom, A. K., Jansson, M., Kyle, M., . . . Hessen, D. O. (2009). Shifts in Lake N:P Stoichiometry and Nutrient Limitation Driven by Atmospheric Nitrogen Deposition. *Science, 326*(5954), 835-837.

Fang, Y. T., Gundersen, P., Mo, J. M., & Zhu, W. X. (2009). Nitrogen leaching in response to increased nitrogen inputs in subtropical monsoon forests in southern China. *Forest Ecology and Management, 257*(1), 332-342.

Filippelli, G. M. (2008). The global phosphorus cycle: Past, present, and future. *Elements, 4*(2), 89-95. doi:10.2113/gselements.4.2.89

Fiore, A. M., Dentener, F. J., Wild, O., Cuvelier, C., Schultz, M. G., Hess, P., . . . Zuber, A. (2009). Multimodel estimates of intercontinental source-receptor relationships for ozone pollution. *Journal of Geophysical Research, 114*(D4). doi:10.1029/2008jd010816

Fowler, D., Pyle, J. A., Raven, J. A., & Sutton, M. A. (2013). The global nitrogen cycle in the twenty-first century: introduction. *Philosophical Transactions of the Royal Society B-Biological Sciences, 368*(1621).

Fu, J. S., Dong, X. Y., Gao, Y., Wong, D. C., & Lam, Y. F. (2012). Sensitivity and linearity analysis of ozone in East Asia: The effects of domestic emission and intercontinental transport. *Journal of the Air & Waste Management Association, 62*(9), 13. doi:10.1080/10962247.2012.699014

Galloway, J. N., Townsend, A. R., Erisman, J. W., Bekunda, M., Cai, Z. C., Freney, J. R., . . . Sutton, M. A. (2008). Transformation of the nitrogen cycle: Recent trends, questions, and potential solutions. *Science, 320*(5878), 889-892. doi:10.1126/science.1136674

Galmarini, S., Koffi, B., Solazzo, E., Keating, T., Hogrefe, C., Schulz, M., . . . Dentener, F. (2017). Technical note: Coordination and harmonization of the multi-scale, multi-model activities HTAP2, AQMEII3, and MICS-Asia3: simulations, emission inventories, boundary conditions, and model output formats. *Atmos. Chem. Phys., 17*(2), 1543-1555. doi:10.5194/acp-17-1543-2017

Geiser, L. H., Jovan, S. E., Glavich, D. A., & Porter, M. K. (2010). Lichen-based critical loads for atmospheric nitrogen deposition in Western Oregon and Washington Forests, USA. *Environmental Pollution, 158*(7), 2412-2421.

Glotfelty, T., Zhang, Y., Karamchandani, P., & Streets, D. G. (2014). Will the role of intercontinental transport change in a changing climate? *Atmospheric Chemistry and Physics, 14*(17), 9379-9402. doi:10.5194/acp-14-9379-2014

Graham, W. F., & Duce, R. A. (1979). Atmospheric Pathways of the Phosphorus Cycle. *Geochimica Et Cosmochimica Acta, 43*(8), 1195-1208.

Gruber, N., & Galloway, J. N. (2008). An Earth-system perspective of the global nitrogen cycle. *Nature, 451*(7176), 293-296.

Guerova, G., Bey, I., Attie, J. L., Martin, R. V., Cui, J., & Sprenger, M. (2006). Impact of transatlantic transport episodes on summertime ozone in Europe. *Atmospheric Chemistry and Physics, 6*, 2057-2072.

Guo, H. Y., Otjes, R., Schlag, P., Kiendler-Scharr, A., Nenes, A., & Weber, R. J. (2018). Effectiveness of ammonia reduction on control of fine particle nitrate. *Atmospheric Chemistry and Physics, 18*(16), 12241-12256.

Guo, J. H., Liu, X. J., Zhang, Y., Shen, J. L., Han, W. X., Zhang, W. F., . . . Zhang, F. S. (2010). Significant Acidification in Major Chinese Croplands. *Science, 327*(5968), 1008-1010.

Hall, J. (2018). *Average Accumulated Exceedance (AAE) of critical loads of acidity and nutrient nitrogen by acid and nitrogen deposition for 2013-15*. Retrieved from: https://doi.org/10.5285/e32745d2-fb56-4f91-a235-6b213a8b45cb

Harrison, J. A., Bouwman, A. F., Mayorga, E., & Seitzinger, S. (2010). Magnitudes and sources of dissolved inorganic phosphorus inputs to surface fresh waters and the coastal zone: A new global model. *Global Biogeochemical Cycles, 24*. doi:10.1029/2009gb003590

Herut, B., Krom, M. D., Pan, G., & Mortimer, R. (1999). Atmospheric input of nitrogen and phosphorus to the Southeast Mediterranean: Sources, fluxes, and possible impact. *Limnology and Oceanography, 44*(7), 1683-1692. doi:10.4319/lo.1999.44.7.1683

Hogrefe, C., Liu, P., Pouliot, G., Mathur, R., Roselle, S., Flemming, J., . . . Park, R. J. (2018). Impacts of different characterizations of large-scale background on simulated regional-scale ozone over the continental United States. *Atmos. Chem. Phys., 18*(5), 3839-3864. doi:10.5194/acp-18-3839-2018

Holland, E. A., Braswell, B. H., Lamarque, J. F., Townsend, A., Sulzman, J., Muller, J. F., . . . Roelofs, G. J. (1997). Variations in the predicted spatial distribution of atmospheric nitrogen deposition and their impact on carbon uptake by terrestrial ecosystems. *Journal of Geophysical Research-Atmospheres, 102*(D13), 15849-15866. doi:10.1029/96jd03164

Holt, J., Selin, N. E., & Solomon, S. (2015). Changes in Inorganic Fine Particulate Matter Sensitivities to Precursors Due to Large-Scale US Emissions Reductions. *Environ Sci Technol, 49*(8), 4834-4841.

Holzer, M., Hall, T. M., & Stull, R. B. (2005). Seasonality and weather-driven variability of transpacific transport. *Journal of Geophysical Research-Atmospheres, 110*(D23). doi:10.1029/2005jd006261

Huang, M., Carmichael, G. R., Pierce, R. B., Jo, D. S., Park, R. J., Flemming, J., . . . Payne, V. H. (2017). Impact of intercontinental pollution transport on North American ozone air pollution: an HTAP phase 2 multi-model study. *Atmos. Chem. Phys., 17*(9), 5721-5750. doi:10.5194/acp-17-5721-2017

Hudman, R. C., Jacob, D. J., Cooper, O. R., Evans, M. J., Heald, C. L., Park, R. J., . . . Ryerson, T. (2004). Ozone production in transpacific Asian pollution plumes and implications for ozone air quality in California. *Journal of Geophysical Research-Atmospheres, 109*(D23).

International Plant Nitrition Institute. (2018). The Nitrogen Cycle. Retrieved from http://www.ipni.net/
Jacob, D. J., Logan, J. A., & Murti, P. P. (1999). Effect of rising Asian emissions on surface ozone in the United States. *Geophysical Research Letters, 26*(14), 2175-2178. doi:10.1029/1999gl900450
Jaffe, D., Price, H., Parrish, D., Goldstein, A., & Harris, J. (2003). Increasing background ozone during spring on the west coast of North America. *Geophysical Research Letters, 30*(12). doi:10.1029/2003gl017024
James, C. N., & Houze, R. A. (2005). Modification of precipitation by coastal orography in storms crossing northern California. *Monthly Weather Review, 133*(11), 3110-3131.
Janssens-Maenhout, G., Crippa, M., Guizzardi, D., Dentener, F., Muntean, M., Pouliot, G., . . . Li, M. (2015). HTAP_v2.2: a mosaic of regional and global emission grid maps for 2008 and 2010 to study hemispheric transport of air pollution. *Atmos. Chem. Phys., 15*(19), 11411-11432. doi:10.5194/acp-15-11411-2015
Janssens, I. A., Dieleman, W., Luyssaert, S., Subke, J. A., Reichstein, M., Ceulemans, R., . . . Law, B. E. (2010). Reduction of forest soil respiration in response to nitrogen deposition. *Nature Geoscience, 3*(5), 315-322. doi:10.1038/ngeo844
Jia, Y., Yu, G., Gao, Y., He, N., Wang, Q., Jiao, C., & Zuo, Y. (2016). Global inorganic nitrogen dry deposition inferred from ground- and space-based measurements. *Sci Rep, 6*, 19810. doi:10.1038/srep19810
Jickells, T. (2006). The role of air-sea exchange in the marine nitrogen cycle. *Biogeosciences, 3*(3), 271-280.
Jickells, T. D., Buitenhuis, E., Altieri, K., Baker, A. R., Capone, D., Duce, R. A., . . . Zamora, L. M. (2017). A reevaluation of the magnitude and impacts of anthropogenic atmospheric nitrogen inputs on the ocean. *Global Biogeochemical Cycles, 31*(2), 289-305.
Jonson, J. E., Schulz, M., Emmons, L., Flemming, J., Henze, D., Sudo, K., . . . Davila, Y. (2018). The effects of intercontinental emission sources on European air pollution levels. *Atmos. Chem. Phys., 18*(18), 13655-13672. doi:10.5194/acp-18-13655-2018
Kanakidou, M., Duce, R. A., Prospero, J. M., Baker, A. R., Benitez-Nelson, C., Dentener, F. J., . . . Zhu, T. (2012). Atmospheric fluxes of organic N and P to the global ocean. *Global Biogeochemical Cycles, 26*. doi:10.1029/2011gb004277
Kanakidou, M., Myriokefalitakis, S., Daskalakis, N., Fanourgakis, G., Nenes, A., Baker, A. R., . . . Mihalopoulos, N. (2016). Past, Present, and Future Atmospheric Nitrogen Deposition. *Journal of the Atmospheric Sciences, 73*(5), 2039-2047. doi:10.1175/jas-d-15-0278.1
Kanakidou, M., Myriokefalitakis, S., & Tsigaridis, K. (2018). Aerosols in atmospheric chemistry and biogeochemical cycles of nutrients. *Environmental Research Letters, 13*(6). doi:10.1088/1748-9326/aabcdb
Kim, S. W., Heckel, A., McKeen, S. A., Frost, G. J., Hsie, E. Y., Trainer, M. K., . . . Grell, G. A. (2006). Satellite-observed U.S. power plant NOxemission reductions and their impact on air quality. *Geophysical Research Letters, 33*(22). doi:10.1029/2006gl027749
Kim, T. W., Lee, K., Najjar, R. G., Jeong, H. D., & Jeong, H. J. (2011). Increasing N Abundance in the Northwestern Pacific Ocean Due to Atmospheric Nitrogen Deposition. *Science, 334*(6055), 505-509.
Köster, E., Köster, K., Berninger, F., Prokushkin, A., Aaltonen, H., Zhou, X., & Pumpanen, J. (2018). Changes in fluxes of carbon dioxide and methane caused by fire in Siberian boreal forest with continuous permafrost. *Journal of Environmental Management, 228*, 405-415. doi:https://doi.org/10.1016/j.jenvman.2018.09.051
Kurokawa, J., Ohara, T., Morikawa, T., Hanayama, S., Janssens-Maenhout, G., Fukui, T., . . . Akimoto, H. (2013). Emissions of air pollutants and greenhouse gases over Asian regions during 2000-2008: Regional Emission inventory in ASia (REAS) version 2. *Atmospheric Chemistry and Physics, 13*(21), 11019-11058. doi:10.5194/acp-13-11019-2013
Laj, P., Klausen, J., Bilde, M., Plass-Duelmer, C., Pappalardo, G., Clerbaux, C., . . . Zardini, A. A. (2009). Measuring atmospheric composition change. *Atmospheric Environment, 43*(33), 5351-5414.
Lamarque, J. F., Bond, T. C., Eyring, V., Granier, C., Heil, A., Klimont, Z., . . . van Vuuren, D. P. (2010). Historical (1850-2000) gridded anthropogenic and biomass burning emissions of reactive gases and aerosols: methodology and application. *Atmospheric Chemistry and Physics, 10*(15), 7017-7039.
Lamarque, J. F., Dentener, F., McConnell, J., Ro, C. U., Shaw, M., Vet, R., . . . Nolan, M. (2013). Multi-model mean nitrogen and sulfur deposition from the Atmospheric Chemistry and Climate Model Intercomparison Project (ACCMIP): evaluation of historical and projected future changes. *Atmospheric Chemistry and Physics, 13*(16), 7997-8018. doi:10.5194/acp-13-7997-2013
Lamarque, J. F., Kiehl, J. T., Brasseur, G. P., Butler, T., Cameron-Smith, P., Collins, W. D., . . . Thornton, P. (2005). Assessing future nitrogen deposition and carbon cycle feedback using a multimodel approach: Analysis of nitrogen deposition. *Journal of Geophysical Research-Atmospheres, 110*(D19). doi:10.1029/2005jd005825
Li, M., Liu, H., Geng, G. N., Hong, C. P., Liu, F., Song, Y., . . . He, K. B. (2017). Anthropogenic emission inventories in China: a review. *National Science Review, 4*(6), 834-866.

Li, M., Zhang, Q., Kurokawa, J., Woo, J. H., He, K. B., Lu, Z. F., . . . Zheng, B. (2017). MIX: a mosaic Asian anthropogenic emission inventory under the international collaboration framework of the MICS-Asia and HTAP. *Atmospheric Chemistry and Physics, 17*(2), 935-963.

Li, Q. B., Jacob, D. J., Bey, I., Palmer, P. I., Duncan, B. N., Field, B. D., . . . Oltmans, S. J. (2002). Transatlantic transport of pollution and its effects on surface ozone in Europe and North America. *Journal of Geophysical Research-Atmospheres, 107*(D13). doi:10.1029/2001jd001422

Li, Q. B., Jacob, D. J., Munger, J. W., Yantosca, R. M., & Parrish, D. D. (2004). Export of NOy from the North American boundary layer: Reconciling aircraft observations and global model budgets. *Journal of Geophysical Research-Atmospheres, 109*(D2).

Li, X. Y., Liu, J. F., Mauzerall, D. L., Emmons, L. K., Walters, S., Horowitz, L. W., & Tao, S. (2014). Effects of trans-Eurasian transport of air pollutants on surface ozone concentrations over Western China. *Journal of Geophysical Research-Atmospheres, 119*(21), 12338-12354. doi:10.1002/2014jd021936

Li, Y., Schichtel, B. A., Walker, J. T., Schwede, D. B., Chen, X., Lehmann, C. M. B., . . . Collett, J. L. (2016). Increasing importance of deposition of reduced nitrogen in the United States. *Proceedings of the National Academy of Sciences of the United States of America, 113*(21), 5874-5879. doi:10.1073/pnas.1525736113

Liang, C. K., West, J. J., Silva, R. A., Bian, H., Chin, M., Davila, Y., . . . Takemura, T. (2018). HTAP2 multi-model estimates of premature human mortality due to intercontinental transport of air pollution and emission sectors. *Atmos. Chem. Phys., 18*(14), 10497-10520. doi:10.5194/acp-18-10497-2018

Liang, Q., Jaegle, L., Jaffe, D. A., Weiss-Penzias, P., Heckman, A., & Snow, J. A. (2004). Long-range transport of Asian pollution to the northeast Pacific: Seasonal variations and transport pathways of carbon monoxide. *Journal of Geophysical Research-Atmospheres, 109*(D23).

Lin, M., Holloway, T., Carmichael, G. R., & Fiore, A. M. (2010). Quantifying pollution inflow and outflow over East Asia in spring with regional and global models. *Atmospheric Chemistry and Physics, 10*(9), 4221-4239. doi:10.5194/acp-10-4221-2010

Liu, F., Zhang, Q., Ronald, J. V., Zheng, B., Tong, D., Yan, L., . . . He, K. B. (2016). Recent reduction in NOx emissions over China: synthesis of satellite observations and emission inventories. *Environmental Research Letters, 11*(11). doi:10.1088/1748-9326/11/11/114002

Liu, H. Y., Jacob, D. J., Bey, I., Yantosca, R. M., Duncan, B. N., & Sachse, G. W. (2003). Transport pathways for Asian pollution outflow over the Pacific: Interannual and seasonal variations. *Journal of Geophysical Research-Atmospheres, 108*(D20). doi:10.1029/2002jd003102

Liu, J. F., Mauzerall, D. L., & Horowitz, L. W. (2005). Analysis of seasonal and interannual variability in transpacific transport. *Journal of Geophysical Research-Atmospheres, 110*(D4). doi:10.1029/2004jd005207

Liu, M. X., Huang, X., Song, Y., Tang, J., Cao, J. J., Zhang, X. Y., . . . Zhu, T. (2019). Ammonia emission control in China would mitigate haze pollution and nitrogen deposition, but worsen acid rain. *Proceedings of the National Academy of Sciences of the United States of America, 116*(16), 7760-7765.

Liu, X., Sheng, H., Jiang, S. Y., Yuan, Z. W., Zhang, C. S., & Elser, J. J. (2016). Intensification of phosphorus cycling in China since the 1600s. *Proceedings of the National Academy of Sciences of the United States of America, 113*(10), 2609-2614. doi:10.1073/pnas.1519554113

Lloret, J., & Valiela, I. (2016). Unprecedented decrease in deposition of nitrogen oxides over North America: the relative effects of emission controls and prevailing air-mass trajectories. *Biogeochemistry, 129*(1-2), 165-180. doi:10.1007/s10533-016-0225-5

Lu, Z., Streets, D. G., Zhang, Q., Wang, S., Carmichael, G. R., Cheng, Y. F., . . . Tan, Q. (2010). Sulfur dioxide emissions in China and sulfur trends in East Asia since 2000. *Atmospheric Chemistry and Physics, 10*(13), 6311-6331.

Luo, J., Wang, X. R., Yang, H., Yu, J. Z., Yang, L. Y., & Qin, B. Q. (2011). Atmospheric phosphorus in the northern part of Lake Taihu, China. *Chemosphere, 84*(6), 785-791.

Luo, R., Fan, J., Wang, W., Luo, J., Kuzyakov, Y., He, J.-S., . . . Ding, W. (2019). Nitrogen and phosphorus enrichment accelerates soil organic carbon loss in alpine grassland on the Qinghai-Tibetan Plateau. *Science of the Total Environment, 650*, 303-312. doi:https://doi.org/10.1016/j.scitotenv.2018.09.038

Mahowald, N., Jickells, T. D., Baker, A. R., Artaxo, P., Benitez-Nelson, C. R., Bergametti, G., . . . Tsukuda, S. (2008). Global distribution of atmospheric phosphorus sources, concentrations and deposition rates, and anthropogenic impacts. *Global Biogeochemical Cycles, 22*(4).

Mahowald, N. M., Artaxo, P., Baker, A. R., Jickells, T. D., Okin, G. S., Randerson, J. T., & Townsend, A. R. (2005). Impacts of biomass burning emissions and land use change on Amazonian atmospheric phosphorus cycling and deposition. *Global Biogeochemical Cycles, 19*(4). doi:10.1029/2005gb002541

Makar, P. A., Akingunola, A., Aherne, J., Cole, A. S., Aklilu, Y.-a., Zhang, J., . . . Jeffries, D. S. (2018). Estimates of exceedances of critical loads for acidifying deposition in Alberta and Saskatchewan. *Atmospheric Chemistry and Physics, 18*(13), 9897-9927. doi:10.5194/acp-18-9897-2018

McNulty, S. G., Cohen, E. C., Myers, J. A. M., Sullivan, T. J., & Li, H. (2007). Estimates of critical acid loads and exceedances for forest soils across the conterminous United States. *Environmental Pollution, 149*(3), 281-292.

Moxim, W. J., Levy, H., & Kasibhatla, P. S. (1996). Simulated global tropospheric PAN: Its transport and impact on NOx. *Journal of Geophysical Research-Atmospheres, 101*(D7), 12621-12638. doi:10.1029/96jd00338

Myriokefalitakis, S., Nenes, A., Baker, A. R., Mihalopoulos, N., & Kanakidou, M. (2016). Bioavailable atmospheric phosphorous supply to the global ocean: a 3-D global modeling study. *Biogeosciences, 13*(24), 6519-6543. doi:10.5194/bg-13-6519-2016

Neff, J. C., Holland, E. A., Dentener, F. J., McDowell, W. H., & Russell, K. M. (2002). The origin, composition and rates of organic nitrogen deposition: A missing piece of the nitrogen cycle? *Biogeochemistry, 57*(1), 99-136.

Nilsson, J. (1988). *Critical Loads for Sulphur and Nitrogen*, Dordrecht.

Paerl, H. W. (2002). Connecting atmospheric nitrogen deposition to coastal eutrophication. *Environ Sci Technol, 36*(15), 323a-326a.

Pardo, L. H., Fenn, M. E., Goodale, C. L., Geiser, L. H., Driscoll, C. T., Allen, E. B., . . . Dennis, R. L. (2011). Effects of nitrogen deposition and empirical nitrogen critical loads for ecoregions of the United States. *Ecological Applications, 21*(8), 3049-3082. doi:10.1890/10-2341.1

Pardo, L. H., Robin-Abbott, M. J., Fenn, M. E., Goodale, C. L., Geiser, L. H., Driscoll, C. T., . . . Dennis, R. L. (2015). *Effects and Empirical Critical Loads of Nitrogen for Ecoregions of the United States* (Vol. 25).

Parrish, D. D., Dunlea, E. J., Atlas, E. L., Schauffler, S., Donnelly, S., Stroud, V., . . . Roberts, J. M. (2004). Changes in the photochemical environment of the temperate North Pacific troposphere in response to increased Asian emissions. *Journal of Geophysical Research: Atmospheres, 109*(D23). doi:10.1029/2004jd004978

Parrish, D. D., Millet, D. B., & Goldstein, A. H. (2009). Increasing ozone in marine boundary layer inflow at the west coasts of North America and Europe. *Atmospheric Chemistry and Physics, 9*(4), 1303-1323.

Paulot, F., Jacob, D. J., & Henze, D. K. (2013). Sources and Processes Contributing to Nitrogen Deposition: An Adjoint Model Analysis Applied to Biodiversity Hotspots Worldwide. *Environ Sci Technol, 47*(7), 3226-3233. doi:10.1021/es3027727

Phelan, J., Belyazid, S., Kurz, D., Guthrie, S., Cajka, J., Sverdrup, H., & Waite, R. (2014). Estimation of Soil Base Cation Weathering Rates with the PROFILE Model to Determine Critical Loads of Acidity for Forested Ecosystems in Pennsylvania, USA: Pilot Application of a Potential National Methodology. *Water Air and Soil Pollution, 225*(9).

Phoenix, G. K., Hicks, W. K., Cinderby, S., Kuylenstierna, J. C. I., Stock, W. D., Dentener, F. J., . . . Ineson, P. (2006). Atmospheric nitrogen deposition in world biodiversity hotspots: the need for a greater global perspective in assessing N deposition impacts. *Global Change Biology, 12*(3), 470-476. doi:10.1111/j.1365-2486.2006.01104.x

Pinder, R. W., Adams, P. J., & Pandis, S. N. (2007). Ammonia Emission Controls as a Cost-Effective Strategy for Reducing Atmospheric Particulate Matter in the Eastern United States. *Environ Sci Technol, 41*(2), 380-386. doi:10.1021/es060379a

Pinder, R. W., Gilliland, A. B., & Dennis, R. L. (2008). Environmental impact of atmospheric NH3 emissions under present and future conditions in the eastern United States. *Geophysical Research Letters, 35*(12).

Posch, M., Duan, L., Reinds, G. J., & Zhao, Y. (2015). Critical loads of nitrogen and sulphur to avert acidification and eutrophication in Europe and China. *Landscape Ecology, 30*(3), 487-499. doi:10.1007/s10980-014-0123-y

Prospero, J. M., Barrett, K., Church, T., Dentener, F., Duce, R. A., Galloway, J. N., . . . Quinn, P. (1996). Atmospheric deposition of nutrients to the North Atlantic Basin. *Biogeochemistry, 35*(1), 27-73. doi:10.1007/bf02179824

Reay, D. S., Dentener, F., Smith, P., Grace, J., & Feely, R. A. (2008). Global nitrogen deposition and carbon sinks. *Nature Geoscience, 1*(7), 430-437. doi:10.1038/ngeo230

Reidmiller, D. R., Fiore, A. M., Jaffe, D. A., Bergmann, D., Cuvelier, C., Dentener, F. J., . . . Zuber, A. (2009). The influence of foreign vs. North American emissions on surface ozone in the US. *Atmospheric Chemistry and Physics, 9*(14), 5027-5042.

Reinds, G. J., Posch, M., De Vries, W., Slootweg, J., & Hettelingh, J. P. (2008). Critical loads of sulphur and nitrogen for terrestrial ecosystems in Europe and Northern Asia using different soil chemical criteria. *Water Air and Soil Pollution, 193*(1-4), 269-287.

Renard, J. J., Calidonna, S. E., & Henley, M. V. (2004). Fate of ammonia in the atmosphere - a review for applicability to hazardous releases. *Journal of Hazardous Materials, 108*(1-2), 29-60.

Richon, C., Dutay, J. C., Dulac, F., Wang, R., & Balkanski, Y. (2018). Modeling the biogeochemical impact of atmospheric phosphate deposition from desert dust and combustion sources to the Mediterranean Sea. *Biogeosciences, 15*(8), 2499-2524. doi:10.5194/bg-15-2499-2018

Richter, A., Burrows, J. P., Nuss, H., Granier, C., & Niemeier, U. (2005). Increase in tropospheric nitrogen dioxide over China observed from space. *Nature, 437*(7055), 129-132. doi:10.1038/nature04092

Riebesell, U., Schulz, K. G., Bellerby, R. G. J., Botros, M., Fritsche, P., Meyerhofer, M., . . . Zollner, E. (2007). Enhanced biological carbon consumption in a high CO2 ocean. *Nature, 450*(7169), 545-U510.

Rodriguez-Lado, L., & Macias, F. (2006). Calculation and mapping of critical loads of sulphur and nitrogen for forest soils in Galicia (NW Spain). *Science of the Total Environment, 366*(2-3), 760-771.

Root, H. T., Geiser, L. H., Jovan, S., & Neitlich, P. (2015). Epiphytic macrolichen indication of air quality and climate in interior forested mountains of the Pacific Northwest, USA. *Ecological Indicators, 53*, 95-105. doi:https://doi.org/10.1016/j.ecolind.2015.01.029

Ruttenberg, K. C. (2003). 8.13 - The Global Phosphorus Cycle. In H. D. Holland & K. K. Turekian (Eds.), *Treatise on Geochemistry* (pp. 585-643). Oxford: Pergamon.

Sanderson, M. G., Collins, W. J., Johnson, C. E., & Derwent, R. G. (2006). Present and future acid deposition to ecosystems: The effect of climate change. *Atmospheric Environment, 40*(7), 1275-1283. doi:10.1016/j.atmosenv.2005.10.031

Sanderson, M. G., Dentener, F. J., Fiore, A. M., Cuvelier, C., Keating, T. J., Zuber, A., . . . Wind, P. (2008). A multi-model study of the hemispheric transport and deposition of oxidised nitrogen. *Geophysical Research Letters, 35*(17). doi:10.1029/2008gl035389

Schwede, D., Zhang, L. M., Vet, R., & Lear, G. (2011). An intercomparison of the deposition models used in the CASTNET and CAPMoN networks. *Atmospheric Environment, 45*(6), 1337-1346.

Shen, J., Chen, D., Bai, M., Sun, J., Coates, T., Lam, S. K., & Li, Y. (2016). Ammonia deposition in the neighbourhood of an intensive cattle feedlot in Victoria, Australia. *Sci Rep, 6*, 32793. doi:10.1038/srep32793

Sickles, J. E., & Shadwick, D. S. (2008). Comparison of particulate sulfate and nitrate at collocated CASTNET and IMPROVE sites in the eastern US. *Atmospheric Environment, 42*(9), 2062-2073.

Simkin, S. M., Allen, E. B., Bowman, W. D., Clark, C. M., Belnap, J., Brooks, M. L., . . . Waller, D. M. (2016). Conditional vulnerability of plant diversity to atmospheric nitrogen deposition across the United States. *Proceedings of the National Academy of Sciences of the United States of America, 113*(15), 4086-4091.

Smil, V. (2000). Phosphorus in the environment: Natural flows and human interferences. *Annual Review of Energy and the Environment, 25*, 53-88. doi:10.1146/annurev.energy.25.1.53

Smith, V. H., & Schindler, D. W. (2009). Eutrophication science: where do we go from here? *Trends in Ecology & Evolution, 24*(4), 201-207.

Stevens, C. J., Duprè, C., Dorland, E., Gaudnik, C., Gowing, D. J. G., Bleeker, A., . . . Dise, N. B. (2011). The impact of nitrogen deposition on acid grasslands in the Atlantic region of Europe. *Environmental Pollution, 159*(10), 2243-2250. doi:https://doi.org/10.1016/j.envpol.2010.11.026

Stjern, C. W., Samset, B. H., Myhre, G., Bian, H., Chin, M., Davila, Y., . . . Tilmes, S. (2016). Global and regional radiative forcing from 20 % reductions in BC, OC and SO4 – an HTAP2 multi-model study. *Atmos. Chem. Phys., 16*(21), 13579-13599. doi:10.5194/acp-16-13579-2016

Stohl, A. (2006). Characteristics of atmospheric transport into the Arctic troposphere. *Journal of Geophysical Research-Atmospheres, 111*(D11).

Stohl, A., Trainer, M., Ryerson, T. B., Holloway, J. S., & Parrish, D. D. (2002). Export of NOy from the North American boundary layer during 1996 and 1997 North Atlantic Regional Experiments. *Journal of Geophysical Research-Atmospheres, 107*(D11).

Sudo, K., & Akimoto, H. (2007). Global source attribution of tropospheric ozone: Long-range transport from various source regions. *Journal of Geophysical Research-Atmospheres, 112*(D12).

Sun, J., Fu, J. S., & Huang, K. (2016). Organic nitrates and other oxidized nitrogen compounds contribute significantly to the total nitrogen depositions in the United States. *Proceedings of the National Academy of Sciences of the United States of America, 113*(31), E4433-E4434.

Sun, J., Fu, J. S., Lynch, J. A., Huang, K., & Gao, Y. (2017). Climate-driven exceedance of total (wet + dry) nitrogen (N) + sulfur (S) deposition to forest soil over the conterminous US. *Earths Future, 5*(6), 560-576.

Sun, Y., Peng, S. S., Goll, D. S., Ciais, P., Guenet, B., Guimberteau, M., . . . Zeng, H. (2017). Diagnosing phosphorus limitations in natural terrestrial ecosystems in carbon cycle models. *Earths Future, 5*(7), 730-749. doi:10.1002/2016ef000472

Tagaris, E., Liao, K. J., Manomaiphiboon, K., Woo, J. H., He, S., Amar, P., & Russell, A. G. (2008). Impacts of future climate change and emissions reductions on nitrogen and sulfur deposition over the United States. *Geophysical Research Letters, 35*(8). doi:10.1029/2008gl033477

Tan, J., Fu, J. S., Huang, K., Yang, C. E., Zhuang, G., & Sun, J. (2017). Effectiveness of SO2 emission control policy on power plants in the Yangtze River Delta, China-post-assessment of the 11th Five-Year Plan. *Environ Sci Pollut Res Int, 24*(9), 8243-8255. doi:10.1007/s11356-017-8412-z

Tan, J. N., Fu, J. S., Dentener, F., Sun, J., Emmons, L., Tilmes, S., . . . Keating, T. (2018). Source contributions to sulfur and nitrogen deposition - an HTAP II multi-model study on hemispheric transport. *Atmospheric Chemistry and Physics, 18*(16), 12223-12240.

Tan, J. N., Fu, J. S., Dentener, F., Sun, J., Emmons, L., Tilmes, S., . . . Keating, T. (2018). Multi-model study of HTAP II on sulfur and nitrogen deposition. *Atmospheric Chemistry and Physics, 18*(9), 6847-6866. doi:10.5194/acp-18-6847-2018

Tao, Z. N., Yu, H. B., & Chin, M. (2016). Impact of transpacific aerosol on air quality over the United States: A perspective from aerosol-cloud-radiation interactions. *Atmospheric Environment, 125*, 48-60. doi:10.1016/j.atmosenv.2015.10.083

Tipping, E., Benham, S., Boyle, J. F., Crow, P., Davies, J., Fischer, U., . . . Toberman, H. (2014). Atmospheric deposition of phosphorus to land and freshwater. *Environmental Science-Processes & Impacts, 16*(7), 1608-1617. doi:10.1039/c3em00641g

Tørseth, K., Aas, W., Breivik, K., Fjæraa, A. M., Fiebig, M., Hjellbrekke, A. G., . . . Yttri, K. E. (2012). Introduction to the European Monitoring and Evaluation Programme (EMEP) and observed atmospheric composition change during 1972–2009. *Atmospheric Chemistry and Physics, 12*(12), 5447-5481. doi:10.5194/acp-12-5447-2012

Unece. (2004). *Manual on methodologies and criteria for modelling and mapping critical loads and levels and air pollution effects risks, and trends*. Retrieved from Berlin, Germany: http://www.rivm.nl/en/themasites/icpmm/manual-and-downloads/manual-english/index.html

van der A, R. J., Eskes, H. J., Boersma, K. F., van Noije, T. P. C., Van Roozendael, M., De Smedt, I., . . . Meijer, E. W. (2008). Trends, seasonal variability and dominant NOxsource derived from a ten year record of NO2measured from space. *Journal of Geophysical Research, 113*(D4). doi:10.1029/2007jd009021

van der A, R. J., Peters, D. H. M. U., Eskes, H., Boersma, K. F., Van Roozendael, M., De Smedt, I., & Kelder, H. M. (2006). Detection of the trend and seasonal variation in tropospheric NO2over China. *Journal of Geophysical Research, 111*(D12). doi:10.1029/2005jd006594

Vet, R., Artz, R. S., Carou, S., Shaw, M., Ro, C. U., Aas, W., . . . Reid, N. W. (2014). A global assessment of precipitation chemistry and deposition of sulfur, nitrogen, sea salt, base cations, organic acids, acidity and pH, and phosphorus. *Atmospheric Environment, 93*, 3-100. doi:10.1016/j.atmosenv.2013.10.060

Vitousek, P. M., Aber, J. D., Howarth, R. W., Likens, G. E., Matson, P. A., Schindler, D. W., . . . Tilman, D. (1997). Human alteration of the global nitrogen cycle: Sources and consequences. *Ecological Applications, 7*(3), 737-750. doi:10.2307/2269431

Vivanco, M. G., Theobald, M. R., Garcia-Gomez, H., Garrido, J. L., Prank, M., Aas, W., . . . Galmarini, S. (2018). Modeled deposition of nitrogen and sulfur in Europe estimated by 14 air quality model systems: evaluation, effects of changes in emissions and implications for habitat protection. *Atmospheric Chemistry and Physics, 18*(14), 10199-10218.

Wang, R., Balkanski, Y., Boucher, O., Ciais, P., Penuelas, J., & Tao, S. (2015). Significant contribution of combustion-related emiscions to the atmospheric phosphorus budget. *Nature Geoscience, 8*(1), 48-54.

Wang, W., Liu, X. J., Xu, J., Dore, A. J., & Xu, W. (2018). Imbalanced nitrogen and phosphorus deposition in the urban and forest environments in southeast Tibet. *Atmospheric Pollution Research, 9*(4), 774-782.

Warfvinge, P., & Sverdrup, H. (1992). Calculating Critical Loads of Acid Deposition with Profile - a Steady-State Soil Chemistry Model. *Water Air and Soil Pollution, 63*(1-2), 119-143.

Weber, R. J., Guo, H. Y., Russell, A. G., & Nenes, A. (2016). High aerosol acidity despite declining atmospheric sulfate concentrations over the past 15 years. *Nature Geoscience, 9*(4), 282-+.

Wesely, M. L., & Hicks, B. B. (2000). A review of the current status of knowledge on dry deposition. *Atmospheric Environment, 34*(12-14), 2261-2282.

Wild, O., & Akimoto, H. (2001). Intercontinental transport of ozone and its precursors in a three-dimensional global CTM. *Journal of Geophysical Research-Atmospheres, 106*(D21), 27729-27744. doi:10.1029/2000jd000123

Wild, O., Pochanart, P., & Akimoto, H. (2004). Trans-Eurasian transport of ozone and its precursors. *Journal of Geophysical Research-Atmospheres, 109*(D11). doi:10.1029/2003jd004501

Xavier, A., Kottayil, A., Mohanakumar, K., & Xavier, P. K. (2018). The role of monsoon low-level jet in modulating heavy rainfall events. *International Journal of Climatology, 38*, E569-E576.

Yienger, J. J., Galanter, M., Holloway, T. A., Phadnis, M. J., Guttikunda, S. K., Carmichael, G. R., . . . Levy, H. (2000). The episodic nature of air pollution transport from Asia to North America. *Journal of Geophysical Research-Atmospheres, 105*(D22), 26931-26945. doi:10.1029/2000jd900309

Yu, H. B., Chin, M., West, J. J., Atherton, C. S., Bellouin, N., Bergmann, D., . . . Tan, Q. (2013). A multimodel assessment of the influence of regional anthropogenic emission reductions on aerosol direct radiative forcing and the role of intercontinental transport. *Journal of Geophysical Research-Atmospheres, 118*(2), 700-720. doi:10.1029/2012jd018148

Yu, H. B., Remer, L. A., Chin, M., Bian, H. S., Tan, Q., Yuan, T. L., & Zhang, Y. (2012). Aerosols from Overseas Rival Domestic Emissions over North America. *Science, 337*(6094), 566-569.

Yuan, Z. W., Jiang, S. Y., Sheng, H., Liu, X., Hua, H., Liu, X. W., & Zhang, Y. (2018). Human Perturbation of the Global Phosphorus Cycle: Changes and Consequences. *Environ Sci Technol, 52*(5), 2438-2450. doi:10.1021/acs.est.7b03910

Zhai, S. J., Yang, L. Y., & Hu, W. P. (2009). Observations of Atmospheric Nitrogen and Phosphorus Deposition During the Period of Algal Bloom Formation in Northern Lake Taihu, China. *Environmental Management, 44*(3), 542-551. doi:10.1007/s00267-009-9334-4

Zhang, J. X., Gao, Y., Leung, L. R., Luo, K., Liu, H., Lamarque, J. F., . . . Nagashima, T. (2019). Impacts of climate change and emissions on atmospheric oxidized nitrogen deposition over East Asia. *Atmospheric Chemistry and Physics, 19*(2), 887-900. doi:10.5194/acp-19-887-2019

Zhang, L., Jacob, D. J., Boersma, K. F., Jaffe, D. A., Olson, J. R., Bowman, K. W., . . . Weinheimer, A. J. (2008). Transpacific transport of ozone pollution and the effect of recent Asian emission increases on air quality in North America: an integrated analysis using satellite, aircraft, ozonesonde, and surface observations. *Atmospheric Chemistry and Physics, 8*(20), 6117-6136.

Zhang, L., Jacob, D. J., Knipping, E. M., Kumar, N., Munger, J. W., Carouge, C. C., . . . Chen, D. (2012). Nitrogen deposition to the United States: distribution, sources, and processes. *Atmospheric Chemistry and Physics, 12*(10), 4539-4554.

Zhang, L., Jacob, D. J., Kopacz, M., Henze, D. K., Singh, K., & Jaffe, D. A. (2009). Intercontinental source attribution of ozone pollution at western US sites using an adjoint method. *Geophysical Research Letters, 36*, 5. doi:10.1029/2009gl037950

Zhang, L., Vet, R., O'Brien, J. M., Mihele, C., Liang, Z., & Wiebe, A. (2009). Dry deposition of individual nitrogen species at eight Canadian rural sites. *Journal of Geophysical Research, 114*(D2). doi:10.1029/2008jd010640

Zhang, Q., Streets, D. G., Carmichael, G. R., He, K. B., Huo, H., Kannari, A., . . . Yao, Z. L. (2009). Asian emissions in 2006 for the NASA INTEX-B mission. *Atmospheric Chemistry and Physics, 9*(14), 5131-5153.

Zhang, Q., Streets, D. G., He, K., Wang, Y., Richter, A., Burrows, J. P., . . . Lei, Y. (2007). NOx emission trends for China, 1995-2004: The view from the ground and the view from space. *Journal of Geophysical Research-Atmospheres, 112*(D22). doi:10.1029/2007jd008684

Zhao, Y., Duan, L., Larssen, T., Hu, L. H., & Hao, J. M. (2007). Simultaneous assessment of deposition effects of base cations, sulfur, and nitrogen using an extended critical load function for acidification. *Environ Sci Technol, 41*(6), 1815-1820.

Zhao, Y., Duan, L., Larssen, T., Mulder, J., Hu, L. H., & Hao, J. M. (2007). Calculating critical loads for acidification for five forested catchments in China using an extended steady state function. *Science of the Total Environment, 387*(1-3), 54-67. doi:10.1016/j.scitotenv.2007.07.014

Zhu, J. X., Wang, Q. F., He, N. P., Smith, M. D., Elser, J. J., Du, J. Q., . . . Yu, Q. (2016). Imbalanced atmospheric nitrogen and phosphorus depositions in China: Implications for nutrient limitation. *Journal of Geophysical Research-Biogeosciences, 121*(6), 1605-1616. doi:10.1002/2016jg003393

APPENDIX

Supporting materials for Chapter 1

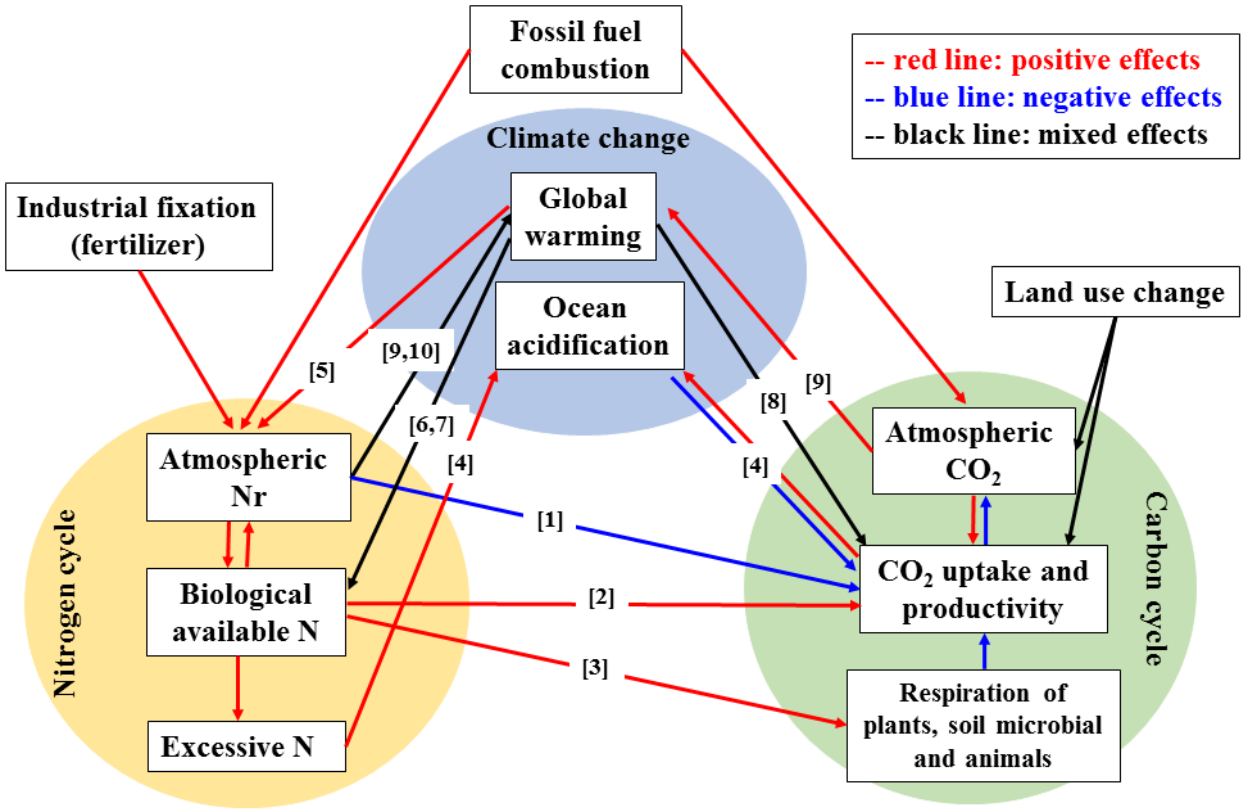

Figure S1. 1 Interaction between emission sources, N and carbon cycles and climate change (modified based on literature (Gruber & Galloway, 2008))

The numbers on the lines are corresponded to the following effects:

[1] Atmospheric NO_x promotes the formation of atmospheric O_3, especially in tropic regions where the solar radiations are strong for the photochemical reactions. The exposure to tropospheric O_3 harms the growth of plants and results in decrease of carbon uptake in the tropic regions.

[2] Increased N supplies the forest and marine ecosystems with biologically available N (inorganic N that can be uptake by plants). For both the terrestrial and aquatic ecosystems, it increases the productivity of the ecosystems and results in increased uptakes of CO_2. For marine ecosystem, increased N also causes ocean acidification, which affects the solubility of CO_2 in the ocean and reduces the CO_2 uptake by ocean. However, studies have found increased consumption of inorganic carbon by marine phytoplankton at increased CO_2 concentration (Riebesell et al., 2007). This over-consumption affects the oceanic carbon sequestration. Global warming changes the precipitation pattern and affects the occurrence of fire. Reduced precipitation in

boreal forest increases the occurrence of fire (Köster et al., 2018). Fires activate the active layer of soils and increase the temperature in the surface layer of the burned area and result in uptake of CO_2 by soils.

[3] High N concentration stimulates the heterotrophic respiration of plants, soil microbial and animals, which increases the CO_2 release into the atmosphere. This effect could partly offset the increased CO_2 sink by the photosynthesis of vegetation. It also increases the decomposition of organic carbon in soils and reduces the CO_2 storage. The over-richness of N also affects the soil sequestration of carbon (R. Luo et al., 2019). The increased nutrient stimulates the microbial and activates the carbon-degrading enzyme in soils, which accelerate the decomposition of soil organic carbon and reduce the soil storage of organic carbon.

[4] The excessive N that can't be uptake by plants enters the marine ecosystems. Both N and CO_2 decrease the ocean pH values and cause ocean acidification. As a result, the solubility of CO_2 is decreased and cause negative effects on oceanic carbon uptake.

[5] High temperature increases the volatilization of NH_3 from soil, which releases the NH_3 gas into the atmosphere and causes loss of nutrient in soils. Global warming changes the precipitation pattern and affects the occurrence of fire. Reduced precipitation in boreal forest increases the occurrence of fire (Köster et al., 2018). Fires activate the active layer of soils and increase the temperature in the surface layer of the burned area and result in uptake of CO_2 by soils.

[6] The soil N cycle is sensitive to soil temperature, moisture and pH values. Soil temperature affects the N uptake, mineralization and nitrification processes.

[7] Climate-driven changes in precipitation affect the leaching of N. Erosion and runoff also influence the mobilization of N.

[8] Increased temperature stimulates the heterotrophic respiration of soil organisms and result in loss of carbon in the tropics and mid-latitudes. Warming thaws the permafrost and increase the uptake in Arctic regions, but at the same time accelerates the decomposition of organic carbon in soils. Reduced precipitation and increased frequency also cause loss of carbon storage in forests.

[9] Greenhouse effects of N_2O and CO_2 accelerate the global warming.

[10] Cooling effects of aerosols. NH_4^+ is one of the main components of aerosols in the air, which have cooling effects on the earth temperature by reflecting the solar radiation and interaction with clouds. The impacts on cloud formation are still unclear.

Supporting materials for Chapter 2

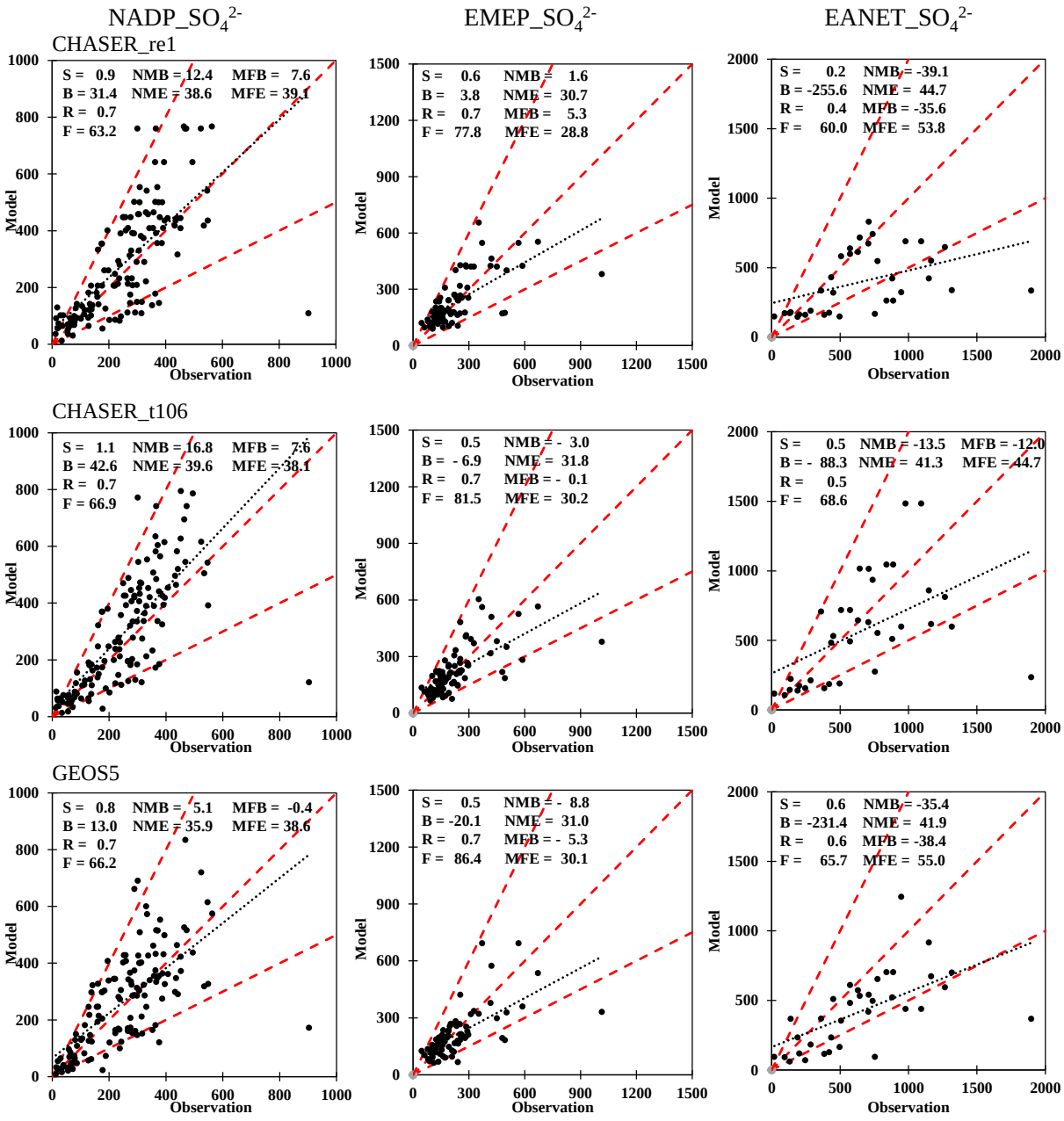

Figure S2. 1 Individual model performances on SO_4^{2-} wet deposition (mg (S) $m^{-2}yr^{-1}$). The model result is the annual deposition in 2010 and the observation is three-year average annual data of 2009-2011.

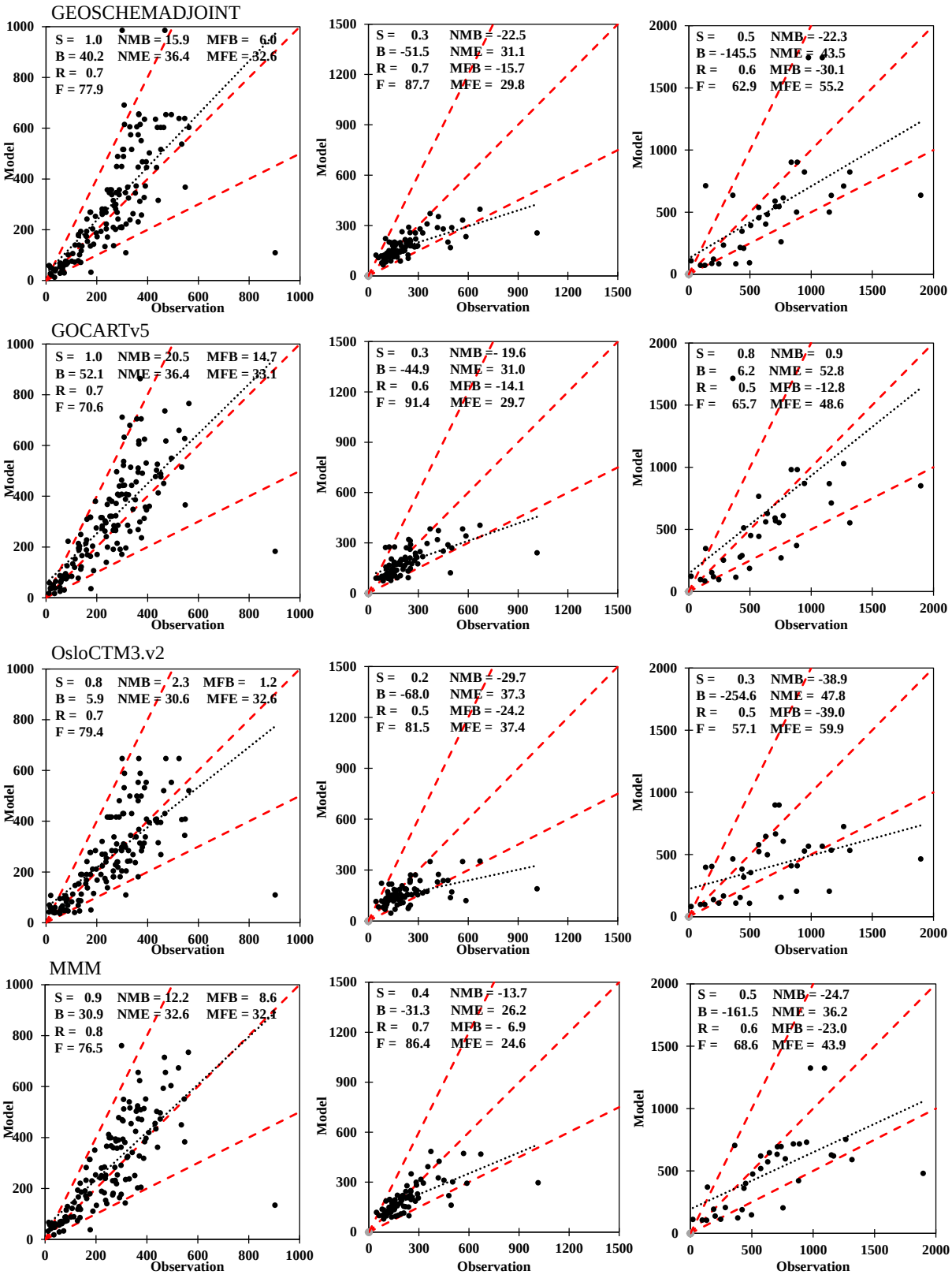

Figure S2. 1 continued.

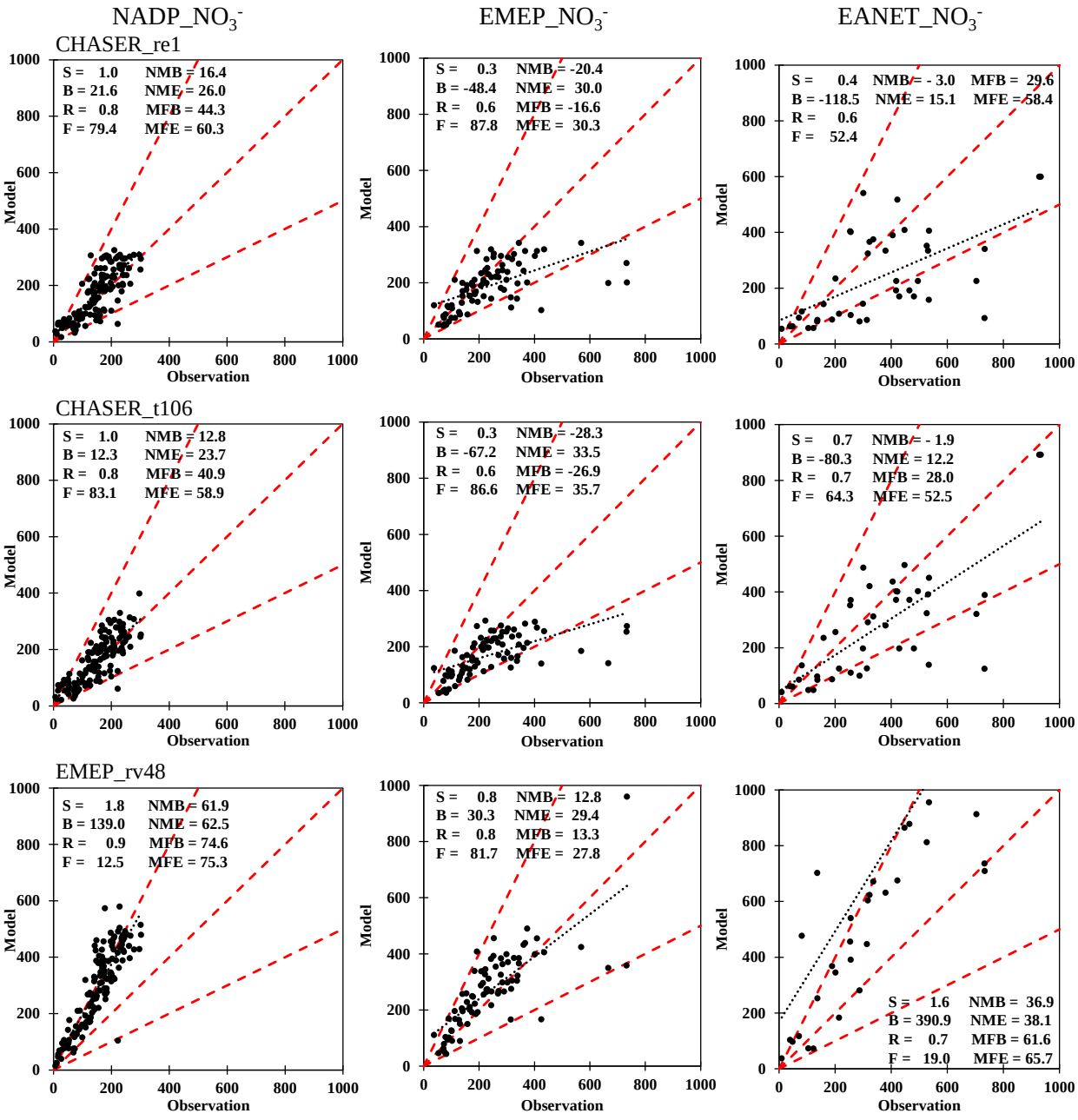

Figure S2. 2 Same as Fig. S2. 1 but for NO_3^- wet deposition (mg (N) $m^{-2}yr^{-1}$).

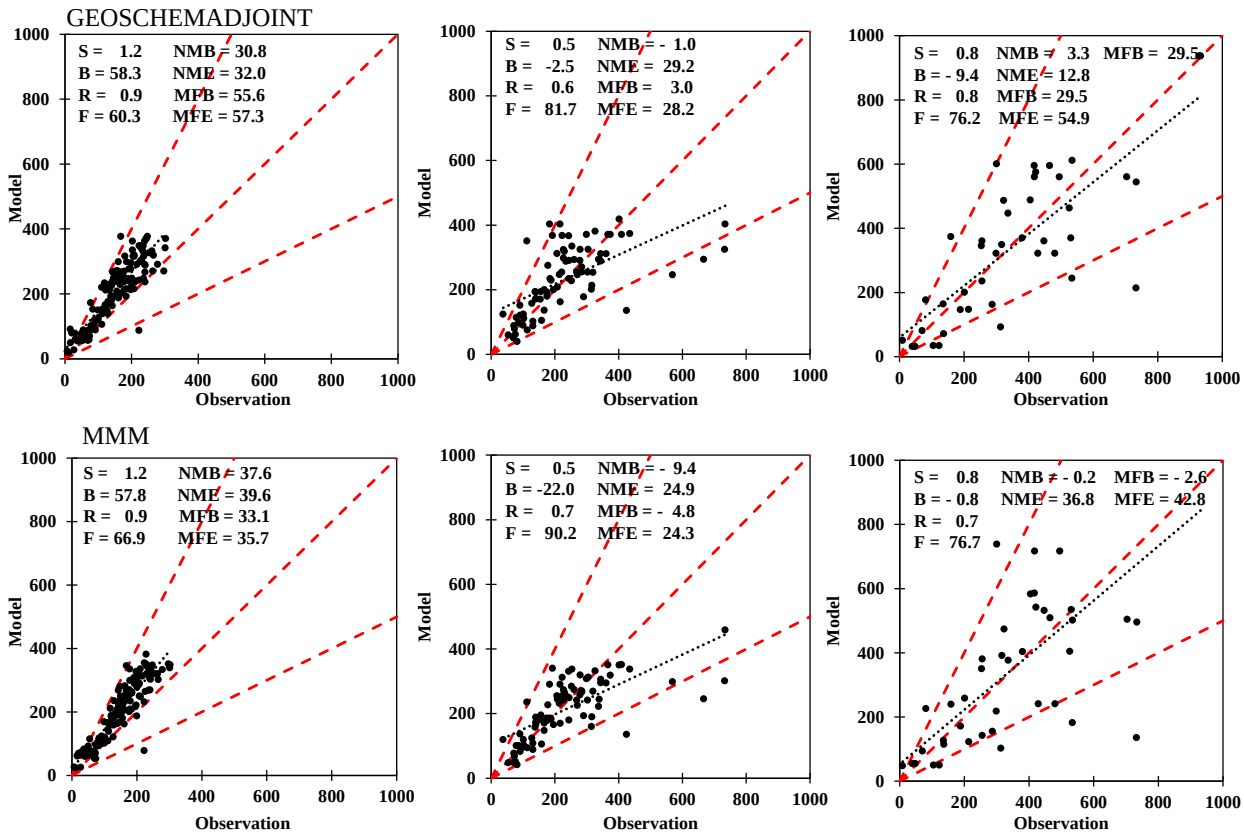

Figure S2. 2 continued.

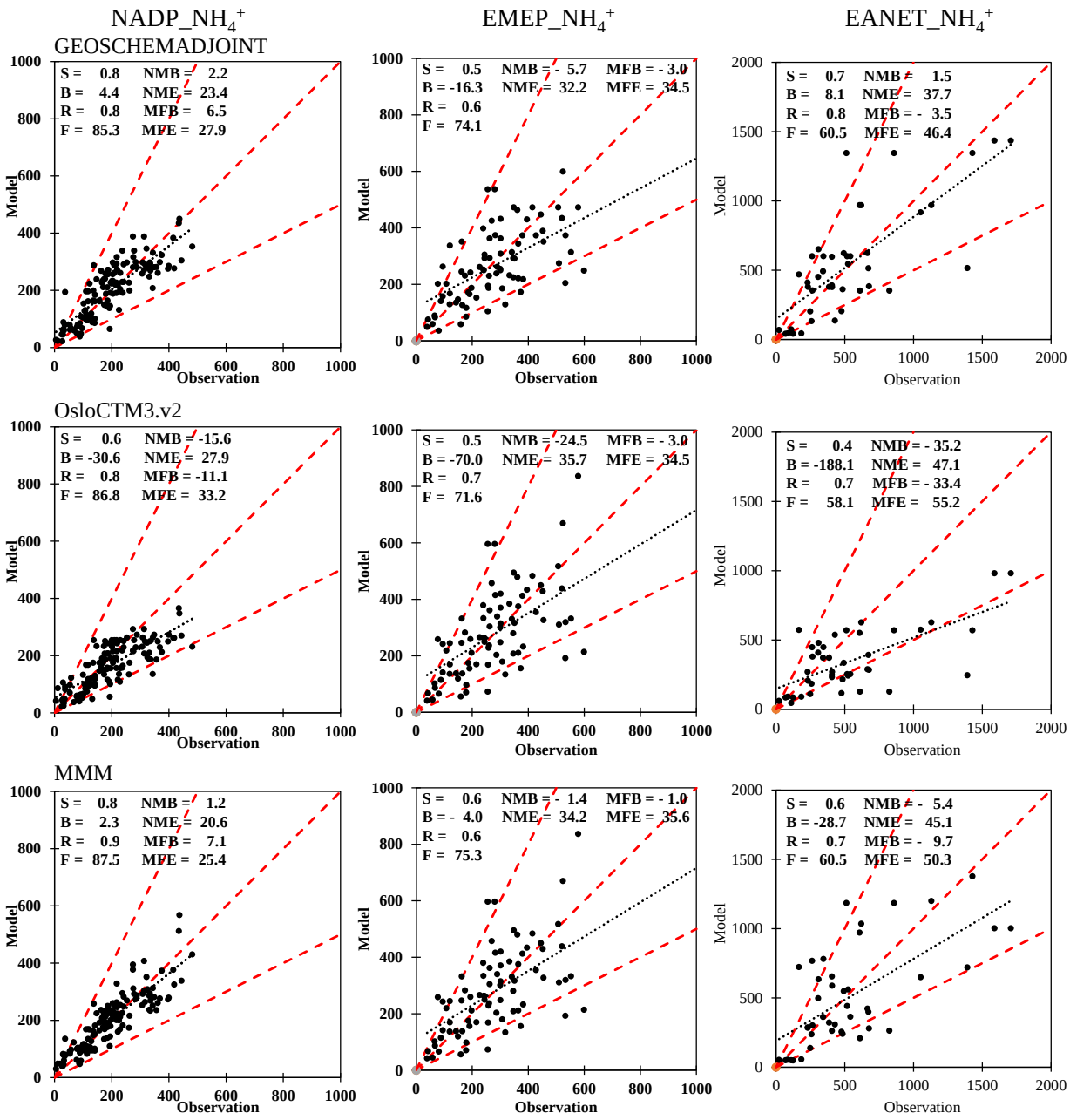

Figure S2. 3 Same as Fig. S2. 1 but for NH_4^+ wet deposition (mg (N) $m^{-2}yr^{-1}$).

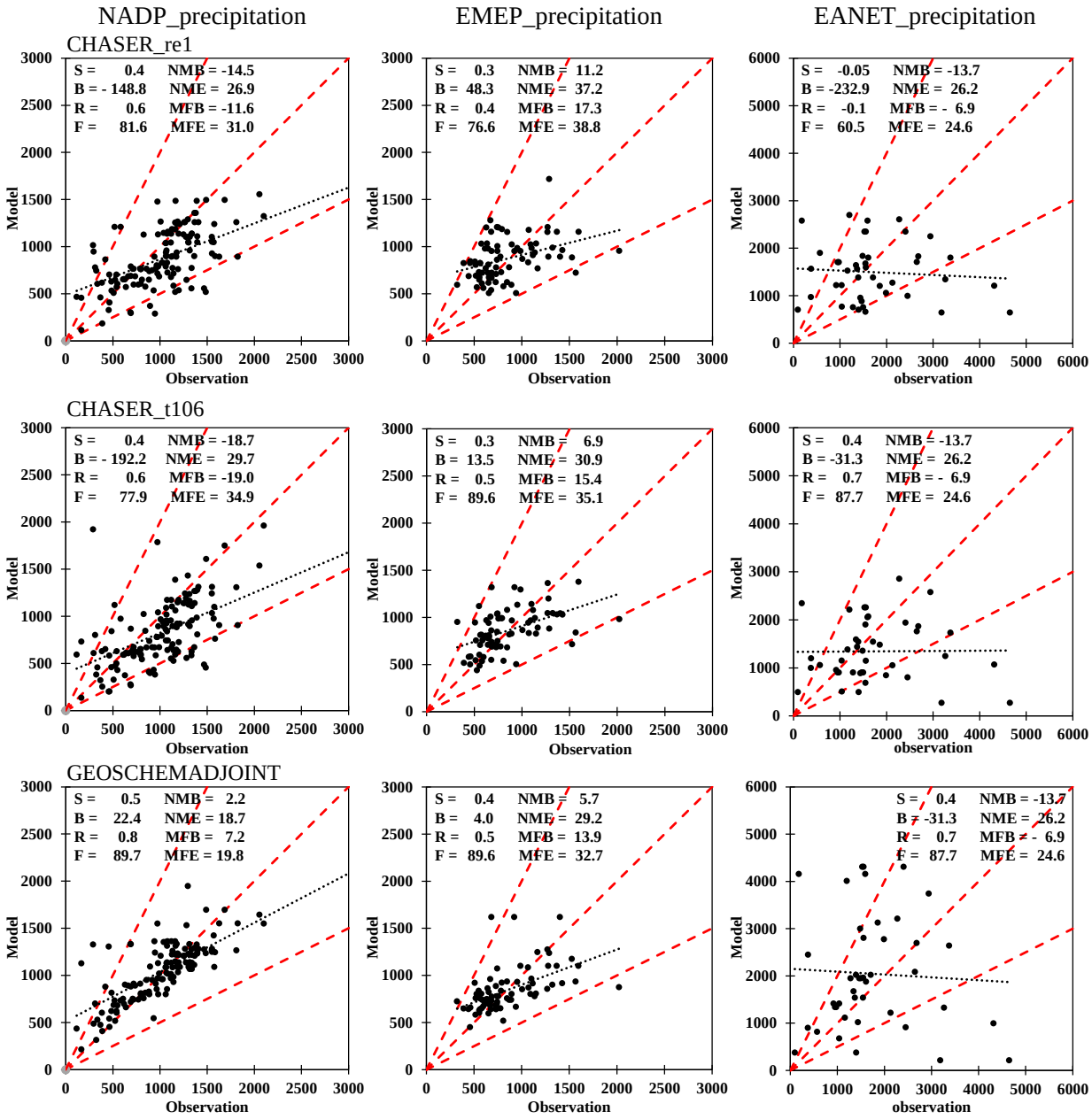

Figure S2. 4 Individual model performances on precipitation (mm yr^{-1}). The model result is the annual precipitation in 2010 and the observation is three-year average annual data of 2009-2011.

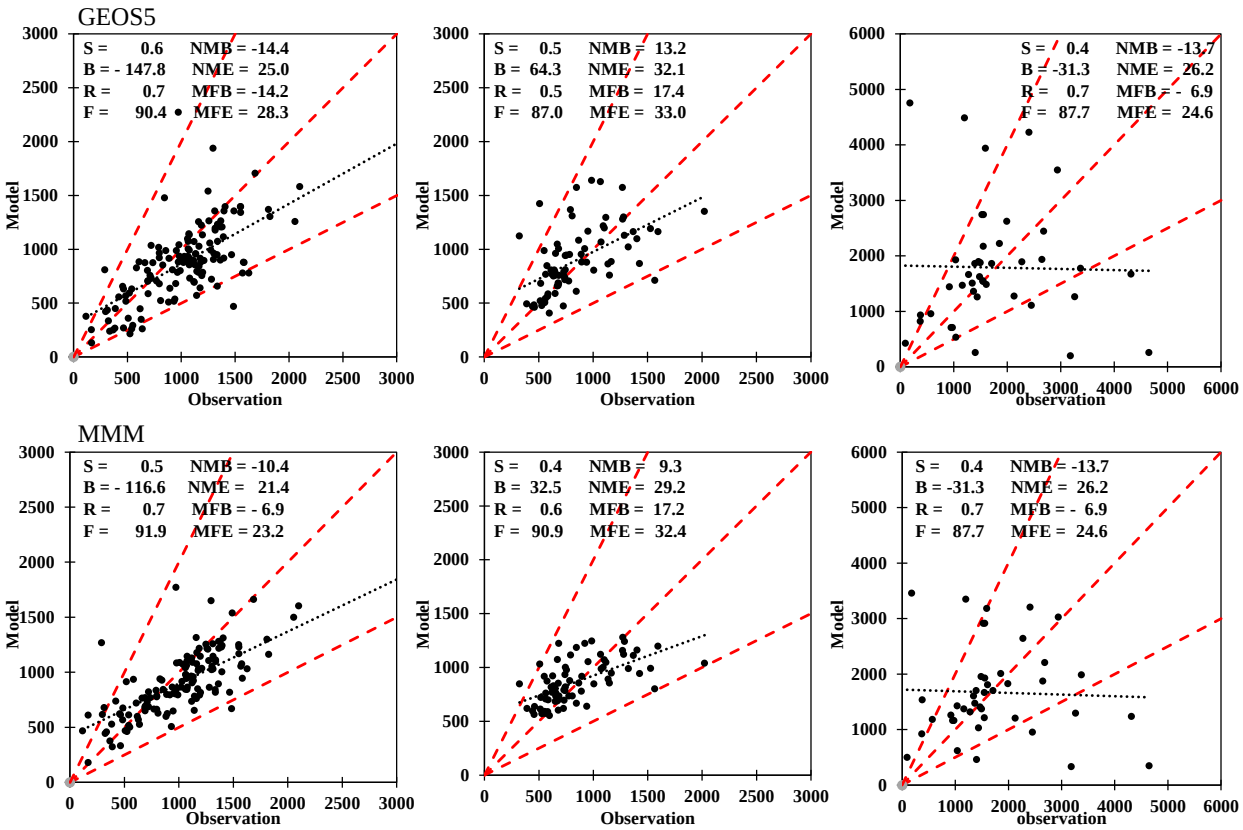

Figure S2. 4 continued.

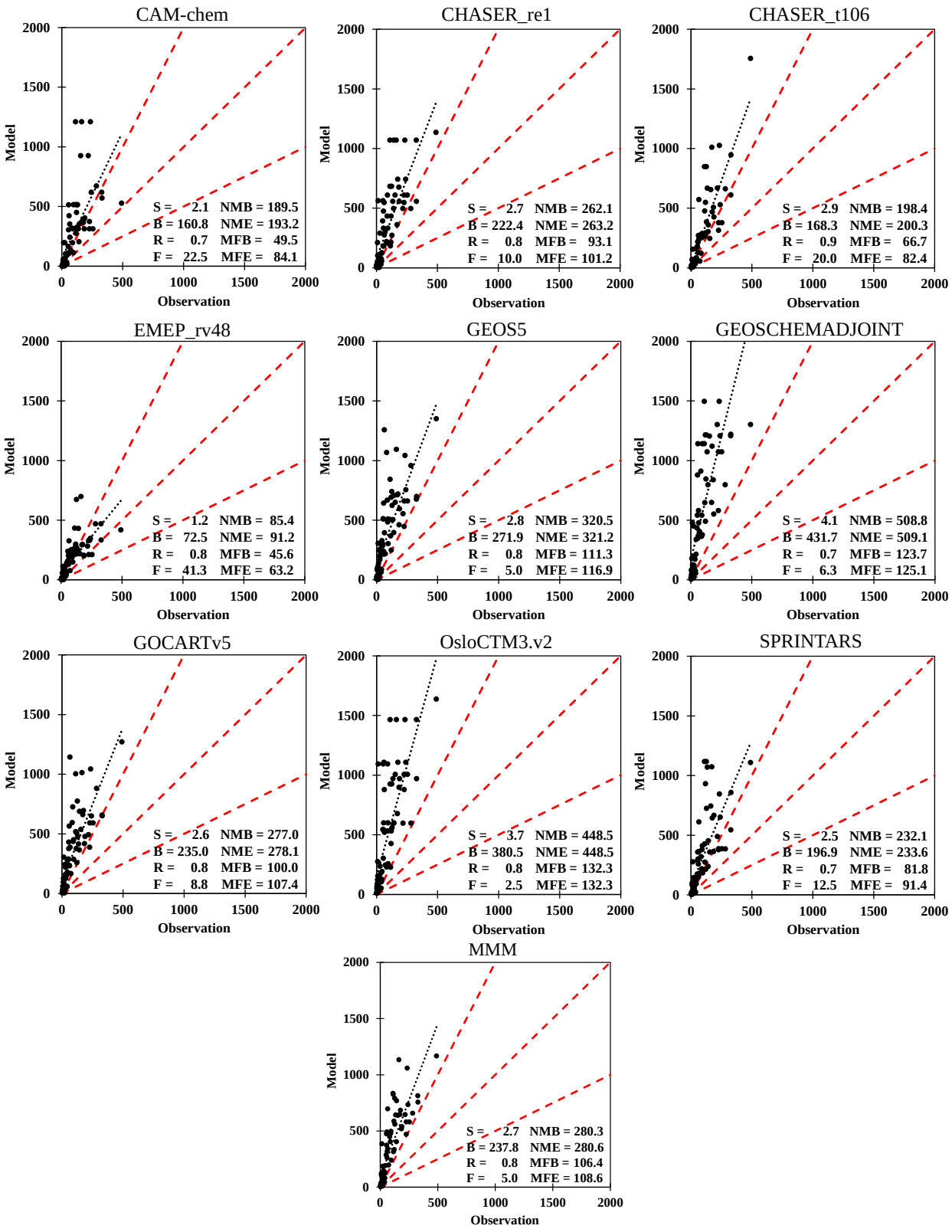

Figure S2. 5 Individual model performances on SO_2 dry deposition (mg (S) $m^{-2}yr^{-1}$). The model result is the annual deposition in 2010 and the observation is three-year average annual data of 2009-2011.

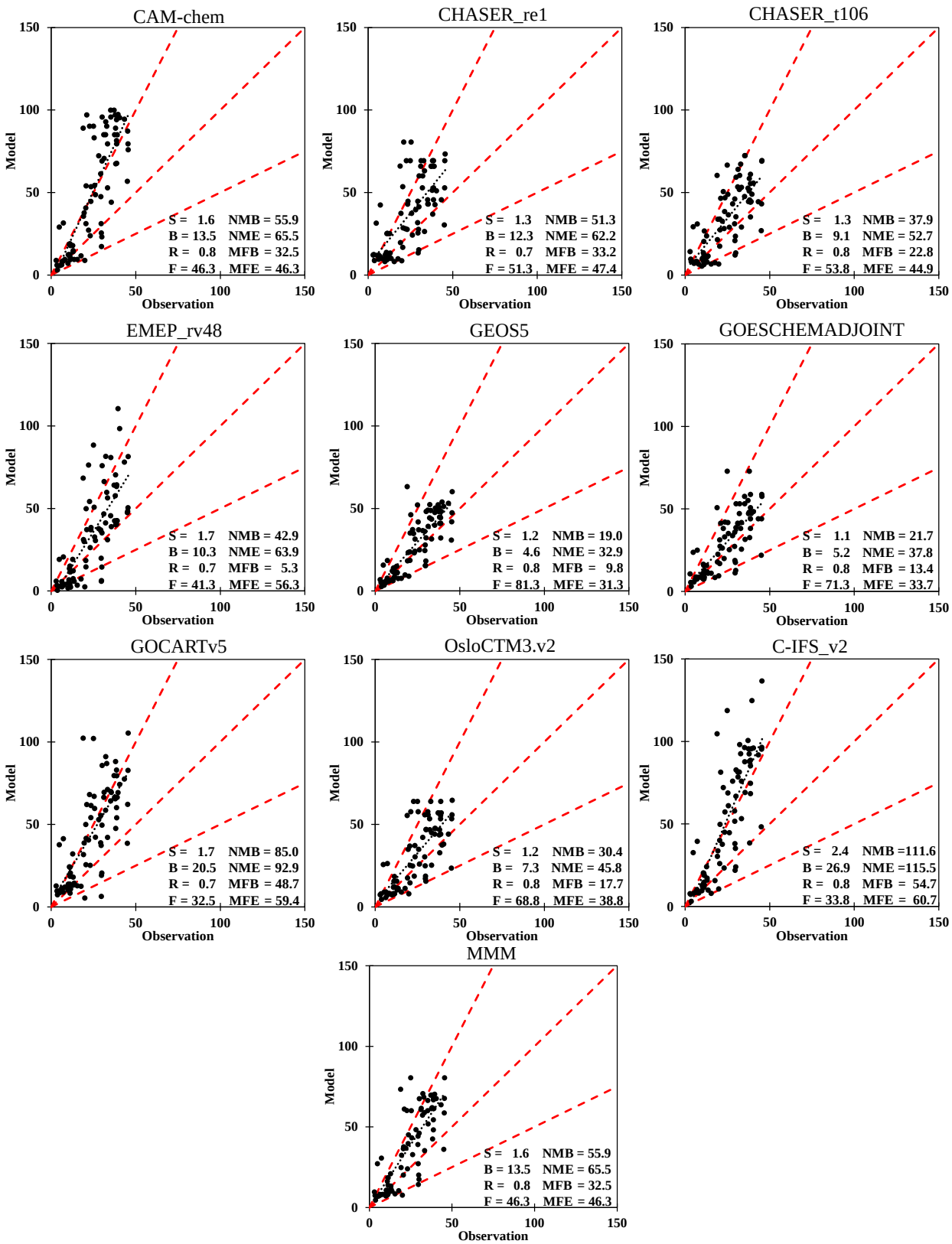

Figure S2. 6 Same as Fig. S2. 5 but for SO_4^{2-} dry deposition (mg (S) $m^{-2}yr^{-1}$).

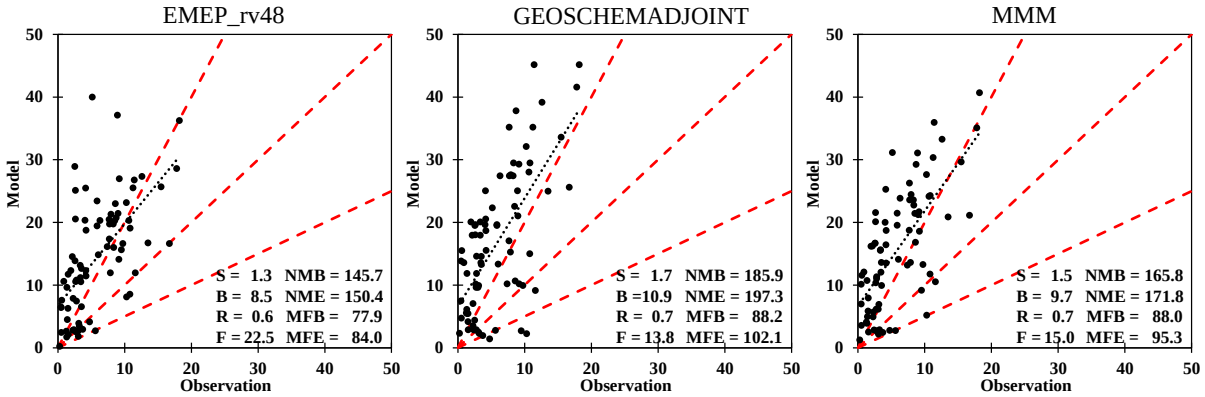

Figure S2. 7 Same as Fig. S2. 5 but for NO_3^- dry deposition (mg (N) $m^{-2}yr^{-1}$).

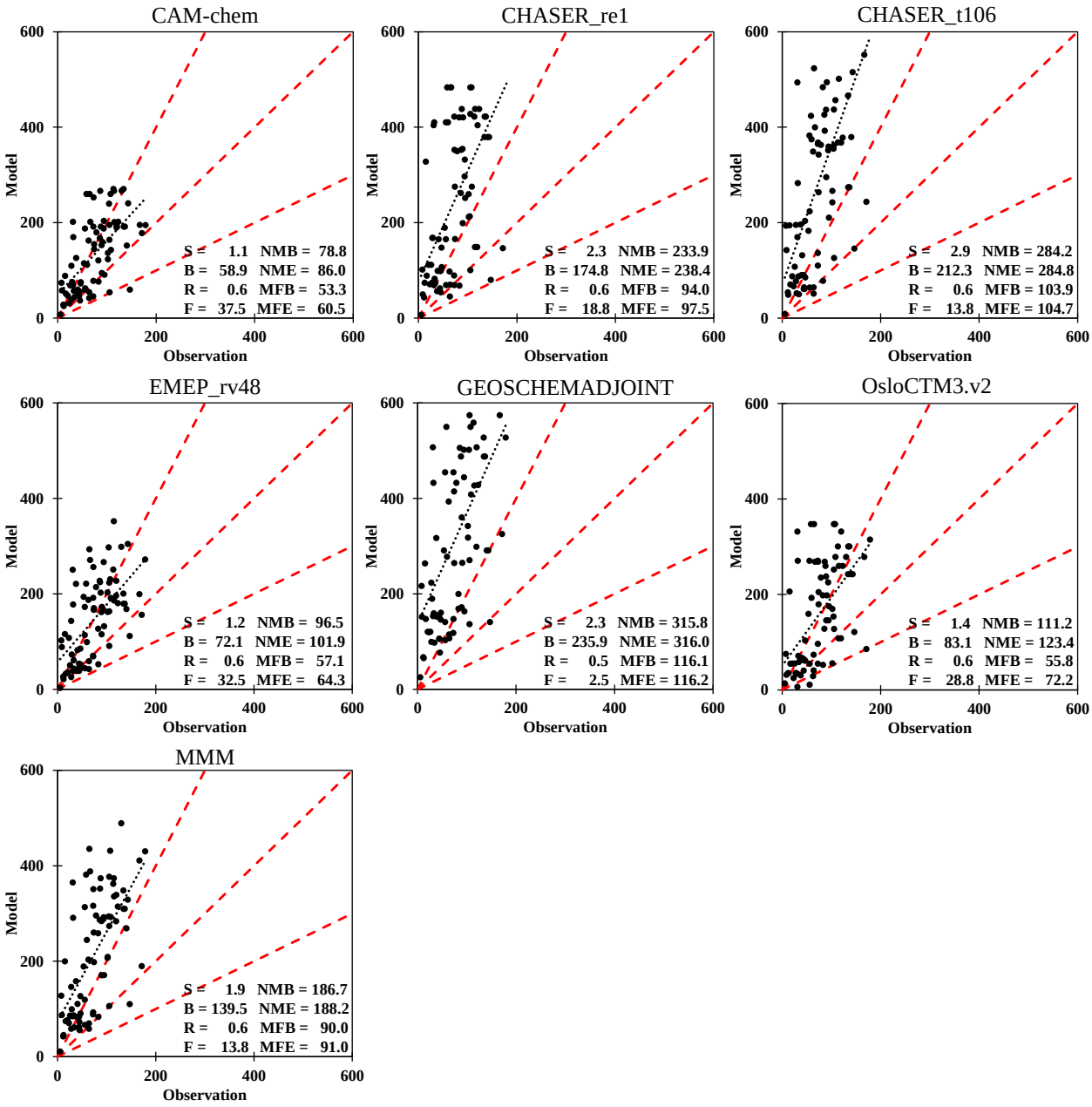

Figure S2. 8 Same as Fig. S2. 5 but for HNO_3 dry deposition (mg (N) $m^{-2}yr^{-1}$).

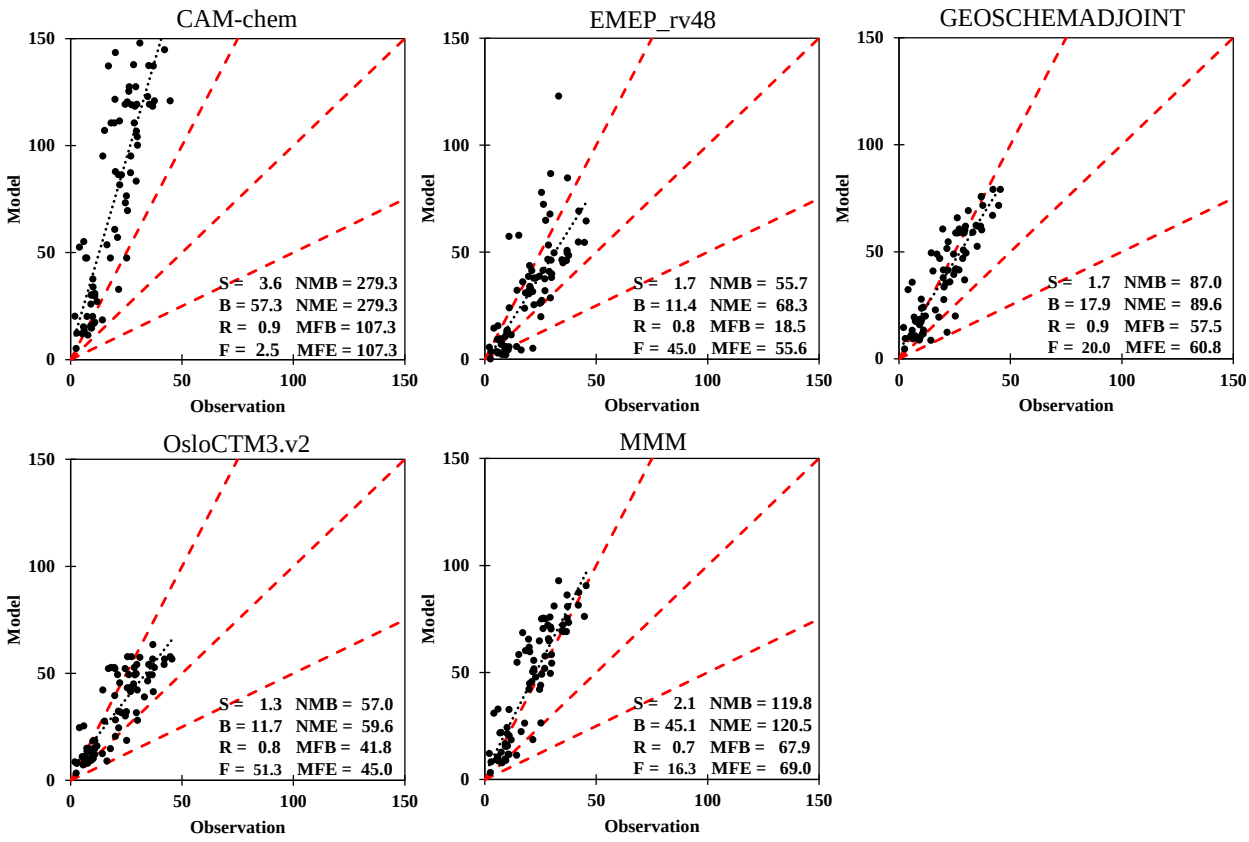

Figure S2. 9 Same as Fig. S2.5 but for NH_4^+ dry deposition (mg (N) $m^{-2}yr^{-1}$).

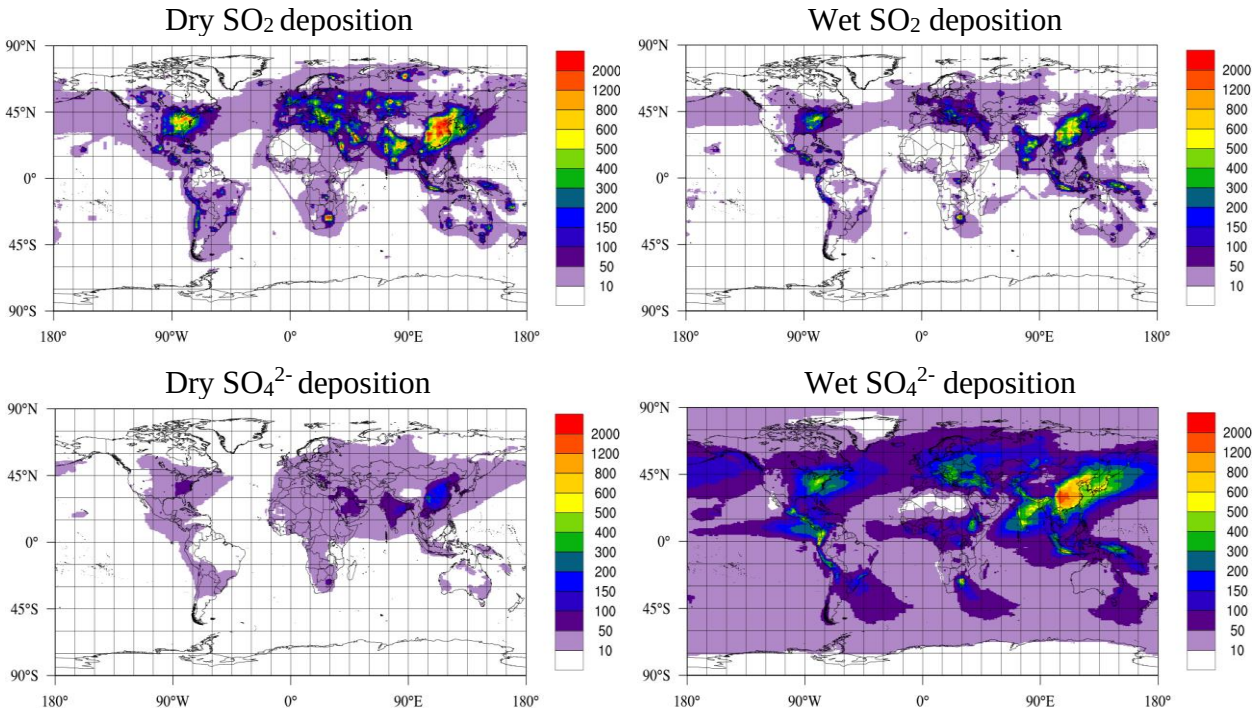

Figure S2. 10 Spatial distribution of SO_2 and SO_4^{2-} deposition in 2010 from MMM results (mg(S) $m^{-2}yr^{-1}$).

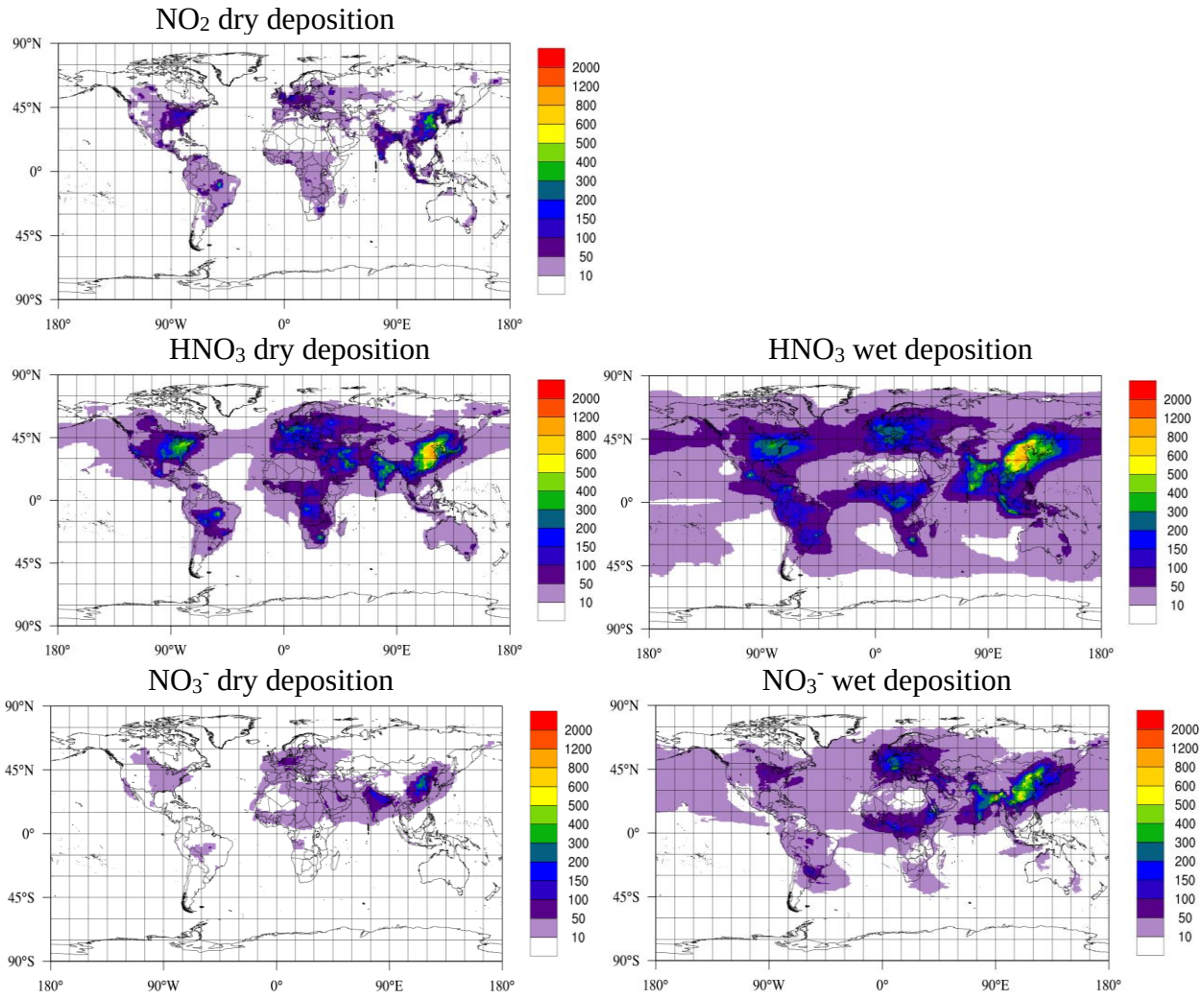

Figure S2. 11 Spatial distributions of NO_2, HNO_3 and NO_3^- deposition in 2010 from MMM results (mg(N) $m^{-2}yr^{-1}$).

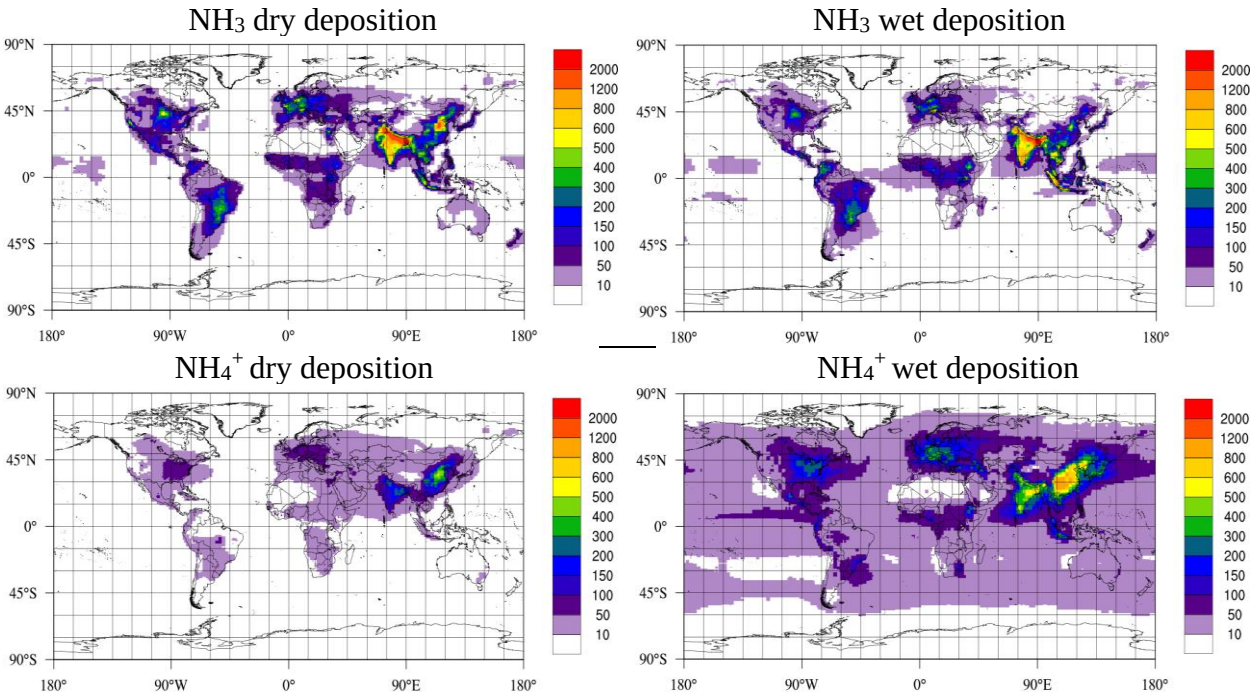

Figure S2. 12 Same as Fig. S2.11 but for NH_3 and NH_4^+ deposition (mg(N) $m^{-2}yr^{-1}$).

Table S2. 1 Multi-model performance on simulating SO_2 concentration at CASTNET sites. The unit is μg (S) m^{-3}.

	CAM-Chem	CHASER_re1	CHASER_t106	EMEP_rv48	GEOSCHEMADJOINT	GOCART	OsloCTM3.v2	SPRINTARS	MMM
mean obs	0.82	0.82	0.82	0.82	0.82	0.82	0.82	0.82	0.82
mean model	5.31	5.79	5.51	1.71	5.36	2.49	4.61	1.72	4.06
Linear Fit Slope	6.77	6.65	7.90	2.22	6.33	2.90	5.43	2.03	5.03
mean bias	0.00	0.00	0.00	0.00	0.00	0.00	0.00	0.00	0.00
Bias[1]	546.66	604.77	570.95	107.92	553.04	203.68	460.86	109.94	394.73
R	0.79	0.81	0.84	0.89	0.76	0.88	0.84	0.76	0.90
F50%	12.50	6.25	12.50	31.25	16.25	21.25	15.00	43.75	11.25
NMB	546.66	604.77	570.95	107.92	553.04	203.68	460.86	109.94	394.73
NME	548.91	606.20	573.30	116.37	554.09	208.21	462.33	117.67	396.47
MFB	104.46	119.52	101.46	21.00	110.67	65.28	105.73	25.09	99.26
MFE	116.11	125.36	110.97	69.95	113.81	88.82	111.67	61.69	106.31
no of station	80	80	80	80	80	80	80	80	80
Spatial resolution	1.9° × 2.5°	2.8° × 2.8°	1.1° × 1.1°	0.5° × 0.5°	2.0° × 2.5°	1.3° × 1.0°	2.8° × 2.8°	1.1° × 1.1°	-

[1] Bias is calculated as dividing Mean Bias with Mean Observation. The unit is %.

Table S2. 2 Same as Table S2.1 but for SO_4^{2-} concentration. The unit is μg (S) m^{-3}.

	CAM-Chem	CHASER_re1	CHASER_t106	EMEP_rv48	GEOSCHEMADJOINT	OsloCTM3.v2	MMM
mean obs	0.64	0.64	0.64	0.64	0.64	0.64	0.64
mean model	1.06	1.24	1.09	0.74	0.70	0.52	0.89
Linear Fit Slope	1.97	1.90	1.80	1.62	1.17	0.96	1.57
mean bias	0.00	0.00	0.00	0.00	0.00	0.00	0.00
bias%	66.99	94.61	71.61	16.30	10.81	-18.18	40.36
R	0.93	0.84	0.88	0.92	0.92	0.87	0.91
F50%	41.25	26.25	40.00	57.50	92.50	82.50	63.75
NMB	66.99	94.61	71.61	16.30	10.81	-18.18	40.36
NME	72.20	95.50	73.78	40.59	23.01	25.30	46.73
MFB	34.17	59.16	45.63	-18.17	6.00	-32.63	23.84
MFE	46.67	60.54	49.32	50.23	23.21	37.75	33.98
no of station	80	80	80	80	80	80	80
Spatial resolution	1.9° × 2.5°	2.8° × 2.8°	1.1° × 1.1°	0.5° × 0.5°	2.0° × 2.5°	2.8° × 2.8°	

Table S2. 3 Same as Table S2.1 but for HNO_3 concentration. The unit is µg (N) m^{-3}.

	CAM-Chem	CHASER_re1	CHASER_t106	EMEP_rv48	GEOSCHEMADJOINT	OsloCTM3.v2	MMM
mean obs	0.17	0.17	0.17	0.17	0.17	0.17	0.17
mean model	0.64	0.83	0.71	0.36	0.64	0.14	0.55
Linear Fit Slope	3.34	4.40	5.10	2.00	2.48	0.72	3.01
mean bias	0.00	0.00	0.00	0.00	0.00	0.00	0.00
bias%	264.73	376.04	309.11	106.39	264.54	-19.82	216.83
R	0.78	0.65	0.82	0.85	0.74	0.76	0.84
F50%	3.75	2.50	1.25	28.75	1.25	76.25	3.75
NMB	264.73	376.04	309.11	106.39	264.54	-19.82	216.83
NME	265.39	376.18	309.11	106.84	264.54	30.38	216.83
MFB	107.09	117.52	105.97	60.13	113.19	-27.44	98.66
MFE	107.50	117.59	105.97	61.55	113.19	42.18	98.66
no of station	80	80	80	80	80	80	80
Spatial resolution	1.9° × 2.5°	2.8° × 2.8°	1.1° × 1.1°	0.5° × 0.5°	2.0° × 2.5°	2.8° × 2.8°	-

Table S2. 4 Same as Table S2.1 but for NO_3^- concentration. The unit is µg (N) m^{-3}.

	EMEP_rv48	GEOSCHEMADJOINT	MMM
mean obs	0.17	0.17	0.17
mean model	0.17	0.63	0.40
Linear Fit Slope	0.67	2.58	1.63
mean bias	0.00	0.00	0.00
bias%	0.05	270.05	135.05
R	0.80	0.74	0.77
F50%	65.00	12.50	17.50
NMB	0.05	270.05	135.05
NME	35.60	279.48	144.21
MFB	2.19	103.34	76.92
MFE	41.98	113.85	87.53
no of station	80.0	80	80
Spatial resolution	0.5° × 0.5°	2.0° × 2.5°	-

Table S2. 5 Same as Table S2.1 but for NH_4^+ concentration. The unit is μg (N) m^{-3}.

	EMEP_rv48	GEOSCHEMADJOINT	MMM
mean obs	0.56	0.56	0.56
mean model	1.13	1.94	1.54
Linear Fit Slope	2.00	3.47	2.74
mean bias	0.00	0.00	0.00
bias%	101.13	244.46	172.79
R	0.91	0.94	0.95
F50%	26.25	1.25	5.00
NMB	101.13	244.46	172.79
NME	101.89	244.46	172.79
MFB	58.09	106.87	88.42
MFE	59.91	106.87	88.42
no of station	80	80	80
Spatial resolution	0.5° × 0.5°	2.0° × 2.5°	-

Table S2. 6 Comparison between models and CASTNET for the velocity of SO_2 dry deposition. The unit is cm s^{-1}.

	CAM-Chem	CHASER_re1	CHASER_t106	EMEP_rv48	GEOSCHEMADJOINT	GOCART	OsloCTM3.v2	SPRINTARS	MMM
mean obs	0.27	0.27	0.27	0.27	0.27	0.27	0.27	0.27	0.27
mean model	0.14	0.17	0.16	0.36	0.33	0.41	0.39	0.50	0.24
Linear Fit Slope	0.16	0.02	-0.01	-0.35	0.20	0.03	-0.62	0.15	0.04
mean bias	-0.13	-0.09	-0.11	0.10	0.07	0.15	0.12	0.23	-0.02
bias%	-47.79	-34.88	-41.44	35.54	25.05	54.32	46.08	87.86	-8.39
R	0.18	0.03	-0.02	-0.23	0.09	0.03	-0.44	0.23	0.06
F50%	36.25	60.00	53.75	56.25	70.00	42.50	50.00	30.00	77.50
NMB	-47.79	-34.88	-41.44	35.54	25.05	54.32	46.08	87.86	-9.03
NME	56.70	44.51	49.62	62.93	55.54	60.74	68.83	88.07	34.88
MFB	-67.47	-39.46	-48.79	27.96	16.61	45.18	36.33	65.08	-3.83
MFE	75.10	52.75	60.26	50.44	42.03	49.40	53.58	65.21	35.00
no of station	80.00	80.00	80.00	80.00	80.00	80.00	80.00	80.00	80

Table S2. 7 Same as Table S2.6 but for velocity of SO_4^{2-} dry deposition.

	CAM-Chem	CHASER_re1	CHASER_t106	EMEP_rv48	GEOSCHEMADJOINT	OsloCTM3.v2	MMM
mean obs	0.13	0.13	0.13	0.13	0.13	0.13	0.13
mean model	0.15	0.09	0.10	0.17	0.13	0.21	0.13
Linear Fit Slope	0.29	0.01	-0.01	0.30	0.11	0.21	0.10
mean bias	0.02	-0.03	-0.03	0.04	0.01	0.08	0.00
Bias %	16.15	-26.92	-24.39	31.34	4.06	63.18	0.30
R	0.42	0.07	-0.16	0.17	0.28	0.27	0.34
F50%	83.75	82.50	85.00	67.50	90.00	36.25	88.75
NMB	16.15	-26.92	-24.39	31.34	4.06	63.18	0.30
NME	26.38	32.21	30.95	45.91	22.36	63.67	21.12
MFB	17.60	-26.05	-22.58	23.00	7.78	50.30	4.56
MFE	26.19	34.91	33.14	37.74	22.75	50.56	21.73
No of stations	80	80	80	80	80	80	80

Table S2. 8 Same as Table S2.6 but for velocity of HNO_3 dry deposition.

	CAM-Chem	CHASER_re1	CHASER_t106	EMEP_rv48	GEOSCHEM ADJOINT	OsloCTM3.v2	MMM
mean obs	1.34	1.34	1.34	1.34	1.34	1.34	1.34
mean model	0.68	1.07	1.41	1.35	1.51	3.55	1.25
Linear Fit Slope	0.03	0.06	-0.37	-0.03	-0.40	-1.24	-0.10
mean bias	-0.66	-0.28	0.06	0.01	0.17	2.21	-0.10
Bias %	-49.12	-20.70	4.60	0.74	12.44	164.52	-7.27
R	0.10	0.05	-0.28	-0.03	-0.29	-0.38	-0.12
F50%	50.00	72.50	77.50	85.00	76.25	16.25	85.00
NMB	-49.12	-20.70	4.60	0.74	12.44	164.52	-7.27
NME	49.92	34.65	36.69	29.96	38.75	165.99	27.47
MFB	-62.09	-27.68	2.14	-0.16	9.65	84.58	-7.01
MFE	63.78	42.88	37.23	30.98	36.88	85.84	29.52
No of stations	80	80	80	80	80	80	80

Table S2. 9 Same as Table S2.6 but for velocity of NO_3^- dry deposition.

	EMEP_rv48	GEOSCHEMADJOINT	MMM
mean obs	0.12	0.12	0.12
mean model	0.29	0.10	0.14
Linear Fit Slope	0.65	0.00	0.06
mean bias	0.17	-0.02	0.02
Bias %	146.99	-16.50	18.69
R	0.26	0.00	0.05
F50%	7.50	77.50	73.75
NMB	146.99	-16.50	18.69
NME	147.73	40.11	37.35
MFB	81.93	-17.07	17.29
MFE	82.58	38.99	32.05
No of stations	80	80	80

Table S2. 10 Same as Table S2.6 but for velocity of NH_4^+ dry deposition

	CAM-Chem	GEOSCHEMADJOINT	MMM
mean obs	0.12	0.12	0.12
mean model	0.22	0.06	0.12
Linear Fit Slope	0.38	0.06	0.13
mean bias	0.10	-0.06	0.00
Bias	81.91	-47.39	-1.72
R	0.40	0.23	0.27
F50%	15.00	60.00	87.50
NMB	81.91	-47.39	-1.72
NME	82.81	48.76	22.13
MFB	60.11	-57.09	2.01
MFE	60.62	59.99	22.67
No of stations	80	80	80

Supporting materials for Chapter 4

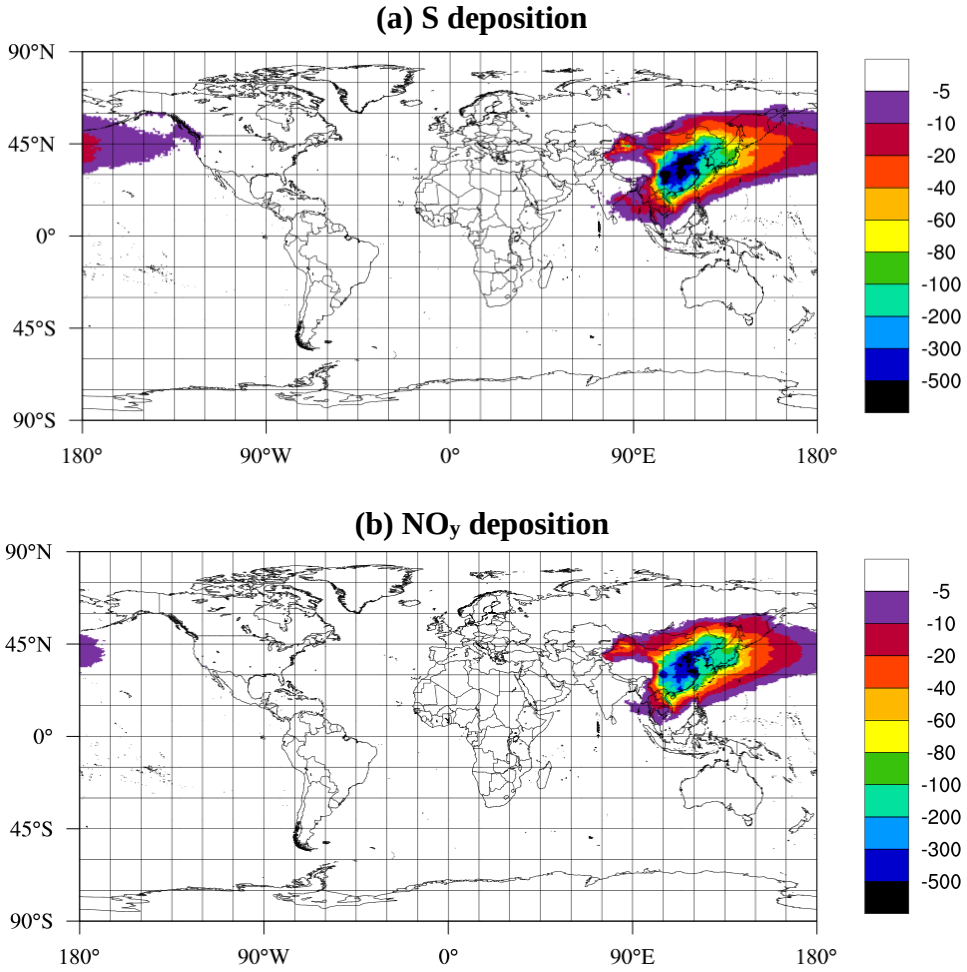

Figure S4. 1 Changes of S and NO_y deposition under 20% emission reduction in EA (unit: mg(S or N) m^{-2} yr^{-1}).

Table S4. 1 Monthly changes of S, NO_x and NH_3 emissions under 20% emission perturbation experiments. The unit is ×0.1 Tg(S or N) month^{-1}).

Emission changes	Seasons	Regions of emission perturbation					
		NA	EU	SA	EA	ME	RU
S emission	Jan	-0.913	-0.646	-0.860	-2.575	-0.505	-0.463
	Feb	-0.886	-0.609	-0.789	-2.119	-0.477	-0.433
	Mar	-0.955	-0.657	-0.876	-2.421	-0.477	-0.428
	Apr	-0.942	-0.591	-0.822	-2.173	-0.452	-0.395
	May	-0.956	-0.483	-0.840	-2.188	-0.436	-0.360
	Jun	-0.996	-0.476	-0.800	-2.249	-0.415	-0.332
	Jul	-1.009	-0.449	-0.805	-2.231	-0.411	-0.323
	Aug	-1.007	-0.392	-0.799	-2.184	-0.425	-0.322
	Sep	-0.961	-0.452	-0.792	-2.168	-0.423	-0.343
	Oct	-0.971	-0.512	-0.834	-2.234	-0.459	-0.385
	Nov	-0.956	-0.514	-0.826	-2.521	-0.472	-0.398
	Dec	-0.911	-0.602	-0.877	-2.820	-0.496	-0.443

Table S4.1 continued

Emission changes	Seasons	Regions of emission perturbation					
		NA	EU	SA	EA	ME	RU
NO_x emission	Jan	-0.698	-0.424	-0.536	-1.434	-0.228	-0.236
	Feb	-0.697	-0.427	-0.484	-1.249	-0.228	-0.231
	Mar	-0.730	-0.462	-0.533	-1.435	-0.227	-0.227
	Apr	-0.729	-0.446	-0.512	-1.362	-0.227	-0.219
	May	-0.728	-0.407	-0.525	-1.369	-0.221	-0.202
	Jun	-0.767	-0.408	-0.505	-1.400	-0.217	-0.195
	Jul	-0.768	-0.388	-0.516	-1.399	-0.210	-0.186
	Aug	-0.768	-0.366	-0.514	-1.389	-0.215	-0.191
	Sep	-0.730	-0.391	-0.492	-1.365	-0.215	-0.194
	Oct	-0.731	-0.424	-0.527	-1.374	-0.229	-0.217
	Nov	-0.730	-0.415	-0.505	-1.494	-0.231	-0.224
	Dec	-0.698	-0.424	-0.537	-1.587	-0.229	-0.232

Continue Table S4.1

Emission changes	Seasons	Regions of emission perturbation					
		NA	EU	SA	EA	ME	RU
NH_3 emission	Jan	-0.391	-0.423	-2.102	-1.122	-0.080	-0.130
	Feb	-0.437	-0.487	-1.805	-1.026	-0.146	-0.235
	Mar	-0.591	-0.780	-2.098	-1.205	-0.246	-0.412
	Apr	-0.694	-0.850	-1.996	-1.487	-0.187	-0.338
	May	-0.719	-0.742	-2.097	-1.765	-0.117	-0.224
	Jun	-0.933	-0.627	-1.996	-1.920	-0.110	-0.200
	Jul	-1.077	-0.571	-2.096	-1.904	-0.113	-0.199
	Aug	-0.903	-0.574	-2.096	-2.038	-0.126	-0.215
	Sep	-0.676	-0.606	-1.996	-1.531	-0.121	-0.214
	Oct	-0.632	-0.642	-2.097	-1.312	-0.094	-0.178
	Nov	-0.592	-0.617	-1.998	-1.360	-0.074	-0.146
	Dec	-0.344	-0.517	-2.109	-1.263	-0.074	-0.133

Supporting materials for Chapter 5

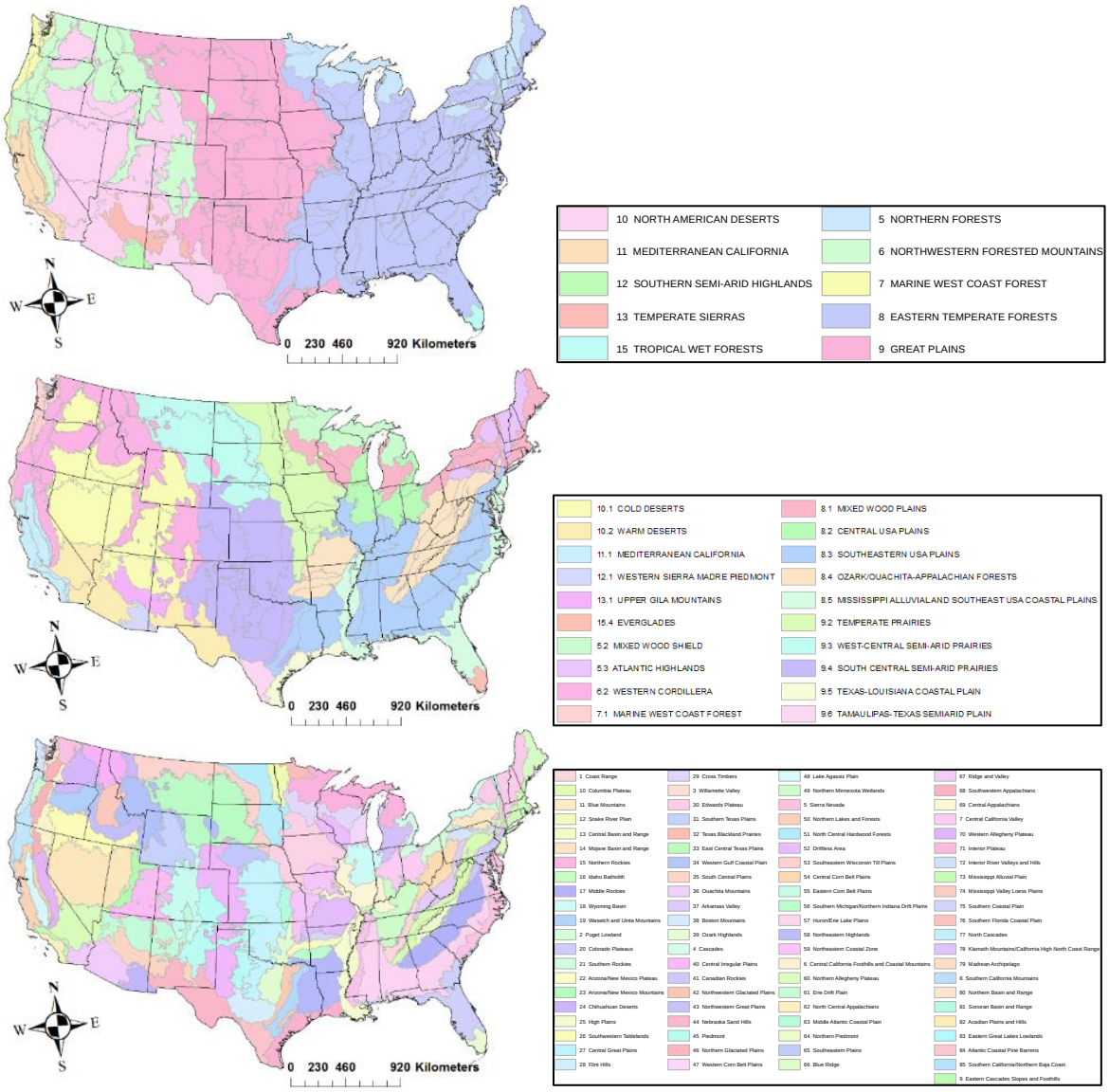

Figure S5. 1 Spatial distributions of U.S. EPA Ecoregion Level I-IV.

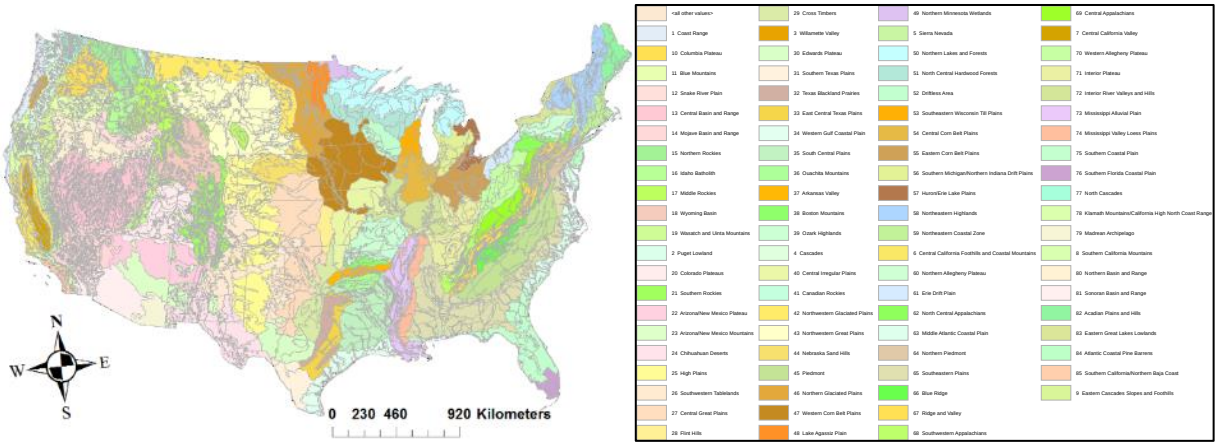

Figure S5. 1 Continued.

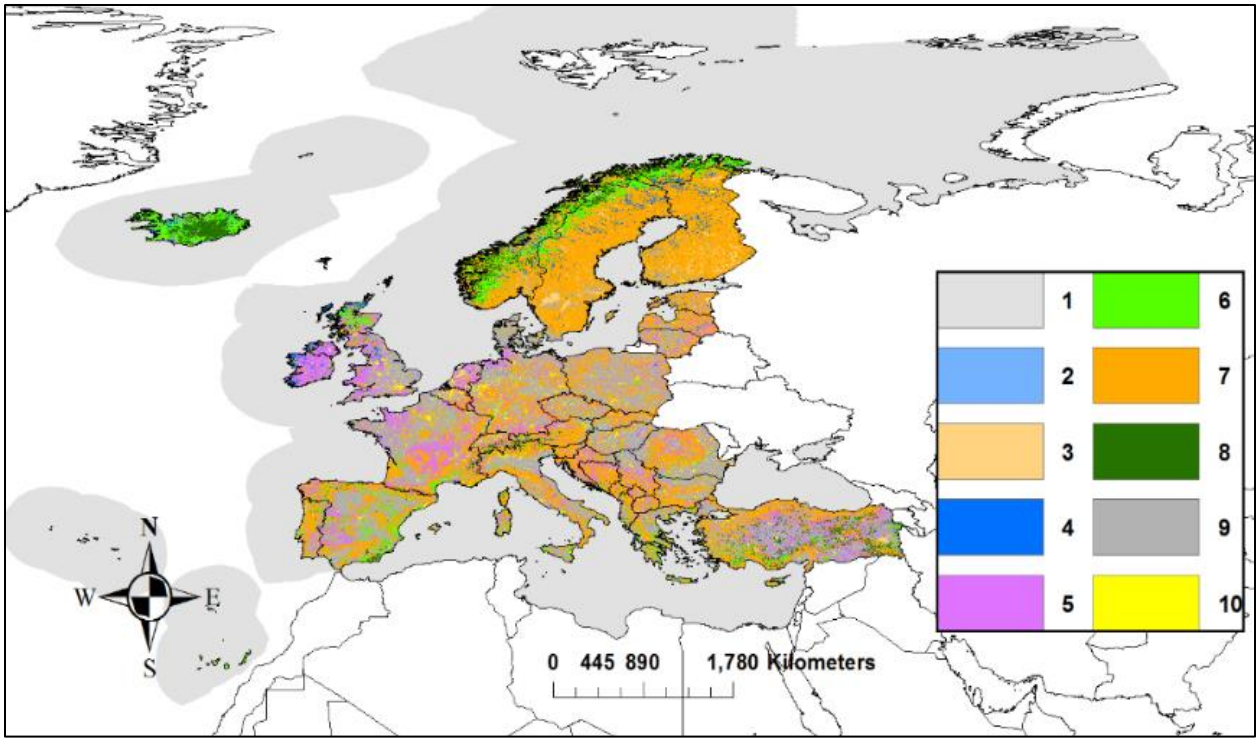

Figure S5. 2 Map of ecosystems in Europe. Number 1 stands for Marine habitats, 2 stands for coastal habitats, 3 stands for inland surface water, 4 stands for mires, bogs and fens, 5 stands for Grasslands and land dominated by forbs, mosses or lichens, 6 stands for heathland, scrub and tundra, 7 stands for woodland, forest and other wooded land, 8 stands for inland unvegetated or sparsely vegetated habitats, 9 stands for regularly or recently cultivated, horticultural and domestic habitats, 10 stands for constructed, industrial and other artificial habitats. The spatial resolution is 1 km.

Supporting materials for Chapter 6

Table S6. 1 Observations of P deposition over North America (part of collection).

Country	Site name	LAT	LONG	MAP[1]	MAT[2]	Sampling Periods	TP	FTP	PO4-P	Note	Database
		deg	deg	mm	ºC		g/m2/a	g/m2/a	g/m2/a		
Canada	Lake Simcoe	44.42	-79.33	863	7.1	1998-2004	0.032	-	-	Terrestrial P deposition, bulk	Tipping et al., 2014
	Ontario (ELA)	49.67	-93.72	580	2.4	1989	0.008	-	-		
	Narrow Lake Alberta	54.58	-113.62	503	1.7	1983	0.020	-	-		
	Rawson Lake, ELA, Ontario	49.77	-94.50	790	2.2	1970	0.033	-	-		
	Kenora	49.77	-94.50	715	1.4	2008	0.124	-	-		
	Buffalo Point	49.02	-95.25	715	1.4	2008	0.055	-	-		
	Sioux Narrows	49.40	-94.12	715	1.4	2008	0.026	-	-		
	Harp Lake, Ontario	45.37	-79.13	860	5.8	1976	0.035	-	-		
	Harp Lake, Ontario	45.38	-79.13	860	5.8	1974	0.074	0.039	0.026		
	N Ontario	46.35	-83.38	953	5.4	1970	0.010	-	-		
	Haliburton / Muskoka Ontario 32 sites	45.00	-79.00	886	5.3	1976	0.020	-	-		
	Clear Lake, Eastern Ontario	45.18	-78.72	900	4.0	1967	0.046	-	-		
Mexico	Chamela	19.02	-105.00	679	24.9	1990	0.016	-	-		
	Yucatan Peninsula	19.33	-89.63	892	25.6	2007	0.027	-	-		
US	Heron Pond, Illinois	37.37	-88.95	1224	14.4	1976	0.110	-	-		
	Hubbard Brook, New Hampshire	43.93	-71.75	1295	5.0	1971	0.010	-	-		
	Lake Michigan	44.00	-87.00	800	8.0	1971	0.017	-	-		
	Tar River, N Carolina	35.58	-77.17	1145	16.4	1975	0.049	-	-		
	Iowa, 6 sites	42.00	-93.00	831	8.9	2003	0.030	-	-		
	South-central Pennsylvania cropland	38.27	-76.40	1079	14.5	2004	0.193	-	-		
	South-central Pennsylvania pasture	38.27	-76.40	1079	14.5	2004	0.110	-	-		
	South-central Pennsylvania woodland	38.27	-76.40	1079	14.5	2004	0.036	-	-		
Canada	Banff National Park	51.27	-115.39	-	-	2008	0.057	-	-	Porter 2012	Brahney et al., 2015
US	New. Hamp., Appalachians	43.95	-71.69	-	-	1972-2010	0.017	-	-	Likens (1995-2010), Hubbard Brook Dataset	
	Colorado Rockies	40.05	-105.59	-	-	2002-2010	0.015	-	-	Mladenov et al 2012	
	California, Sierra Nevada	39.11	-120.34	-	-	1994-2004	0.019	-	-	Sahoo et al 2010, Vicars 2010	
Canada	Harp Lake	45.38	-79.14	-	-	2003–2007	-	-	-	Yao, H., McConnell, C., Paterson, A., 2010Variable sampling periods (<31 days)	Vet et al., 2014
	Heney Lake	45.18	-78.82	-	-		0.014	-	-		
	Plastic Lake	45.13	-79.10	-	-		0.015	-	-		
	Turkey Lakes	47.03	-84.38	-	-	2000–2005	0.006	-	-	Semkin, R., April, 2010. Weekly sampling periods	

Continue Table S6. 1

Country	Site name	LAT	LONG	MAP[1]	MAT[2]	Sampling Periods	TP	FTP	PO4-P	Note	Database
		deg	deg	mm	ºC		g/m2/a	g/m2/a	g/m2/a		
US	Narraganseet, RI	41.5	-71.5	-	-		0.007	-	-	Graham and Duce, 1979, Table 3	Mahowald et al., 2008
	New Haven, CT	41.3	-74	-	-	1973-1975	0.012	-	-		
	New York State	43	-76	-	-		0.04	-	-		
	Lake Huron	45	-83	-	-		0.01	-	-		
	Southern Lake Huron	43.5	-82.5	-	-		0.027	-	-		
	Lake Superior	47.5	-87	-	-		0.01	-	-		
	Northern Minnesota	48	-92	-	-		0.014	-	-		
	Clear Lake, Ontario	48	-83	-	-		0.027	-	-		
	Western Ontario	50	-92	-	-		0.05	-	-		
	Sudbury, Ontario	46.5	-81	-	-		0.02	-	-		
	Cochocton, OH	39.1	-84.5	-	-		0.017				

Note:
1 - MAP: mean annual precipitation.
2 - MAT: mean annual temperature.

Table S6. 2 Observations of P depositions over South & Center America.

Country	Site name	LAT	LONG	MAP	MAT	Sampling time	TP	TDP	PO_4-P	Note	Database
		deg	deg	mm	ºC		g $m^{-2}a^{-1}$	g $m^{-2}a^{-1}$	g $m^{-2}a^{-1}$		
Brazil	Manaus	-3.13	-59.87	2622	26.0	1996 -1997	-	0.007	0.002	Bulk	Tipping et al., 2014
	Rio Negro	-3.00	-66.00	1997	27.0	1964	0.018	-	-		
	Lake Prato	-2.70	-60.75	2083	26.7	1991	-	0.030	-		
	Ducke Forest Preserve	-2.95	-59.61	2476	25.0	1968 - 1972	0.037	-	-		
	Central Amazon Basin	0.00	-55.00	2053	25.6	1987	-	-	0.011		
	Manaus	-3.13	-59.87	2622	26.0	1965 - 1968	0.027	-	-		
Columbia	Middle Caqueta	-0.73	-72.08	3400	24.0	1995 - 1997	-	-	0.033		
	Cordillero Central, 2550 m	4.83	-75.55	2115	12.2	1986	-	-	0.072		
	Cordillero Central, 3370 m	4.83	-75.50	1453	7.7	1986	-	-	0.048		
Costa Rica	Turrialba	9.88	-83.67	2195	17.0	1979 - 1981	0.020	-	0.009		
Equador	Loja	-4.00	-79.08	2220	16.2	1999	-	-	0.060		
Honduras	Siguatepeque	14.62	-87.83	1132	21.9	1978	-	-	0.008		
Puerto Rico	Luquillo	-18.33	-65.83	565	16.5	1988 - 2002	-	-	0.011		
Venezuela	Lake Valencia	10.14	-67.63	750	23.1	1976 - 1978	0.168	-	0.030		
	San Eusebio	8.62	-71.35	1576	17.0	1973	0.110	-	-		
Colombia	Vander (Montane)	5	-75.50	-	-	1986-1987	0.060	-	-	Bulk, Veneklaas 1990	Brahney et al., 2015
Ecuador	Cordillera Real (Montane)	-4	-79.08	-	-	1998-2003	0.093	-	-	Bulk, Boy et al 2008	
	Podocarpus National Park	-4.11	-78.92	-	-	2002-2006	0.260	-	-	Wet, Fabian et al 2009	
North Andes	Montane (Mean)	-4	-79.00	-	-	1998-2006	0.138	-	-	Boy et al 2008, Fabian et al 2009	
Chile	Torres del Paine (Patagonia)	-50.94	-73.41	-	-	1984-1993	0.013	-	-	Galloway et al 1996, Wet	
Costa Rica	Turrialba	9.91	-83.59	-	-	1979-1981	0.019	-	-	Hendry et al., 1984; Tsuka et al., 2006	Mahowald et al., 2010
Venezuela	Lake Valencia	10.1	-67.87	-	-	1976-1977	0.168	-	-	Lewis, 1981; Tsuka et al., 2006	
Brazil	Manaus	-3	-60	-	-	1973-1975	0.029	-	-	Graham and Duce, 1979, Table 5	

Table S6. 3 Observations of P depositions over Europe (part of collection).

Country	Site name	LAT	LONG	MAP	MAT	Sampling time	TP	FTP	PO4-P	Note	Database
		Deg	Deg	mm	ºC		g $m^{-2}a^{-1}$	g $m^{-2}a^{-1}$	g $m^{-2}a^{-1}$		
Austria	Piburger See	47.20	10.89	1083	2.4	1977 - 1980	0.036	-	-	Terrestrial P deposition, direct measurements of bulk TP, FTP and PO4-P	Tipping et al., 2014
Denmark	Denmark	56.00	9.27	600	8.6	1989 - 2010	0.004	-	-		
Estonia	Estonia	58.67	25.67	600	5.2	1990 -2002	0.003	-	-		
	Lake Vortsjarv	58.28	26.03	759	4.6	1995	-	-	0.014		
Finland	Lake Pyhajarvi	60.98	22.28	618	5.0	1992	0.027	-	-		
France	Capo Cavallo, Corsica	42.52	8.67	600	15.0	1985 - 1987	0.040	-	-		
	Madeleine	43.60	3.90	478	13.8	1966 - 1968	0.070	-	-		
	Grabels	43.60	3.90	602	13.8	1966 - 1968	0.080	-	-		
	Rouquet	43.60	3.90	662	13.8	1966 - 1968	0.100	-	-		
	Gabriac	43.60	3.90	709	13.8	1968	0.110	-	-		
Greece	Finokalia, Crete	35.33	25.67	760	19.3	1999 - 2000	-	-	0.002		
UK	Cheshire	53.17	-2.58	400	9.3	1965 - 1966	0.080	-	-		
	Lake District	54.15	-3.17	1710	8.8	1962 - 1965	0.033	-	-		
	Kincardineshire	56.92	-2.50	750	7.2	1965 - 1966	0.020	-	-		
	Merlewood	54.19	-2.92	1050	8.5	1965 - 1966	0.100	-	-		
	N Yorkshire	54.25	-1.47	700	8.5	1965 - 1966	0.080	-	-		
	Moor House	54.70	-2.40	1861	7.1	1964 - 1966	0.022	-	-		
	Berkshire	51.42	-1.00	802	9.7	1975 - 1977	0.122	-	-		
	Heigham Holmes	52.73	1.62	600	10.0	2012	0.021	-	-		
	Yarner Wood	50.60	-3.71	1196	9.6	2012	0.026	-	-		
	Cockley Beck	54.40	-3.16	1309	8.8	2012	0.013	-	-		
	Monkswood	52.40	-0.23	625	9.5	2012	0.013	-	-		
Sweeden	North (Area 12)	65.36	19.14	-	-	1998-2000	0.024	-	-	Kuslt 2001, bulk	Brahney et al., 2015
Norway	Hurdal Central (HU)	60.44	11.06	-	-	1998	0.015	-	-	Svein et al 1998, bulk	
	Langtjern Central (LA)	58.90	11.60	-	-	1998	0.018	-	-		
	Fagernes Central (FA)	60.96	9.20	-	-	1998	0.013	-	-		
	Sogne South (SG)	58.09	7.79	-	-	1998	0.021	-	-		
	Birkenes South (BI)	58.16	7.83	-	-	1998	0.023	-	-		
	Valle South (VA)	58.10	7.31	-	-	1998	0.016	-	-		
Fella, England	South lake district (Merlewood)	53.90	-2.87	-	-	1962-1965	0.100	-	-	Carlisle 1967, bulk	
Italy	08FR12 Northeast	46.63	13.10	-	-	1998-1999	0.004	-	-	Mosello et al 2002, bulk	
	10LOMI Northeast	46.21	9.77	-	-	1998-1999	0.019	-	-		
	17TREI Northeast	46.32	11.21	-	-	1998-1999	0.114	-	-		
	20VENI Northeast	45.83	12.22	-	-	1998-1999	0.007	-	-		
	07FRII Northeast	46.08	15.96	-	-	1998-1999	0.016	-	-		
Spain	St Nicholas Valley	42.67	1.00	-	-	1990	0.061	-	-	Camarero and Catalan 1996, bulk	
	St Nicholas Valley	42.63	0.77	-	-	1997-1998	0.009	-	-	Ventura et al 2000, bulk	
	Sierra Nevada	36.57	-3.28	-	-	2001-2002	0.016	-	-	Morales-Baquero et al 2006	
Slovakia/Poland	Tatra Mountains	49.46	20.23	-	-	1998-2009	0.021	-	-	Kopacec et al 2011, bulk	

Table S6. 4 Observations of P depositions over Asia (part of collection).

Country	Site name	LAT	LONG	MAP	MAT	Sampling time	TP	TDP	PO4-P	Note	Database
		Deg	Deg	mm	ºC		g $m^{-2}a^{-1}$	g $m^{-2}a^{-1}$	g $m^{-2}a^{-1}$		
China	Lake Taihu	31.67	120.37	1206	15	2002	0.056	-	-	Bulk	Tipping et al., 2021
	Upper Reach, Changjiang River	30.72	111.28	1202	15	1998	0.006	-	0.004		
	Middle Reach, Changjiang River	31.03	116.63	1392	15	1998	0.008	-	0.004		
	Lower Reach, Changjiang River	31.35	121.98	1179	15	1998	0.009	-	0.005		
India	Dal Lake, Kashmir	34.12	74.87	500	10	1981	0.018	-	-		
Japan	Ashiu	35.33	135.72	2339	12	2000-2004	0.024	-	0.005		
Malaysia	Upper Segama, Sabah	4.97	117.80	2800	27	1989	-	0.0300	-		
Russia	Lake Baikal	53.50	109.50	500	-2	1960s/1980s	0.017	-	-	Bulk; Counted as 1 year in analysis	
India	Kumaun Himalaya (2050 masl)	19.38	79.46	-	-	1981-1982	0.1	-	-	Bulk, Pandey et al. 1983	Brahney et al., 2015
China	Xizang Agriculture and Animal Husbandary	30.1	94.57	625	9	March-october 2017	-	0.088	-	Bulk, Annual value calculated from 8 months	Wang et al., 2018
	National Field Scientific Observation Station of Alpine Forest Ecosystem	30.08	95.2	839	-1		-	0.102	-		
China	Aksu	40.62	80.85	66	11	2013	0.004	-	-	Agriculture	Zhu et al., 2016
	Ailao Mountains	24.53	101.02	1146	13		0.020	-	-	Forest	
	Ansai	36.86	109.32	493	9		0.004	-	-	Agriculture	
	Beijing	40.02	116.57	549	12		0.005	-	-	Forest	
	Inner Mongolia Grassland	43.63	116.70	391	0		0.004	-	-	Grassland	
	Changshu	31.55	120.70	1204	14		0.253	-	-	Agriculture	
	Daxinganling	52.07	122.05	492	-7		0.007	-	-	Forest	
	Dangxiong	30.85	91.08	518	-4		0.011	-	-	Grassland	
	Dinghu Mountain	23.16	112.55	1733	22		0.043	-	-	Forest	
	Dongling Mountain	39.97	115.43	539	7		0.010	-	-	Forest	
	Dongting Lake	29.50	112.80	1310	17		0.008	-	-	Lake	
	Duolun	42.03	116.28	517	-1		0.025	-	-	Grassland	
	Erdos	39.49	110.19	395	6		0.030	-	-	Grassland	
	Fengqiu	35.02	114.55	629	14		0.019	-	-	Agriculture	
	Fukang	44.29	87.93	143	7		0.032	-	-	Desert	
	Gongga Mountain 1600m	29.65	102.12	939	11		-	-	-	Forest	
	Gongga Mountain 3000m	29.58	102.00	939	11		-	-	-	Forest	
	Haibei	37.62	101.32	344	0		0.048	-	-	Grassland	
	Hailun	47.45	126.93	554	2		0.013	-	-	Agriculture	
	Heshan	22.68	112.90	1848	22		0.077	-	-	Forest	
China	Lake Taihu	31.40	120.22	-	-	2003	0.004-0.044	-	-	Six sample every season, dry depo only	Luo et al., 2011
India	Karala Coast	11.00	76.00	-	-	1973-1975	-	0.480	-	Graham and Duce, 1979, Table 5	Mahowald et al., 2008

Table S6. 5 Observations of P deposition over Africa.

Country	Site name	LAT	LONG	MAP	MAT	Sampling time	TP	FTP	PO_4-P	Note	Database
		Deg	Deg	mm	ºC		g $m^{-2}a^{-1}$	g $m^{-2}a^{-1}$	g $m^{-2}a^{-1}$		
Cameroon	Korup National Park	5.07	8.85	5370	25.1	1992	0.107	-	-	Terrestrial P deposition, bulk	Tipping et al., 2014
Cambia	Yundum	13.33	-16.67	1055	26.3	1963	0.031	-	-		
	Jenoi	13.48	-15.57	1007	26.9	1963	0.016	-	-		
	Yoroberi Kunda	13.50	-14.75	709	27.4	1963	0.027	-	-		
Ivory Coast	Taï National Park	7.33	-5.87	1833	26.0	1990	0.013	-	-		
Nigeria	Samaru	11.17	7.63	1176	25.0	1959	0.250	-	-		
RSA	Pella	-33.52	18.53	381	16.4	1980	0.019	-	-		
Tanzania	Bukoba, Lake Victoria	-1.33	31.82	1612	21.5	1999	0.190	-	0.068		
	Mwanza, Lake Victoria	-2.52	32.90	1027	22.5	1999	0.270	-	0.087		
	Seronera, Lake Victoria	2.33	34.92	1062	22.0	1999	0.180	-	0.047		
Nigeria	Northern Nigeria	11	8	-	-	1973-1975	0.260	-	-	Graham and Duce, 1979, Table 5	Mahowald et al., 2008
Gambia	The Gambia	13	343	-	-		0.022	-	-		
-	Natal Coast, South Africa	-29	32	-	-		0.430	-	-		

Table S6. 6 Collection of observations over Oceania.

Country	Site name	LAT	LONG	MAP	MAT	Sampling time	TP	TDP	PO_4-P	Note	Database
		Deg	Deg	mm	ºC		g $m^{-2}a^{-1}$	g $m^{-2}a^{-1}$	g $m^{-2}a^{-1}$		
Australia	Richmond River catchment NSW	-30.00	153.00	1420	18.9	1994 -1996	0.036	-	-	Bulk	Tipping et al., 2014
Fiji	Viti Levu	-17.98	177.28	2100	24.0	1990 -1991	0.008	-	-		
New Guinea	Eastern highlands montane forest	-6.00	145.18	3985	20.8	1970	0.053	-	-		
New Zealand	Ngapuna	-38.08	176.27	1401	12.9	1974	0.040	-	-		
	Taita Experimental Station, Wellington	-41.00	175.00	1352	12.4	1956 - 1958	-	0.022	-		
	Kelburn	-41.17	174.46	1300	12.8	1983 - 1992	-	-	0.005		
	Lauder	-45.02	169.41	530	7.6	1983 - 1994	-	-	0.001		
	Puruki	-38.43	176.22	1500	13.1	1987 - 1991	-	-	0.002		
	Whakarewarewa Forest	-38.14	176.25	1524	10.0	1954 - 1956	-	0.026	-		
	Kaingaroa Forest	-38.14	176.25	1524	10.0	1955 - 1957	-	0.038	-		
Samoa	Tutuila Island	-14.30	-170.70	2900	27.0	1975	0.014	-	-		
New Zealand	North Island	-38.5	176	-	-	1973-1975	0.028	-	-	Graham and Duce, 1979, Table 5	Mahowald et al., 2008
		-38.5	176	-	-		0.022	-	-		
	New Zealand	-34.5	173	-	-	1970s	0.015	-	-	Chen et al., 1985	

Table S6. 7 Transport of P among different earth cycles from literature.

	Regions	TP fluxes	Reference	Note
	Unit	10^{10} g a^{-1}		
Manure	Global	1700 (600, 900,1700)	(L. Bouwman et al., 2013)	2000 (1900,1950,2000)
Runoff	Global	400 (100,100,400)	(L. Bouwman et al., 2013)	2000 (1900,1950,2000)
	China	157 (47,78,157)	(X. Liu et al., 2016)	2012 (1960,1990,2012), fig 1
Phosphine from freshwater wetlands and rice paddies	Global	0.020 (0.0038 - 0.036)	(R. Wang et al., 2015)	-
Atmosphere to Ocean	Global	60	(Ahlstrom & Cornell, 2018)	-
Biosphere to Oceans	Global	1200	(Ahlstrom & Cornell, 2018)	-
Oceans to Lithosphere	Global	600 - 3300	(Ahlstrom & Cornell, 2018)	-
Lithosphere to Biosphere	Global	4500	(Ahlstrom & Cornell, 2018)	-
Lithosphere to Atmosphere	Global	140	(Ahlstrom & Cornell, 2018)	-
Continent to Ocean	Global	100	(Graham & Duce, 1979)	-
	Global	400-600	(Filippelli, 2008)	-
	Global	145 (DIP)	(Harrison, Bouwman, Mayorga, & Seitzinger, 2010)	Export from river to coastal region

VITA

Jiani Tan was born in Shanghai, China. She received her Bachelor's and Master's degrees from the department of Environmental Science and Engineering of Fudan University, China in 2011 and 2014. She joined the Department of Civil and Environmental Engineering of the University of Tennessee in August of 2014. She finished the Ph.D. program in December 2019 with an interdisciplinary graduate minor in computational science.